Estimation of the Risk for Mine Induced Seismicity in Large Scale Mining in the Garpenberg Mine

By M.J.G. van Koppen

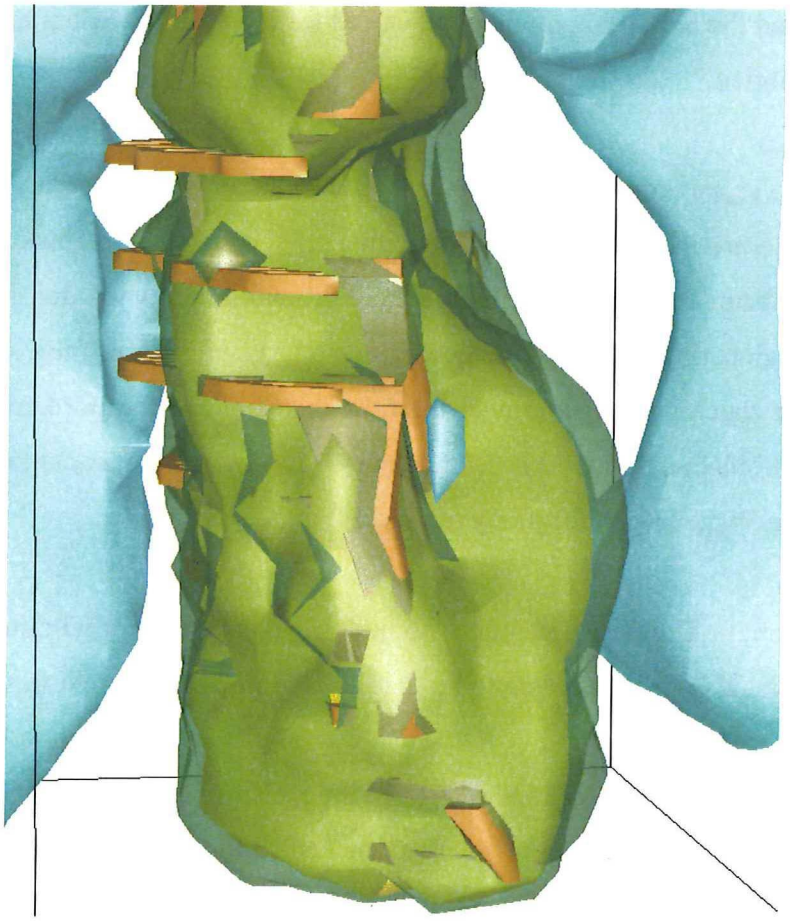

TU Delft

NEW BOLIDEN

TEKNILLINEN KORKEAKOULU
TEKNISKA HÖGSKOLAN
HELSINKI UNIVERSITY OF TECHNOLOGY

Preface

This thesis is the final project for the degree of Master of Science in Mining Engineering at the Delft University of Technology in the Netherlands. The project was provided and supported by New Boliden AB in Sweden. This thesis tries to provide some insight in the potential for mine induced seismicity in the Lappberget orebody in Garpenberg. The thesis started with a two-month period at the mine in Garpenberg and the remaining months were used for modelling, writing and figuring out data in Boliden.

I would like to express my thanks to the various production crews at Garpenberg for taking me underground and providing me with a sense for the way things work at Garpenberg, Shaun Duggan for taking me underground, Franz Vyskytensky for trying to teach an engineering student some geology on a large number of mine visits, Simon Granbacka for checking the geology chapter, Lennert Lehtola for more mine visits and stability problems, Sari Koivisto for answering an incredible amount of questions and André van Wageningen for many practical things.

Thanks goes out to Thomas Askemur, who not only gave a very good mine tour in Zinkgruvan, but also provided data to model the case study to relate it to seismicity.

I would like to thank Prof. Pekka Särrkä from the Helsinki University of Technology and ir. Hans de Ruiter from Delft University of Technology for their feedback and support and, hopefully, acceptance of this thesis.

Last but, as one of the worst clichés will agree, certainly not least are the people in the Boliden office. Thanks goes out to the whole department, but especially to Anders Nyström and Per-Ivar Marklund who not only had to put up with some of my ridiculous and far fetched theories but also with my horrific Swedish.

Maarten van Koppen
Boliden, August 2008

Summary

A few years ago a licentiate thesis was presented by K. Larsson on seismicity in Swedish mines compared with experienced seismicity abroad. This thesis was mainly focused on cut and fill mining and sublevel caving methods. Recently the Swedish mining company New Boliden started implementing transverse open stoping in the Lappberget ore body in the Garpenberg mine. The ore varies from being a homogeneous massive sulfide of zinc ore to a schistose biotite in a foliated quartzitic rock. In the early stage of Lappberget when using cut and fill mining stress induced fractures could be seen in the rock when mining the subsequent cut and this led to believe that the stresses are high enough to exceed the strength. The occurrence of a violent sill pillar failure in the Kanalmalmen ore body in Garpenberg gave reason to investigate the potential for instability at high extraction ratios of Lappberget and in particular if there is a potential for seismic events and associated violent failures.

An effort was made in this thesis to summarize all of the relevant geomechanical information available on Lappberget. Fundamental factors in rockbursting have been discussed and the information on the various elements – geology, state of stress, mining sequencing and rock mass properties – are discussed. A brief description of the fundamentals of the used numerical methods and the set-up of the models is described followed by the mechanisms behind two types of seismic events, where strain related seismicity and fault-slip seismicity are distinguished.

In discussing the results the tradeoff between the calculated strain energies in three-dimensional elastic (non-failure) models were compared to the two-dimensional plastic (failure) models. An indication of the stress reduction due to the plastic zones in the footwall and hanging wall was provided to estimate the potential for seismic events. This included analysis of the loading history, strain energies and indicated plastic zones.

Two case studies were analyzed in a similar fashion and it was concluded that the potential for strain related events is low, as rock will likely fail gradually instead of instantly and thereby dissipating the strain energy through small scale fracturing. The fault slip potential is harder to assess, as there are no significant geological features in

the vicinity of Lappberget to present knowledge. Fault slip mechanisms close to the hanging wall are not likely to accumulate high energies due to the weak hanging wall – ore contact. If a significant structure turns out to be present close to Lappberget the Excess Shear Stress method is suggested to provide an upper-bound estimation of potential events and as a starting point for more detailed analysis.

Furthermore it should be noted that the only definite way of finding the potential for seismic events is by the occurrence of seismic events. Seismic events do not automatically lead to structural failure. The lack of potential for seismic events does not exclude other types of structural failure.

The failure state of the stopes should be closely watched through observations and possibly convergence measurements. The numerical models can be improved by calibrating the failure criterion in the ore by using the observations and measurements. They will also improve by gaining a better understanding of the geology of the hanging wall to get a better idea of the plastic zones and the associated stress reduction in the ore. A three-dimensional numerical code capable of incorporating plasticity can provide a better understanding of the interaction of plasticity in various rock masses, provided that an adequate geomechanical model can be constructed.

Table of contents

List of figures and tables

1. Introduction

1.1 Background

Many underground hard rock mines are placed around geological anomalies that already have a complex stress pattern due to a variety of reasons such as residual, gravitational or tectonic sources of stress. When creating openings in and around stressed rock masses it causes the already complicated stress pattern to alter, leading to reduced stresses in some locations and increased stresses in others. These alterations can cause failure of the rock, however the fundamental factors that determine the extent and consequence of failure depend on the state of stress, the mining activities and the properties of the rock mass, including discontinuities such as faults and joint sets.

Naturally failure requires an interaction between all of these factors and for violent failure to occur it requires some specific conditions. Since a lot of development within mining is of a temporary nature failure can often be dealt with by means of support (e.g. shotcrete, bolts) or is simply being accounted for (e.g. dilution in open stopes). It is the violent failure that can prove to be particularly problematic. Violent failure is generally called a rockburst, but displaced volumes or masses are not quantified, as this appears to differ for each mine. As a result the following definitions have been introduced.

Seismicity	The rock mass response to deformation and failure.
Seismic event	The sudden release of potential or stored energy in the rock.
Rockburst	Mining induced seismic event that causes damage to openings in rock.

In 2004 a study was carried out to investigate the occurrences of, knowledge of and experiences with induced seismicity in mines throughout Sweden (Larsson, 2004). These were then compared with other mines in the Sudbury basin as well as two other mines in Scandinavia. This comparison was mostly aimed at sublevel caving and cut and fill mines. A few years ago longhole methods slowly started to replace the cut and fill mining in the Lappberget ore body, which is a major ore body in the Garpenberg

mine. Ground conditions in Lappberget are varying from homogenous massive sulphide ore to bands of mainly zinc ore and locally schistose biotite in a foliated quartzitic rock.

In the development drifts some stress induced spalling and slabbing has occurred at the pillar noses between cross cuts. In the cut and fill mining in Lappberget stress induced cracks can be seen at the face. This implies that the stresses are high enough to exceed the strength of the rockmass close to the drifts. Experience has been gained from stress induced pillar failures when mining sill pillars in other areas of the Garpenberg mine and this gives reason to examine the expected mining conditions at high extraction ratios. The focus of this thesis is to see if there is risk for stability issues and in particular induced seismicity to any degree when mining Lappberget by the current transverse open stoping design.

1.2 Objective and scope of the thesis

The objective of this thesis is to estimate the risk for seismicity when mining the Lappberget orebody in Garpenberg using longhole stoping methods. The emphasis will be around the sill pillar near the end of life of the lower mining block (1080-896) and the infrastructure around the levels in the lower part. As stresses are higher in the lower part it is this part that is expected to have the highest likelihood to display some degree of seismicity.

Numerical modelling software will be used for the analysis in which energy balances will play an integral part. The numerical modelling software will be provided by Phase2 and Examine3D, which are a 2D finite difference model and a 3D boundary element model, respectively. By using these programs the Excess Shear Strain (ESS) and the Energy Release Rate (ERR) can be calculated which should provide an indication of the most burst prone areas in Lappberget.

In order for the models to have any meaning special care must be taken in selecting the input place parameters and entering the geometry of the geology and planned excavations. This will play a paramount role in the success of the thesis.

In addition two case studies will be discussed. The first case study, the Burkland ore body at Zinkgruvan mine, has a seismic monitoring system installed. This case was selected as the rock conditions and stope designs are similar to Lappberget. The second case is a seismic event that occurred in a sill pillar in another orebody in the Garpenberg mine. Experiences and recommendations from these two cases will be discussed and compared to Lappberget.

1.3 Outline of the thesis

Following the introduction is an historical background on the area, the mine and the orebody for general reference. Chapter 3 will discuss the geology of the Lappberget orebody and surrounding host rock. The planned mining methods and execution of those is discussed in Chapter 4.

Chapter 5 will encompass the sizes and orientations of the far field stresses and discuss the acquisition of these values. In addition some convergence measurements are discussed. The rock mass parameters are derived from the available data and are discussed in Chapter 6 and assumptions will be highlighted and explained. Chapter 7 deals with the background and set-up of the numerical models, while Chapter 8 is about calculation of the seismicity indicators. Chapter 9 describes the model outcomes and relates them to the potential for seismicity.

Chapter 10 will discuss the case studies and this thesis will conclude and discuss its findings in Chapter 11. The final Chapter will also include recommendations for further work. Appendixes can be found at the end of the report.

1.4 References

Larsson, K., 2004, *Mining induced Seismicity in Sweden*, Licentiate thesis, 2004:80, Luleå University of Technology, Luleå, Sweden

2. Introduction to Garpenberg

2.1 The mining history in the area

The Garpenberg mine lies on the edge of the Bergslagen district, shown in Figure 2.1. The Bergslagen has been an important mining area since the Middle Ages and still hosts a number of mines, including Garpenberg and Zinkgruvan.

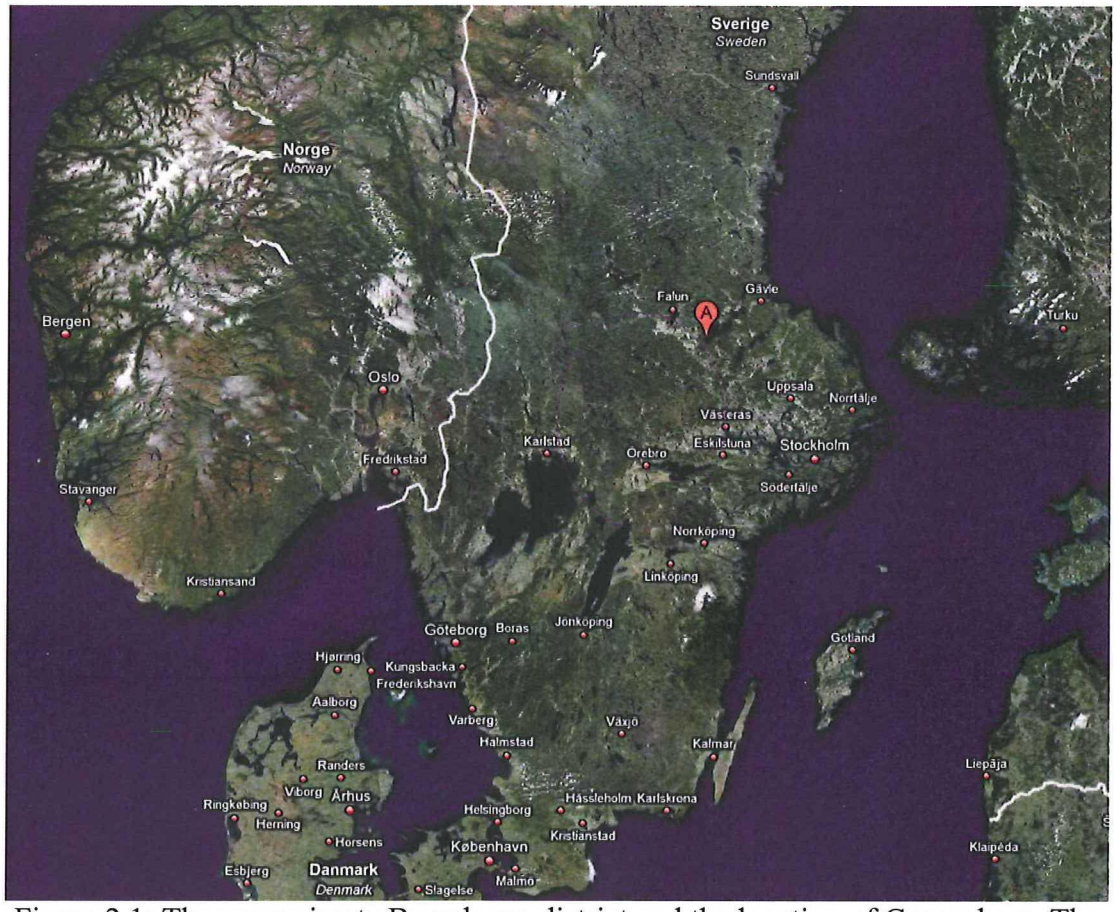

Figure 2.1: The approximate Bergslagen district and the location of Garpenberg. The red balloon indicates Garpenberg, whereas the blue ellipsoid indicates Bergslagen. (Google Maps, 2008)

The earliest mining in the Bergslagen district are estimated between 400 and 300 BC. In Riddarhyttan, approximately 70km southwest of Garpenberg, seven primitive iron smelters were found that were dated back to 380 BC. The iron that was produced originated from an iron-rich soil, which is abundant in the area. Tests in the 80's showed that 4.5 kg of forgeable iron could be obtained from as little as 11 kg of soil.

A major discovery was made in Lapphyttan, approximately 40km south of Garpenberg, where a complete medieval industrial complex was found. The complex dates back to the 12th century and had ore and coal storage facilities, smelters, blacksmiths, warehouses and accommodation facilities.

The earliest mining in Garpenberg was dated back to the Viking era by carbon dating. The famous writer, scientist and part-time geologist – nowadays his illustration is shown on the Swedish 100 Kroner bill – Carl Linnaeus wrote that it was not sure when mining started in Garpenberg, but that he thought that mining in Garpenberg went as far back as before Christ's birth. Medieval mining in Garpenberg was mainly for copper, although iron and silver were mined too. The ore probably reached the surface, because mining took place so early in time. The earliest written record that mentions the Garpenberg mining industry is a document from July 14th 1402. In this statement a certain Olof Finne gives his share of an inheritance in Finnhyttan to his brother.

In 1724 explosives were introduced in Garpenberg. Up to 1724 fires were built underground to heat up the rock and afterwards cold water was thrown over the rock. This made the rock a little more brittle which made it easier to hammer it from the wall. The earliest explosives were received with great skepticism. They were dangerous, expensive and could cause some stability problems. It wasn't until the 1860's when Alfred Nobel discovered some neat properties of nitroglycerin that dynamite was introduced on a large scale in mining.

Even with explosives the working conditions of the underground mines were far from favorable. Carl Linnaeus wrote about a visit to the mines in Falun: "in these underground holes 1200 people go down, like devilish black laborants, who are engulfed in soot and darkness and surrounded by smoke and fumes. There is no room for a clean breath and sweat pours out like water from a woolen bag…"

In the middle of the 17th century the Garpenberg mining operations produced approximately 60 tonnes annually of raw copper, which made Garpenberg the second largest copper producer in Sweden. The number one producer was Falun, where 2000 tonnes of copper were produced annually.

Halfway the 19th century the ore had become poorer and poorer. In 1848 all mining stopped and in 1878 the smelter was shut down. In the 19th century a lot of changes happened. The Swedish population, for example, grew from 3.5 million in 1850 to about 5.7 million in 1913 (excluding the 1.2 million Swedes who migrated to the USA). Production of food and other goods were mechanized and industries were no longer bound by streams of water to power their factories. Money started to play an important role and people were no longer exclusively paid in goods. Under influence of the rising Marxism unions were slowly starting to arise during the second half of the 19th century. (Andersson, 2007)

Mining started again in 1906. In 1923 AB Zinkgruvor became the new owner of the Garpenberg operations. The mining operations survived the depression of the '30s and the Second World War and between 1950 and 1953 a new shaft was sunk. Figure 2.2 shows a picture of the head frame under construction. In 1957 the company Boliden AB took over Garpenberg. The Garpenberg Norra area was taken into production in 1972. A connection drift started in 2000 and the two mines were finally joined together on the 24th of March 2004 (Söderman, 2006)

Figure 2.2: Construction of the new south shaft in the 50's. (Andersson, 2007)

2.2 Boliden and the Garpenberg Mine

Boliden is one of the leading European metal companies in exploration, mining, smelting and recycling, with the focus on zinc and copper. Boliden employs approximately 4500 people. The Boliden operations are shown in Figure 2.3. Tara and Garpenberg are the main underground mines, whereas the Aitik open pit mine produces the majority of the copper. The production statistics for 2007 are listed in Table 2.1. There are four smaller mines in the Boliden area. Renström and Kristineberg are both underground mines. Storliden closed down in June 2008. Maurliden is a small open pit mine under the responsibility of the Kristineberg operation. The production of this mine is subcontracted.

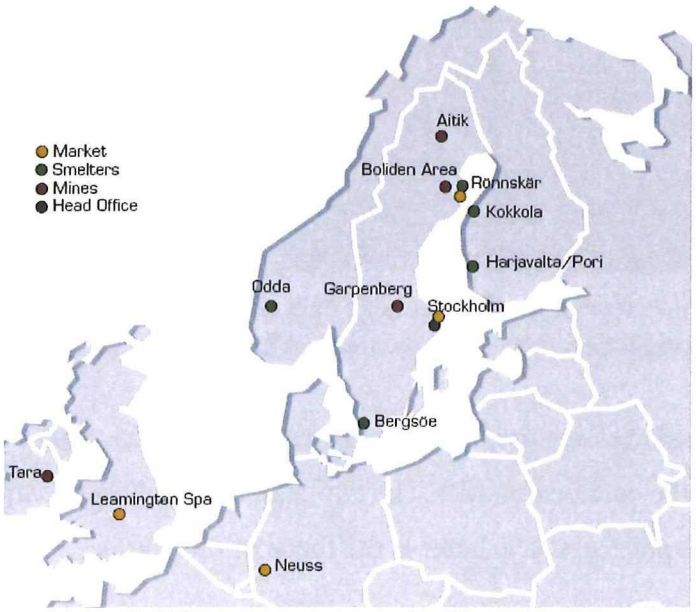

Figure 2.3: Boliden operations and offices (Boliden, 2008)

Table 2.1: Production of the Boliden operations in 2007 (After Boliden, 2008).

Mine	Production	Metal contents				
	Ore, 1000 tonnes	Cu, tonnes	Pb, tonnes	Zn, tonnes	Ag, kg	Au, kg
Aitik	18,200	50,487	-	-	42,301	1,178
Garpenberg	1,250	682	25,139	71,464	117,789	244
Tara	2,650	-	25,618	190,916	1,850	-
Boliden area		11,633	3,409	70,913	79,753	1,412
- Kristineberg	580					
- Renström	255					
- Maurliden	325					
- Storliden	278					

The modern Garpenberg mine is shown in Figure 2.4. Two shafts allow access to the mine in addition to a ramp at the Garpenberg Norra shaft. The two mines are connected by a connection drift, which is indicated on Figure 2.4 as well.

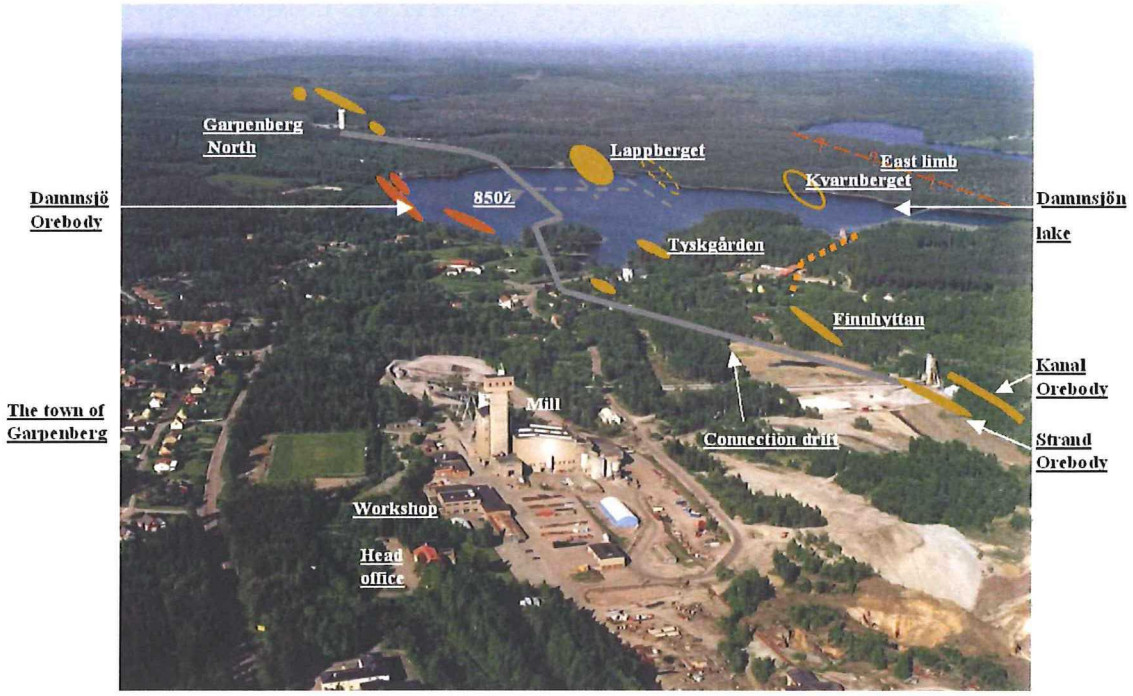

Figure 2.4: Aerial view of the Garpenberg operations. The main ore bodies and the connection drift are indicated. (After Söderman, 2006)

An artist's impression of the ore bodies is shown in Figure 2.5. It shows most of the ore bodies along the connection drift. The two major orebodies in Garpenberg are Dammsjön and Lappberget. The latter is the focus of this thesis.

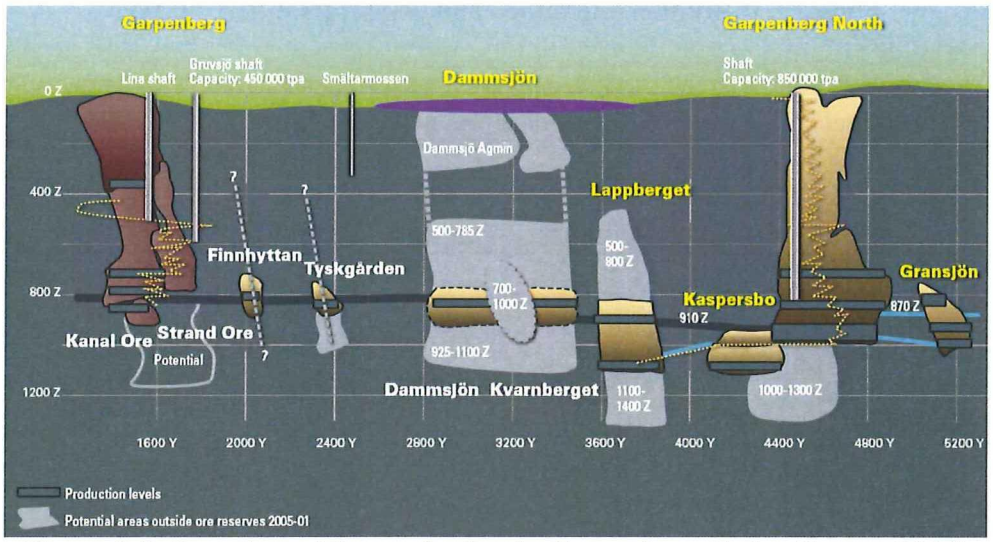

Figure 2.5: Location of the ore bodies in Garpenberg (Atlas Copco, 2006)

Fagerstöm, P., 2007, *Gruvnära prospektering i Garpenbergsområdet maj 2002 – mars 2007, Lappberget i fokus*, New Boliden internal report. Boliden, Sweden. (in Swedish)

Google Maps, 2008, http://maps.google.com/

Koivisto, S., *Personal communication*

Söderman, T., 2006, *Garpenberg area*, presentation on the New Boliden AB operations in Garpenberg.

2.3 Discovery of the Lappberget orebody

In 1997 a borehole was drilled from the ramp at 820 level in the southern direction. It hit a mineralised zone that later became the Kaspersbo ore body. The borehole was 100 meters long and it showed an anomaly in the borehole electromagnetic survey (BHEM) at the end of the hole. The borehole unexpectedly encountered a wide limestone section that caused the drill hole to get such a length. An exploration drift – the U-drift – was driven on 910 level to further investigate the future Kaspersbo orebody and the anomaly afterwards.

In 2001 the exploration drift had come to a stage where the anomaly could be drilled. Three boreholes with the same azimuth were drilled towards 800, 900 and 1000 m in the direction of the anomaly. Each of those holes hit the Lappberget orebody. The BEHM surveys could neither indicate the top or the bottom of the ore. Drilling continued in 2002 and eventually BEHM surveys indicated the top of the mineralization to be around 450 to 500 meter elevation. Drilling to further define the Lappberget orebody continues to present day both in the upper part and the deeper part of Lappberget as well as in the known areas to fine-tune the economic boundaries for stope and infrastructure design. (Fagerström, 2007)

Mining of Lappberget begun in March 2003 by cut and fill mining on the 870 level. In February 2007 longhole mining was introduced between 1060 and 1080 levels as the first transverse open stopes were excavated. The transverse open stoping will complement the cut and fill mining at first and replace the cut and fill mining completely around the end of 2010. (Koivisto, 2008)

2.4 References

Andersson, B.O., 2007, *Djupt i Garpeberget, gruvarbetarnas fackliga historia*, Garpenberg, Sweden. (In Swedish)

Atlas Copco, 2006, *Pioneering precision at Garpenberg*, Mining & Construction, p35-37 No 3 2006, Stockholm, Sweden

Boliden, 2008, *Fact sheet 2008 Mines and Concentrators*, Boliden intranet

3. Geology of Lappberget

This chapter starts off by briefly describing the regional geology in the Garpenberg area. Since the geology is rather complicated and the author is not a geologist it will be a very crude summary of work done earlier, primarily by Rodney Allen and colleagues in 2003. The rock types found in and around Lappberget are described later in this chapter. This will be in large part a translation from the work done by Pia Fagerström. The different zones that can be distinguished in Lappberget are described in the last part of this chapter and this is largely based on the work by Pia Fagerström, on the maps and interpretations by Franz Vyskytensky and by observations made by the author.

3.1 Regional (structural) geology at Garpenberg

The Garpenberg area is thought to be a volcanogetic hydrothermal ore deposit that has been formed by a stratabound replacement process below the sea floor in a caldera vent of a larger shallow marine rhyolite-dacite volcano. There is evidence to believe that the replacement process took place just before or just after the caldera forming eruption. The limestone reef formed prior to the volcanic eruption and provided an excellent physical and chemical trap for the hydrothermal solutions to focus the precipitation of base metals along the base of this limestone unit. Later tectonic deformations contributed to the formation and location of economically viable ore bodies.

The northern part of the Garpenberg mine is situated on the Northwest part of a regional syncline. The rock mass has been jointed, folded and faulted in a complex system. Figure 3.1 shows the geological map of the Garpenberg syncline. This complex system of geological features has a strong influence on the geometry, location and grades of the ore bodies. A cross section on 4540Y (Figure 3.3) shows the geology in detail as a lot of information could be obtained from diamond drilling, geochemical analysis of systematic sampling and underground mapping. The cross section on 4000 Y is shown in figure 3.4 and shows the Lappberget anticline, but at

the time of the analysis there was less information on this area as drill hole information was limited. (Allen et al, 2003)

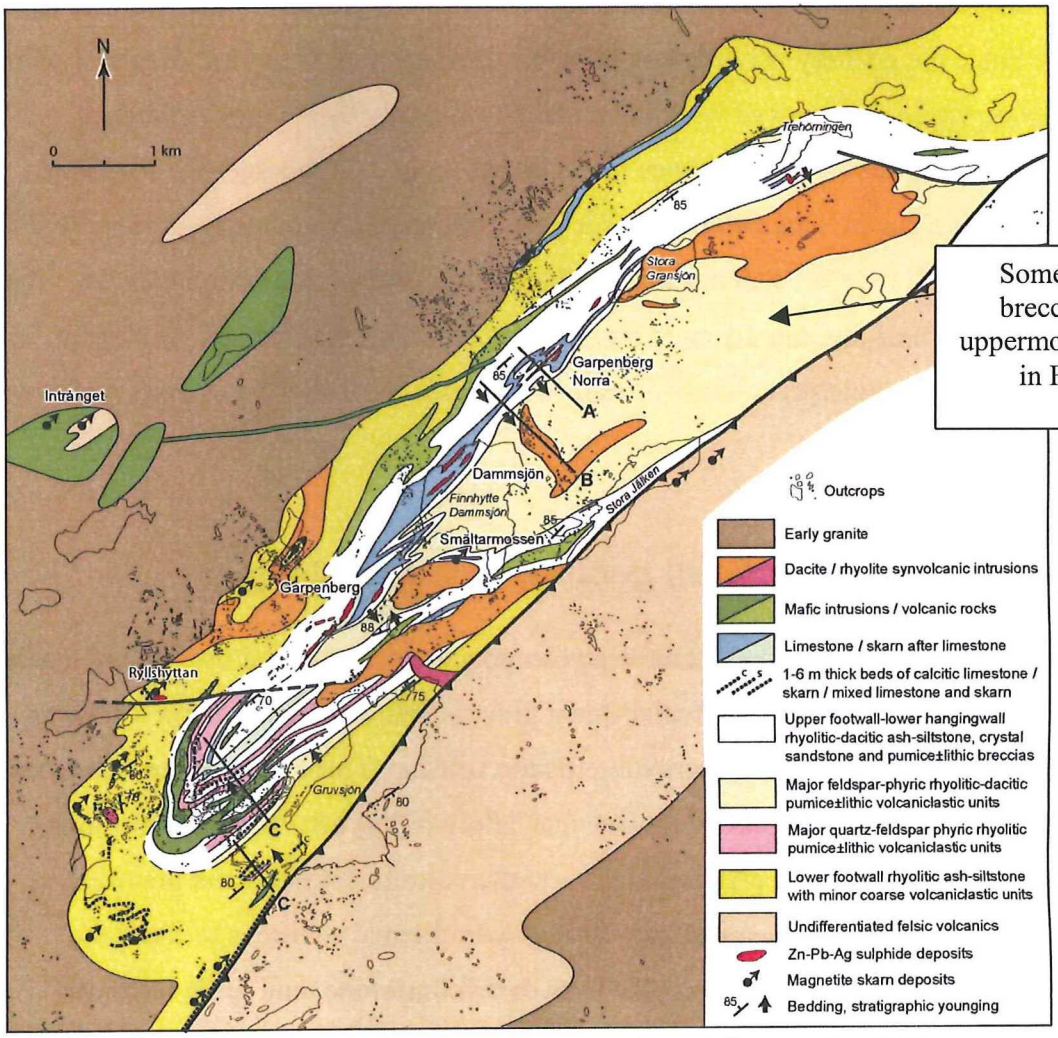

Figure 3.1: Geological map of the Garpenberg syncline (Allen et al., 2003)

Three major deformations are found in the structure at Garpenberg Norra:

(1) A first generation of folding on a large scale that is masked by later deformations.

(2) A second generation of tight folding and associated shear zones.

(3) A third generation of shear zones and faults with associated minor folding

The most prominent folds in the limestone are thought to be due to a complex pattern of the second-generation parasitic folds and at least in part products of interference between the first generation and second-generation folds. The parasitic folds occur as

steeply dipping cone- or arch-shaped anticlines and funnel- or through-shaped synclines. The steeply dipping structures give rise to the idea that the associated shear zones are of a dip-slip type. The third generation of shear zones and faults mainly focus along the anticlinal centres and on the northwest part of each fold. These faults and shear zones are of a dip-slip type as well. Figure 3.2 shows two probable relationships between the first two generations mentioned above. (Allen et al, 2003)

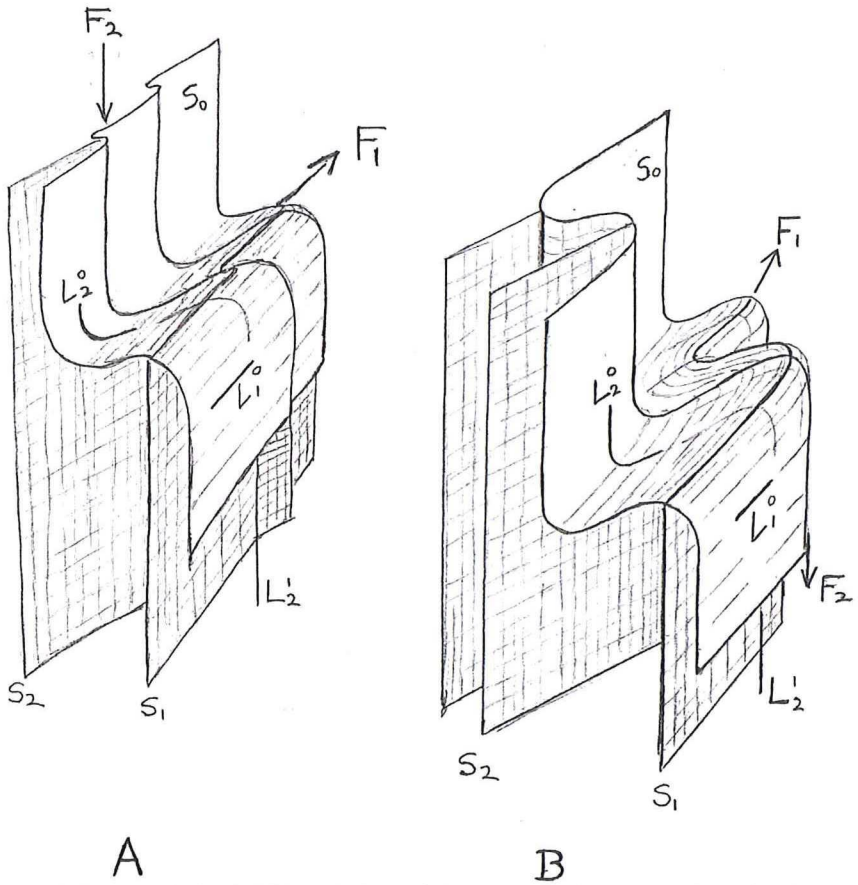

Figure 3.2: Possible folding (F1 and F2) and foliation (S1 and S2) mechanisms at Garpenberg Norra. A: possible case of a horizontal folding (F1) followed by a weak vertical folding (F2). B: more realistic case where both F1 and F2 folding are strongly developed. In reality all structures are steeply oriented due to stretching subparallel to L2' during F2 folding. (Allen et al., 2003)

While the exact structures in the cross section at 4540Y (Figure 3.3) do not reach the cross section at 4000Y (Figure 3.4), the sort of structures is believed to be very similar. The cross section at 4540Y will be described into more detail, as only a general interpretation is available at the 4000Y cross section which includes Lappberget.

In Figure 3.3 small second generation folds are shown with a plunge and plunge direction that is consistent with larger parasitic second-generation folds. The parasitic folds are highly irregular and have slightly different orientations in the limestone and felsic rock masses due to different competences. The folds in the felsic rock masses are generally more regular whereas the folds in the limestone are more irregular due to plastic flow during the folding process.

When comparing Figure 3.3 with a plan view of the geology at 250 m depth (Figure 3.5) the structures should become clearer. The limestone at 1000X and 300 m depth and upwards can be seen as a second generation syncline that plunges between 40 and 70 degrees SSW and has been folded in a complex pattern. Third generation shear deformations have sliced the syncline up around the hinge region into panels, or so it seems from the footwall-limestone contacts. Two ore zones in Garpenberg Norra are associated in this area with the third generation shears.

The limestone around 850X and 250m depth is folded in an anticline/syncline system by pair of folds. This pair of folds seems to plunge 60 degrees SW at the southern end, but flattens towards the north and flips over to 70 degrees NE around 4630Y. South of 4500Y the fold pair fades away into the regional syncline structures. Third generation shear zones that happen to host the B lens ore bodies cut the western limb of the syncline. The anticline has the crude shape of a cone that can be attributed to a strong stretching strain during the second generation folding. This structure can be summarized as a second generation parasitic fold pair that has been altered by third generation shear zones parallel to the steep western limb of the fold pair.

The structure in the limestone unit on cross section 4540Y around 600 meters depth varies between a monocline and anticline/syncline. The fold pair has a relatively flat plunge for at least 100 meters on either side of the cross section. What happens to the structure beyond these points is not entirely clear. As with the structure described before, third-generation shear zones deformed this structure and it hosts another ore zone.

Below 600 meters a new parasitic anticline-syncline pair of folds deformed the limestone. The syncline has a narrow tight shape and the hinge region seems to be cut

off by a fault which runs SE of the deep F ore zone. Reason to believe there is a fault is the presence of opposite facing stratigraphies on either side of the F ore zone, although they cannot be matched in detail. The anticline is a large complex that extends the drilling towards the SE and seems to be plunging steeply towards the NE.

In conclusion it can be noted that the steeply dipping rock mass at Garpenberg Norra is characterised by a large extent by second-generation parasitic folds. These folds are locally flat lying to plunging to either direction. On cross section the limestone appears to be situated in plateaus or benches. The structures should be seen more as a system as interchanging and interpenetrating cone- and arch-shaped structures, where arches or cones start off at the flank of adjacent structures. The area between 4540Y and 4600Y on Figure 3.5 appears to feature doubly plunging anticlines side by side and this can be interpreted as a first generation NW-SE trending anticline that is later deformed by second-generation parasitic folds. (Allen et al, 2003)

The exact folding mechanism of the Lappberget anticline is not entirely sure, but there are two general theories behind it. The first one is that two generations of folding perpendicular to each other formed a dome-based structure. The second one is called sheath folding and this is basically a folding process and stretching process in one, where the flanks of the dome are stretched and the centre is not which creates a concentration of ore in the centre of the dome. A schematic sketch of a similar large-scale structure is shown in Figure 3.6. The extreme height of the Lappberget anticline (as it is more than a kilometre) is, as of yet, unique to the Garpenberg syncline. Relatively high contents of copper and gold in joint infillings and a higher concentration of remobilised ore veins on the southern end of Lappberget suggest tectonic shear zones in that area, similar to shear zones found towards the north. (Allen et al, 2003, Allen, 2008)

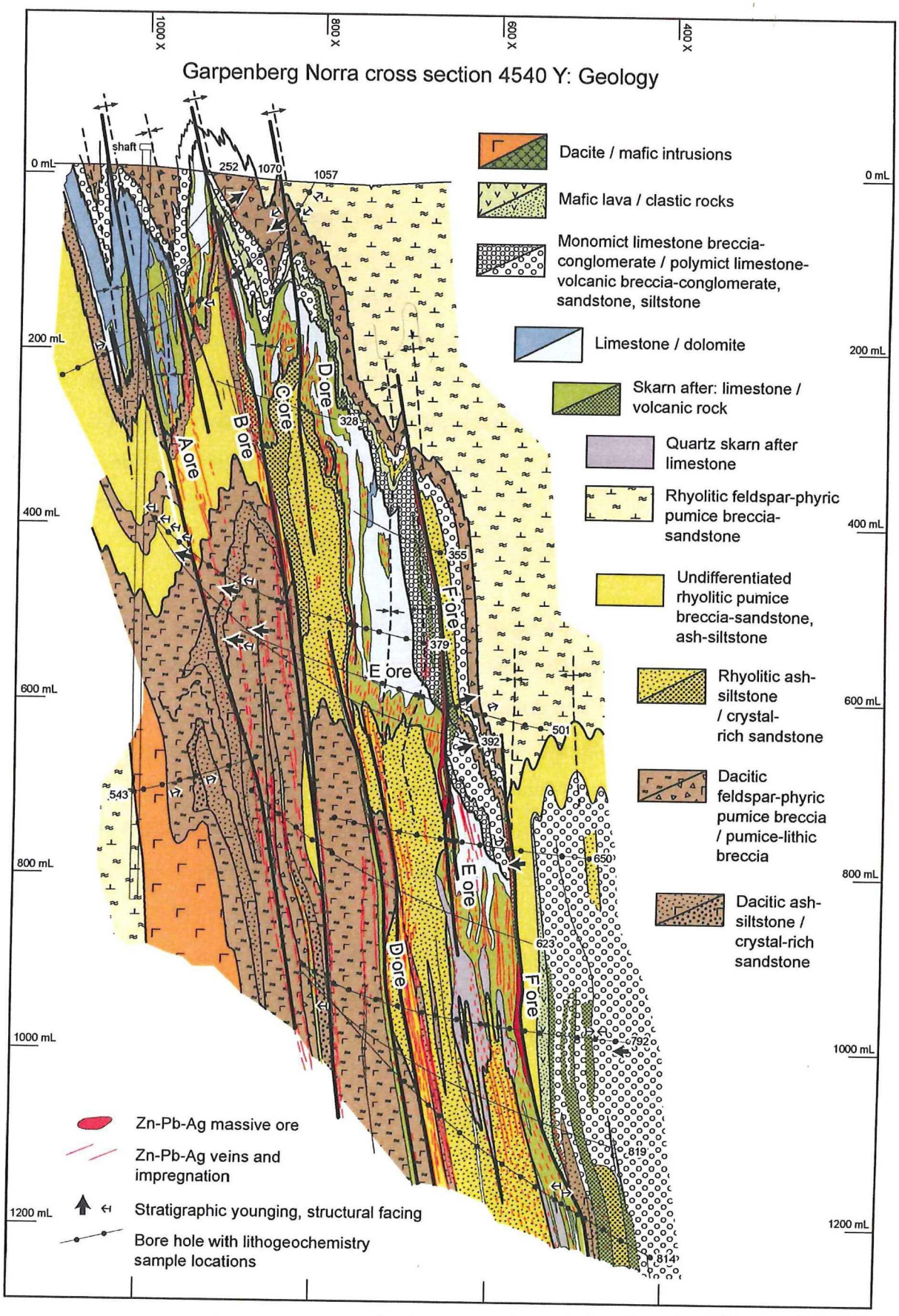

Figure 3.3: Cross section at 4540 Y. It is shown on Figure 3.1 as line A. (Allen et al, 2003)

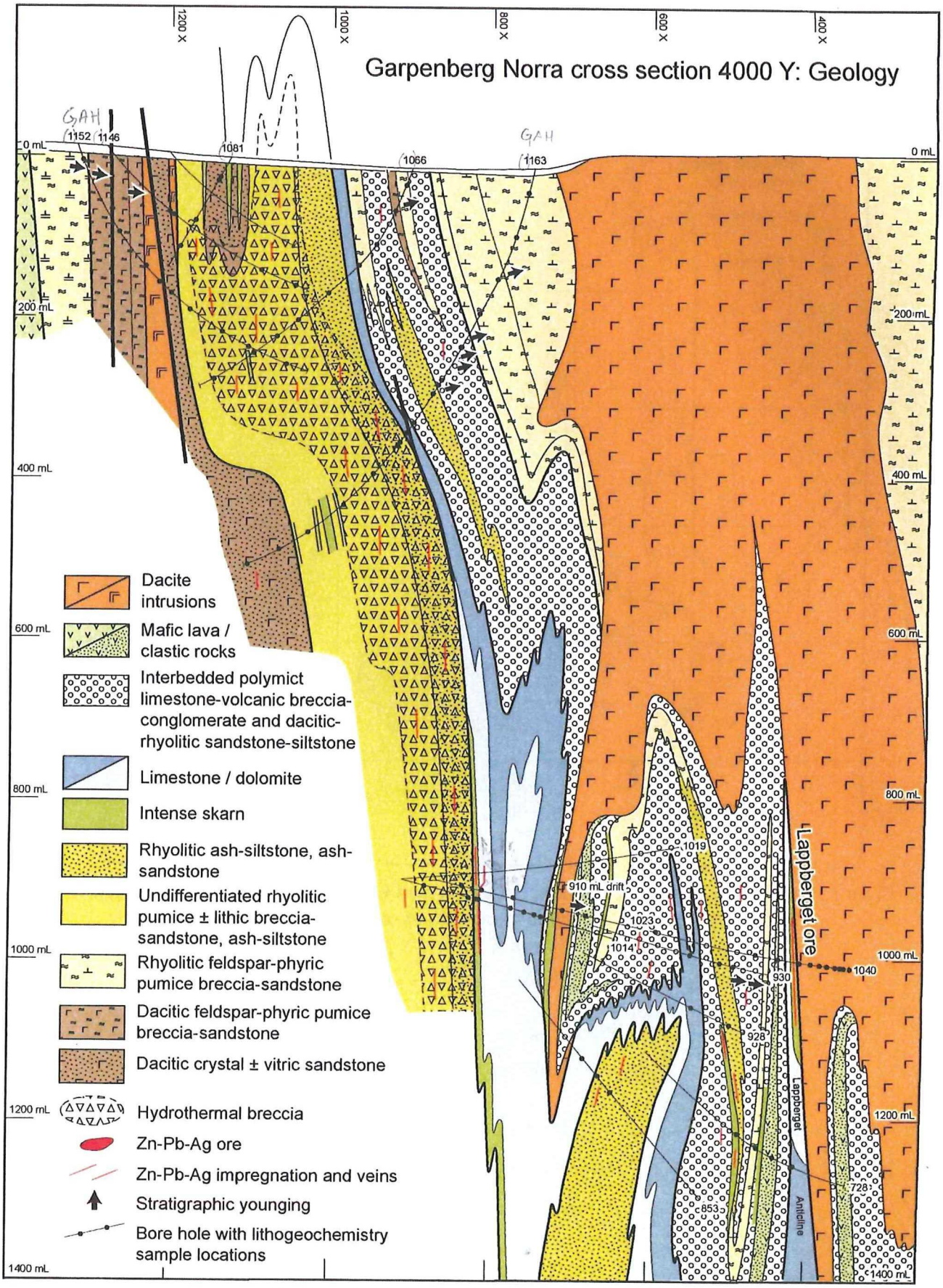

Figure 3.4: Cross section at 4000Y. This is shown on Figure 3.1 as line B. (Allen et al., 2003)

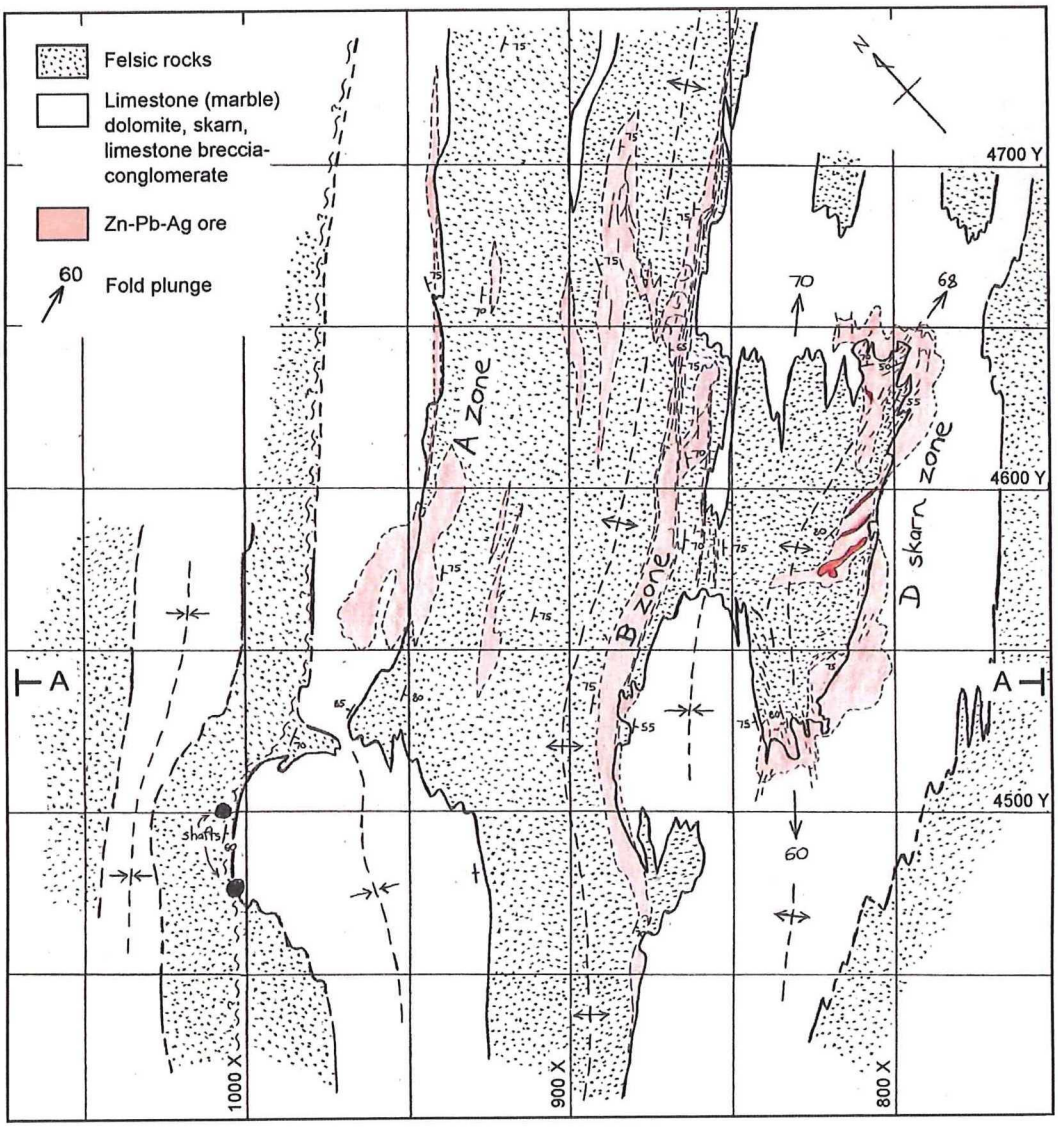

Figure 3.5: Geological plan view of the 250m level in Garpenberg Norra. The location of the 4540Y cross section is marked by A-A. (Allen et al., 2003)

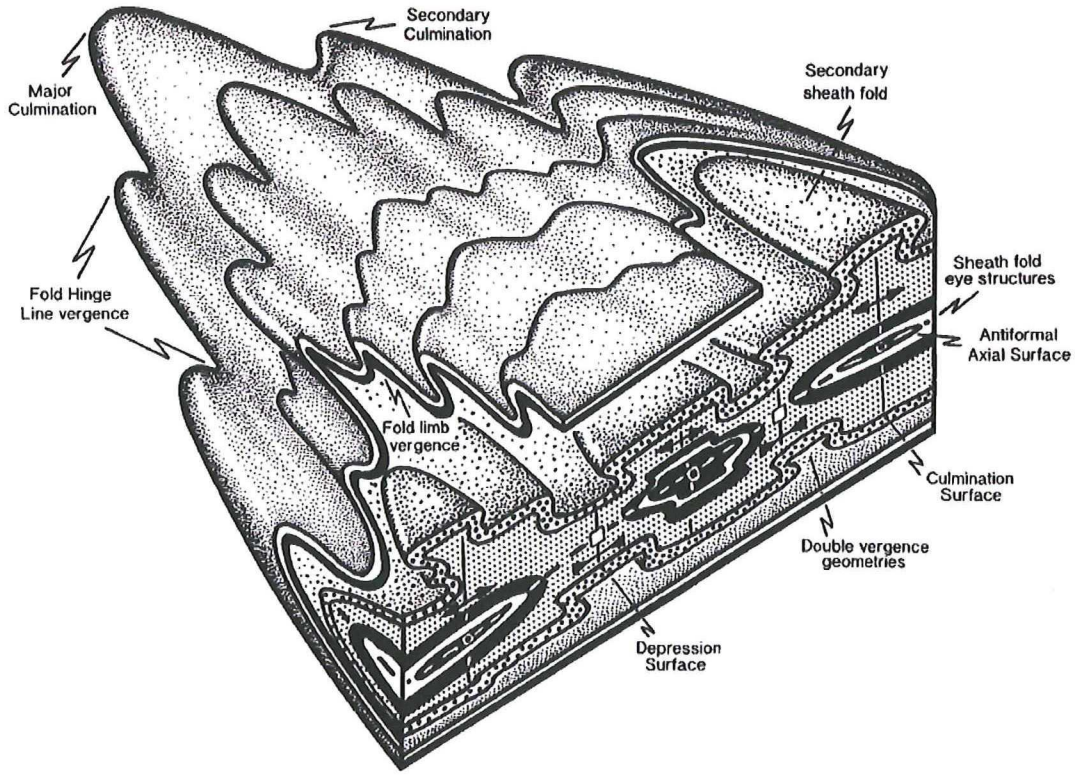

Figure 3.6: Schematic three-dimensional sketch illustrating the geometry of a major antiform with sheath folding that appears to have similarities to the Lappberget ore body. (Alsop and Holdsworth, 1999)

3.2 Stratigraphy and rock types at Lappberget

The general stratigraphy is shown in Figure 3.7. The general sequence in Lappberget from the top is:

- Young volcanogetic rocks and volcanic/clastic sediments
- Limestone, which is in contact with the ore.
- Ore, mainly sulphides, skarn and impregnated quartzite
- Old volcanogetic rock types, often fine-grained.

The above is a very general sequence as there are a lot of unclear intrusive rock types and sill type structures in the area. A more detailed description is given in this chapter following this general stratigraphy. (Fagerström, 2007)

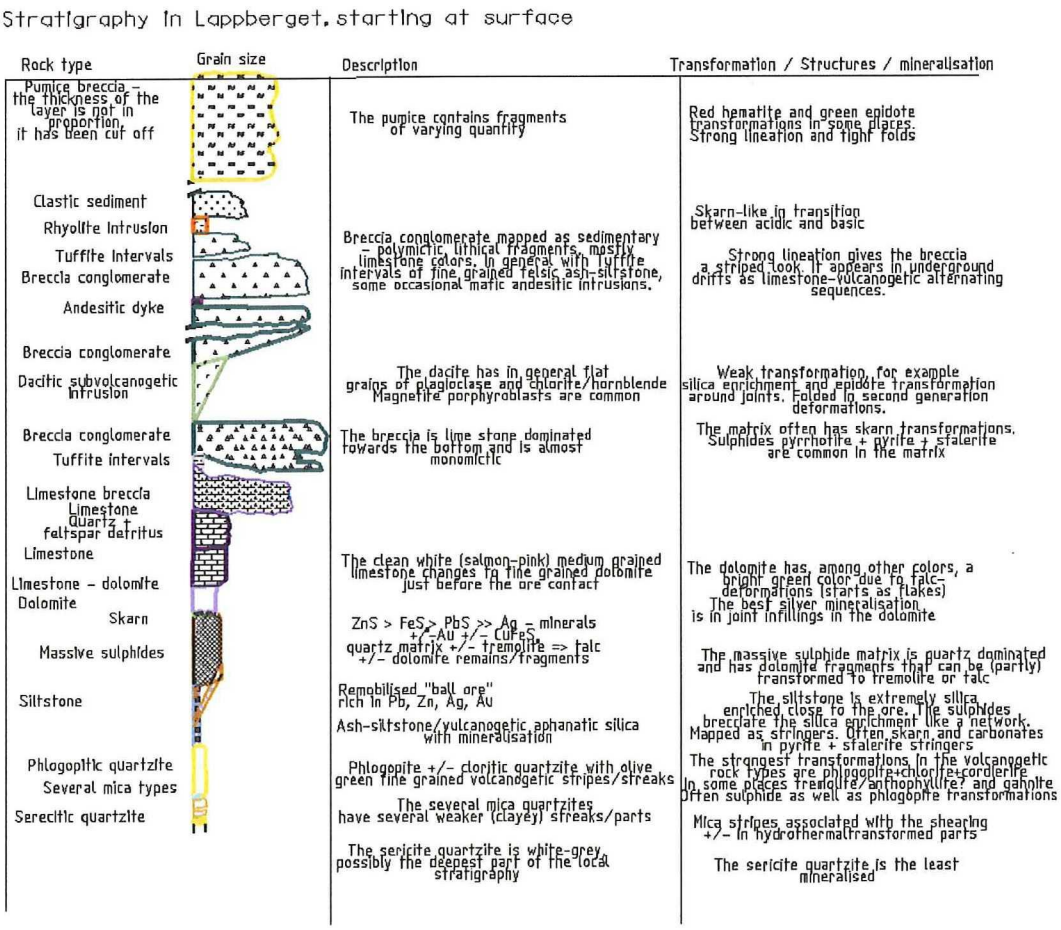

Figure 3.7: Stratigraphy in Lappberget. The stratigraphy is not to scale and grain size is relative. The stratigraphy is open at the bottom end, but future core drilling in the bottom part of Lappberget might provide more information. (After Fagerström, 2007)

Figure 3.8: Pumice breccia, the grey version on the left and red on the right. (Fagerström, 2007)

The first rock type is the **pumice breccia** as shown in Figure 3.8. Note that the pumice component is somewhat misleading here; it has been metamorphosed and does not resemble the rock that is used for washing clothes, nor does it float when cast into water. The pumice breccia is rhyolitic in chemical composition and is therefore very hard. The rock is brown-greyish but various transformations are known. Examples are the impregnation with hematite that gives the rock a red colour and the impregnation with epidote that gives the rock a green colour around contacts with joints. The formation is vast in size and is a result of a Caldera formation. The formation consists of multiple individual layers with distinct clast sizes (autochthony fragments within the cemented matrix). (Fagerström, 2007). The pumice breccia fills up the bulk of the caldera/syncline. The centre of the syncline is shown in Figure 3.1 (Granbacka, 2008)

Figure 3.9: Breccia-conglomerate (Fagerström, 2007)

The **breccia-conglomerate** (Figure 3.9) has varying thickness up to several tens of meters. The fragment sizes vary from a few centimetres up to several decimetres. The main part of the rock type is limestone and it often occurs in large fragments. The rhyolite parts of the rock type are usually smaller and often rounded off at the edges, which could indicate erosion due to transportation. The rock has been partly transformed into Skarn. The matrix of the breccia-conglomerate consists of fine to medium grained grey-green chlorite/mica/skarn. The matrix can be irregularly silica cemented and the entire material is poorly sorted.

Within the breccia-conglomerate distinct layers of fine-grained **grey siltstone layers** consisting of quartz, feldspars and biotite are commonly found without any apparent mechanism. The thickness of these layers varies from 5 centimetres up to 2 meters. Less common are the coarse sand and gravel layers. These layers can be well graded

and more transformed than the siltstone layers. The fine-grained dark layers that typically carry amphibolites are less common. These layers could be intrusive as the layers contacts are sharp

Sulphides are commonly present in the matrix of the breccia-conglomerate, especially in the bottom part of the formation that indicates the proximity of the ore mineralization. The sulphides appear irregularly as an impregnation of iron sulphides (pyrite, pyrrhotite) and zinc sulphides (sphalerite). Some massive sulphides have been found in drill cores (often high grades of sphalerite), but it is unclear where or when those sulphides originate.

Most **heterogeneous clastic sediments** occur in the syncline south of the Lappberget anticline, stratigraphically under the pumice formation. The transition between the clastic sediment and the pumice is often unclear. Clastic sediments occur as layers in the breccia-conglomerate as well.

The typical clastic sediment in the southern syncline is a dark green-grey rock type with a fine-grained matrix with sparsely occurring fragments as shown in Figure 3.10. The fragments are only a few centimetres large and are usually not rounded off. There has often been a transformation into skarn. (Fagerström, 2007)

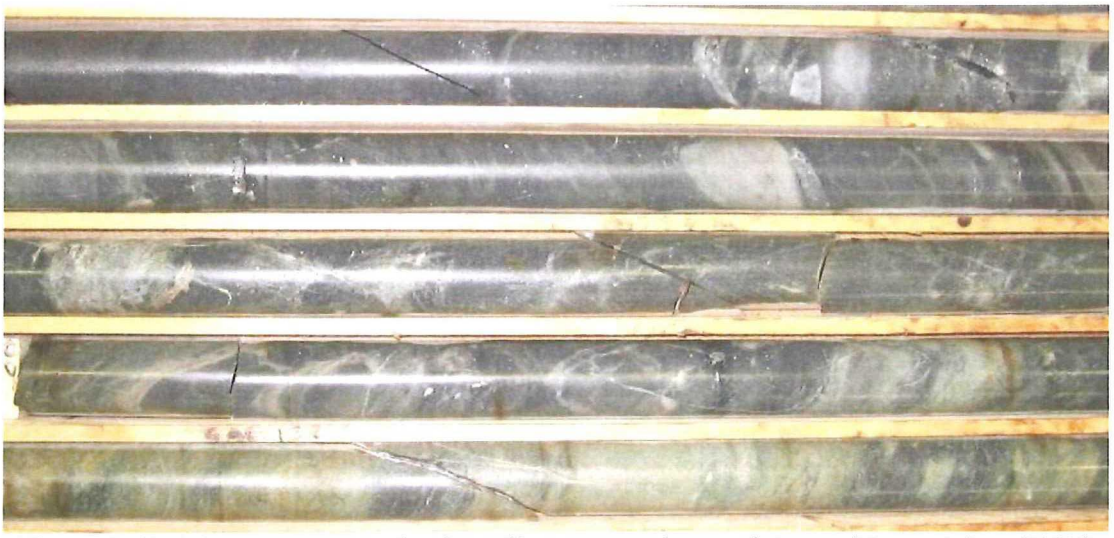

Figure 3.10: Heterogeneous clastic sediment carrying rock type. (Fagerström, 2007)

Dacite is a half understood sub-volcanic rock type that has intruded trough the hanging wall up to the end of the fault structure. The dacite looks homogeneous and grey with fine flat grains, but often porphyritic with plagioclase crystals up to 1mm and mafic crystals up to 2 mm. The dark mafic minerals are primarily assumed to be amphibole, though a large part has been transformed into chlorite. Pyrrhotite porphyroblasts, and to a lesser extend magnetite minerals, occur regularly, which explains the excellent response of the dacite intrusion to magnetic geophysics. (Fagerström, 2007)

Figure 3.11: Limestone breccia (Fagerström, 2007)

Figure 3.11 shows drill core fragments of **limestone breccia**, which is the transition between the breccia-conglomerate and the limestone. The breccia has fragments from a single source and is often brecciated in-situ. The matrix is a fine-grained silt material, sometimes with irregular quartz concentrations or clasts. (Fagerström, 2007)

Figure 3.12: Limestone with quartz clasts (indicated by arrows). (Fagerström, 2007)

Limestone is a medium grained, white, clean, metamorphically recrystallized rock type that really should be called marble. In some places it shows orange to salmon-red colours. The limestone can have small layers of siltstone material and in some places quartz minerals mixed with calcite can be found. The limestone is shown in Figure 3.12.

The limestone altered to dolomite closer to the ore due to a magnesium alteration. The dolomite has finer grains than the limestone but is white as well. The colour alteration to light green is associated with the talc transformation which is very common close to the ore. Some of the dolomitic limestone can be included as part of the ore as dark joint infillings are rich in silver.

The **massive sulphides** are described in detail for the different zones in chapters 3.3, 3.4 and 3.5. Stratigraphically speaking they are buried below the limestone/dolomite and partly under the volcanogetic rock masses. The metal bearing fluids have partly repressed the limestone in places where the limestone is missing completely and where the ore is directly in contact with the limestone breccia. (Fagerström, 2007)

Figure 3.13: Siltstone with a silica transformation and some sulfides (Fagerström, 2007)

There is some silica addition directly under the vast compact ore of the A zone which is mapped as aphanitic (individual grains are indistinguishable) **siltstone**. An example of the siltstone is shown in Figure 3.13.

The underlying volcanic rocks are named based on the transformation process. Examples are **phlogopitic quartzite** (Figure 3.14, "Flogopitkvartsit" in Swedish), **chloritic quartzite** ("kloritkvartsit"), **cordieritic quartzite** ("kordieritkvartsit"), **sericitic quartzite** ("sericitkvartsit") and **combinations of the aforementioned** if the rocks consist of quartzite and addition such as mica. If there are several mica minerals in the rock sample of which none is dominating the rock is simply named **mica quartzite** ("glimmerkvartsit"). Note that the quartzite name is used here, but that it has nothing to do whatsoever with the sedimentary clastic (real) quartzites. (Fagerström, 2007)

Figure 3.14: Phlogopitic quartzite (Fagerström, 2007)

3.2.1 Zones

At the earliest stage in mining Lappberget the ore was divided in to three distinct zones; the A, B and C zone. The A and B zone are very similar but are separated by a rock mass without sufficient mineralization. This intermediate rock mass includes a few planes of weakness with mica minerals and talc. The C zone is adjacent to the A zone but is geologically different from the A and B zone as will be described in

Chapters 3.3, 3.4 and 3.5. A plan view is shown in Figure 3.15. In this figure the approximate locations of the A, B and C zones are indicated.

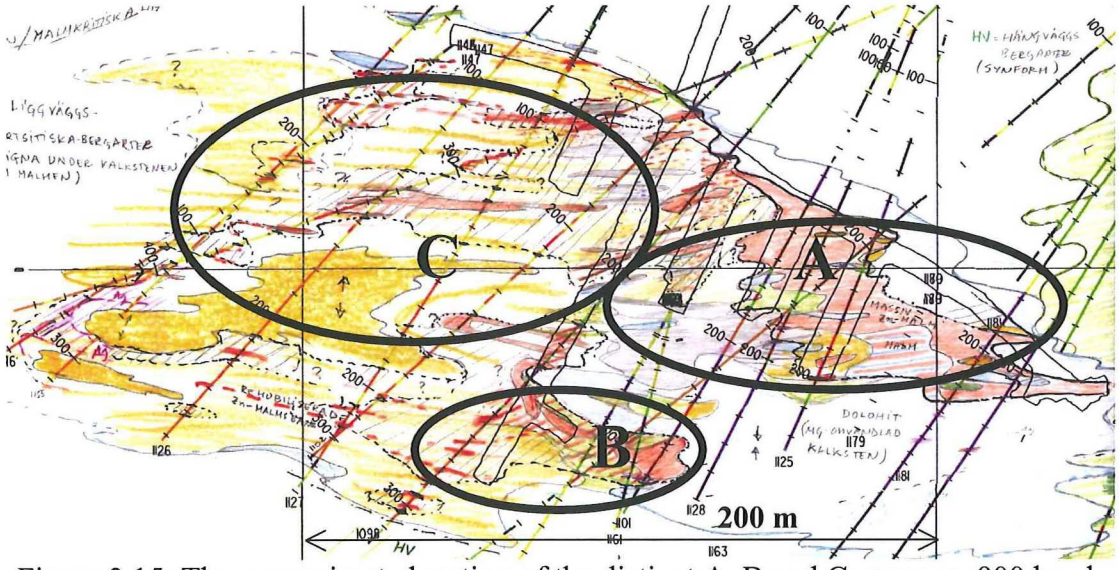

Figure 3.15: The approximate location of the distinct A, B and C zones on 900 level. Red is compact sulphide ore, blue is limestone and yellow is quartzite or tuff. (after Nyström, 2005)

3.2.2 Significant Geological features

On the hanging wall ore contact at both the A and C zone there are some deformation zones that contain talc as well as mica minerals such as biotite and chlorite. These zones are typically 1 to 5 meters wide and impose significant issues with the hanging wall stability. The origin of these zones is connected to the contact between the limestone and volcanic rocks where the hydrothermal fluids penetrated.

3.3 The massive sulphides; A and B zones

Lappberget has three ore zones; A, B and C. Zone A and B are massive sulphide ores and are very similar in mineralogy, stratigraphy and in grades. The C zone is in another stratigraphic region and has lower grades. Only parts in the C zone are massive, so this zone is described in the next chapter.

Geological maps can be found in Appendix A. These maps and interpretations were made by Franz Vyskytensky and are excellent tools in three-dimensional visualisation of the geology, especially for the bottom part of Lappberget.

The massive A zone is richest and most persistent in both height and width of the three ore zones. The A zone is confirmed between 650 and 1300 elevation, but core drilling is on going to further define the ore body outline. The A zone is 150 meters long and 20 to 40 meters wide on 900 elevation for example. The mineralization took place in the limestone/dolomite and in the contact underneath the limestone. During the ore formation process the metal bearing fluids reacted with the limestone buffer and the metals precipitated out of the solution. The limestone or calcite ($CaCO_3$) reacted with magnesium and transformed into dolomite ($CaMg(CO_3)_2$) and skarn minerals, as did the silica-based minerals with magnesium. When the ore forming solutions reacted with dolomite they also formed diopside and tremolite(skarn), which can also be seen in the matrix. Together the silica based minerals, the skarn minerals and the dolomite formed the matrix for the massive sulphides or the intermediate masses in between the massive sulphides.

The massive B zone is similar to the A zone in texture, mineralogy and stratigraphic position (the same limestone/dolomite base). The B zone is a separated area (as indicated on Figure 3.15), probably caused by folding or shearing mechanisms in the limestone. The A and B zone were probably connected prior to a separating deformation process took place. Based on information available at present the B zone decreases in size towards the surface. It is approximately 50 to 80 meters long and 10 to 15 meters wide. The B zone runs, according to the present knowledge, between 1000 and 450 elevations. The metal contents are somewhat lower than in the A zone due to large lumps of dolomite and quartz minerals in between the sulphides. It does contain more pyrite than the A zone.

The massive sulphide ore in Lappberget contains sphalerite, pyrite, galena, silver containing minerals and to lesser extent magnetite, chalcopyrite, pyrrhotite and gold minerals. The host rock contains pyrite, sphalerite (in the hanging wall breccia), pyrrhotite and magnetite. The magnetite often occurs in the dacite intrusions as individual grains and as massive bands (1-20cm) in the dolomite in the northern

contact of the A ore. Arsenopyrite occurs as well, albeit rarely, and most occurrences are in mafic rocks.

The massive A ore consists mostly of sphalerite (ZnS) and pyrite (Fe_2S) together with in general galena and sometimes some silver minerals such as acanthite. The silver minerals have not been identified in the drill cores on a macroscopic scale. The ore often has dolomite inclusions, 5-10 cm lumps with varying amounts of silica: lots of quartz, skarn minerals (tremolite, diopside), mica (phlogopite, sericite, chlorite) as well as talc. These minerals are in reducing occurrences as written in this order. A typical A zone ore is shown in Figure 3.16. Talc and skarn are the most common minerals in the matrix if the metal bearing fluids represses the dolomite. Where quartz dominates as the matrix mineral it could be due to the dolomite having a larger content of silica minerals (volcanic-sedimentary material) and the proximity to the transition zone with the underlying volcanic rock. (Fagerström, 2007) The quartz can also be due to intense silicification of the dolomite. There are zones where the dolomite/limestone has been completely replaced by quartz due to that process, e.g. in the hinge zone between 600 and 500 elevation. (Granbacka, 2008)

Figure 3.16: Rich A zone ore with a quartz based matrix. (Fagerström, 2007)

The B zone is very similar to the A zone as mentioned before. The ore minerals are the same as in the A zone, but the matrix often consists of skarn, talc and mica minerals. Higher contents of gold (and copper) are closely situated to the B ore zone. The gold content is probably more dependant on tectonic movements than the presence of the B ore zone (see the chapter about metamorphosis and deformation).

High silver contents up to the cut of grade can be found in the dolomite north (north in the local mine coordinate system) of the A zone and in between the A and B zones. The silver mineralization or ore occurs as a network of veins in the heavily jointed dolomite. The joints are thin (often less than 1 mm), roughly perpendicular to the foliation and appear to be formed in a late stage of the ore formation process. Very high silver contents are associated with the silica addition/replacement process in the upper part of Lappberget. The silver can come in all sorts of minerals, of which most are silver-antimony and/or lead combinations as well as silver rich chalcopyrite and silver inclusions in the galena minerals. (Fagerström, 2007)

Figure 3.17: Joint infillings with high silver grade in the dolomite (Fagerström, 2007)

The silver minerals are in the joint infillings in a network of joints. This joint network can get so dense that silver contents up to 2 to 3 kg/t can be reached (Figure 3.17). (Diopside/tremolite-) skarn-transformations can produce these high grades of silver too. This occurs in proximity to the massive ore and dolomite, the Kaspersbo ore is an example of such a silver rich orebody that is hosted mainly by skarn. Joints in quartz intrusions can host silver as well, as is illustrated in Figure 3.18. (Fagerström, 2007)

Figure 3.18: Silver (possibly native in this picture) in joints in a quartz intrusion. (Fagerström, 2007)

In the dolomite east of the A ore near the contact with the massive sulphides decimetre wide streaks or bands of massive magnetite can be found. Magnetite mainly occurs in the upper part of Lappberget at 1000m level and upwards. The magnetite is thought to be related to manganese skarn as they often occur simultaneously.

Higher contents of Au and Cu are found in the southern ore contact of the B zone as well as east of the B zone (Fagerström, 2007). This also occurs below the B zone, below 1000z (Granbacka, 2008). Au contents are low though, on average 1-2 g/t (on average in Lappberget it is 0.2 g/t). The copper content is not economical (<1%) but is thought to be associated with the gold content. The gold content starts to increase below 1000 meters and continues in the deeper parts of Lappberget. It will be interesting to see how the gold content increases with depth exactly, as drill cores confirmed this observation. (Fagerström, 2007)

There is a coarse metal zoning in the massive sulphide ore in Lappberget. It is rich in silver in the top part, dominated by zinc in the middle and possibly higher grades of copper and gold in the deeper part. Otherwise the zinc-lead-silver ore is generally found in the entire Lappberget orebody as this is the main type of ore. (Fagerström, 2007)

3.4 C zone

The C zone is the most difficult to describe of the three zones. The mineralization is heterogeneous and irregular in concentrations and grades. The C zone is situated stratigraphically in the underlying volcanic rock below the limestone and massive sulphides of the A and B zones. The footwall rock types have different degrees of silica alteration. The strongest transformation took place in the siltstone below the A zone. The border between the A and C zone is at the contact between the massive sulphides and the volcanic rock as a result.

It appears that the metal bearing fluids have penetrated and/or brecciated the silica altered rocks, in which the silica alteration should have happened in an early stage of the ore formation process. The appearance has similarities with stringer

mineralization, which complies very well with the classic model of stringer zones below the massive replacement ores of zones A and B.

The C zone contains sulphides, most commonly sphalerite and pyrite, which occur in branching bands or streaks and branching spots, as well as remobilised mineralization. The remobilised ore will be described in chapter 3.6.

The transition between the A and C zone can be very clear if the underlying volcanic rock is strongly altered by addition of silica and if the sulphides only occur as brecciated edges (see Figure 3.19). (Fagerström, 2007)

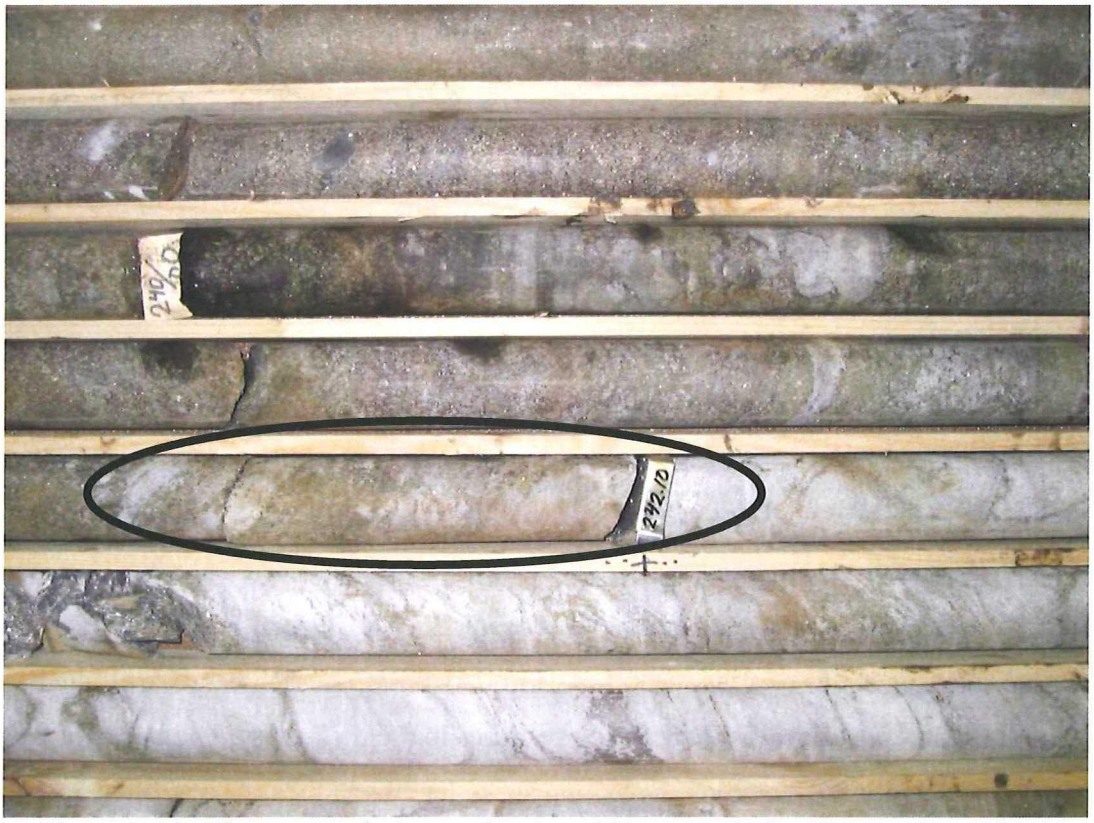

Figure 3.19: The contact between the A and C zones. (After Fagerström, 2007)

The ore minerals are most often fine to medium grained, 0,5-3 mm. The pyrite builds 0,5-5mm crystals in an early stage in the sphalerite. Sphalerite has the bad tendency to build crystals so the mineral size varies greatly. The sphalerite has several colour variations; from orange to brick red to dark brown. This reflects the ratio between quantities of iron and zinc in the mineral. The darker brown the mineral is the more iron is present.

Galena occurs both as a medium grain size (1-5mm) crystal aggregate and as a fine-grained (<0.5mm) joint infilling. The silver mineralization most often occurs as a dendritic joint infilling together with the galena infilling in the dolomite inclusions and in the contact skarn in the outer part of the ore. Typical C zone ore is shown in Figure 3.20. (Fagerström, 2007)

Figure 3.20: Typical C zone ore with remobilised ore and bands or streaks of massive sulphides. (Fagerström, 2007)

3.5 Remobilised ore

Aside from the stringer mineralization (see chapter 3.4) the C zone in general has massive sulphide bands of a few centimetres in thickness. The rich bands are called remobilised and they follow the tectonic structures in the rock mass. The bands have sharp contacts with the host rock, have long strike lengths in the area and often have the same orientation as the large regional faults or the large folding planes. Despite their limited length three or four of those bands will provide enough metal contents for a full drift. This remobilised mineralization has formed after the main ore was formed, because it was found in drill cores through the massive ore. The remobilised ore is as a result independent of the stratigraphy and can run from the C zone into the A zone. The remobilised ore has high contents of zinc, lead silver and gold. Especially silver and lead are relatively high in comparison to zinc. The result is that lots of remobilised ore has a grey tone of colour (Figure 3.21). (Fagerström, 2007)

Figure 3.21: The grey remobilised band of ore with galena, sphalerite and some pyrite. (Fagerström, 2007)

The remobilised ore has a special texture: the ore minerals are often fine grained although the pyrite minerals can be somewhat larger. The usual matrix is lacking and instead coarse round quartz minerals (90%) and some chlorite or mica minerals (10%) can be found. These silica minerals have been rounded and recrystallized due to the faulting process that took place during the tectonic movements that moved the ore and produced the remobilised ore (Figure 3.22). (Fagerström, 2007)


Figure 3.22: Remobilised ore with large round pieces of quartz. (Fagerström, 2007)

3.6 remaining issues

There is still a debate if the domes and basins, such as Lappberget, are formed by two different folding mechanisms or if it is due to one (sheath-)folding event as pictured in Figure 3.6. (Granbacka, 2008)

The exact mechanism of the structural geology is not entirely sure. As of now the geology can be mapped and the ore can be mined, but the deeper understanding of the structures is lacking. With a better understanding of the Lappberget structure a more educated guess can be made in future exploration targets.

The C zone in the deeper part of Lappberget is not entirely understood as well. The remobilisation ore follows certain trends but if this will continue to deeper elevations and if the occurrences will justify a large-scale mining method remains to be seen.

3.7 Pillars of strong rock types

A new hoisting shaft is planned in the vicinity of Lappberget with the coordinates X536.3 and Y3932.7. As part of the field investigation diamond drill cores were recovered. The drill cores primarily contained volcanogetic rock types, but some sections of sandstone and clastic sediment were encountered, as well as a small section of limestone. The rock strength of these rock types is high and a high RQD value was observed (Nyström, 2008). More about the latter can be found in Chapter 6.

3.8 References

Allen, R., S. Bull, M. Ripa and R. Jonsson, 2003, *Regional Statigraphy, Basin Evolution, and the Setting of Stratabound Zn-Pb-Cu-Ag-Au Deposits in Bergslagen, Sweden*. Final report for SGU-FoU project 03-1203/99, jointly founded by SGU and Boliden Mineral AB.

Allen, R., 2008, *personal communication*

Alsop, G.I., and R.E. Holdsworth, 1999, *Vergence and facing patterns in large-scale sheath folds*, Journal of Structural Geology 21 (1999) 1335-1349.

Fagerström, P., 2007, *Gruvnära prospektering i Garpenbergsområdet maj 2002 – mars 2007, Lappberget i fokus*, New Boliden AB internal report, Boliden, Sweden (in Swedish)

Granbacka, S., 2008, *personal communication*

Nyström, A., 2005, *Numerical analysis of stope dimensions for large scale mining of the Lappberget ore body and prognosis of mining conditions*. New Boliden AB internal report TG_REP2005/004. Boliden, Sweden. (in Swedish)

Nyström, A., 2008, *Estimation of rock conditions for a new hoisting shaft in Garpenberg*, New Boliden AB internal report, Boliden, Sweden

Vyskytensky, F., 2008, *numerous mine visits, personal communication and geological interpretations of levels 1080, 1060, 1040, 1016, 822, 801 and 776*. Garpenberg mine, Sweden.

4. Mining Lappberget

Lappberget is now one of the major orebodies in Garpenberg and is located near the North shaft as shown in Figure 4.1.

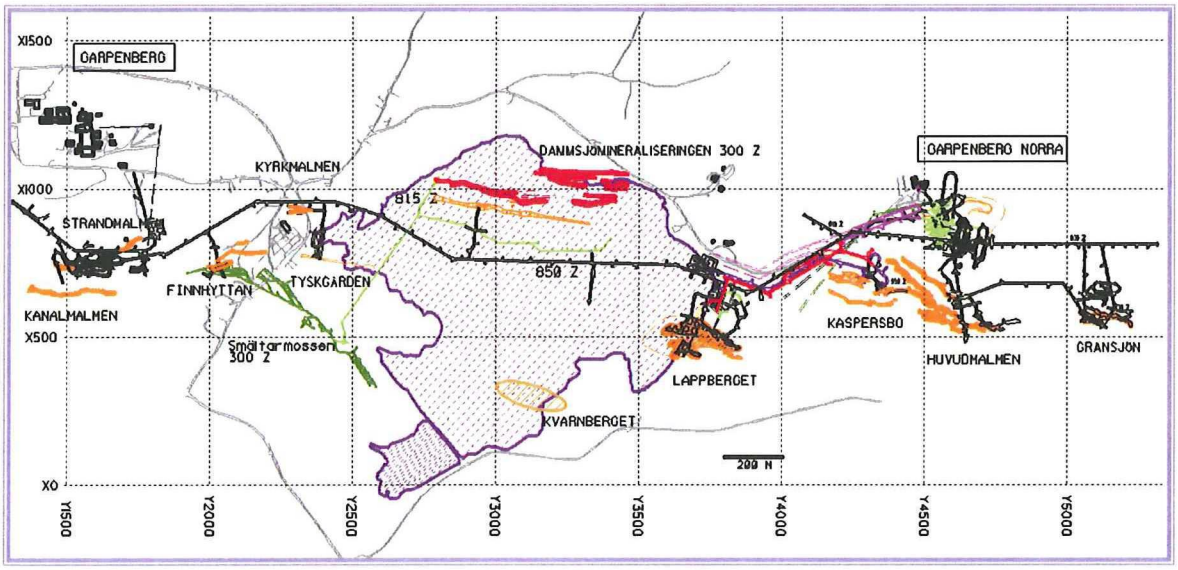

Figure 4.1: Plan view of the Garpenberg operations. The main ore bodies and the connection drift are indicated. (Söderman, 2006)

The Lappberget orebody is accessed by a ramp located at some distance away from the footwall drifts. A second ramp is being excavated at the moment of writing and is located directly at the footwall drifts, which should improve traffic tremendously. The footwall drifts are located north of the ore body. The ore is hauled from the production levels to a central crusher location at 800 level where it is skipped through the North skip shaft to surface. The ore is then transported by trucks to the mill at the South shaft.

4.1 Mining methods

The mining methods currently applied in the Lappberget ore body are post pillar cut-and-fill mining and transverse open stoping mining. In the past Rill mining has been applied as well, a combination of avoca and eureka mining. Rill mining stopped by the end of 2007 and will not be further described here.

4.1.1 Post pillar cut and fill mining levels 881-822

The cut-and-fill mining started on 881 elevation and is planned to be continued up to 822 elevation. This was the first ore being mined at Lappberget for the simple reason that it is a common method in the rest of the Garpenberg mine. At the time of discovery rapid production from Lappberget at its early stage was needed to feed the mill. A longitudinal view of the remaining mining is shown in Figure 4.4, in which the cut and fill mining are the long rectangular areas below 822.

The cut and fill mining started in 2003 and will likely be finished by the end of 2010, but the last two cuts might be mined by some longhole method instead which would cause termination of cut and fill mining in Lappberget earlier. (Koivisto, 2008)

The cut and fill on these elevations is a post pillar mining method, which means that pillars are left behind on each cut on the exact same location as the previous cut. The resulting pillars continue from sill pillar to sill pillar through all the intermediate cuts. Figure 4.2 illustrates a post pillar mining operation.

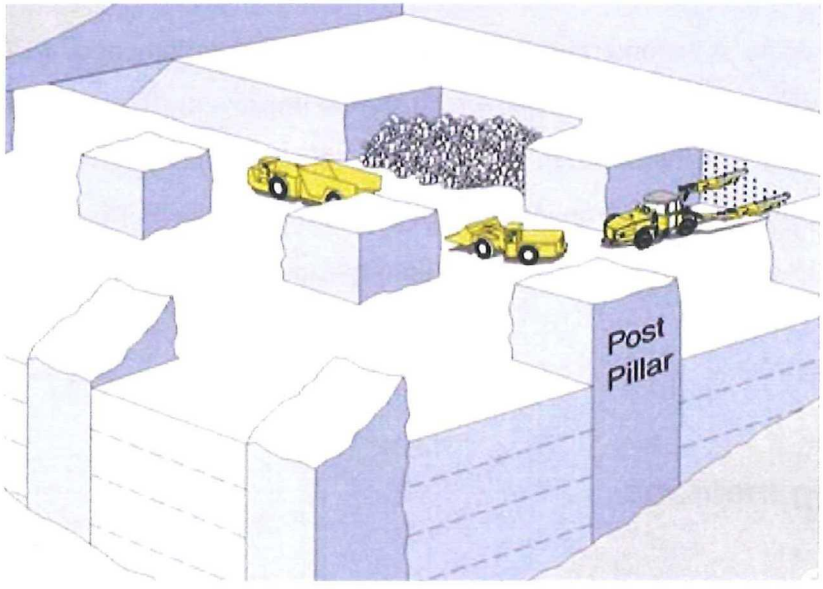

Figure 4.2: Post pillar mining (After Atlas Copco rock drills AB, 2000)

The stopes are backfilled with waste rock produced in other areas in the mine. The rockfill is often augmented with hydraulic fill whenever the infrastructure is available to do so. This produces a level fill and thus provides a proper floor in the succeeding

cut. The succeeding cut is then drilled with a drill and blast pattern very similar to an ordinary development heading. Slashing, or breasting, the ore into the waste is usually not done to minimize secondary dilution and because the gap between floor and ore is often uneven.

4.1.3 Transverse open stoping

Transverse open stoping is a longhole method in which a drift parallel to the ore is developed in the footwall, hence the name footwall drift. The ore is accessed by means of cross drifts perpendicular to the footwall drift. Access is created to the stopes on the bottom to be able to mine the stope. The first step after the development is done is to create a box hole cut, or drop raise, to provide a free face for the longhole blasting. After the box hole is created rings can be drilled, charged and blasted. Both the longhole drilling and the charging equipment at Garpenberg is capable of dealing with downholes as well as uppers. Remote mucking takes place in the bottom drift to prevent people from working under unsupported ground. A fill fence is built at the bottom access once the stope is mined out to enable paste filling.

An example of an transverse open stoping mine is shown in Figure 4.3. This example is from the Williams gold mine in Northern Ontario and shows a similar practice as the method that is applied to the Garpenberg mine. Some differences are that the secondary stopes are mainly backfilled with paste instead of rockfill and that boxhole raises are used instead of the raisebore raises. The dimensions differ as well.

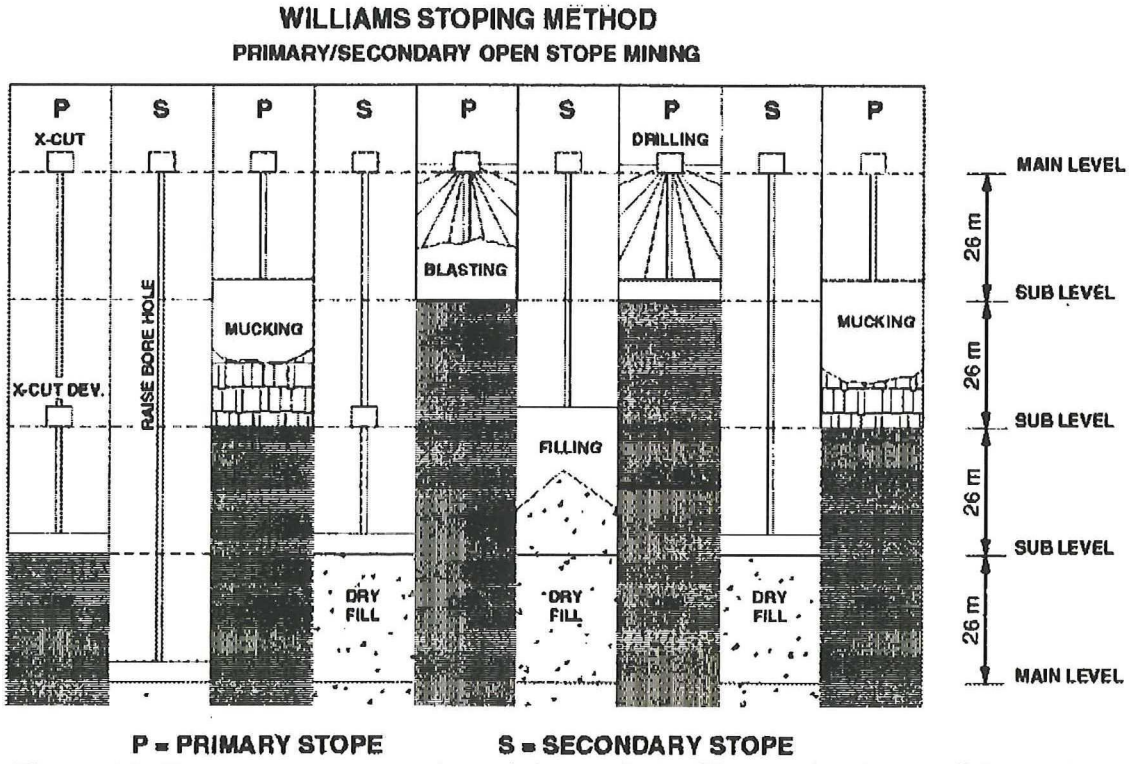

Figure 4.3: Transverse open stoping mining at the Williams mine (Hustrulid, 2001)

The paste requires a curing time of 7 to 10 days before it can be accessed on the top. The cycle repeats itself on the stope above once the paste is sufficiently cured. The mine is scheduled is such a way that blasting the secondary stopes is always a long time after the neighbouring primary stopes have been backfilled. The paste is produced at the paste plant on surface near the Garpenberg Norra shaft and is pumped to the stopes underground. The paste is a combination of the sand fraction of the tailings produced by the mill and a binder. The sand fraction of the tailings is pumped as slurry from the mill to the paste plant where the water is taken out by a hydrocyclone followed by thickener system for the finer fraction or by vacuum pump for the coarser fraction. The resulting paste backfill has estimated strengths between 200 and 1500 kPa, depending on the requirements for the paste in the mine (Marklund, 2003, see Chapter 6 for more on this topic).

Sequencing follows a typical pyramid shape with a saw tooth pattern and more about this can be read in section 4.3. Stope dimensions were initially calculated using the Modified Stability Graph method (Polk et al., 2004). The Modified Stability Graph is an empirical method to design dimensions for open stopes in a variety of longhole

methods. The method is based on approximately 350 case studies in the mining industry. The parameters in this design method are:

- Rock Quality Designation (RQD)
- The number of joint sets in a rock mass
- Roughness and shape of the joint surfaces
- Condition of the joint surfaces
- The increase in stress in the centre of the new excavation compared to the Unconfined Compressive Strength (UCS) of the rock, obtained by 2D or (preferably) 3D numerical stress modelling.
- The orientation of joints and faults in respect to the excavation
- The inclination of a surface of the excavation that is analysed.

The combination of the parameters mentioned above result in a Stability Number noted as N. This number is then correlated to a hydraulic radius, which is the ratio between surface area and perimeter. The hydraulic ratio dictates the maximum stope dimensions based on the case studies used for this method. In the study by Snowden two mining methods were proposed; transverse open stoping for the A zone and a longitudinal retreat method for a combined B and C zone. Their base case stope dimensions were evaluated using the aforementioned Stability Graph. (Polk, 2004)

A more detailed study was done by Anders Nyström who used a three dimensional boundary element program, Examine3D, to model the depth of fracturing with an impressive amount of different stope dimensions. The used failure criterion he used was calibrated by looking at the depth of failure in pillars in a new workshop close to Lappberget. Those pillars were of different sizes and shapes. Based on those results more detailed recommendations were made about the design criteria and the expected plastic zones for both the transverse open stoping and longitudinal retreat methods. (Nyström, 2005)

The picked stope dimensions for Lappberget are shown in Figure 4.3.

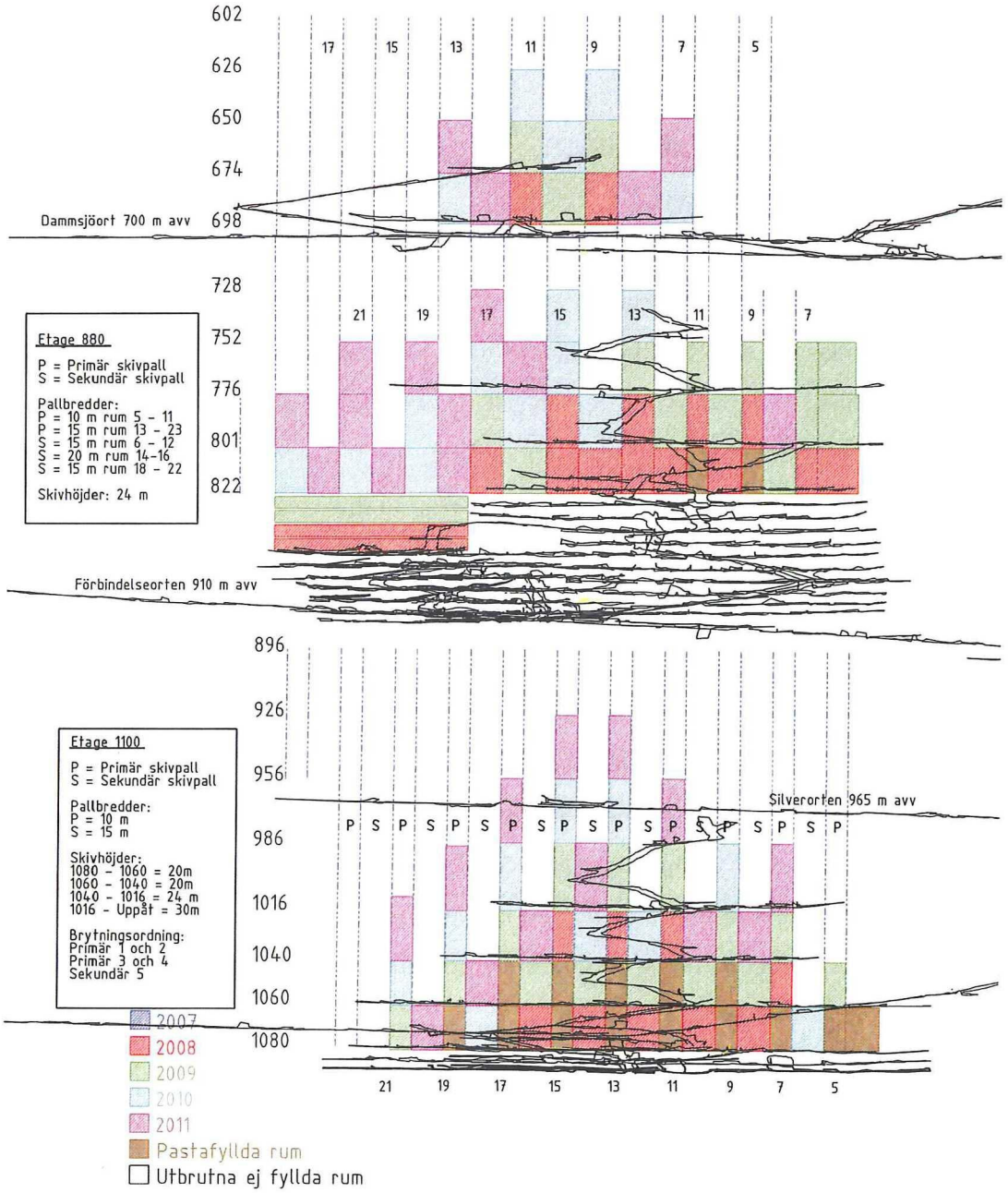

Figure 4.4: Longitudinal view of the Lappberget mining layout for longhole stoping of the A and C zones. (Koivisto, 2008). Pallbredder are stope widths, skivhöjder are stope heights, primär skivpall is primary stope, sekundär skivpall is secondary stope, förbindelseorten is the connection drift and pastafyllda rum is pastefilled stope.

At the moment ramp development is in progress and the connection between 1080 and Silverorten has just been completed. From Silverorten the ramp will continue upwards to the 910 connection drift close to the new workshop. In the same fashion a ramp is driven up from the 822 level up to Dammsjöorten on 700 elevation and should eventually end up at the connection drift on 500 elevation. Once the main

ramp is augmented by the new ramp close to Lappberget ventilation and traffic will be largely simplified.

The recovery is assumed to be close to 100% while using 10% dilution in the calculations.

4.1.4 The B- zone between 1080 and 1040

In the initial pre-feasibility study this part of the ore body was to be mined by a longitudinal retreat method (Polk et al., 2004). Once access was gained to the ore it turned out to be too irregular and complex to be mined by a longhole method. The decision was made to apply the post pillar cut and fill mining similar to the cut and fill mining between 881 and 822 until the ore will show more homogeneous characteristics. Cut and fill mining will be applied up to at least 1040 level. The pillars in this section are not going to be recovered. How the B zone is going to be mined above 1040 remains to be seen. The B zone is moving towards the A and C zones at higher elevation, but further core drilling will provide more insight.

The decision to start mining the B zone with the post pillar cut and fill mining was made as there was not enough knowledge about the geology available to justify a longhole method. The cut and fill method requires little pre-production development and can achieve decent production numbers. Post pillar mining means that there are some restrictions on the flexibility of locating the succeeding cuts and that the recovery rates are lower than by a longhole method.

The ore is now accessed through stope number 10 on the 1080 level. This is a secondary stope, but now acts as an attack ramp for the post pillar cut and fill mining. Both stope number 9 and 11 are primary stopes and have been backfilled with paste. Stope number 10 is scheduled to be mined in 2008, but only after mining the B zone up to 1062 elevation has been completed. Stope number 21 on 1060 level will then become the new attack ramp to access this area. The change to access the B zone through stope 21 was to allow the planned scheduling to take place without

disturbance from the cut and fill mining. How the B zone is going to be mined from level 1040 and upwards is unclear at the moment.

Recovery is expected to be roughly 75%, while the calculations include 10% dilution.

4.2 Production numbers

Mining commenced at 880 level in 2004 and cut-and-fill mining will likely be applied up to 822 level until the end of 2010. Long hole stoping begun on 698 level in June 2008, on 822 level in July 2007 and on 1080 level in February 2007. It is very likely that a lot of the reserves can be turned into resources after more core drilling.

Table 4.1: Production numbers for Lappberget. Numbers in ktonnes (Koivisto, 2008)

Mining	**2007**	**Up to May 2008**
Cut and fill	220	125
Transverse open stoping	282	158
Rill	43	0
Development	204	82
Total	**749**	**365**

The numbers for Lappberget are in Table 4.1. For 2007 production from Lappberget averaged a little over 2000 tonnes per day. Currently the mucking capacity is the bottleneck in production. This will be solved within the near future.

4.3 Mine layout and sequencing

The objectives of mine sequencing are to:

- Maximize the extraction of the resource
- Create a sustainable rate of extraction
- Minimize the costs per tonne extracted
- Minimize the up-front development capital
- Provide a grade control strategy
- Minimize ground control problems

These objectives are not complementary as the upfront capital may for example increase to minimize ground control. The overall objective should be a combination of the objectives listed to maximize the Net Present Value of the project. (Pelley, 2006).

By using a sawtooth primary-secondary open stoping pattern as shown in Figure 4.4 a large number of stopes is created over the entire width of the ore body to enable a sustainable rate of extraction and the potential for grade control. As the stopes are placed in a pyramid shape the stresses should be pushed towards the abutments and into the secondary stopes. While pillarless mining (just primary stopes) might eliminate highly stressed secondary stopes, it restricts the flexibility of the overall mining operation as only two stopes per level can be mined simultaneously versus four stopes in the ideal primary-secondary sequence.

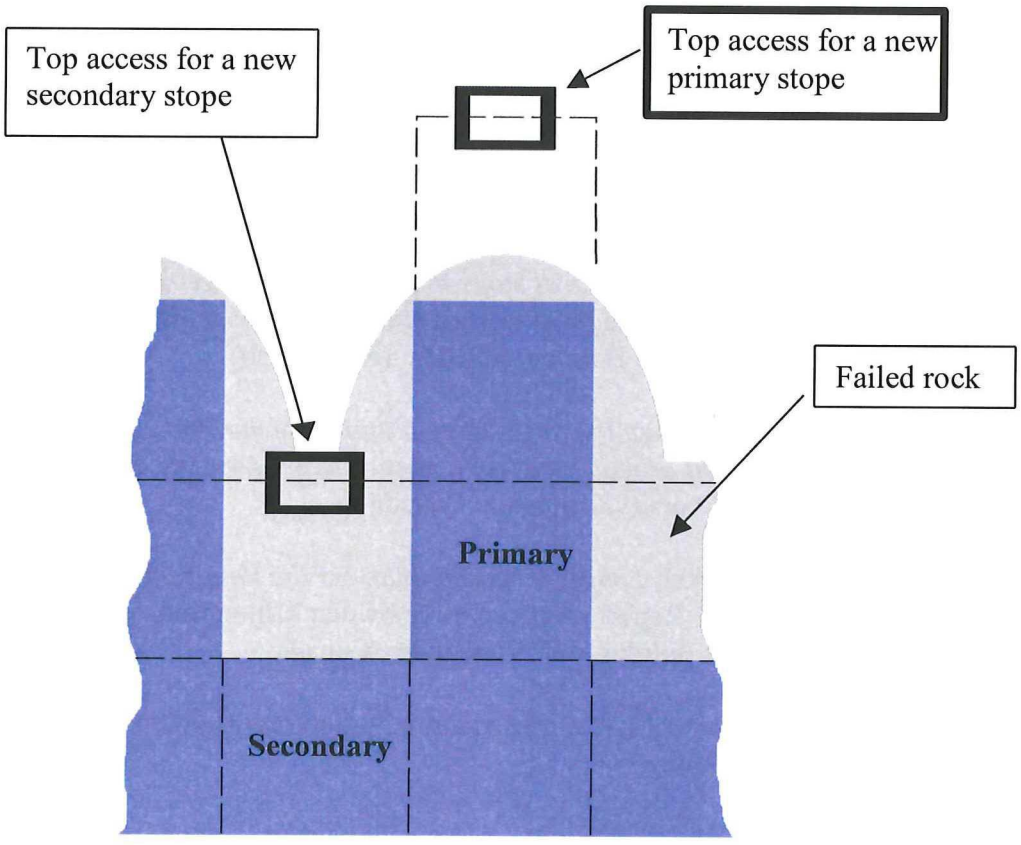

Figure 4.5: Conceptual sketch for the layout in Lappberget (After Nyström, 2005)

Figure 4.5 shows a conceptual sketch of the expected ground conditions. The drifts for the primary stopes should be fairly straightforward to construct as they are in undisturbed rock. The drifts for the secondary stopes will probably pose more difficulties as the rock mass will be highly stressed. It is expected that the ore in the secondary stopes is either at a failed (naturally destressed) state or at the brink of failing. Whichever it may be, it is important that these top accesses are excavated at the last possible moment just prior to mining the stope underneath. (Nyström, 2005). Numerical modelling later in this thesis should indicate the state of stress in the secondary stopes.

4.4 References

Atlas Copco Rock Drills AB, 2000, *Underground mining techniques*, Örebro, Sweden

Hustrulid, et al., 2001, *Underground Mining Methods: Fundamentals and International Case Studies*, SME, USA.

Koivisto, S. 2008. *Personal communication.*

Marklund, P.I., 2003, *Pastafyll*, presentation on pastefill for a course on rock support, Boliden, Sweden. (in Swedish)

Nyström, A., 2005, *Numerical analysis of stope dimensions for large scale mining of the Lappberget ore body and prognosis of mining conditions*, Boliden internal report, TG_REP2005/004, Boliden, Sweden. (in Swedish)

Pelley, C., 2006, *Mine sequencing, the long range planning of mining activity throughout the overall orebody*, course notes for MINE444: underground mining, Queen's University, Kingston, Canada

Polk, A. and R. Goodwin, 2004, *Longhole mining plan for the Lappberget deposit, Garpenberg, Sweden.* Report prepared by Snowden Mining Industry Consultants for New Boliden AB. Vancouver, Canada.

Söderman, T., 2006, *Garpenberg area*, presentation on the New Boliden AB operations in Garpenberg.

5. Stresses

5.1 Introduction to stresses

The state of stress is essential in most, if not all, geomechanical related topics. In assessing the potential of seismicity in Lappberget virgin stresses and induced stresses will play an integral part of the analysis. Therefore it is fitting to briefly introduce stresses here.

Stresses can be divided into two categories; mine induced stresses and virgin stresses (also known as far field and in situ stresses). Virgin stresses are the stresses in a rock mass before any opening in the rock has been excavated and can be caused by a number of reasons, e.g. gravitational (lithostatic) stresses, residual stresses and tectonic stresses. Once an opening has been excavated, the stress pattern will locally be altered and the resulting alterations are known as mine induced stresses.

The state of stress can be described by a stress tensor. For convenience the main principal stress component has the same orientation as the maximum stress orientation and is denoted as σ_1 and the minor principal stress component is perpendicularly orientated in the direction of the minimum stress and is denoted as σ_3. The result of doing so is the elimination of shear stresses. Often the main principal stress component is assumed to be vertical, but this would be true if the only source of stress is gravitational.

Introducing an opening into a rockmass creates a disturbance of the state of stress. The stresses will tend to "streamline" around the excavation. Figure 5.1 illustrates the state of stress after an excavation is introduced in an elastic rock mass. For excavations with a simple geometry (e.g. circular, ellipsoid and spherical excavations) in elastic rock masses analytical solutions may suffice to calculate the altered state of stress. Numerical modelling has to be used as soon as situation gets more complicated, for example the calculation of induced stresses of several excavations or excavations with more complex geometries.

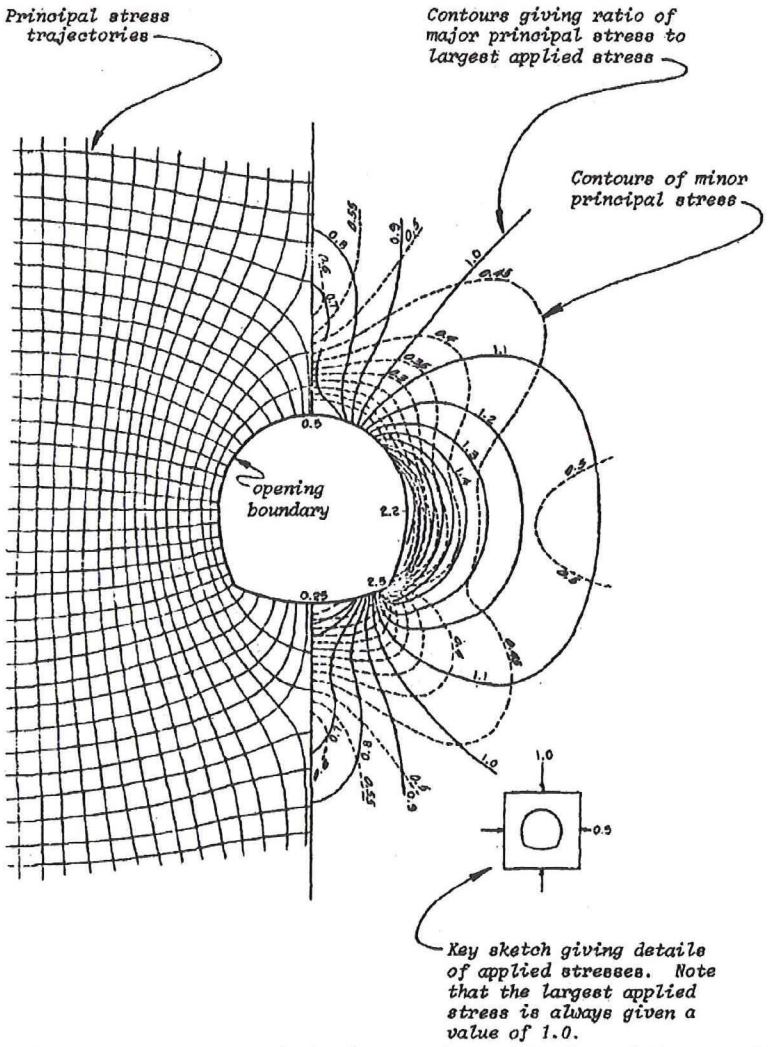

Figure 5.1: Stresses around single openings (Hoek and Brown, 1980)

Figure 5.1 shows an increase in stress along the surface of the excavation parallel to the principal stress component in the virgin state of stress. On the back and the floor relaxation takes place as result of the redistribution. Whether or not the rock will fail depends on a great number of things of which the state of stress plays an important role.

A similar situation may occur in an open stope as illustrated in Figure 5.2. Note that the major principal stress component is horizontal. Analogous to the opening in Figure 5.1 compression occurs along the surface parallel to the main principal stress. Relaxation occurs along the walls of the stope as result of the redistribution. Depending on the strength of the rock (among other factors), the rock might fail due

to an excess stress in the back or might cave in on the walls due to the lack of confining stress.

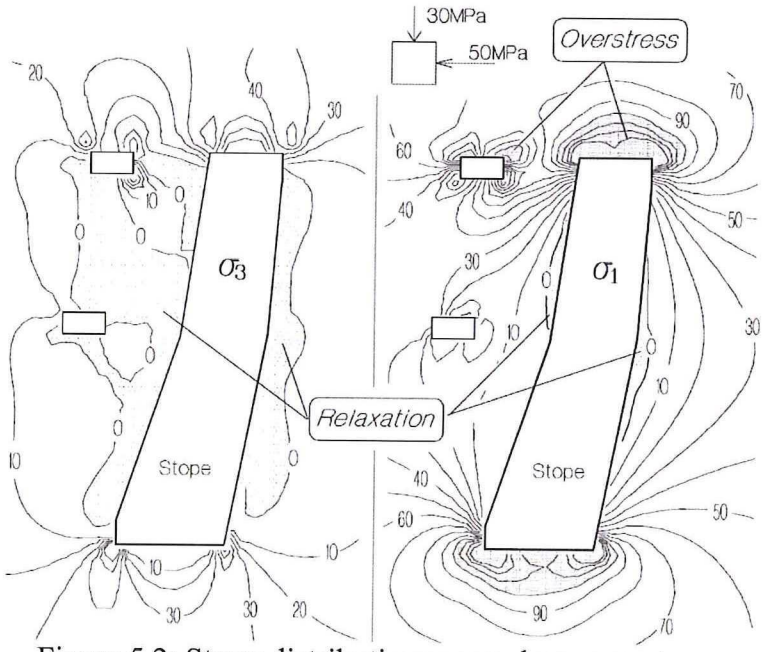

Figure 5.2: Stress distributions around an open stope (Hutchinson and Diederichs, 1996)

5.2 Stress measurements

Stress measurements are time consuming and therefore expensive measurements to carry out. In addition it takes experience and specialized equipment. Stresses are not measured directly, but instead strains are measured and then back calculated by elastic relationships to stresses. By rotation of the stress components the orientation and size of the principal stresses (either three dimensional or two dimensional in the plane of the measurements) can be determined. Two series of stress measurements have been taken in or in close proximity to Lappberget by SINTEF from Norway. The measurements will be described here.

5.2.1 Overcoring

The stress measurements were carried out using the overcoring technique and were carried by SINTEF. In these measurements a 72 mm diamond drill hole is drilled to the required depth. Then a 36mm hole is drilled within the 72mm diamond drill hole to approximately 30 cm past the point where the diamond drill hole stopped. A three-

dimensional strain measurement cell with known orientation is then glued into the small hole and the zero strain state is recorded. After this is done the diamond drilling continues to "overcore" the measurement cell and the core is taken out. The three-dimensional state of stress can then be back calculated once the rock mechanical properties of the rock are known from laboratory testing. The samples are the cores taken from the actual measuring holes and testing includes biaxial load tests. The samples have a diameter of 62 mm and a length/diameter ratio of 2.5. The results are included in Table 5.1 (Nilsson, 2004).

Table 5.1: Rock properties of the limestone. The E modulus and Poisson's ratio have been calculated from the biaxial load tests. (after Nilsson, 2004)

	E-modulus (GPa)	Poisson's ratio	UCS (MPa)	Sound velocity (m/s)	Density (kg/m^3)
883 level	55	0.17	73	4217	2714
967 level	60	0.12	100	4860	2722

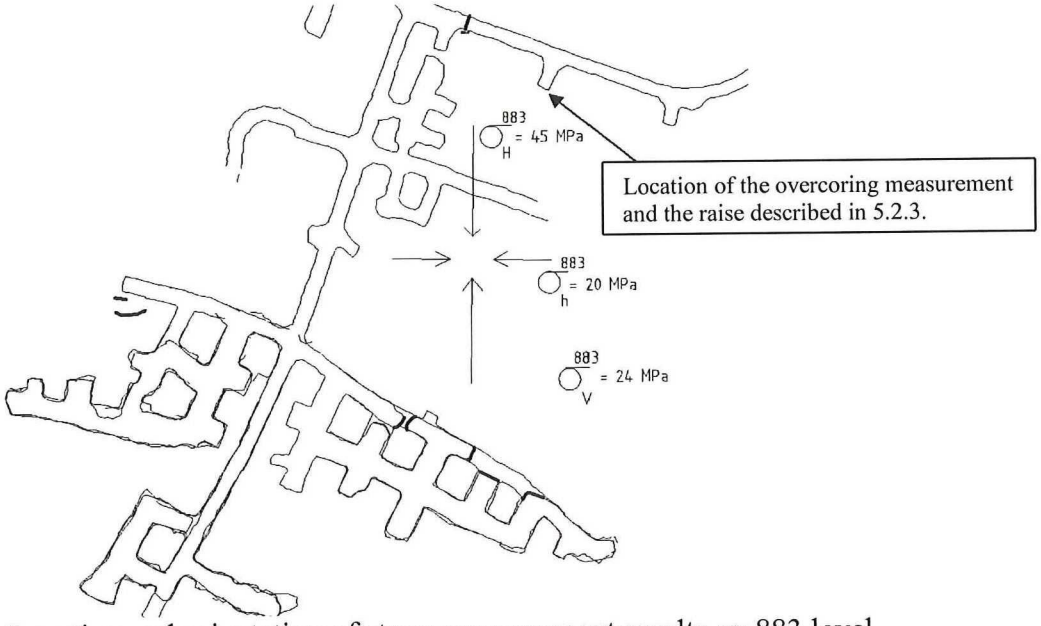

Figure 5.3: Location and orientation of stress measurement results on 883 level (after Nyström, 2005*a*)

Figure 5.3 shows the location of the stress measurement at 883 level. A large electric workshop was constructed at the time of the measurements. The dimensions of the workshop are 6x40x50 meters and the shop is located on average 25m away from the measuring point. Numerical modelling in a two-dimensional boundary element program showed that the horizontal stresses are not influenced and that the vertical stress increases by about 10% due to the excavation. The measurement was oriented

N150E (approximately perpendicular to the drift orientation) on a 6 degree incline and ended up being 18.5 meters long. The major rock type was limestone with some darker and lighter parts. The measurements were taken in between 14.5 and 18.5 meters into the hole. (Nilsson, 2004)

The measurement at 967 elevation is taken in foliated limestone that only has a few joints. The foliation has the approximate orientation of the ore body with a strike and dip of N060E/75SE. The orientation of the hole was identical to the 883 hole and a sketch of the location can be seen in Figure 5.4.

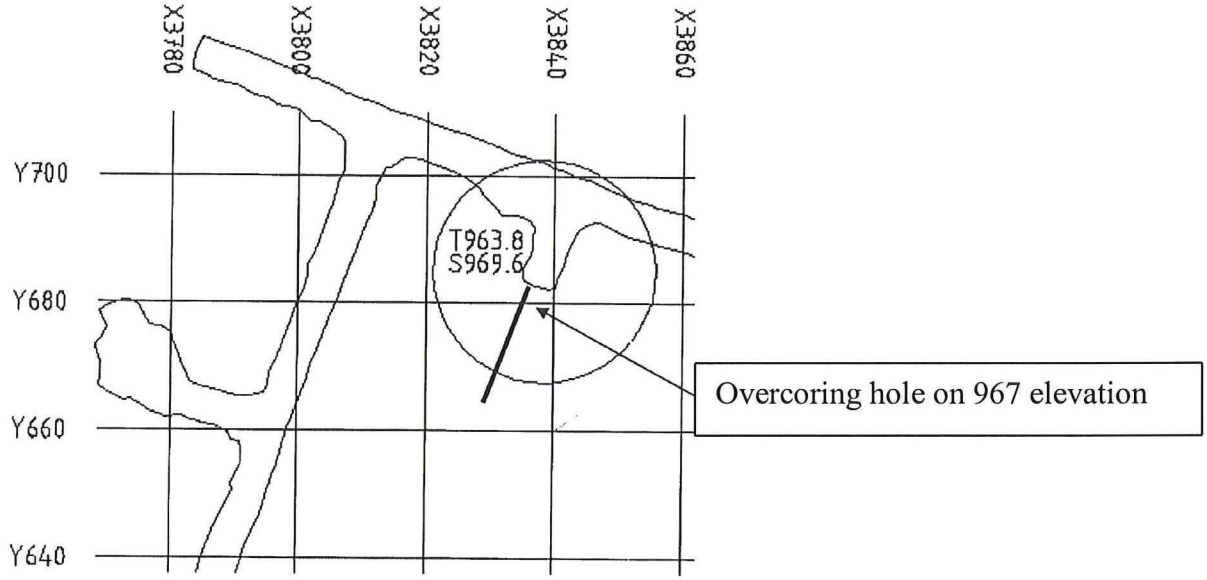

Figure 5.4: Location and orientation of the measurement at 967 level (Nilsson, 2004)

The stress orientations are illustrated in Figure 5.5 and the values are summarized in Table 5.2. The theoretical lithostatic horizontal and vertical stresses as calculated with the Poisson's ratios and an average density of the overburden of 2.7 t/m^3. It is easily observed that the measured horizontal stresses greatly exceed the theoretical ones. This indicates a large amount of tectonic or residual stresses. The vertical stress on 883 elevation is very close to the theoretical stress, but on 967 level the measured vertical stress is a lot lower than the theoretical stress.

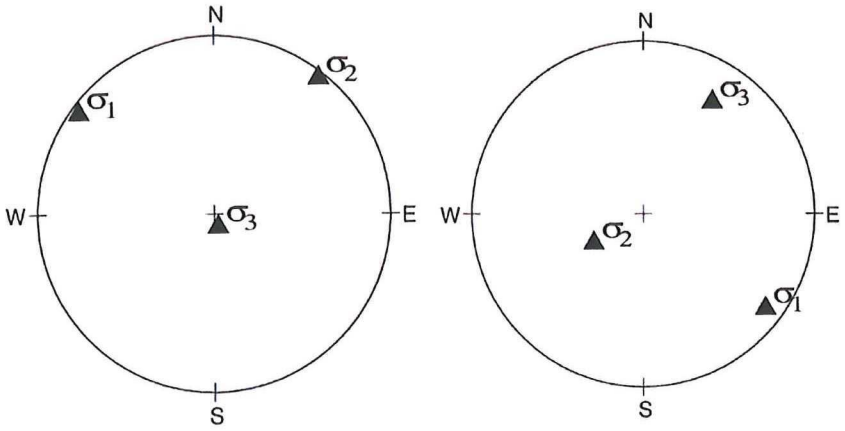

Figure 5.5: Stereographic representation of the states of stress at 967 (left) and 883 (right) elevations. (Nilsson, 2004) Orientations with respect to the true North, not the local mine coordinate system.

Table 5.2: Magnitudes of the measured and theoretical (lithostatic) stresses (Nilsson, 2004)

	967	883
σ_1	26.2 MPa	45.2 MPa
σ_2	17.8 MPa	23.8 MPa
σ_3	10.7 MPa	20.2 MPa
σ_v	25.6 MPa	23.4 MPa
σ_h	3.5 MPa	4.8 MPa

It is hard to find the reasons for the stress deviations and for the large differences between the 967 and 883 elevations. Induced stresses from nearby excavations might play a larger role than expected. There could be a significant difference between the elastic properties of the massive sulphide ore and the host rock that could cause stress accumulations in certain areas in the host rock near the ore contact. From experience in Scandinavia it is not unusual to see the main stress component in (sub-) horizontal direction. (Nilsson, 2004).

5.2.2 Doorstoppers in the post pillars in Lappberget

The doorstopper measurements are in a way very similar to the overcoring measurements in that strain is converted to stress after a sample is destressed. The doorstopper method is a two-dimensional method. At the end of a hole the doorstopper is glued, which basically consists of four strain measurement strips in 45-degree intervals. The zero-strain is recorded and overcoring drilling takes place. The new strain values are then used to back calculate the two-dimensional state of stress (perpendicular to the borehole direction). For this calculation the elastic relationships

and laboratory test results of rock samples are needed (Dahle, 2005). The state of stress at the end of the borehole is not equal to the in-situ stress as the borehole itself imposes, albeit small, induced stresses (Figure 5.6). Correction factors based on the Poisson's ratio are available and should be used. (Myrvang, 2001)

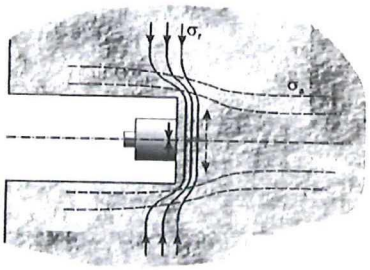

Figure 5.6: Stress concentration near the bottom of the hole (Myrvang, 2001)

The measurements took place in two post pillars on 852 elevation in the cut and fill post pillar mining part of Lappberget (see chapter 4.1.1). The location of the test holes is shown in Figure 5.7. The first hole is 6.5 meters deep and 8 measurements were taken from 0.4 to 5.6 meters into the hole. The second hole was drilled to 7 meters depth and 7 measurements were taken between 0.6 and 6.5 meters into the hole. The measurement at 6.5 meters was unsuccessful and is therefore discounted in the calculations on the total load on the pillar. The cores recovered from the holes showed only one serious joint in hole one. This joint had clay infilling. (Dahle, 2005)

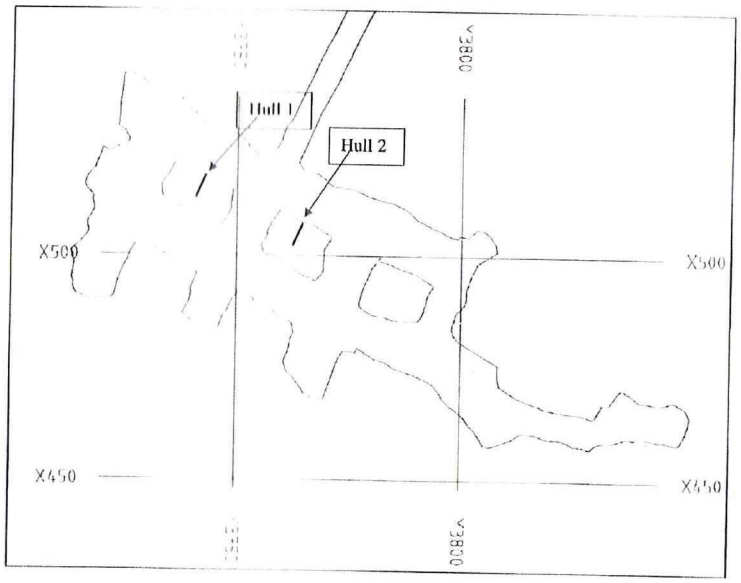

Figure 5.7: Location of the doorstopper measurements in Lappberget at 852 elevation (Dahle, 2005). "Hull" is Norwegian for hole.

The recovered cores from the measurement holes were tested by uniaxial loading tests. The average values of the different parameters are summarized in Table 5.3. The rock mass is heterogeneous and therefore the values vary a bit depending on the location in the borehole. (Dahle, 2005)

Table 5.3: Rock properties of the ore for the doorstopper measurements (Dahle, 2005)

Measurement location	E-modulus (GPa)	Poisson's ratio	UCS (MPa)	Sound velocity (m/s)	Density (kg/m^3)
Hole 1	84.7	0.15	196	5147	3331
Hole 2	90.7	0.15	146	4687	3270

Figure 5.8 shows the state of stress along the length of the boreholes. The lowest stresses were measured near the collar of the hole. The factors of safety – defined here as $UCS/\sigma_{1,max}$ – are 5.5 for hole 1 and 3.1 for hole 2. The factor of safety (FOS) for the second hole is based on a single high value, if the FOS is calculated over the average stress it increases to 5.4 (Dahle, 2004). The FOS should be between 3 and 5 as failure is generally initiated at a FOS below 2 (Myrvang, 2001).

These values are to be used with some caution as the E modulus varied over the length of the borehole. The results give a good impression of the state of stress in the pillars nonetheless. (Dahle, 2004).

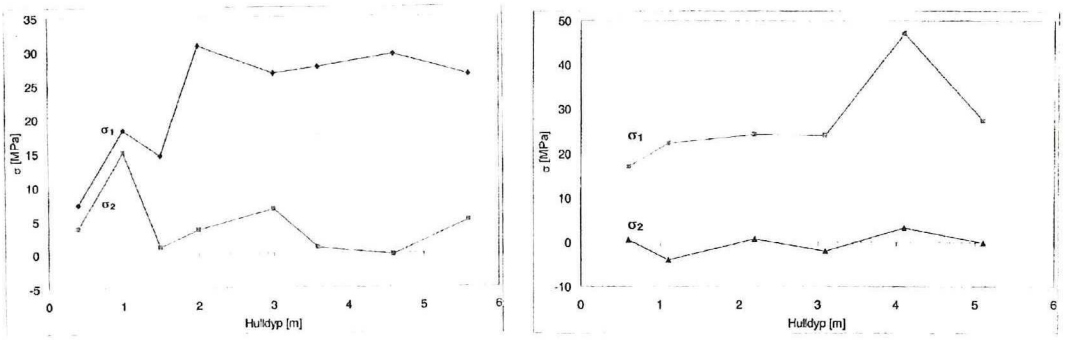

Figure 5.8: Stress profiles along hole 1 (left) and hole 2 (right) (Dahle, 2005)

5.2.3 Observations from a bored raise

For ventilation purposes a raise was constructed from 883 level to 827 level. The raise was bored using a raisebore on the exact location of the stress measurement. Since the raise was bored, a smooth surface was created. After construction, parts of the raise failed in the circumference that complies with the stress measurement. As discussed

in section 5.1, the stresses around a circular opening occur on the circumference parallel to the major principal stress component and as a result the major stress orientation is indicated by the locations of the failures. Figure 5.9 is a picture taken in the raise and Figure 5.10 provides the associated major principal stress orientation that is consistent with the overcoring measurements described in 5.2.1. (Nyström, 2005*b*). The location of the raise is indicated on Figure 5.3 as well.

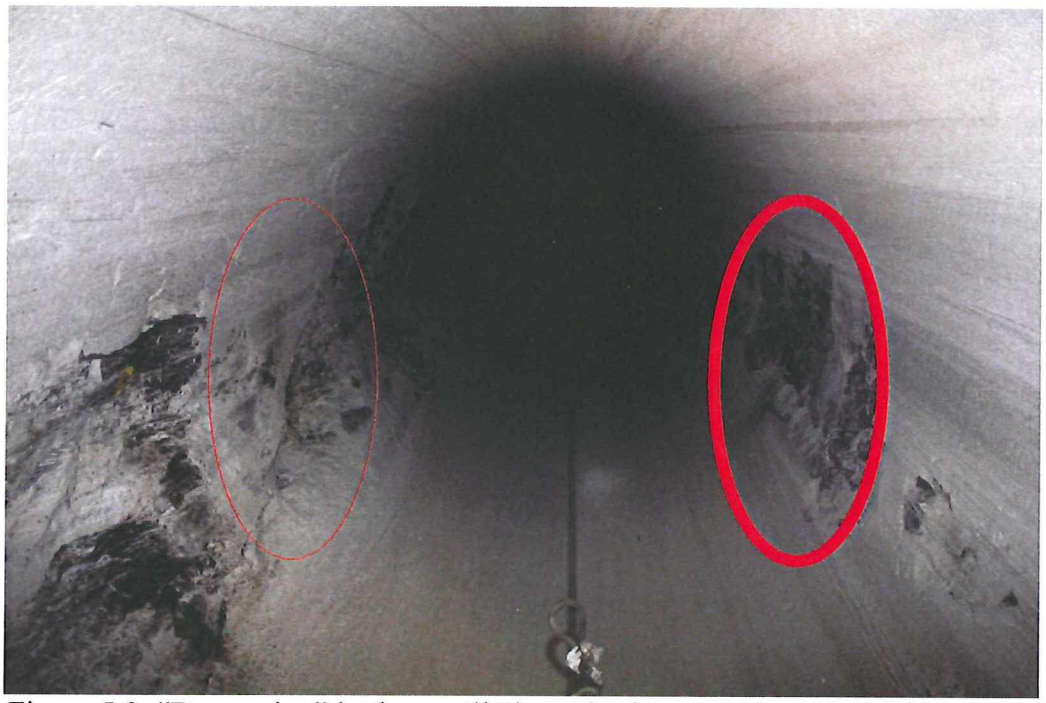

Figure 5.9: "Dog earing" in the ventilation raise between the 883 and 827 levels (Nyström, 2005*b*).

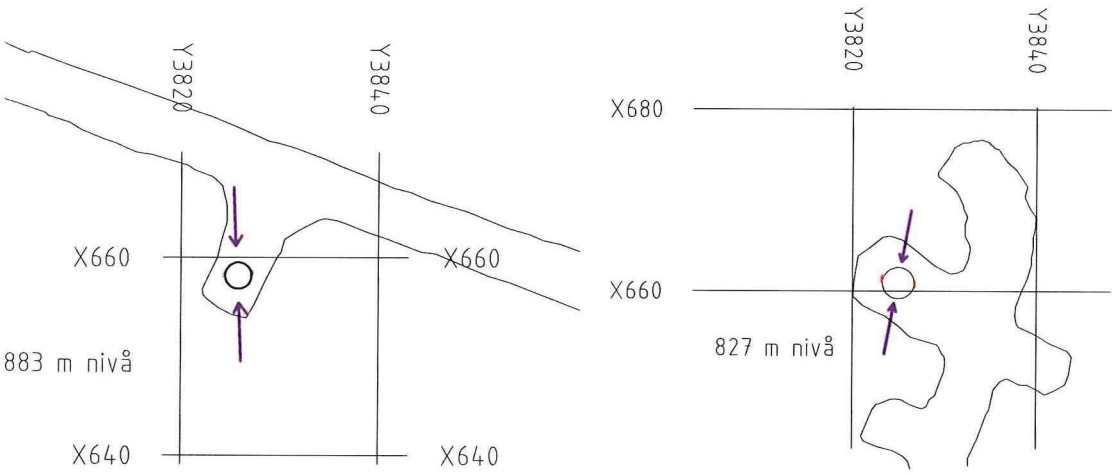

Figure 5.10: Location of the raise –883 level on the left and 827 level on the right side - and the major stress direction associated with the failures (Nystöm, 2005*b*). "Nivå" means level.

5.3 Stress related observations in Lappberget

Problematic stress induced failures have been relatively sparse. There have to date not been any rockbursts or other problematic failures due to high compressive stresses. The few structural failures experienced in Lappberget were due to geological structures and stress induced fractures. Those occurrences were limited to the open stopes and the talc zone in the hanging wall contact.

5.3.1 Stress induced joints in the ore

The redistribution of stresses around fresh openings causes the rock to react and fractures might be created. This was displayed in the cut and fill mining between 896 and 822 elevation as can be seen in Figure 5.11. In this picture the back of the previous cut can be observed. This back was scaled at time of the creation, so the lions share of the observed joints have to be stress induced. These joints have an orientation parallel to the main principal stress analogous to the major principal stress trajectories in Figure 5.1 (note that the major principal virgin stress component is roughly orientated horizontally). These fractures can be dealt with by applying support to ensure an interlocking system of rock fragments.

Figure 5.11: Horizontal stress induced fractures above the back of the previous cut in cut and fill mining in the A zone. (Nyström, 2005*a*)

If the relative stiff ore is in contact with a softer contact zone a situation as in Figure 5.12 might be the result. The induced fractures in the ore are continuous right up to

the footwall – ore contact. The contact zone consists of a soft rock mass. What happened in the case of Figure 5.12 is that a cross cut drift for the bottom access of the transverse stoping at level 822 was driven perpendicular over top of the last cut of the cut and fill mining. The old cut and fill drift below has been backfilled with rockfill, so that can be effectively seen as a void from a convergence point of view even if tight fill would have been achieved (as the stiffness of the rockfill mass is far lower).

Figure 5.12: Horizontal stress induced fractures in the ore up to the footwall contact. (Nyström, 2008)

The result is that the stiff ore pushes the softer contact rock into the void as sketched in Figure 5.13. The resulting induced fractures are parallel to the contact and perpendicular to the major principal stress. (Nyström, 2008)

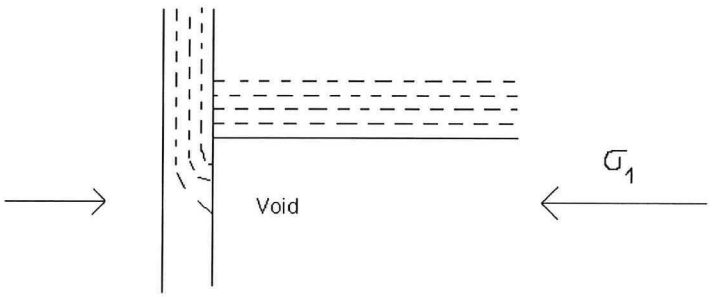

Figure 5.13: Sketch of ore at a soft contact (after Nyström, 2008)

5.3.2 Pillar and brow deterioration

Gradual deterioration of the pillars in between the crosscuts, footwall drift and stopes can be observed, most notably on the corners with the footwall drift. This deterioration is mainly stress induced as the pillars are thoroughly scaled by mechanical scaler, yet slabbing can be seen after mining activities in the proximity. An example of this deterioration can be seen in Figure 5.14. The pillars near the intersection between the footwall drift and ramp access are the ones most affected at the moment due to the span they have to support and because the secondary stopes have been mined in that area.

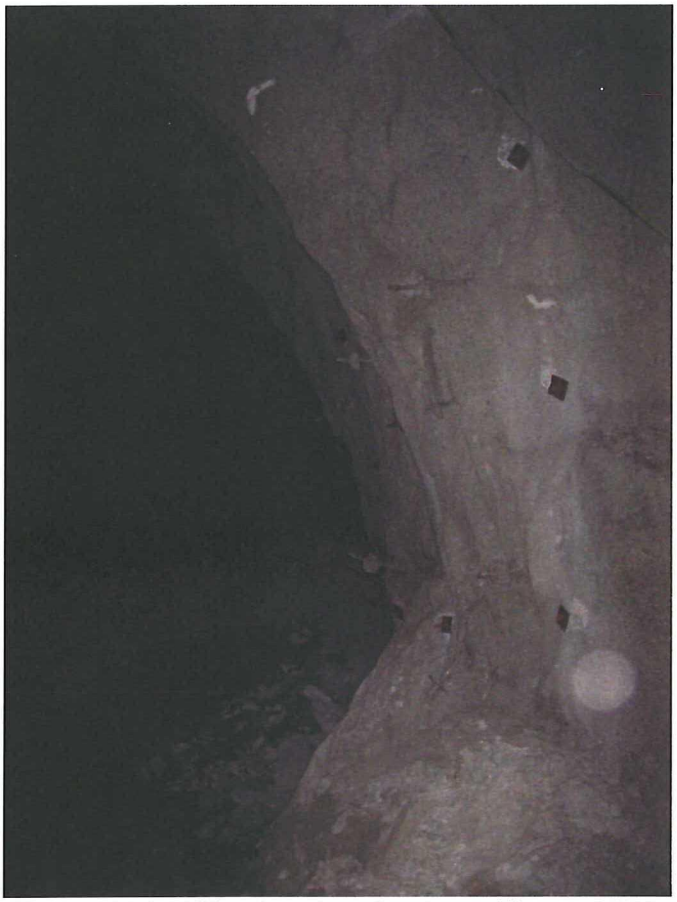

Figure 5.14: Pillar deterioration in a pillar on 1080.

The explanation of the deterioration is that the stresses are redistributed due to taking out the stopes. A simplified model was made in Examine 3D (Rocscience Inc., 2003) to illustrate the stress changes by showing the major principal stress component for the pillars in the middle row in different stages in the mining history. The different stages of the model are shown in Figure 5.15 and the associated stresses in the middle row of pillars are shown in Figure 5.16. As the primary stopes are taken out the stress

is redistributed partially though the pillars, which explains an increase in stress near the accesses to the secondary stopes. When the secondary stopes are taken out as well the pillar is loaded in a different manner. Once the stope above is taken out the pillar on the top access of the first stope will at least partially disappear in a stress shadow or area of relaxation, which results in a significant reduction of stresses. It quickly becomes clear that these pillars are subject to dynamic loading and unloading due to progressive mining activities. If the loading and unloading at some point exceed the elastic capacity of the rock plasticity, or irreversible deformation, takes place that leads to the visually observable deterioration of the pillar.

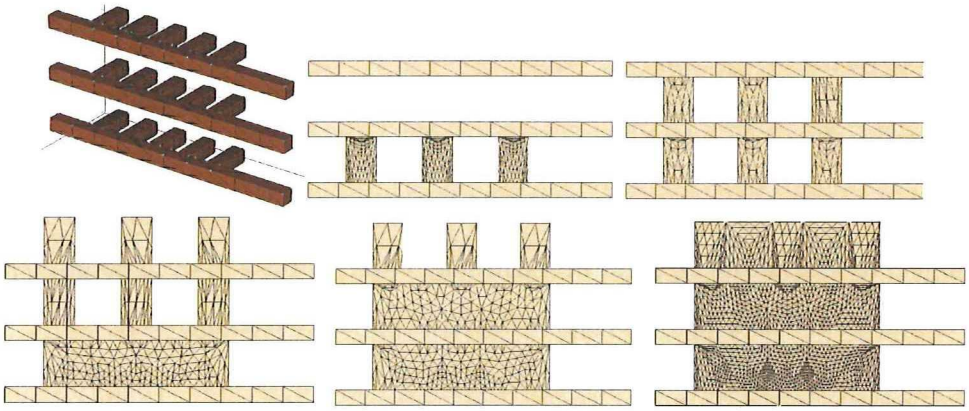

Figure 5.15: The six models representing different stages. The first stage is shown in isometric view, while the other five subsequent stages are in longitudinal view.

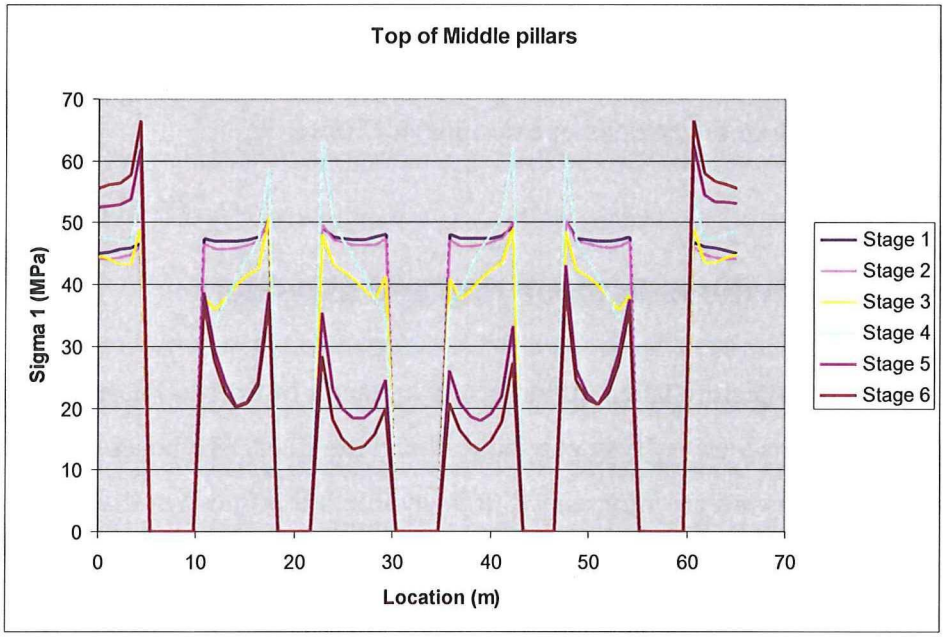

Figure 5.16: Stress changes in the upper part of the pillars in the middle row of the model. Values are taken 5 meters from the brow at the level of the back. Note that the crosscuts to the primary rooms are located at 5 – 10m, 30 – 35m and 55 – 60m. Access to the secondary rooms is gained between 17.5 – 22.5m and 42.5 – 47.5m.

Problems could occur in the brows somewhat similar to the slabbing in the pillars. The explanation is identical to the aforementioned pillar deterioration, although they will disappear in the stress shadow as soon as the stope is excavated. The brows are important and they are not allowed to collapse, as people will operate the remote scoops from underneath these.

Based on a study by Nyström in 2006, it was shown that the pillars will most likely show a degree of plasticity at the edges as the models were calibrated to the observations of pillars in a large workshop not far from Lappberget. It was recognised that additional support is needed in the pillars when the crosscuts to the secondary stopes are developed on the bottom level (1080). The levels above 1080 are subject to a change in stress, but will end up in the stress shadow behind the mined ore and the stresses are eventually significantly reduced. There is, however, always a risk for the need of rehabilitation of the pillars. This report prognosis the round at the ore contact to be subject to high stress changes in the mining cycle and it will need additional support as a result. The support design is adjusted for these findings. Before developing the crosscuts into the secondary stopes the pillars will need additional rebar and the round at the ore contact should be supported with additional shotcrete and a denser bolt pattern (Nyström, 2006).

A more detailed analysis on pillar and brow stability will follow with more detailed numerical modelling of the actual stope designs in Chapter 9.

5.3.3 Induced fractures in stope roof and shoulders

Figure 5.17 shows a picture taken in the secondary stope 14 on 1060 near the hanging wall contact. There is a cavity between the wall and the floor. The hoses coming out of the marked collars are geology related. It is unclear if the fractures that can be seen in the wall are natural, stress or blast induced, but the rock is more fractured than the untouched counterparts.

When it comes to the backs of the secondary stopes it is hard to conclude anything. At the moment there are only a few secondary stopes in production and all of them are shotcreted, which obscures the ability to observe the rock.

Figure 5.17: Natural, blast or stress induced fractures in 1060 stope 14.

Whether or not the fractures are stress induced in the shoulders of the stope is in some ways irrelevant. As the rockmass in the shoulders is destressed, fractured ground falls can occur. Just recently a remote scoop got buried because of such a ground fall from one of the shoulders.

5.4 Measured convergences

As part of the monitoring program for Lappberget convergence measurement were taken over time on the 1080 stope 10 and 1060 stope 10. These are secondary stopes which at present allow access to the B zone through the A zone. The convergence measurements should allow more insight in any mechanisms at work in Lappberget.

A few measurements were taken to get the total picture. The convergence in the roof itself was measured using Multi Point Borehole eXtensometers (MPBX) and is

described in 5.4.1. The roof convergence relative to a "fixed" point in the footwall drift was measured to get the convergence of the roof perimeter itself. This is described in 5.4.2. The width of the access drift is measured at different points at two depths into the wall and is described in 5.4.3.

5.4.1 MPBX

MPBX is an acronym for Multi Point Borehole eXtensometer. Two of these cables have been installed in the back of the drift in 1060 stope 10. MPBX1 is installed in the ore, while MPBX2 is installed at the HW-ore contact. The extensometers are custom-built with anchor points at the positions indicated in Table 5.4. All readings are relative to Anchor 1. The anchor that is called 'collar' in Table 5.4 is installed 10 cm into the hole.

Table 5.4: Positions of the anchors on the extensometer (After Lehtola, 2008)

Anchor 1	Anchor 2	Anchor 3	Anchor 4	Anchor 5	Anchor 6	Collar
10.00 m	7.50 m	5.00 m	2.50 m	2.00 m	1.00 m	0.00 m

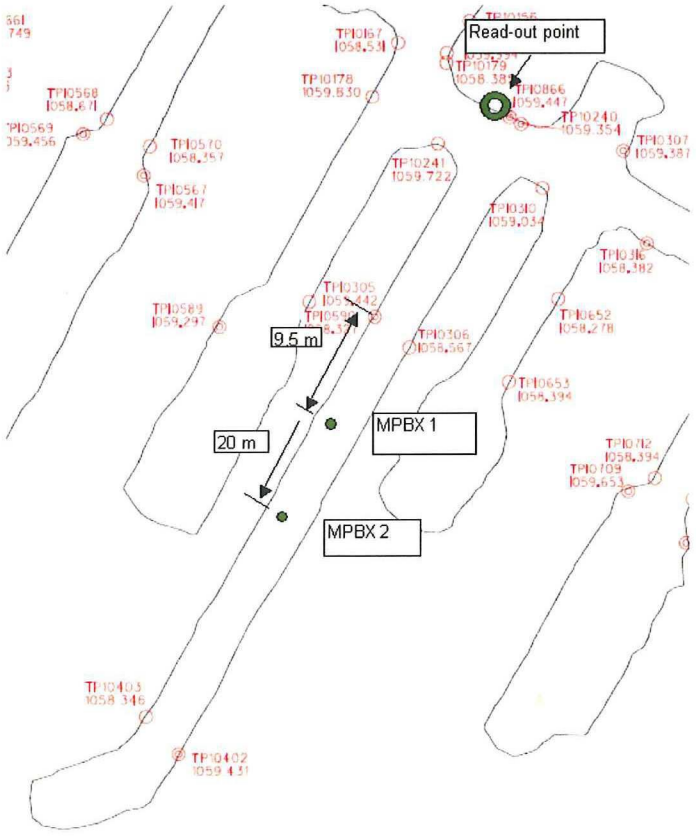

Figure 5.18: Location of the MPBXs in 1060 stope 10. (After Lehtola, 2008)

The readings of MPBX1 do not show any significant movement in the roof as all indicated displacements are less than 1mm. MPBX2 shows a lot more activity as shown in Figure 5.19.

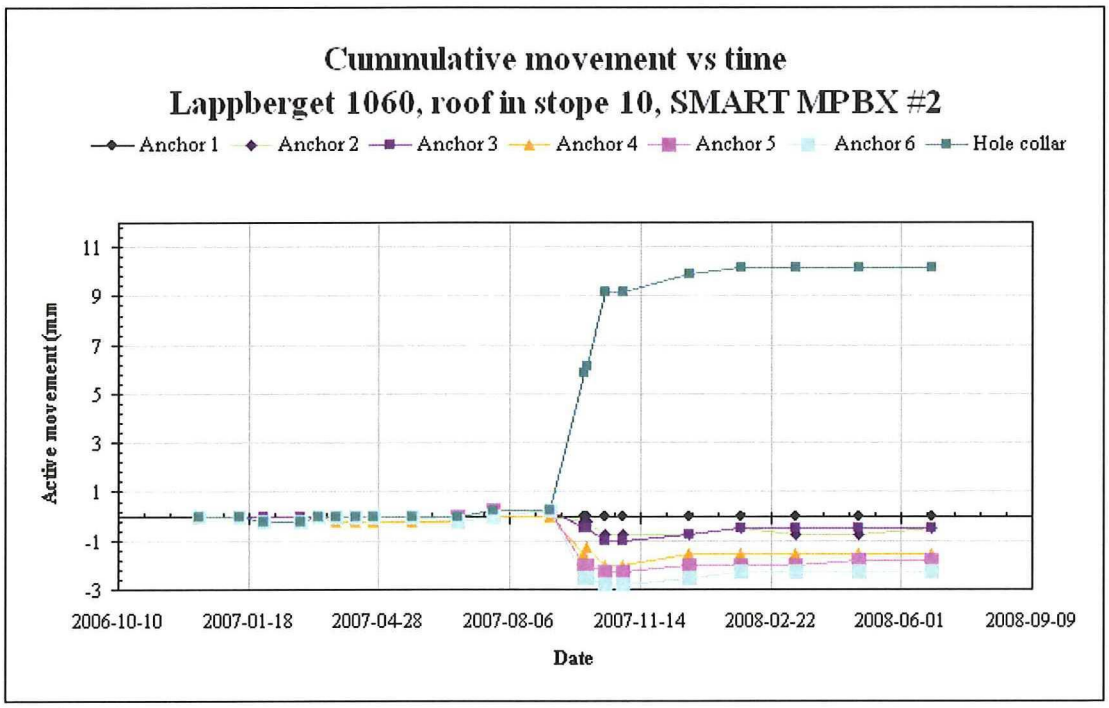

Figure 5.19: Movement on the MPBX2 (After Lehtola, 2008)

Up to September 2007 there was hardly any movement and this part of the graph is very similar to all readings from MPBX1. Data from that point started to deviate. The first meter into the hole from the collar the rock expanded nearly 14mm, while the remaining 9 meters into the hole shrunk up to 3 mm. The large change was measured between the 6th of September and the 18th of October 2007. In this time the adjacent stope 11 and stope 13 were mined between 1060 and 1040. This change would have to be plastic, as elastic relationships would give a maximum stress in the order of magnitude of 15 mS x 60 GPa = 900 MPa.

5.4.2 Roof convergence

The roof convergence measurements were taken in stope 10 on both the 1060 and 1080 levels as shown in Figure 5.20. The roof convergence measurements are relative to TP0, which is placed in the footwall drift. Each measurement point has two rock anchors that are measured. One of them is anchored at approximately 600mm into the

rock and is denoted with a K ("Kort", or short in Swedish) and the other is anchored at approximately 2.7m into the rock and is denoted with an L ("Lång", or long in Swedish).

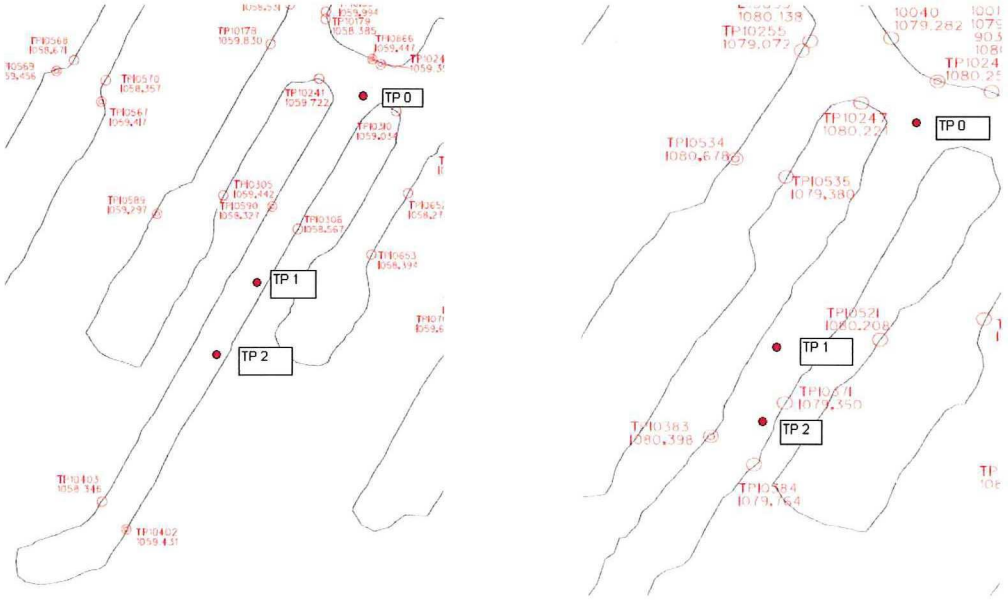

Figure 5.20: Roof convergence measuring points on 1060 (left) and 1080 (right) (After Lehtola, 2008)

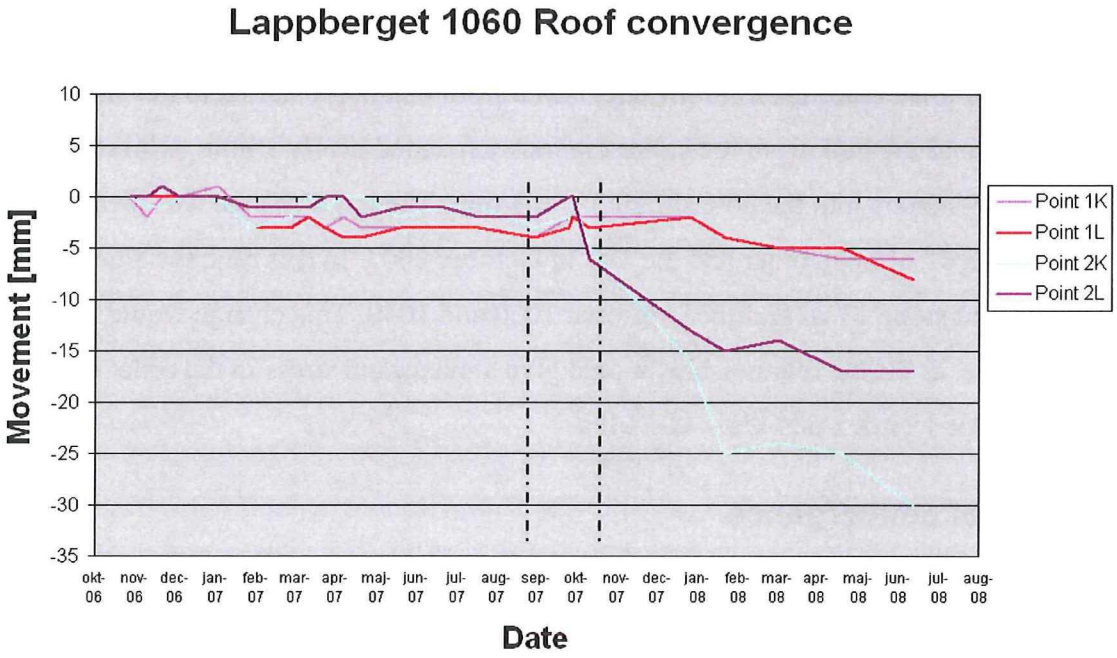

Figure 5.21: Roof convergence in 1060. The time between the dashed lines is the time interval where the major change took place in extensometer MPBX2, which is close to TP2. (After Lethola, 2008)

The roof convergences on 1080 vary between +1mm to –5mm and do not show any clear trend. The measurements on 1060 are shown in Figure 5.21.

It appears that TP2 was affected by mining rooms 11 and 13 as convergences started to increase significantly. This is not the case for point TP1. The convergences stabilize in the borehole extensometers, whereas the convergence of 2L only starts to stabilize approximately three months after rooms 11 and 13 were mined out. The difference between the 2K and 2L points is consistent with the MPBX2 difference between collar and anchor 5, which both indicate plasticity within a short distance from the perimeter.

5.4.3 Wall convergence

The wall convergences are measured on four different spots in 1060 and 1080. The distance between bolts was measured accurately between bolts that are the same as in the roof convergences.

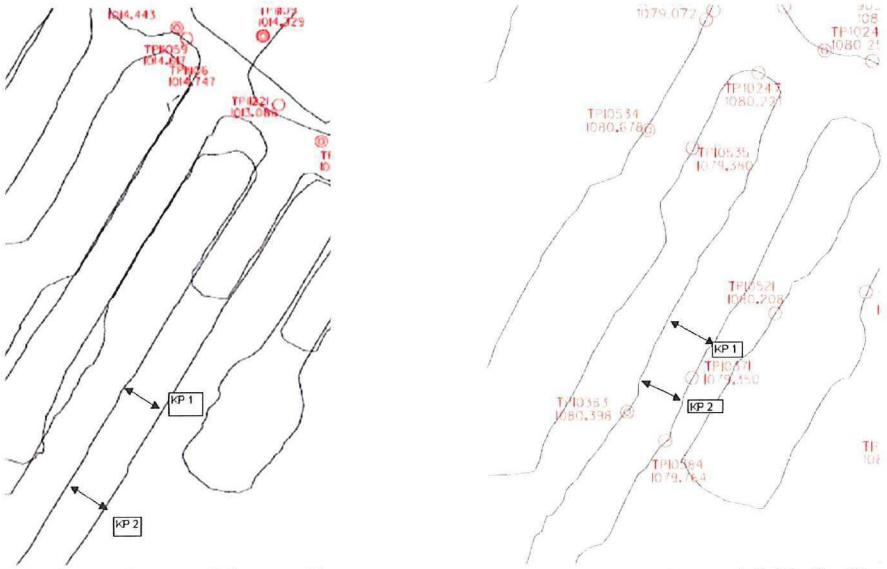

Figure 5.22: Locations of the wall convergence measurements on 1060 (left) and 1080 (right). (After Lehtola, 2008)

The results for 1060 level are shown in Figure 5.23. It appears that the convergences for KP2 were mainly impacted by stope 11 on 1080 and by stopes 11 and 13 on 1060. Positive numbers mean that the distance between the points on the walls on either side of the drift increased. For KP2 it is interesting to see that the distance between the

long bolts increased while the distance between the short bolts decreased after stope 11 on 1080 was blasted. From these numbers it is not sure which wall moved in what direction, but for the case of the large spike in September 2007 it seems reasonable to think that the major part of the deformation is due to wall movement towards stope 11.

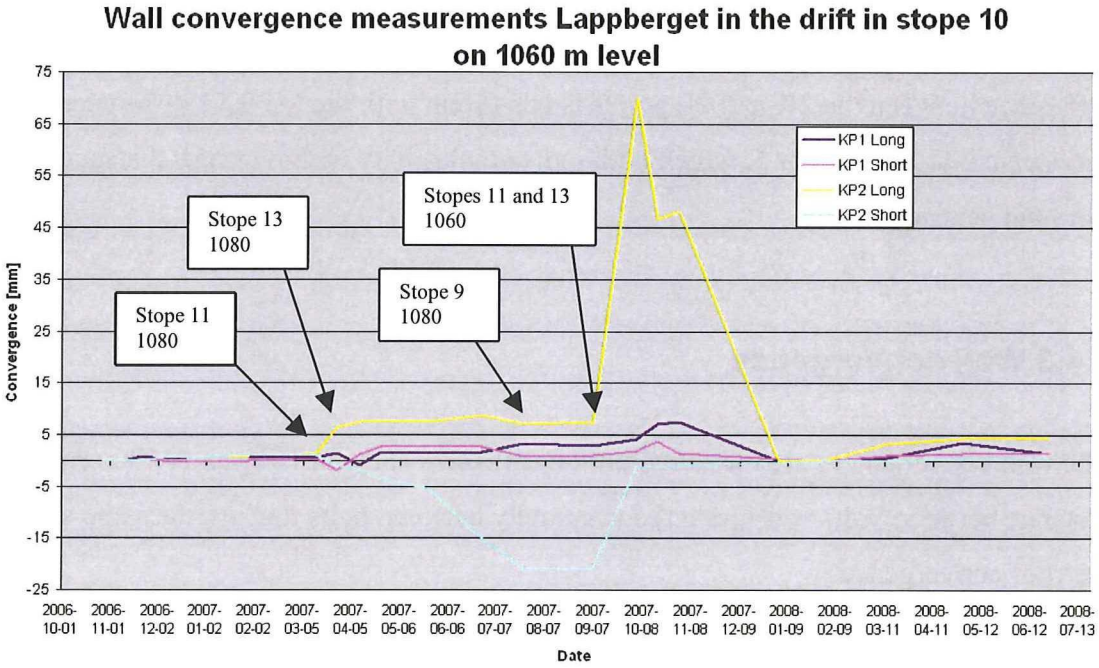

Figure 5.23: Wall convergences for 1060 level. (After Lehtola, 2008)

Unlike the wall convergences in 1060, the convergences in 1080 are only increasing, which is to say that the distance between the walls is increasing, as is shown in Figure 5.24. The explanation for the difference between KP1 on 1080 and KP1 on 1060 is not straightforward, as a similar pattern would be expected. Another point in the drift in stope 10 on 1080 was measured, close to the two survey points 10383 and 10584 in Figure 5.22. This point had two 2.7m 1" rebars installed in the walls. This point is in or very close to the ore-hanging wall contact, but the measurements were terminated as the bolts broke off twice.

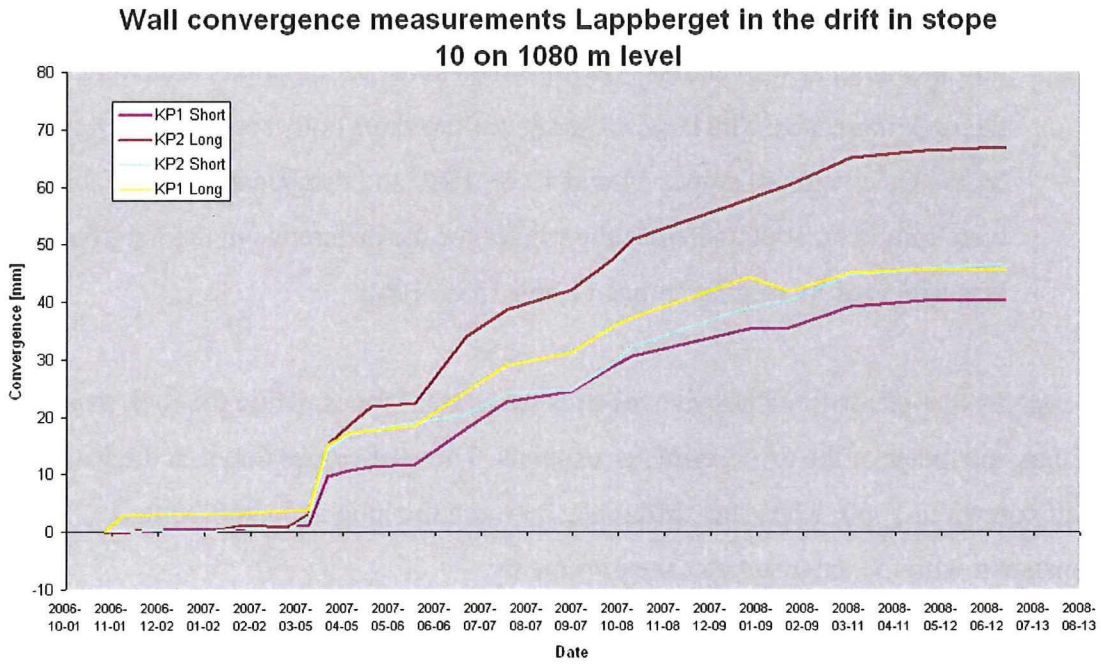

Figure 5.24: Wall convergences for 1080 level. (After Lehtola, 2008)

5.4.4 Convergence conclusions

From 5.4.1 to 5.4.3 the following conclusions can be drawn:

- The roof convergences measured on 1060 within the hanging wall contact mainly happens within one meter from the drift perimeter. The change happened over a relatively small amount of time and is sufficiently large to indicate plasticity.
- The roof itself doesn't move much in comparison with the footwall drift on 1080 level. On 1060 level the difference gradually increased over time starting from the point where a large increase was measured in the borehole extensometers. The increase is larger for the measurement point near the hanging wall contact, and the point measured 60 cm into the rock moved more than the point measured 2.7m into the rock.
- The distance measured on the walls increased on 1080 level, whereas the distances measured on 1060 level increased at large mining activities and then started decreasing again. The larger numbers were found for the hanging wall contact. The convergence on 1080 was triggered by mining stope 11 on 1080 and gradually increased with time.

- On 1060 level the distance between the walls decreased for the points 60 cm into the hanging wall contact. The distance between the points bolted 2 m into the rock increased. The largest change for the short bolts seems to be triggered by the excavation of stopes 11 and 13 on 1080 and disappear when 11 and 13 were mined on 1060, whereas the trigger for the difference in the long bolts was triggered by mining stopes 11 and 13 on 1060.

It appears that the drift walls move towards excavated stopes, while the rock mass within one meter of the drift perimeter expands. The roof comes down in the hanging wall contact in 1060, where the difference between the long and short bolts is consistent with the extensometer measurements.

5.5 References

Dahle, H., 2005, *Pilarspenningsmålinger i Lappberget, Garpenberg, Sverige*, SINTEF Berg og geoteknikk report for New Boliden AB, Trondheim, Norway. (in Norwegian)

Hoek, E. and E.T. Brown, 1980, *Underground excavations in hard rock*, A.A. Balkema, Rotterdam, the Netherlands.

Hutchinson, D.J. and M.S. Diederichs, 1996, *Cablebolting in Underground Mines,* Vancouver, Canada.

Larsson, K., 2004, *Seismicity in mines, a review*, technical report, 2004:22, Luleå University of Technology, Luleå, Sweden.

Lehtola, L., 2008, *Personal communication and convergence data.*

Martin, C.D., 1997, *The effect of cohesion loss and stress path on brittle rock strength*, Canadian Geotechnical Journal 34: 698-725.

Myrvang, A., 2001, *Bergmekanikk*, course notes for rock mechanics at the NTNU - institutt for geologi og bergteknikk, Trondheim, Norway (in Norwegian)

Nilssen, P., 2004, *Bergspenningsmålinger i Garpenberg Norra gruve*, SINTEF Bygg og miljø report for New Boliden AB, Trondheim, Norway. (in Norwegian).

Nyström, A., 2005*a*, *Description and evaluation of rock conditions for the Lappberget ore body*, Boliden AB internal report, Boliden, Sweden. (in Swedish)

Nyström, A., 2005*b*, *Besiktning av raiseborrstigen mellan 827 och 883 m nivå*, Boliden AB internal report, Boliden, Sweden. (in Swedish)

Nyström, A., 2005*c*, *Numerical analysis of stope dimensions for large scale mining of the Lappberget ore body and prognosis of mining conditions.* Boliden AB internal report TG_REP2005/004, Boliden, Sweden. (in Swedish)

Nyström, A., 2006, *Förstärkning av inslag i fältorter i Lappberget*, Boliden AB internal report, Boliden, Sweden. (in Swedish)

Nyström, A., 2008, *personal communication*, Boliden, Sweden

Rocscience Inc., 2003, *Examine3D v 4.0997*, Toronto, Canada

6. Rock mass properties

One of the key elements in a geotechnical model are the properties of the rock mass. This chapter will deal with the literature that is available on the rock types in Lappberget and on any assumptions on the missing data.

6.1 Information from core drilling

In the internal report by Anders Nyström cores from 28 holes were analysed by their geomechanical characteristics with a total length of 5894 meter. The holes were spread over Lappberget with several orientations. (Nyström, 2005)

6.1.1 Unconfined Compressive Strength by point load testing

The Unconfined Compressive Strength for the several rock types was analysed by point load testing for three holes. The point load testing was done by diametral testing only, as illustrated in Figure 6.1. (Nyström, 2005)

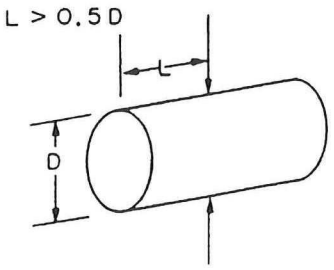

Figure 6.1: Diametral testing. (Sjöström and Sjöberg, 2000)

The results of these tests are presented in Figure 6.2. The weaker rock types are found throughout the cores, but rocks with a UCS of 100MPa and more dominated the majority. (Nyström, 2005). For some rock types there is a large spread depending on the mineral content of the tested samples. This is especially applicable for biotite quartzite, mica quartzite, sericite quartzite and sericite mica.

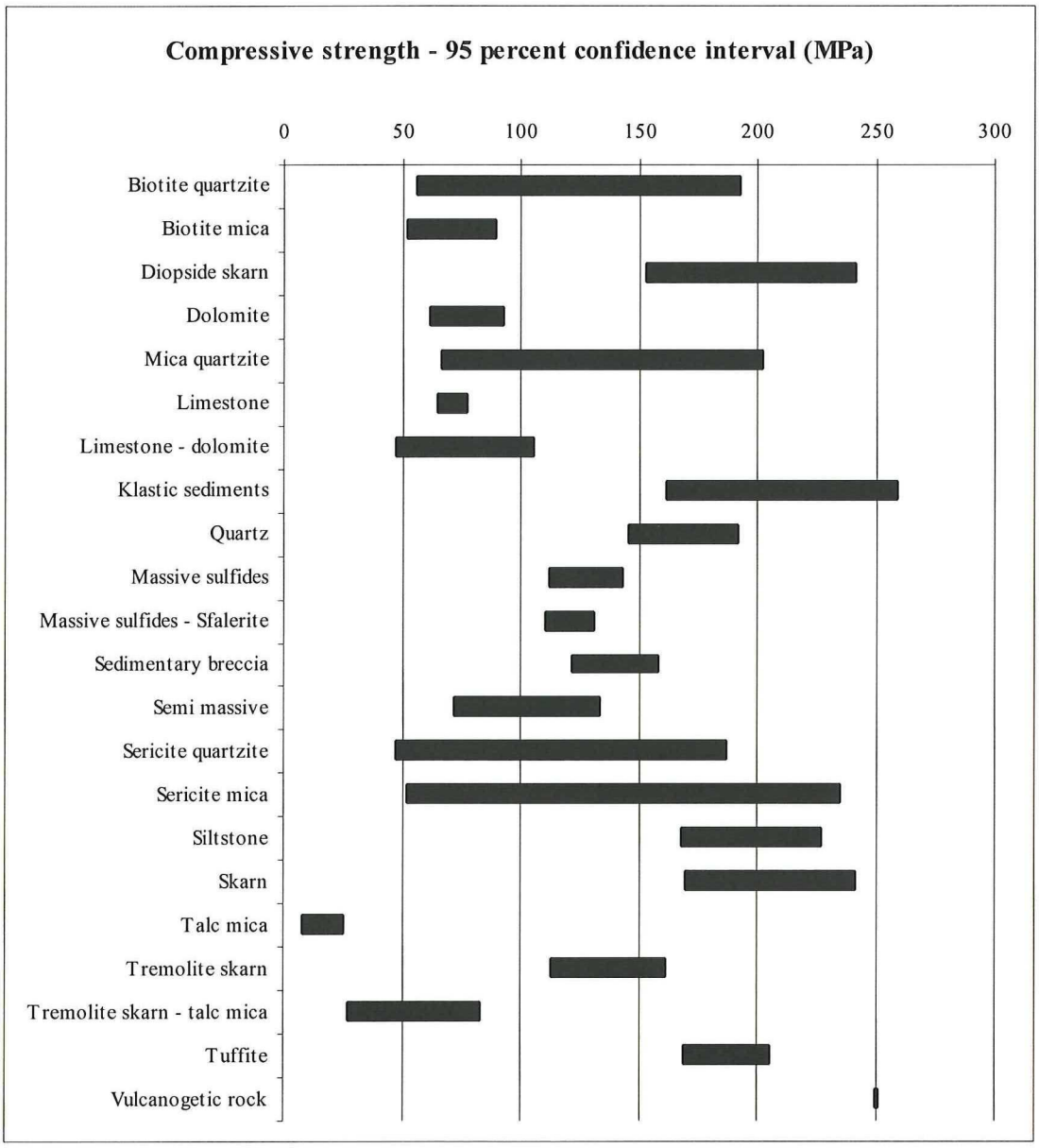

Figure 6.2: Compressive strength by point load tests for various rock types in Lappberget. (After Nyström, 2005)

6.1.2 Boliden Rock Quality Designation (BRQD)

The Rock Quality Designation (RQD) is a widely used measure of the quantity of joints within a rock sample. The RQD was developed in the sixties and Boliden developed its own variation on it called the Boliden Rock Quality Designation or BRQD. The BRQD is a more sensitive method for rocks with high joint frequencies and it is determined by the sum of the length of all the bits divided over the total length of the section. The bits are intact pieces of a specified length. For drill cores of

42mm in diameter and more the bit length is 10cm, anything less has a bit length of 5 cm. All discontinuities are counted except for the handling breaks to fit the cores in their boxes. An example is given in Figure 6.3 (Sjöberg and Sjöman, 2000)

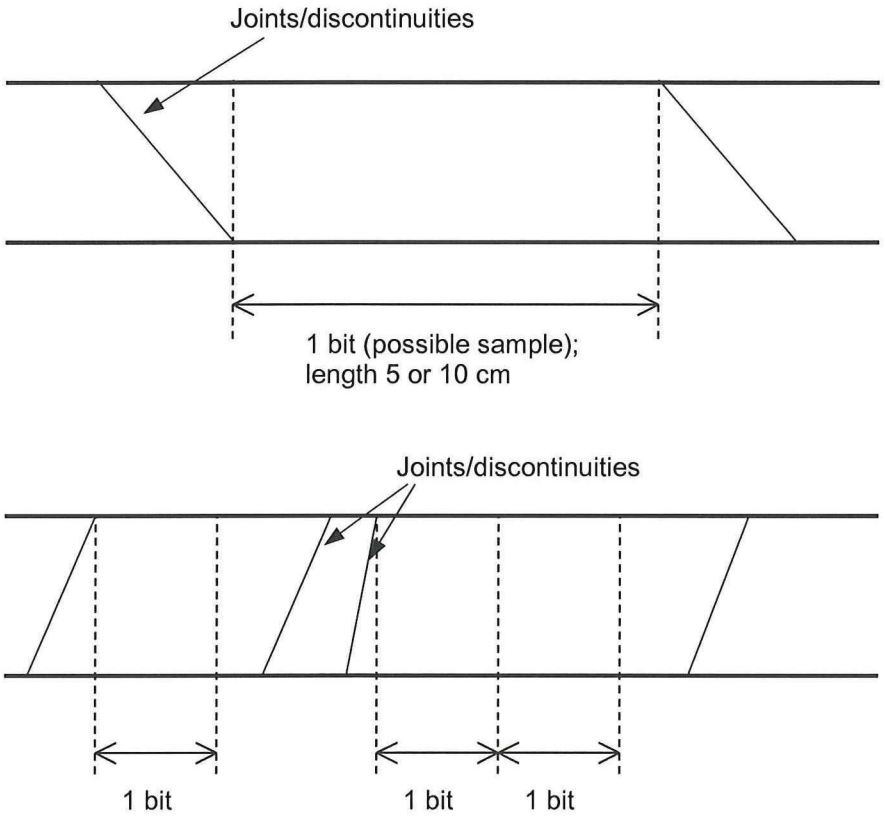

Figure 6.3: Examples of BRQD (Sjöberg and Sjöström, 2000)

The BRQD is used in a rock mass classification system (described later this chapter), which is based on the RQD system. The BRQD is always lower than the RQD. While an exact correlation is lacking, it is observed that the BRQD is approximately 20% lower. How the BRQD and RQD relate to the rock mass classification system is listed in Table 6.1. (Sjöberg and Sjöström, 2000)

Table 6.1 *RMR*-rating from *BRQD*-values. (Sjöberg and Sjöström, 2000)

BRQD (%)	*RQD* (%)	*RMR*-rating
0	< 25	3
0 - 25	25 - 50	8
25 - 50	50 - 75	13
50 - 75	75 - 90	17
75 - 90	90 - 100	20
90 - 100	90 - 100	20

The result of the BRQD assessment of over 5.5 km of core is shown in Figure 6.4. In total there was 26m (0.4%) with a BRQD of 0. Those sections are listed in Table 6.2. The joints commonly had joint infillings between 0-1mm thickness and contained talc or chlorite. (Nyström, 2005)

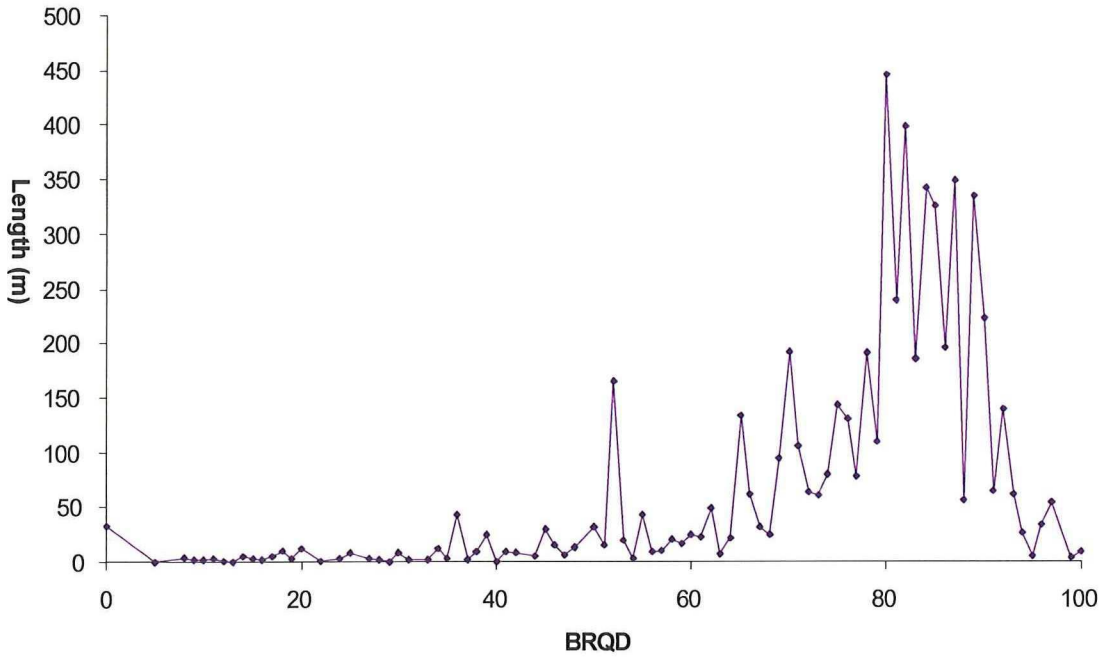

Figure 6.4: BRQD for 5754m of drill core in Lappberget (After Nyström, 2005)

Table 6.2: Sections of zero BRQD (After Nyström, 2005).

	Joint zone, joint spacing 0-5cm	Crushed zone	Clay infilling	Missing core	Core disking
Number of sections	14	18	1	1	2
Total length	11,2 m	5,4 m	0,05 m	5 m	0,5 m

6.1.3 Rock Mass Rating (RMR)

The RMR system is one of the widely used rock mass classification systems. It takes the properties of a rock mass (UCS, RQD, joint spacing, joint conditions and ground water) and assigns a score to it. Based on the sum of the assigned scores a rock mass is rated from very poor to very good rock. (Sjöberg and Sjöström, 2000).

For Lappberget 28 holes were mapped for RMR with a total length of 5894m. (Nyström, 2005) The results for each rock type are shown in Figure 6.5 and the overall results for the mapping are shown in Table 6.3.

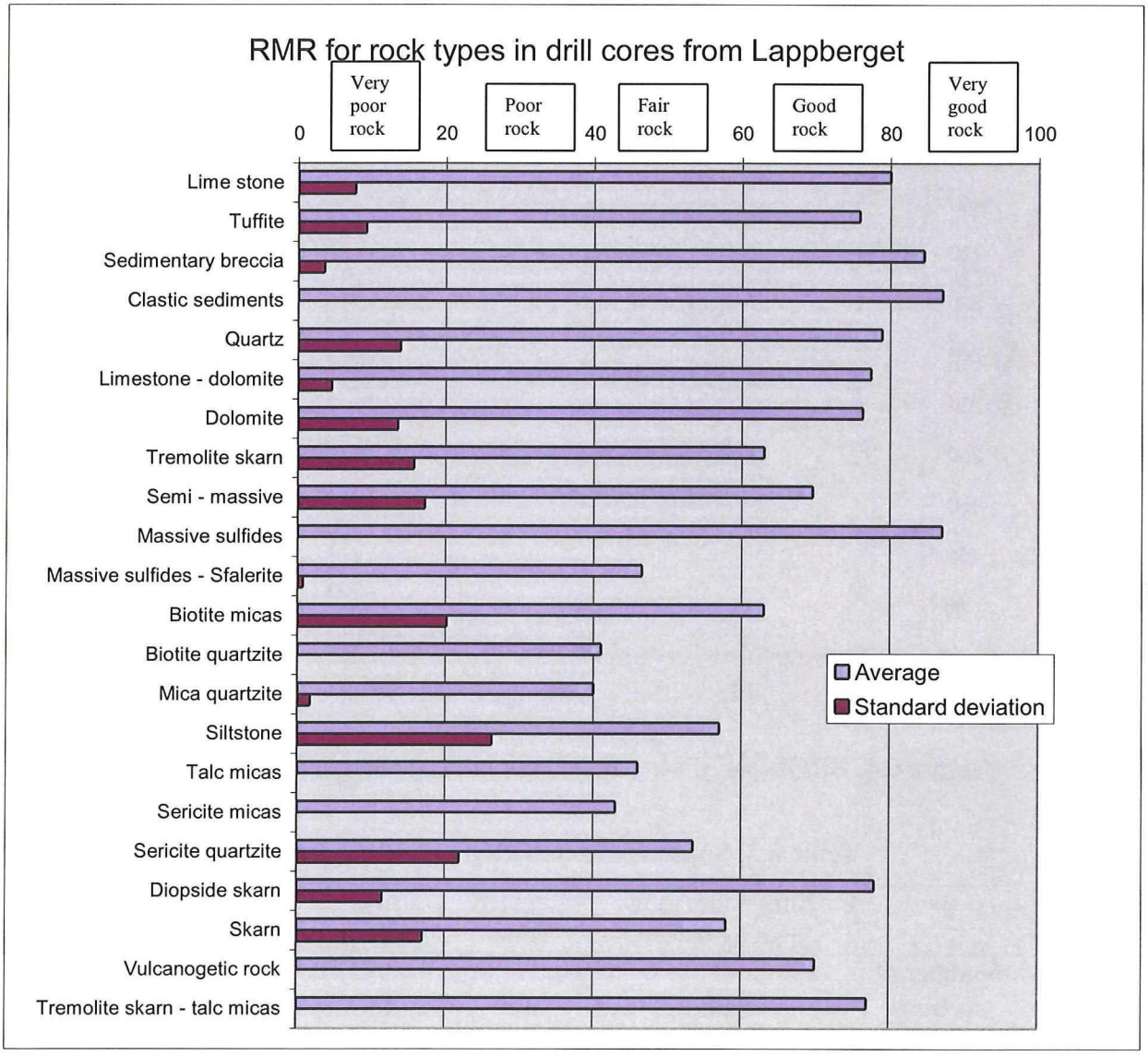

Figure 6.5: RMR from drill cores for various rock types. (After Nyström, 2005)

Table 6.3: RMR-classification of the mapped rocks (After Nyström, 2005).

Class	Percentage of the total mapped length
Very poor rock	0 %
Poor rock	1 %
Fair rock	20 %
Good rock	39 %
Very good rock	40 %

6.1.4 Mapped joints and structures

Some drifts in the cut and fill mining in the A-zone have been mapped for joints and large structures. The mapping was carried out in 2003 and the results are shown in Figure 6.6. Observations show that the joint orientation parallel to the existing foliation is dominating. Weaker zones with talc and/or mica were found in some small areas, but generally speaking the A zone has very few joints. The weaker zones are steeply dipping and are commonly found near the hanging wall contact. The B-zone is flanked by these zones on both sides. In the C-zone no strong weakness zones were identified other than the jointing parallel to the foliation. (Nyström, 2005)

Two sub vertical joint concentrations were identified. These are consistent with the change of orientation of the foliation from the A zone to the C zone as shown in Figure 6.6. These have the orientations of N46E/90 and N72E/90. Locally some sub horizontal joints were found too.(Nyström, 2005)

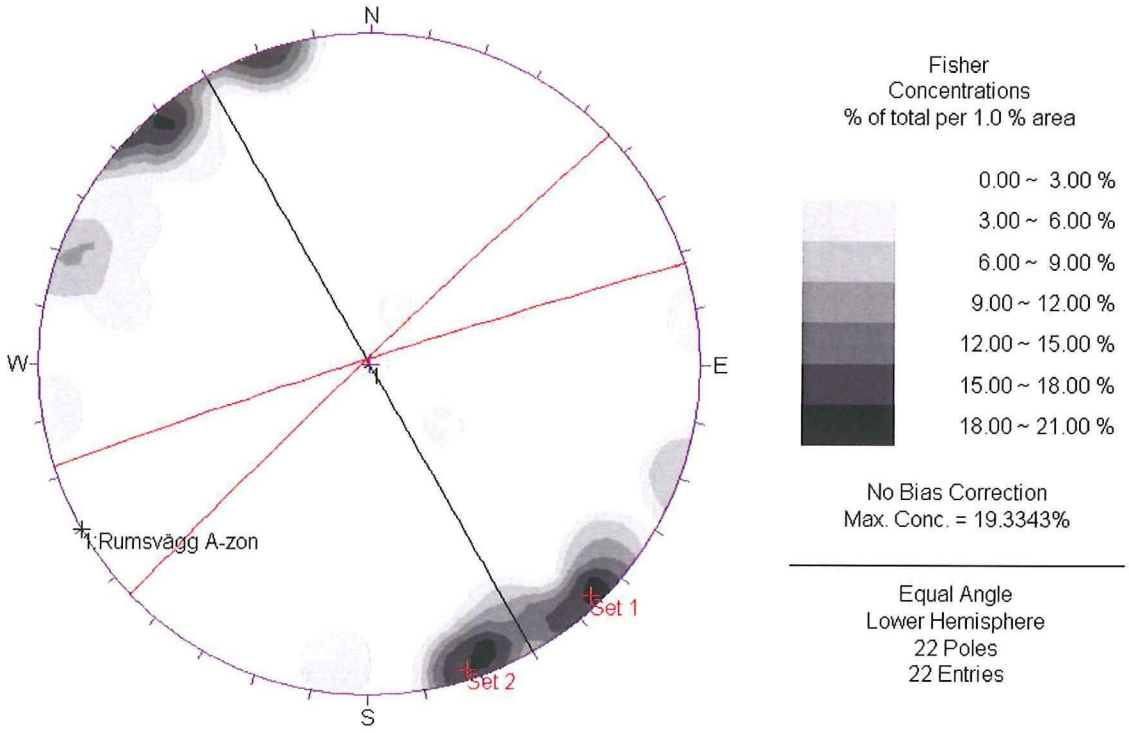

Figure 6.6: Stereographic representation of joints in drifts in Lappberget. The black plane (with associated pole Rumsvägg A-zon) is perpendicular to the strike of the A zone ore. The orientations are with respect to the geographic North. (Nyström, 2005)

6.2 Rock conditions for a potential nearby shaft

As part of the feasibility study on a new shaft close to Lappberget (~150m away, Figure 6.7) a drilling program was set up. Approximately 1250 meters of core was analysed along the planned shaft location. The majority of the cores consisted of dacite and tuffite, although some sections of sandstone, clastic sediment and limestone were found. The rock strength is high. It was estimate to be in the 100-250 MPa range. Some pieces of core have been point load tested and those results are in Table 6.4. (Nyström, 2008)

Table 6.4: Point load tests along the potential shaft outline. (Nyström, 2008)

Rock type	Number of samples	UCS (MPa)
Tuffite	6	191 ± 52
Dacite	1	176
Sandstone	3	207 ± 58

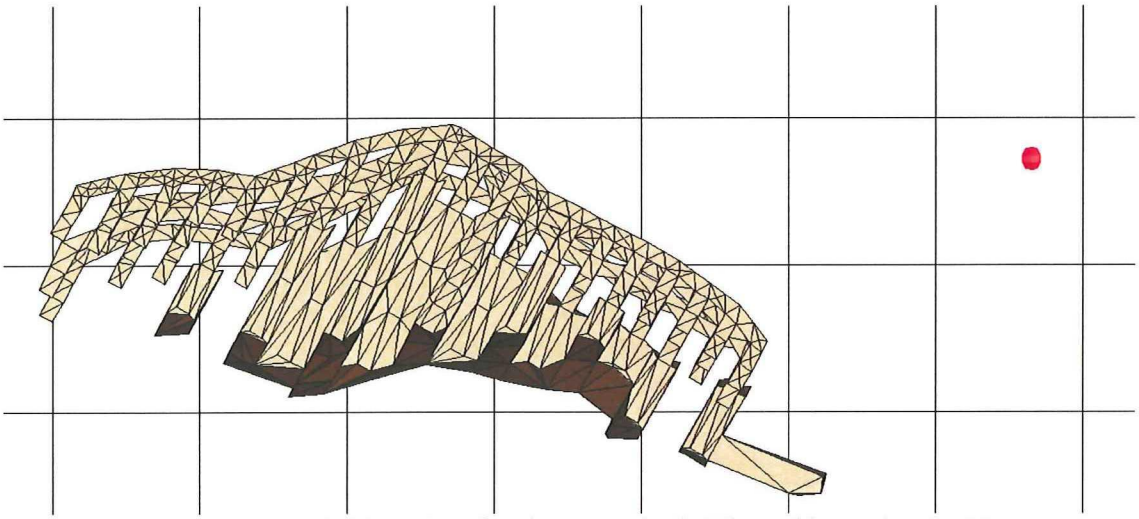

Figure 6.7: Potential location for the new shaft. The grid spacing is 50m.

Similar to the other drill cores that have been analysed the BRQD and RMR were determined. The joints were rough with hard joint infillings in the worst cases. Discoloured joint were found down to 100m below surface. Nearby ventilation shafts are dry from depths of 300m and down, where a grout curtain was successfully applied to limit the water inflow down to 200m. (Nyström, 2008). The RMR ratings are shown in Table 6.5.

Table 6.5: RMR-rating from logging of drill hole 1757 and 1774 (Nyström, 2008)

Rock mass class	Percentage of total length of drill cores (%)
Very poor rock	0
Poor rock	0
Fair rock	1
Good rock	70
Very good rock	29

The BRQD for the upper sections has quite a few traces of joints running along the core that causes the BRQD to drop significantly. In the lower section, which is the field of study in this thesis, the BRQD is exceptionally high as shown in Figure 6.8.

The presence of a very strong rock mass with very few joints in close proximity is likely significant in the analysis in this thesis. As a large intact strong rock mass can sustain a lot of stresses it can potentially cause a stiff unloading system in the Lappberget area. There is more information on unloading systems in paragraph 8.1.1.

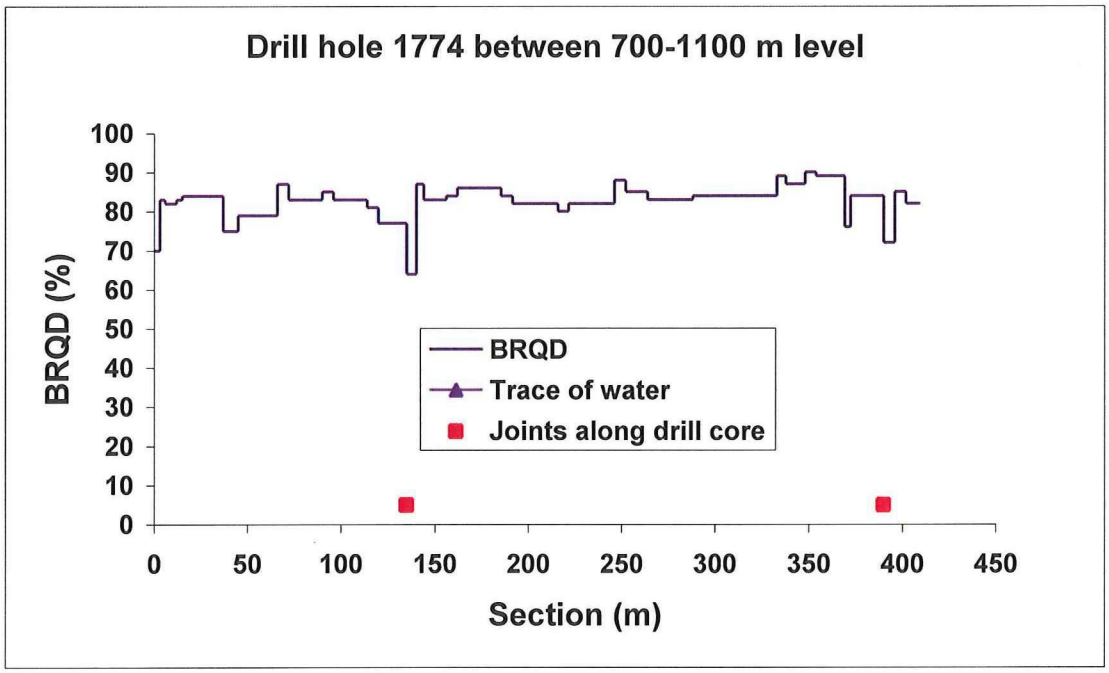

Figure 6.8: The BRQD for the lower section of the potential new shaft. (Nyström, 2008)

6.3 Elastic properties

The elastic measurements of the rock types in Lappberget are limited to the stress measurement data by Dahle and Nilssen as described in Chapter 5. The results of their biaxial tests are listed in Tables 6.6 and 6.7.

Table 6.6: Rock properties by biaxial tests for the limestone. (after Nilsson, 2004)

	E-modulus (GPa)	Poisson's ratio	UCS (MPa)	Sound velocity (m/s)	Density (kg/m^3)
883 level	55	0.17	73	4217	2714
967 level	60	0.12	100	4860	2722

Table 6.7: Rock properties by biaxial tests for the ore. (Dahle, 2005)

Measurement location	E-modulus (GPa)	Poisson's ratio	UCS (MPa)	Sound velocity (m/s)	Density (kg/m^3)
Hole 1	84.7 $^+/_-$ 10.4	0.15 $^+/_-$ 0.03	196 $^+/_-$ 65.1	5147	3331
Hole 2	90.7 $^+/_-$ 15.6	0.15 $^+/_-$ 0.04	146 $^+/_-$ 14.0	4687	3270

6.4 Pastefill

Paste is used for backfill in major parts of Lappberget. The secondary stopes might be (partly) filled with rockfill. Pastefill has the advantages that it is homogeneous throughout the process, it binds with water (limited run-off) and that the entire fine

fraction from the mill can be used. The paste is produced in the paste plant on surface near the Garpenberg Norra shaft (Figure 6.9) from where the paste is distributed underground by pipelines. The resulting paste has the viscosity between toothpaste and peanut butter when it is poured into the empty stope. (Marklund, 2003)

Figure 6.9: The paste plant near the Garpenberg Norra shaft (Marklund, 2003)

The requirements of the fill depend on the stope dimensions and sequencing. Because the fill needs to maintain its integrity when blasted in the adjacent stope the fill requirements become important. When the primary stopes become larger they need to be stable for larger spans and the required paste strength will increase. The recipe of the paste is adjusted accordingly, following the guidelines in Table 6.8.

For secondary stopes the main objective is to provide a stable fast curing work floor, because the fill in de secondary stopes will not be subject to a large open spans. To provide a more rugged floor the top part of the stope is filled with a layer of rockfill.

Table 6.8: Recipes for the paste. (After Marklund, 2003)

Required strength	Percentage binder	Lab strength
200 kPa	2 %	320 kPa
200 – 500 kPa	2.5 %	480 kPa
500 – 1000 kPa	4.5 %	1150 kPa
1000 – 1250 kPa	5 %	1300 kPa
1250 – 1500 kPa	5.5 %	1450 kPa

Figure 6.10 shows the lower part of Lappberget with the calculated fill requirements, for which the recipes from Table 6.8 are used. These numbers are based on the open spans the stopes are exposed to.

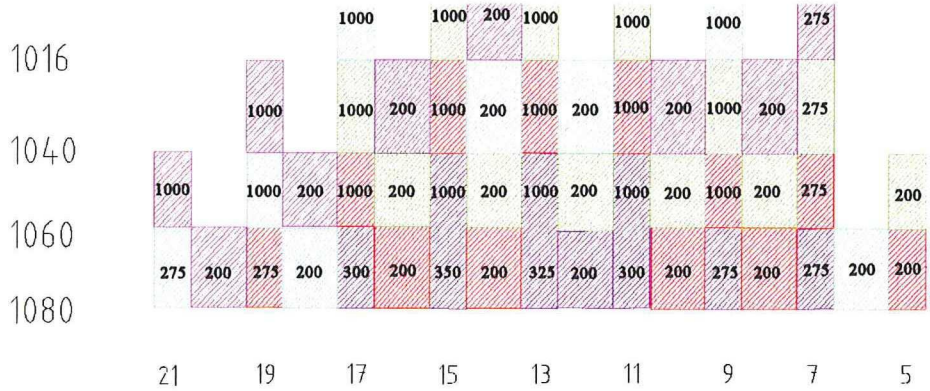

Figure 6.10: Paste requirements for the lower part of Lappberget. The numbers in the stopes refer to the UCS of the paste in kPa. (Marklund, 2003)

6.5 References

Dahle, H., 2005, *Pilarspenningsmålinger i Lappberget, Garpenberg, Sverige*, SINTEF Berg og geoteknikk report for New Boliden AB, Trondheim, Norway. (in Norwegian)

Marklund, P.I., 2002, *Pastafyll*, presentation on pastefill for a course on rock support, Boliden, Sweden. (in Swedish)

Nilssen, P., 2004, *Bergspenningsmålinger i Garpenberg Norra gruve*, SINTEF Bygg og miljø report for New Boliden AB, Trondheim, Norway. (in Norwegian).

Nyström, A., 2005, *Description and rock conditions for the Lappberget ore body*, Boliden internal report TG_REP2005/008. (in Swedish)

Nyström, A., 2008, *Estimation of rock conditions for a new hoisting shaft in Garpenberg,* Boliden internal memo, Boliden, Sweden

Sjöberg, J. and J. Sjöström, 2000, *Rock Mechanics Core Logging – Boliden Standard*, Boliden internal report B6/00.

Sjöström, J. and J. Sjöberg, 2000, *Point Load Testing of Drill Cores – Boliden Standard*, Boliden internal report B7/00

7. Numerical modelling

Numerical modelling can provide more insight in the problem and is widely used throughout the industry. Model verification is probably one of the most important aspects of modelling. It is vital to have reliable models by evaluating the mechanisms of events that happened in the past to meaningfully predict future conditions. Misleading models are a waste of time and money at best; in the worst case they can compromise the safety of personnel and equipment.

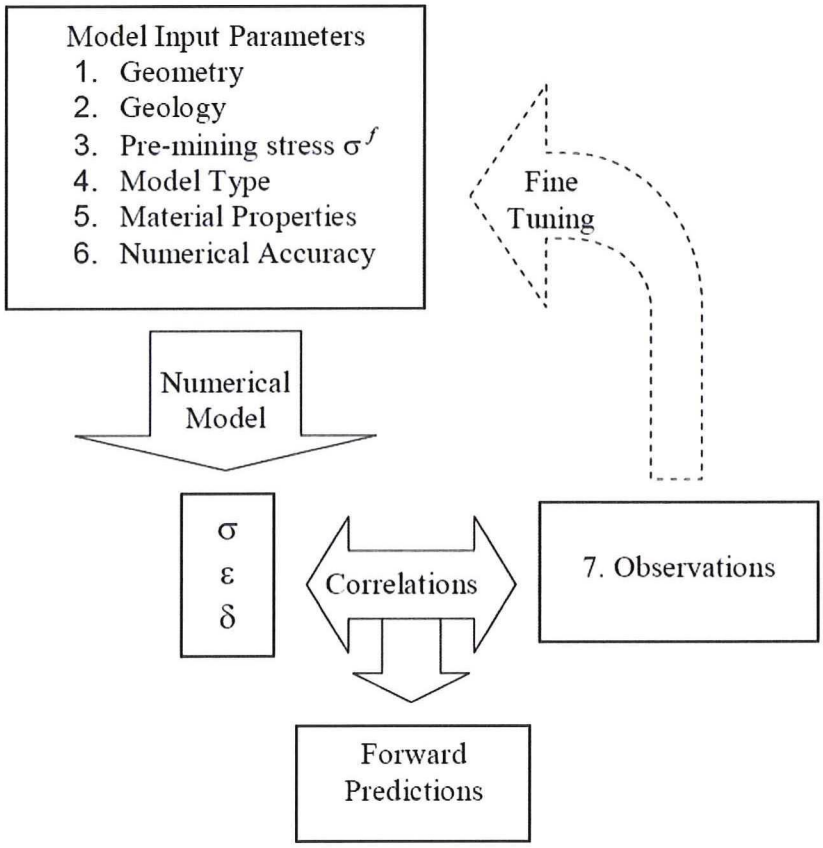

Figure 7.1: Model inputs and verification process (Wiles, 2007)

An effort will be made to follow the schedule in Figure 7.1. The observations seen in Lappberget have to show in the model or else the model needs to be revised. Simple models are preferred to more complex models as the limited number of input parameters can be calibrated easily. The total error is determined by the error in each component, so care must be taken in looking at the entire picture to determine where the largest source of error is and how it can be reduced while making sure the

improvement of one parameter is not at the expense of one or more other parameters. (Wiles, 2007)

In addition it should be noted that anticipating the solutions and possible model outcomes is an important aspect of numerical modelling. A model is a simplification of reality rather than an imitation of reality. It should also be driven by the questions that it is supposed to answer rather than trying to get every single detail right. The two methods used in this thesis have a lot of limitations, yet combined they could/will provide some insight each from their own perspective. The numerical model is a mere tool in coming to a solution, instead of being the goal on itself. (Starfield and Cundall, 1988)

7.1 Numerical methods

While the choice of method is limited to the available software, it might be worthwhile to look at the codes that are available. For this thesis the methods are limited to a three-dimensional boundary element method and a two-dimensional finite element method.

7.1.1 Boundary Element Method (BEM)

The boundary element method (BEM) is a method to evaluate the influence of a geometry in an infinite continuous elastic medium. The following is a simplified explanation about 2D BEM from Hoek and Brown while avoiding the mathematical formulations.

The problem is to determine the tractions on a boundary of an excavation. Prior to excavation, the rock (to be removed) will provide support to the surrounding rock. This support can be seen in terms of normal and tangential tractions on the boundary and these tractions will vary in magnitude from point to point, depending on the orientation of the boundary on that point. This is illustrated on the left two sketches in Figure 7.2. When the rock is removed the support it gave prior to that reduces to zero and the action can be seen as applying negative tractions to the boundary, illustrated

by the upper right sketch in Figure 7.2. The resulting state of stress is then a combination of the initial state of stress and the stress changes due to the excavation. Finding the distribution of the forces that were induced by introducing negative tractions is the next step.

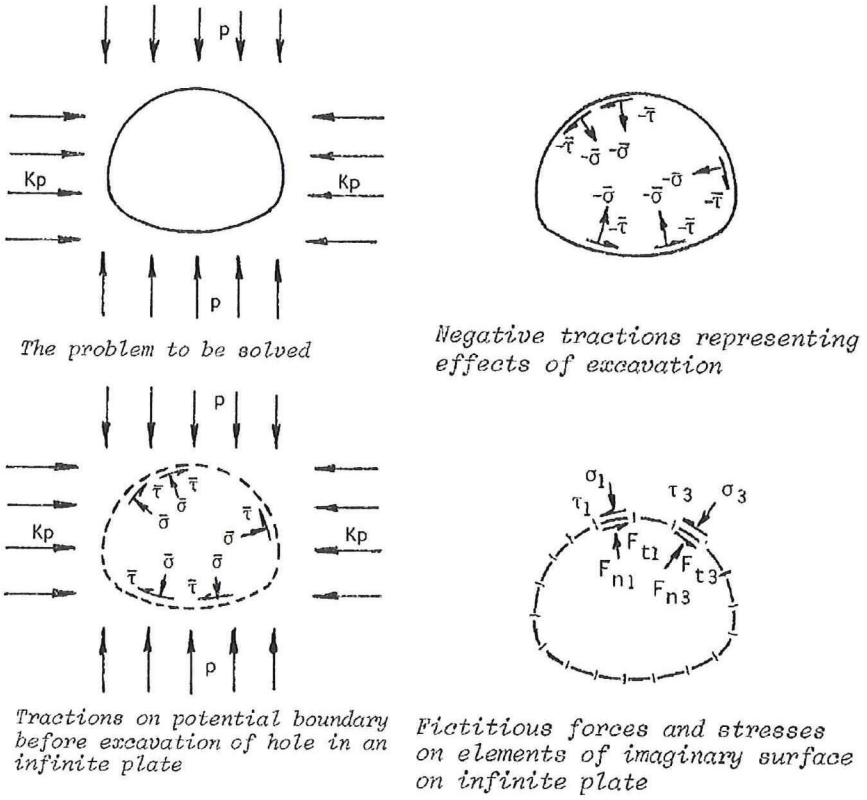

Figure 7.2: Sketches illustrating 2D BEM (Hoek and Brown, 1980)

The fourth sketch in Figure 7.2 should be seen as an imaginary solid plate with the boundary drawn on it. The plate is unstressed in infinity. The boundary is split up into elements and forces are applied (uniformly or other) on each element. There are two forces for each element; normal and tangential forces. These forces are referred to as fictitious forces, as they do not correspond with any real forces applied on the original boundary. The procedure is to adjust the fictitious forces until the state of stress in the middle of the element is sufficiently equal to the negative tractions in that point. Once the load is applied on element 1 so that the stresses in the middle of element 1 correspond to the tractions, it will influence all the other elements by the adjustment. By adjusting the load on element 2, it will in turn influence the state of stress in

element 1 and all other elements. By iteration an approximation for the loads on the elements can be found.

Once the iteration is complete, the tractions on the imaginary and "real" plate are the same. These tractions determine the induced state of stress, so the change in state of stress at any point may be calculated from the imaginary plate as well. Using standard expressions for point loads on all loads applied in the imaginary plate results in the calculation of the induced state of stress. As the loads are applied on elements instead of points the point load equations should be integrated according to the way the load is distributed on the elements.

To come to the stresses following excavation the induced stresses have to be added to the virgin state of stress. Displacements can be calculated in a similar fashion, as there are standard equations for the calculation of displacements in an infinite medium from point loads, similar to the procedure to calculate the altered state of stress. (Hoek and Brown, 1980)

7.1.2 Finite Element Method (FEM)

The Finite Element Method (FEM) takes the area surrounding an excavation and divides the domain into discrete, interacting elements. Unlike the BEM there is a boundary to the modelled domain, upon which boundary conditions can be applied. Figure 7.3 shows such a problem area and a conceptual discretization with boundary conditions. The problem is to find the state of total stress, and the excavation-induced displacements, through the assembly of a finite number of elements. (Brady and Brown, 2004)

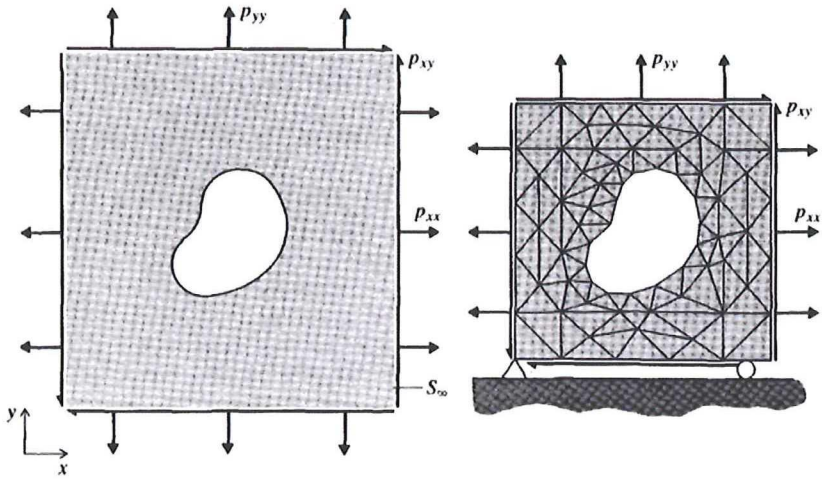

Figure 7.3: Problem discretization in 2D FEM. (Brady and Brown, 2004)

The main steps in the FEM are (McKinnon, 2006):

1. **Discretization of the continuum**
   The first step is to divide the domain in triangles or other, more complicated, shapes.
2. **Selection of the displacement model.**
   This has to be some polynomial function to describe the displacement between the nodes in the elements. The simplest function is linear. More complicated interpolation functions can be used too, as long as it returns the nodal displacements at the nodes.
3. **Derivation of the stiffness matrix.**
   The stiffness matrix contains the coefficients of the material and geometric properties of the element. The stiffness relates the displacements a node to the applied forces of that or another node in the element.
4. **Assembly of algebraic equations for the overall discretized continuum.**
   This is the assembly of all the stiffness matrixes of the elements into one matrix for the entire problem (Global matrix). All elements connected to one node have to have the same nodal displacements for that node. The initial load is also taken into account by constructing an internal load vector.
5. **Solution of unknown displacements from the global stiffness matrix**
   The global stiffness matrix, the initial loading vector and the boundary conditions provide sufficient data to provide the nodal displacements. This is

relatively simple if the displacement models are linear and requires some effort for more complex functions.

6. **Calculation of stresses and strains from the nodal displacements.**
   The stresses and strains in the elements can now be readily calculated from the nodal displacements.

7.1.3 Software

Examine3D

There is a software package available at Boliden for a three-dimensional Boundary Element Method called Examine3D (Rocscience, 2003). The model-building module of this program accommodates DXF files to import triangulations and outlines as well as basic CAD functions. There are some convenient features in the model-building feature, such as the option to check for overlapping and invalid elements and the option to check if the model is "watertight". Locations of seismic events can be inserted in the model to calculate the modelled stresses and displacements in these points.

Once the model is finished and valid, it can be calculated in the computation-module. The models can be calculated in batches. The most important bottleneck in this process is internal memory of the computer. It makes a significant difference in calculation time if the solution matrix to compute the fictitious loads can fit in the internal memory. If this is not the case the matrix has to be spit up into several matrixes and that requires much more iteration. Most model matrixes fit in the 1024 MB internal memory that was available for the program on the computer available for computation by Boliden.

The results-module can generate any kind of combination of the stress tensor components and the displacements. Aside from the obvious ones, such as Sigma 1 and total displacement, there is a function which allows the user to compute any parameter from the stress tensor and displacements. This is relevant as the strain energy could be calculated as well as the potential for shear failure.

Since the BEM is a fully elastic method it does not account any failed zones. There is a function, however, that indicates the zone of failure based on the inserted failure criteria.

Phase2

Phase2 is another program made by Rocscience. It is a user-friendly two-dimensional elasto-plastic finite element program. It allows multiple stages per model and has a range of possible failure criteria built in. Furthermore liners, bolts and other forms of support can be added with various degrees of complexity.

Similar to Examine3D there are three different modules to the program. The model-building, the computational and the interpretation modules. In the interpret stage queries can be made on all sorts of data without specifying the location of the measurement point in the model-building stage, which is of great comfort.

The user friendliness allows the user to easily build in all sorts of complex operations, which is both an advantage and a disadvantage. Care has to be taken in selecting parameters and properties that make sense.

7.2 Models in Examine3D

As described in the previous section Examine3D is mainly evaluating the influence of geometry of the excavations on the state of stress. This is a good starting point to evaluate the strain energies in the rock, to see what the area is for potential slip and how this changes over the life of the orebody. In this thesis, only the part of the ore body between 1080 and 822 will be evaluated, as this is the deepest part currently in production. If there is any potential for seismicity it will likely manifest itself in the deepest part due to higher stresses.

7.2.1 Geometry

Simultaneously with this thesis a new planning software package (iGantt) is taken into use. For the planning software all of the latest stope designs with the rough dimensions needed to be implemented by means of triangulating the stopes individually (Koivisto, 2008). Those triangulations were also used to model the geometry in Examine3D (Rocscience, 2003). The triangulations were converted from Microstation files (Bentley, 2006) to DXF files, which could in turn be converted with a little utility that comes with Examine3D to a GEO format that was then imported into Examine3D. The imported file had to be manipulated to create a consistent "watertight" solid. In the manipulation process the triangulations had to be simplified in some spots, although effort was made to keep that to a minimum.

The triangulations for the mined cut and fill area between 822 and approximately 880 were lacking, because they are not relevant for the planning software (as this is already mined). For modelling purposes a simple geometry is thought to be sufficient to redirect the stresses into the sill pillar. The cut and fill area is therefore made by taking the ore outline at 896 level, moving it up to 881 elevation and then extruding it to 821 elevation. The 896 ore outline was somewhat simplified by reducing the number of nodes on the string to reduce the amount of elements.

The infrastructure associated with this part of Lappberget was partly not designed yet and partly not updated for new ore outlines. A simple design for the footwall drifts and crosscuts was therefore made by taking the ore outlines from Microstation (Bentley, 2006) and by drawing the wall outlines in AutoCAD (Autodesk, 2004). Drawing could have been done in Microstation too, but the author has no proficiency in this software package. The wall outlines were then imported into Examine3D, manipulated and then stored as portable triangulations for Examine3D. This has the advantage that they can be imported into any model.

The simplified infrastructure has drifts that are 5x5m square drifts. The drifts are oriented parallel to the orientation of the stope and the drifts are centred on the stopes, which means that the centrelines of the crosscuts are effectively 12.50m apart. The distance between the stopes and the roughly perpendicular footwall drift is 15 meters.

The design is illustrated in Figure 7.4 and the resulting portable infrastructure is shown in Figure 7.5. The infrastructure is lacking a floor and back at this stage to minimise the amount of elements in the construction phase.

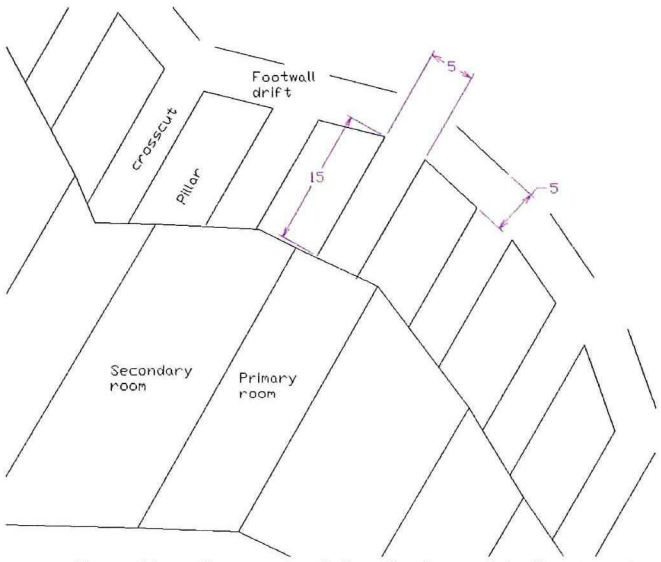

Figure 7.4: Some wall outline for part of the designed infrastructure for 956 level.

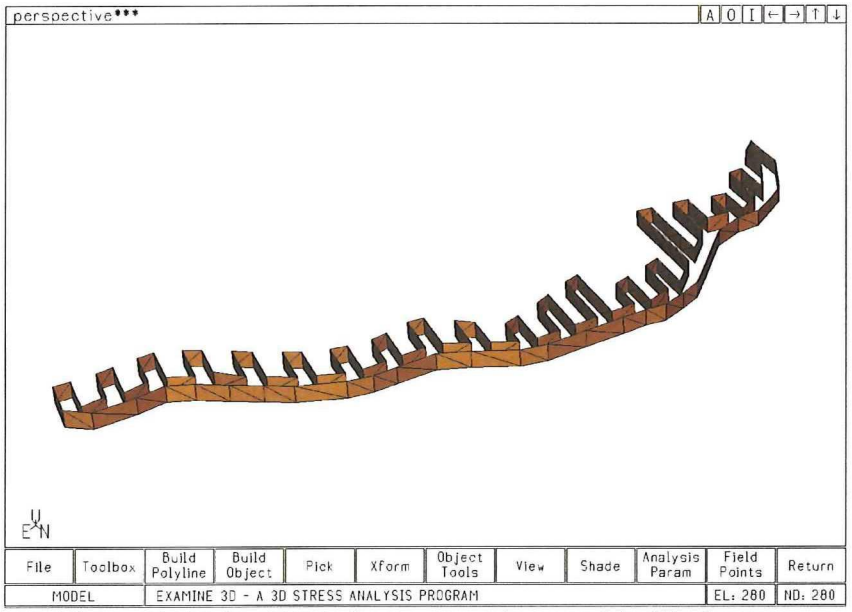

Figure 7.5: The 956 infrastructure in portable file format.

Once the infrastructure was imported into the appropriate stages it had to be knitted to the solid made out of stopes. In the end all stages had to be separate models that need to be "watertight". The several stages are described in 7.2.2.

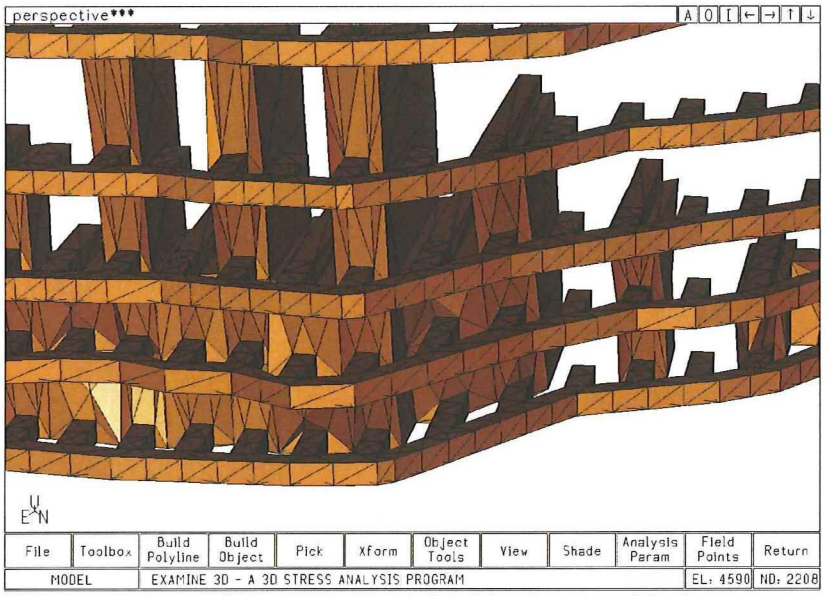

Figure 7.6: Part of the 2009 model with associated infrastructure.

Figure 7.6 shows a part of the model for 2009 with the infrastructure tied into it. As can be seen in this picture the top accesses of the drifts run to the end of the stope for both primary and secondary stopes. The mesh density will be discussed in 7.2.3.

7.2.2 Progressive stages in mining Lappberget

At present time the stopes in Lappberget have been sequenced up to 2011 (Koivisto, 2008). In order to get a picture of the entire life of the lower part of Lappberget the remaining stopes had to be sequenced as well. This was done according to Figure 7.7. The idea behind the sequencing is to maintain the sawtooth pyramid shape as much as possible. While the actual sequence can and probably will change and is not necessarily within the correct time frame, it should provide sufficient understanding of the underlying mechanisms. If the actual stope sequence is then not followed as the quick design used in determining the different stages should not matter too much as long as the general sawtooth pyramid shapes are maintained as much as possible.

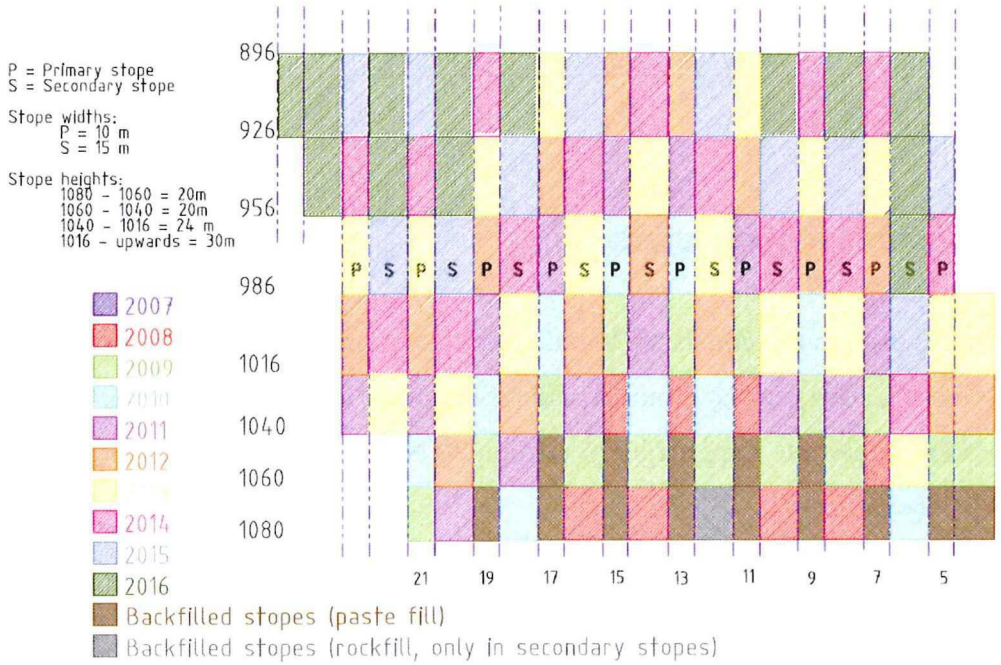

Figure 7.7: Sequencing of the lower part of Lappberget.

Models were constructed in Examine3D with the appropriate stopes as indicated in Figure 7.7. Isometric views of all of the models can be found in Appendix B.

7.2.3 Mesh density

The mesh density is a trade-off. It influences the mathematical accuracy of the model and at the same time increases the calculation time dramatically. The element sizes in the models depend a bit on the location of the element in the model, but are generally smaller than 5 meters across on the hanging wall and stope walls and smaller than 2 meters across on the infrastructure and footwall side. The total amount of elements and nodes is shown in Table 7.1.

Table 7.1: Nodes and elements in the Examine3D models

Model	Elements	Nodes
2008	14488	7190
2009	19016	9421
2010	23288	11532
2011	26016	12870
2012	36736	18200
2013	38128	18856
2014	38240	18882

2015	38960	19220
2016	39928	19676

7.2.4 Geotechnical parameters

The parameters used in all models are based on the stress measurements done by SINTEF (Nilssen, 2004) and by a model calibration on the rock strength of pillars in the new workshop close to Lappberget (Nyström, 2005). The stress measurements are described in Chapter 5.

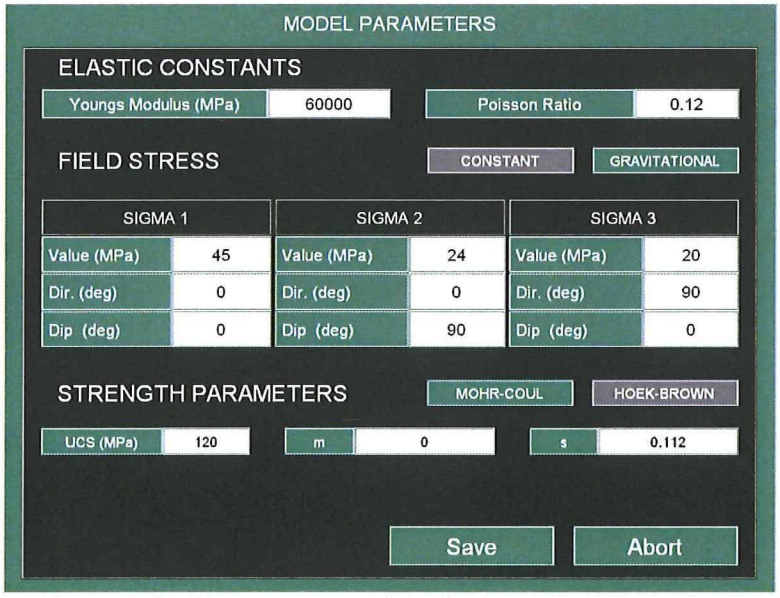

Figure 7.8: Parameters used in the Examine3D models.

Figure 7.8 shows the required input parameters. The strength parameters are used to indicate areas where the stresses have exceeded the strength of the rock and this is not used for further calculation. The elastic constants are taken from the stress measurements at 967 elevation (Nilssen, 2004). Since the stresses measured at 883 are quite a bit higher than the ones measured at 967 it seems justified to use these conservative numbers and use them as constant stresses for the entire lower part of Lappberget.

In calibrating the strength factor of the models it was found that the depth of failure in the limestone pillars in the new workshop corresponded with an UCS between 100

and 150 MPa, while taking s at 0.112 and reducing m to zero in the Hoek Brown criterion (Nyström, 2005). The effective failure criterion then becomes $\sigma_1 - \sigma_3 = {}^1/_3\ \sigma_c$, which was found to be the point where shear failure initiates according to a Canadian study in intact granite (Martin, 1997). This should provide an indication for the depth of failure in the Limestone footwall. The number can be changed for the ore by setting the failure criterion at a revised strength factor. A calibration such as the study around the workshop is not available for the ore.

The model tolerance was left at the default level. Computation times for all models were approximately 23 hours altogether.

7.3 Models in Phase2

Complimentary to the elastic models in Examine3D a simple model was built in Phase2 to look at the influence of the weak talc zone in the hanging wall and the influence on any potential zones where plasticity might occur. The model was largely conceptual, as the geometry of the weakness zones is not exactly known. In addition there is the problem with representing a complex three-dimensional geometry in a two-dimensional plane.

7.3.1 3D geometry in 2D software

Two-dimensional models are ideally constructed for situations of plane strain. This means that the stresses normal to the plane of the model would have to be constant over a large distance, such that the strains acting normal to that plane are constant and can be neglected. In the case of Lappberget the geometry of the stopes do not allow for such a situation as stresses are guided around the primary stopes into the secondary stopes.

Even for the last stage in Lappberget when only a sill pillar is left a two-dimensional elasto-plastic model would not suffice, as the stresses were not evenly distributed in previous stages. This would lead to an uneven distribution of plasticity, which in turn influences the state of stress in the last stage because plasticity is irreversible.

Nevertheless a simplified model could be useful in analysing the talc zone in the hanging wall and potential plastic zones. It should be noted that the magnitude and orientation of stresses and the associated displacements and plasticity differs from the modelled values. For primary stopes the induced effects are probably less dramatic, because there are two pillars (secondary stopes) on either side. For the secondary stopes it should be noted that the amount of stress, plasticity and displacements is probably higher, as stresses have already been guided around the primary stopes.

7.3.2 Progressive stages in mining Lappberget

Similar to the Examine3D models, a progressive mining model was built. In Phase2 all progressive stages can be modelled in one model to account for plasticity along the process. The ore body outline between stope 9 and 10 was selected. The outline coordinates in three dimensions were recalculated to get the outline in one plane so only two dimensions were left.

By adding stages in the model the mining sequence can be simulated. These stages are shown in Appendix C. Figure 7.9 shows the model for the 1016 level. Instead of modelling the pastefill as a material, loads were applied on the circumference of the previous stages. These loads are based on the silo sidewall pressures in Figure 7.10.

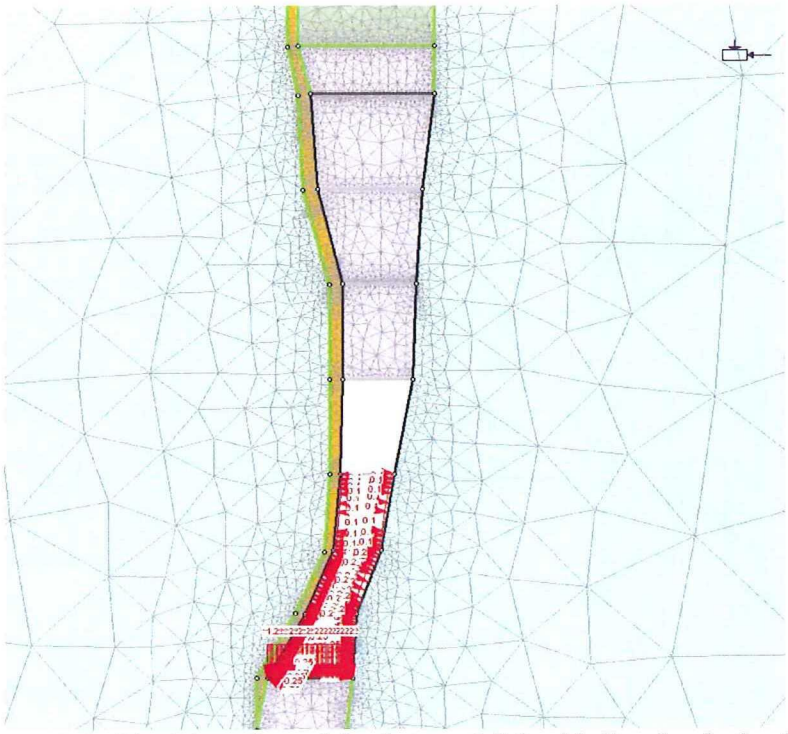

Figure 7.9: The Phase2 model of stope 9/10 with line loads for fill.

The loads are applied as uniformly distributed line loads. This is not exactly correct, as the loads increase over depth. While it is possible to apply linearly distributed loads in Phase2, it is not possible to change it in an appropriate way for the different stages. The error made is deemed to be small, as pressures are only up to 250 kPa and the in situ stresses are up to 45MPa, so that the backfill pressures are only about 0.5% of sigma 1. The load applied on the floor of 1080 is the lithostatic pressure for a backfill with a density of 2200 kg/m^3.

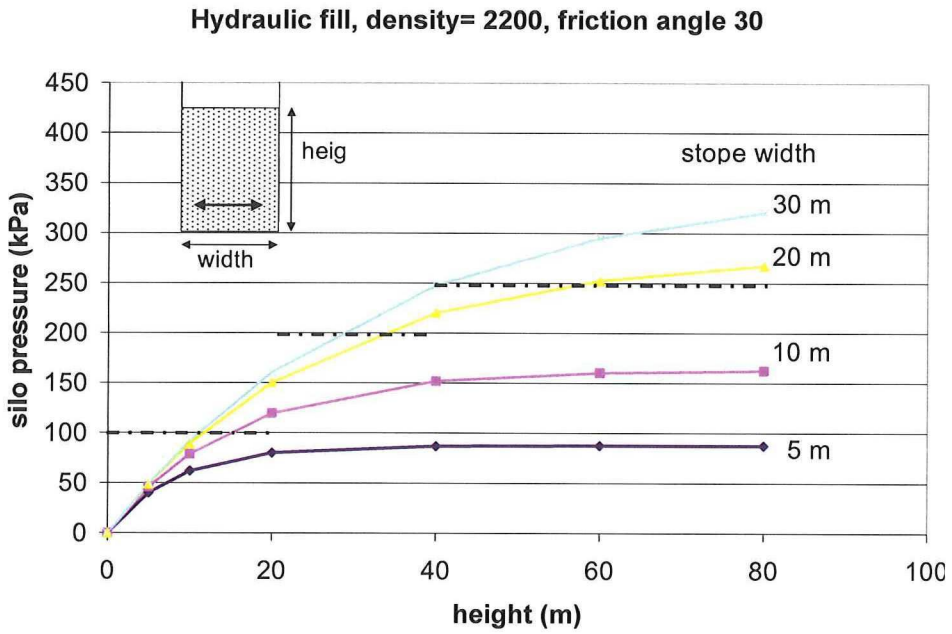

Figure 7.10: Silo sidewall pressures for hydraulic fill. (Marklund, 2008) The pressures at the dashed lines were used in the model.

A standard discretization for the boundaries and materials was made and a standard meshing with three nodes per element was selected. The mesh density around the stope and particularly around the levels was increased to avoid numerical instability and inaccuracy. The number of elements and nodes for each stage is listed in Table 7.2. Similar to the Examine3D models a constant stress was applied and for simplicity's sake σ_1 was taken as horizontal (45MPa) and σ_3 as vertical (20MPa).

Table 7.2: Elements and nodes for each stage in Phase2.

Stage	Elements	Nodes
BASE	7984	4021
1080	7472	3824
1060	7097	3650
1040	6967	3596
1016	6781	3519
986	6507	3410
956	5990	3170
926	5287	2861

The tolerance was left at the default level of 0.001 with the default maximum number of iterations of 500. The convergence type is based to calculation of minimum amount of potential energy.

7.3.3 Geology and geotechnical parameters

The Phase2 model is relatively simple, but deemed sufficient for analysis of the failure of the talc zone in the hanging wall and growth of a plastic zone. The limitations in 7.3.1 should be borne in mind.

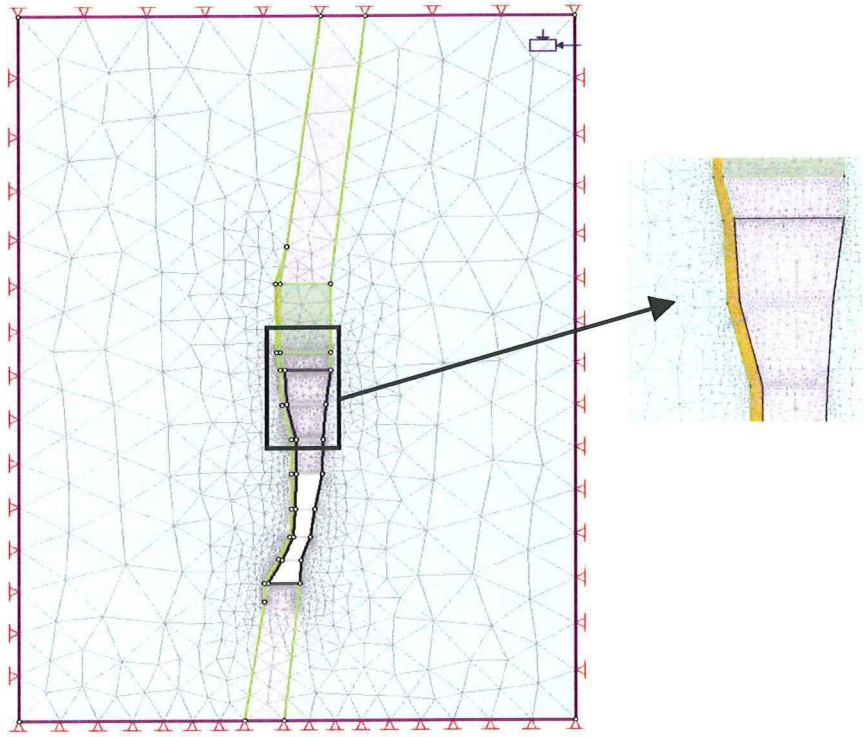

Figure 7.11: The entire Phase2 model

The stope outlines were entered as described in 7.3.2. The cut and fill area was taken as rectangular similar to the Examine3D models. The ore continues linearly towards the boundary. On the hanging wall a talc layer was modelled with a thickness of 5m that runs from below 1080 to above the cut and fill area. The cut and fill area is filled with backfill. The material in both the hanging wall and footwall was taken as limestone. There are two main reasons for doing so. The first reason is that the geology of the hanging wall is not entirely known. The skarns that are in the hanging wall can vary from tremolite skarn with talc and micas (especially near the ore contact) to diopside skarn and there is a large range of strengths in between (see Figure 6.2). Taking the properties of limestone is probably somewhat conservative. The second reason is that the model should be as simple as possible for the mechanism that needs to be analysed. The main objective is to see how the talc reacts to the excavation.

Table 7.3: Material properties for the Phase2 model.

Parameter	Talc	Limestone	Ore		Fill
Young's Modulus	20 GPa	60 GPa	90 GPa		285 MPa
Poisson ratio	0.3	0.12	0.15		0.3
Failure criterion	Hoek-Brown	Hoek-Brown	Hoek-Brown		Mohr-Coulomb
UCS	30 MPa	120 MPa	200 MPa	Tensile strength	0 MPa
m	1	0	0	Fric. angle	33°
s	0.001	0.112	0.112	Cohesion	0.24 MPa
Dilation	0°	0°	0°	Dilation	0°
m residual	1	0	0	Fric. Angle residual	33°
s residual	0.001	0.112	0.112	Cohesion residual	0.24 MPa

The material properties are shown in Table 7.3. The Young's modulus and poisons ratio for the limestone and ore are given by the stress measurements described in Chapter 5 and 6. The values for the failure criterion are based on the philosophy that failure initiates at one third of the UCS. (Martin, 1997).

For the talc no elastic properties are known. The Young's modulus was estimated at 20 GPa from looking at micas ("Glimmerskifer") with similar UCS values in the NTH/NTNU/SINTEF database. (Myrvang, 2001). The values for the failure criterion other than the UCS were left at the default settings. The values for the backfill are taken from some in-situ values for cemented rockfill (Brady and Brown, 2004).

All materials are modelled as elasto-plastic materials, which means that they will remain their peak strength at the point of failure. While this is unrealistic when the minor principal stress is close to zero, it is not too far off from triaxial test results. Dilation, the amount of expansion when reaching the peak strength, was left at 0°.

7.4 Considerations

As pointed out before, both methods have their limitations. In addition there is a complicated geology that is not captured by either model, both on small scale and large scale.

On a larger scale there are a few things to keep in mind. The strong rock types at the location of the new potential shaft for example should be taken into account. Perhaps Lappberget is flanked by such a rock mass on the other side as well, which could make a difference in the mine unloading stiffness if the extend of those rock masses is large enough. The B-zone was neglected in the analysis for three reasons. The first reason is that the B zone comes closer to the A and C zone towards the upper part of the piece of Lappberget that was analysed. The second reason is that the data for the current mining of the B zone at 1080 was not as readily available as for A and C zone. The third reason is that there are still some uncertainties in the mine designs around the B zone. In addition, the B-zone will probably fall in the stress shadow of the A and C zone under current planned sequencing.

On a smaller scale the geometry and location of the various rock masses are hard to model as they are largely unknown. Even if this would be known in detail it could not be captured by either method used here. The three-dimensional BEM only allows for a homogeneous elastic material that extends into infinity while the two-dimensional FEM would not be able to capture the full picture with only two dimensions as the geometry and location of the various rock masses is highly irregular.

While the models used have their limitations as pointed out, they do provide a basis in the analysis. It is important to keep the model outcomes in mind as a guideline instead of the absolute truth.

7.5 References

Autodesk, 2004, *AutoCAD LT 2004*, San Rafael, USA

Bentley Systems Inc., 2006, *Microstation*, version 08.05.02.70 Windows x86, Exton, USA

Brady, B.H.G., and E.T. Brown, 2004, *Rock mechanics for underground mining*, Kluwer Academic Publishers, Dordrecht, the Netherlands

Hoek, E. and E.T. Brown, 1980, *Underground excavations in rock*, Instn Min. Metall.: London, United Kingdom

Koivisto, S., 2008, *personal communication and triangulations of the stopes*

Marklund, P.I., 2008, *personal communication*

Martin, C.D., 1997, *The effect of cohesion loss and stress path on brittle rock strength.* Can. Geotech. J. 34: 698-725 (1997).

McKinnon, S.D., 2006, *Numerical Modelling,* course notes for MINE469: Stability analysis in mine design, Queen's University, Kingston, Canada

Myrvang, A., 2001, *Bergmekanikk*, course notes for rock mechanics at the NTNU - institutt for geologi og bergteknikk, Trondheim, Norway (in Norwegian)

Nilssen, P., 2004, *Bergspenningsmålinger i Garpenberg Norra gruve*, SINTEF Bygg og miljø report for New Boliden AB, Trondheim, Norway. (in Norwegian).

Nyström, A., 2005, *Numerical analysis of stope dimensions for large scale mining of the Lappberget ore body and prognosis of mining conditions*, New Boliden AB internal report TG_REP2005/004, Boliden, Sweden. (in Swedish)

Rocscience, 2003, *Examine3D*, version 4.0992, Toronto, Canada

Rocscience, 2008, *Phase2*, version 6.028, Toronto, Canada

Starfield, A.M. and P.A. Cundall, 1988, *Towards a Methodology for Rock Mechanics Modelling,* Int. J. of Rock Mech. And Mining Sciences, Vol. 25 No. 3 p99-106.

Wiles, T.D., 2007, *Evidence based model calibration for reliable predictions*, Proc. 4th Int. Seminar on Deep and High Stress Mining, p. 3-20, Perth, Australia

8. Tackling seismicity – considerations and methods

The causes for seismicity and a few methods for prediction of seismicity will be introduced in this chapter. These methods for prediction are suitable to be used without any seismic records and generally provide a guideline what areas to focus on. As noted earlier the following definitions will be used. Seismicity is the rock mass response to deformation and failure. A seismic event is the sudden release of potential or stored energy in the rock. The released energy is then radiated as seismic waves. A rockburst is defined as a mining induced seismic event that causes damage to openings in the rock (Larsson, 2004). Seismicity is not necessarily a bad thing. In the Coeur d'Alene district for example it was found that most seismicity is a normal, safe and desired rock mass response to mining. There only a small minority of seismic events constitutes a rockburst hazard. (Whyatt et al., 2002)

8.1 Mine induced seismicity

Seismic events can be divided in two categories; seismicity due to excess compressive stress and seismicity due to excess shear stress. The first two types, strain bursts and pillar bursts, described in this paragraph are in the first category. The third type, fault slip, falls in the second category.

8.1.1 Strain burst

Rockbursts due to compressive stresses are often explained in terms of crushing of rock in soft and stiff loading compression. Two types of testing machines illustrate the analogy that is often used. The first one is the displacement-driven test machine with a stiff unloading curve (AGH). The reaction of the rock to this unloading curve is stable and needs an external source of energy to propagate failure. The energy deficit can be seen as the energy in area AEG in Figure 8.1. The other type of loading system is the load-driven test machine or soft loading system (ADS). The reaction to the rock is in this case self-sustaining as there is an excess energy that needs to be dissipated. The excess energy is represented as the area ADE in Figure 8.1. The combination of a soft loading system with a strong and brittle rock mass can result unstable or uncontrollable and potentially violent failure. (Brummer and Andrieux, 2002)

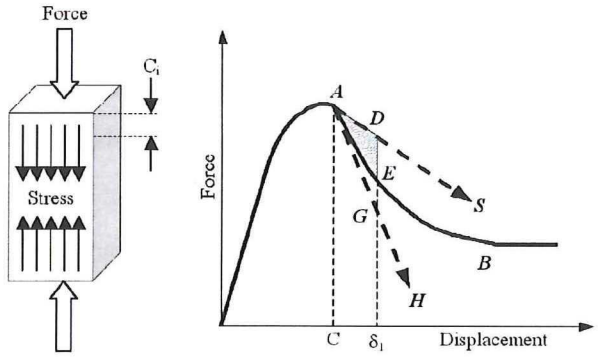

Figure 8.1: Brittle rock failure in soft (ADS) and stiff (AGH) loading systems (Brummer and Andrieux, 2002)

It should be noted that the energy is accumulated in the rock sample as stored strain energy and that this energy is dissipated in free surfaces, both internal and external. The potential for violent failures is thus greater for homogeneous (undisturbed) samples. The more inhomogeneous the rock is, the more energy can be dissipated through the discontinuities and formation of microfractures. This can also been seen as an effective softening of the rock mass. This is also the objective of the preconditioning type of destress blasting. Preconditioning has been successfully applied in the past (e.g. in mines in South Africa) to "soften up" the rock mass prior to mining, where confined blasts in the rock mass ahead of the face are detonated to create fractures. (Brummer and Andrieux, 2002)

The stiffness of the loading system in a mine is often hard to determine as it depends on mine geometry as well as rock mass properties (Brummer and Andrieux, 2002). A simplified explanation is illustrated in Figure 8.2. When the stiffness of the excavated rock is higher than the stiffness of the host rock failure could potentially be violent as a soft loading system is simulated (left situation in Figure 8.2). When the stiffness of the excavated rock is lower than the stiffness of the host rock a stiff loading system is simulated and the failure process is more likely to be non-violent. If there is only one rock type there is still a potential for strain bursts depending on the local loading system (influenced by mine geometry for example). (Larsson, 2004)

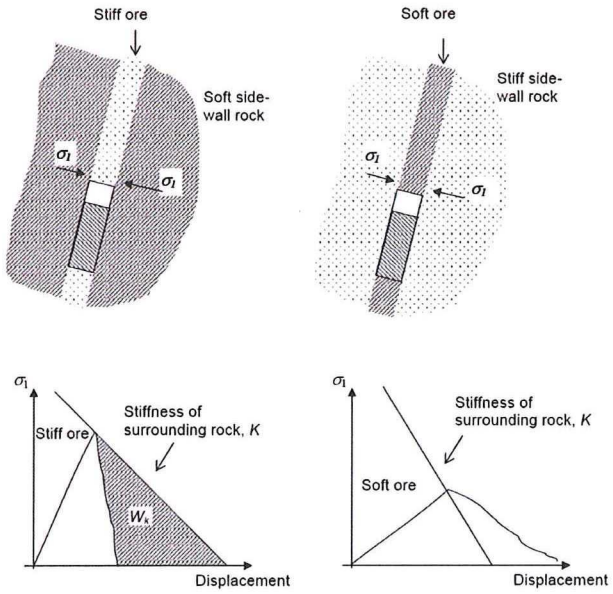

Figure 8.2: the two distinct loading systems caused by difference in stiffness (Larsson, 2004)

The difference in stiffness is a potential cause for rockbursts to occur. In Fraser mine in Sudbury, Canada some rockbursts occurred as pyroxene boulders embedded in the host rock unloaded their stored strain energy when encountered by the face. The size of these boulders varied from the size of basketballs to small houses (Falconbridge presentation and Larsson, 2004). An example of such a stiff boulder is shown in Figure 8.3. Another example is the Nygruvan ore body in Zinkgruvan mine where the ore is stiffer than the host rock. Rockbursts have been experienced and this led to the installation of a microseismic monitoring system. Another ore body in Zinkgruvan will be described in more detail in Chapter 10.1.

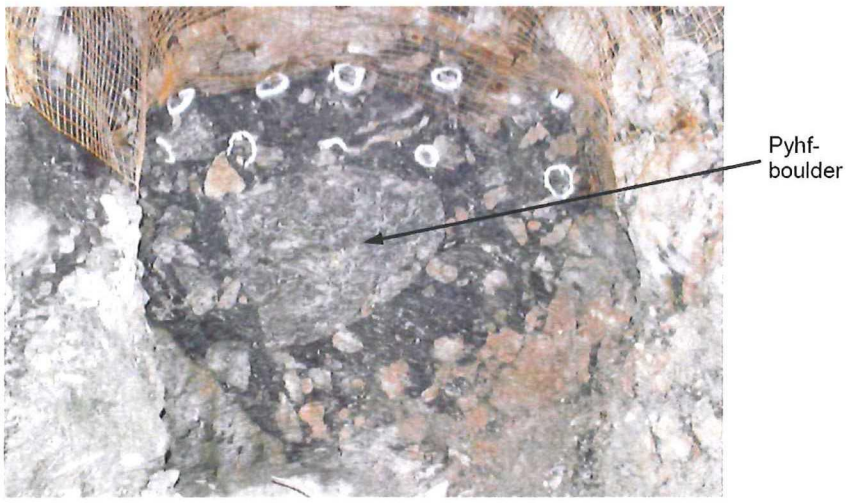

Figure 8.3: Pyhf-boulder in the center of the face (Larsson, 2004)

The above is a general description of seismicity due to compressive stresses. The term strain bursts is generally used to describe events of violent failure where relatively small pieces of rock are ejected from the boundary of an excavation. This type of failure causes spalling or slabbing in the exposed rock and pre-existing geological discontinuities are thus not a requirement. Strain bursts are arguably the most occurring type of rockbursts in the mining and civil industries. The term face burst is sometimes used for bursts due to release of stored strain energy just ahead of the face causing violent ejection of material from the face into the excavation (Larsson, 2004)

The relevance for Lappberget is here in the evaluation of faces of the cross cuts in secondary stopes and in general when the sill pillar is approached. Another relevant point is to evaluate if there are any large bits of stiff rocks (boulder size bits of quartzite for example) that might release their stored strain energy in a violent fashion. At present it appears that those kinds of boulders are lacking. Precautions should be taken if they do occur.

8.1.2 Pillar burst

Pillar bursts are violent pillar failures. Pillar bursts are a result of (local) stress redistributions and they are subsequently the cause of further (local) stress redistributions. The damage of a pillar burst can be severe depending on the location and condition of the failed pillar and the pillars in the proximity. The energy released in a pillar burst is usually much higher than the case with strain bursts and the radiated seismic energy can also cause damage or loose falling down in other areas. The rapid loss of support due to failure of a pillar causes stress redistribution on the remaining support pillars. (Larsson, 2004)

If the remaining pillars fail as well a domino effect can be initiated, of which the multiple pillar failure in the Quirke mine (room and pillar mine with rib pillars of varying dimensions) in Elliot lake (Ontario, Canada) might be the most famous example. One of the questions raised following the chain reaction failure of pillars was why squat pillars failed so violently while slender pillars failed non-violently. Two factors were identified to be contributing to the pillar bursts: the pillars were

highly stressed due to an extraction rate of 75 to 80% and the pillars were in different orientations. The latter resulted in some pillars being weaker or being less effective in transferring stresses through them. (Hedley, 1992)

The high stresses in the pillars were a prerequisite, yet pillars in other areas were equally stressed and did not start the initial violent failure. The weakness due to an unfavorable orientation of some rib pillars is considered to be the cause of the first rockbursts. During mining no problems were encountered, but as the mine expanded this area got to a more central location of mining activities. It was found that the slender pillars would fail non-violently first and the resulting stress redistribution caused stress to accumulate in the squat pillars. The squat pillars would then fail violently as mine stiffness became very low. The latter can be explained as the load the squat pillars were carrying could almost be seen as a dead weight (and therefore hardly decreasing with increasing displacement). (Hedley, 1992)

The relevance for Lappberget is the evaluation of the sill pillar and the pillars in between cross cuts on the footwall drift. In case of the latter the pillars on the bottom level of the mining horizon (on level 1080 for example) and the on the top level (the one accessing the stopes just below the sill pillar from the top) might be the most interesting as these pillars might partially be in the area of compression due to stress redistribution.

8.1.3 Fault slip

Fault slip failures are a result of mine induced stress redistributions as well, albeit on a larger scale. As a mine expands the influence on the surrounding rock mass expands with it. The stress alteration can lead to reactivation of existing faults and/or violent creation of fractures through intact rock. The term fault slip is used to describe displacement along the fault or other geological structure. Mining activities can trigger fault slip bursts by reducing the stress normal to the fault and thereby reducing the shear resistance, by increasing the shear stresses parallel to the fault or by a combination of these two. The damage to excavations is caused by energy that is released when the slip occurs. Once the radiated seismic energy hits the free face of

the excavation it causes existing wedges to eject, tensile failure due to the rarefaction wave and failure due to the compressional wave. (Larsson, 2004).

The mechanisms behind fault slip bursts and earthquakes are more or less the same, so the problem of predicting earthquakes applies to fault slip bursts too. The generally accepted theory is that stress and strain accumulate over time, which is suddenly released by displacement along the fault. In the most simplistic model the time and magnitude can be modeled based on the static and dynamic friction coefficients, but the results remain questionable. Statistics might be applied to small events as the amount of small events can justify statistical models. Larger events cannot be described by statistics, as there is a lack of data to support it. Prediction remains a problem even for long term prediction (in the scale of tens of years) even with the knowledge of stresses, strains and fault characteristics, so stating that prediction on the timescale of minutes to days remains a bit of a challenge is an understatement. (Larsson, 2004)

The relevance for Lappberget is a difficult one. The only real significant geological feature seems to be the hanging wall contact along the ore in which displacement might take place. Three-dimensional elastic-plastic modeling combined with verification of convergence measurements might provide more insight in potential mechanisms. For this thesis the areas of weakness will be evaluated by analyzing the induced state of stress in the boundary element models and some simple 2D finite difference models to put things into perspective.

8.2 Energy balances and equations

The first energy balance can be seen as a balance between action and reaction. On the left side of equation 8.1 the action of creating an opening is placed, which are the change in potential energy as a result of displacements in the remaining rock mass (W_t) and the stored strain energy in the removed rock mass (U_m). This energy has to be dissipated somehow. On the right-hand side of equation 8.1 are the energy changes due to the creation of the opening, which are the increase in stored strain energy in the remaining rock (U_c), energy absorbed by the support and backfill (W_s) and the excess energy denoted as released energy (W_r).

$$W_t + U_m = U_c + W_s + W_r \quad \text{[Eq. 8.1]}$$

$$W_r = U_m + W_k \quad \text{[Eq. 8.2]}$$

$$W_k = W_t - (U_c + W_s) \quad \text{[Eq. 8.3]}$$

Equation 8.1 is based on the assumption that the rock mass is elastic and that no energy is used in fracturing or non-elastic behavior. The rock mass responds to an instant removal of rock before an equilibrium can be reached. In the process of reaching such equilibrium energy is dissipated in the form of seismic and damping energy (kinetic energy). The released energy can be further divided (equation 8.2) as the stored strain energy in the removed rock (U_m) – as that energy is released from the system – and kinetic energy (W_k). Substituting [8.2] in [8.1] produces [8.3]. (Hedley, 1992)

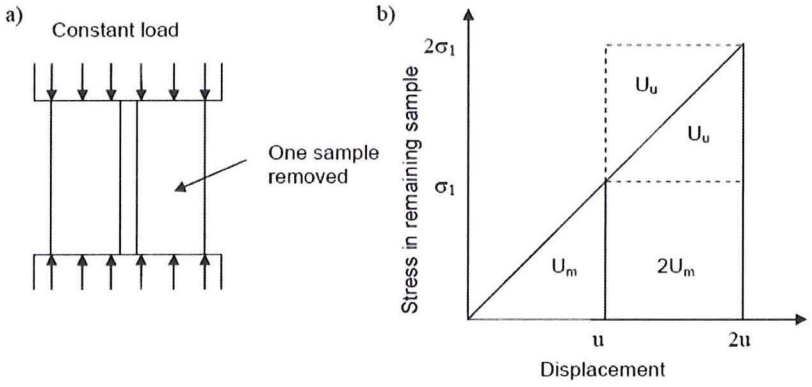

Figure 8.4: Energy changes (b) after one sample is removed in (a). (Larsson, 2004, after Hedley, 1992)

Figure 8.4 illustrates the relationships of removing rock from underneath load. The energy stored in both samples prior to removal of one sample is U_m. Once a sample is removed the displacement increases to 2u as σ_1 doubles. The remaining sample would then carry the increase in stored strain energy. The increased displacement causes the potential energy to change. The following relationships were deduced:

$$U_c = 2U_m + U_u \quad \text{[Eq. 8.4]}$$

$$W_t = 2(U_m + U_u) \quad \text{[Eq. 8.5]}$$

$$W_r = U_m + U_u = W_t/2 \quad \text{[Eq. 8.6]}$$

$$W_k = U_u \quad \text{[Eq. 8.7]}$$

U_u is the stored strain energy if the increase in load was applied to an unstressed sample. Equations 8.4 to 8.7 are shown to be valid for all mining configurations. (Hedley, 1992)

$$\Delta W_t = \Delta U_c, \quad \Delta W_r = \Delta U_m \quad \text{and} \quad \Delta W_k = 0 \qquad \text{[Eq. 8.8]}$$

The conditions in equation 8.8 are the limiting conditions for mining in infinitely small steps. Some interesting points can be seen from these energy balances. (Hedley, 1992).

- Without support, all energy components can be expressed in U_m and U_u.
- If mining takes place in infinitely small steps no kinetic energy is released. Mines that utilize incremental mining and still experience rockbursts have other sources of energy that are being liberated due to non elastic behavior such as slip along faults.
- The change in potential energy is the driving force; reduce this and other energy components will be reduced accordingly.
- Support such as backfill has two beneficial effects. The change in potential energy is reduced as volumetric convergence is restricted and the available kinetic energy is reduced as energy is absorbed in deforming the support.

8.3 Prediction of seismicity

The selected prediction methods can be used without any seismic records and provide an insight in the areas that are most likely to display seismicity and provide a crude evaluation of mining layouts.

8.3.1 Energy Release Rate (ERR) and stored strain energy

The Energy Release Ratio, ERR, is the stored strain energy in the rock to be removed in the area ($\Delta U_m/\Delta A$). The method was developed in South Africa for gold mines to

evaluate the rockburst potential in various mine layouts. In these mines there is a strong relationship between ERR and damage in mines. (Hedley, 1992)

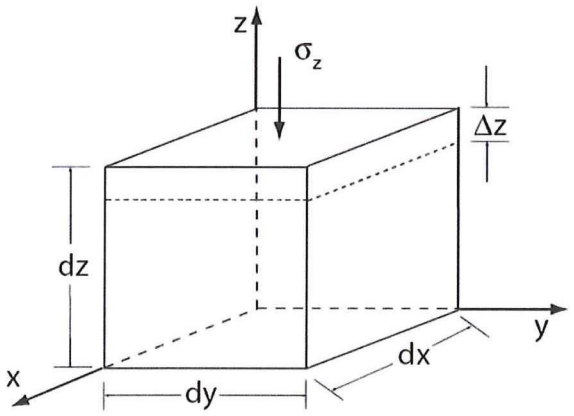

Figure 8.5: Sketch on uniaxial loading per unit volume (McKinnon, 2007)

Figure 8.5 illustrates uniaxial loading on a unit volume. In this sketch all stress components other than σ_z are assumed to be zero. The work done on this unit volume due to σ_z on the area dxdy is given by equation 8.9. (McKinnon, 2007)

$$dW = \frac{1}{2}\sigma_z dx dy \varepsilon_z dz \qquad \text{[Eq. 8.9]}$$

The three dimensional state of stress is illustrated by Figure 8.6. In this figure 9 different stress components can be distinguished. Three shear stress components, however, can be substituted by considering the moment equilibrium of the unit rock mass, as $\tau_{yx} = \tau_{xy}$, $\tau_{yz} = \tau_{zy}$ and $\tau_{zx}=\tau_{xz}$ (Brady and Brown, 2004)

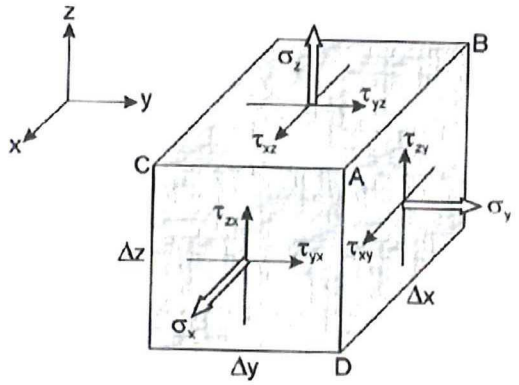

Figure 8.6: Stress components in a three dimensional state of stress (Myrvang, 2001)

The work done in a three dimensional state of stress is given in equation 8.10

$$dW = \frac{1}{2}\begin{pmatrix} \sigma_z dxdy\varepsilon_z dz + \sigma_y dzdx\varepsilon_y dy + \sigma_x dydz\varepsilon_z dx + \\ \tau_{xy} dydz\gamma_{xy} dx + \tau_{yz} dxdz\gamma_{yz} dy + \tau_{zx} dxdy_{xy} dx \end{pmatrix} \quad \text{[Eq. 8.10]}$$

To simplify equation 8.10 the work per unit volume is taken in equation 8.11. Substituting 8.11 into 8.10 obtains the much simpler equation 8.12. (McKinnon, 2007)

$$w_0 = \frac{work}{volume} = \frac{dw}{dxdydz} \quad \text{[Eq. 8.11]}$$

$$w_0 = \frac{1}{2}\left(\sigma_x\varepsilon_x + \sigma_y\varepsilon_y + \sigma_z\varepsilon_z + \tau_{xy}\gamma_{xy} + \tau_{yz}\gamma_{yz} + \tau_{zx}\gamma_{zx}\right) \quad \text{[Eq. 8.12]}$$

To further simplify the calculation process, the work per unit volume will just be expressed in terms of stresses and elastic properties. To do this, use is made of stress-strain relations in equations 8.13 and 8.14.

$$\varepsilon_x = \frac{1}{E}\left[\sigma_x - \upsilon(\sigma_y + \sigma_z)\right] \quad \text{[Eq.8.13]}$$

$$\gamma_{xy} = \frac{\tau_{xy}}{G} \quad \text{[Eq. 8.14]}$$

If 8.13 and 8.14 are then substituted into 8.12 equation 8.15 emerges.

$$w_0 = \frac{1}{2E}\left(\sigma_x{}^2 + \sigma_y{}^2 + \sigma_z{}^2\right) - \frac{\upsilon}{E}\left(\sigma_x\sigma_y + \sigma_x\sigma_z + \sigma_y\sigma_z\right) + \frac{1}{2G}\left(\tau_{xy}{}^2 + \tau_{yz}{}^2 + \tau_{zx}{}^2\right) \quad \text{[Eq. 8.15]}$$

This can be simplified somewhat if the principal stresses are used. The shear stresses vanish as a result, as can be seen in equation 8.16. (McKinnon, 2007)

$$w_0 = \frac{1}{2E}\left[\left(\sigma_1^{\,2} + \sigma_2^{\,2} + \sigma_3^{\,2}\right) - 2\upsilon\left(\sigma_1\sigma_2 + \sigma_1\sigma_3 + \sigma_2\sigma_3\right)\right] \qquad \text{[Eq. 8.16]}$$

Equation 8.16 calculates the strain energy per unit volume rock. This can be seen as a combination of the change in potential energy (W_t) and the strain energy in the removed rock (U_m), as it covers the entire area under the curve in Figure 8.4. This is the energy that is available and needs to be dissipated, either as strain energy in the remaining rock, through deformation of the support or as released energy. The ERR, defined as $\Delta U_m/\Delta A$, will not be calculated. This is partly because the geometry is not as straightforward as for the narrow vein gold mines it was developed for. Furthermore, it is difficult to define a proper begin and end stadium in the mining process and the ERR might be higher in between the two. Evaluation of the total energy that is available in the surrounding rock versus failure criteria is deemed sufficient.

Strain energy and Examine3D go well together as both are based on the assumption of full elastic properties of the rock mass. As described in the case study of Kanalmalmen calculation of the strain energy in the surrounding rock mass can provide a powerful tool in the evaluation.

8.3.2 Seismic activity along geological features

The energy release ratio (ERR) described in the previous part is based on elastic properties of the rock mass to calculate strain energies only. To state the obvious; this method does not take any non-elastic features such as fault zones into account. For that purpose the excess shear stress method was introduced.

The excess shear stress (ESS) gives a measure of potential released energy along a geological feature. The ESS is given by equation 8.18. Slippage occurs when the shear stresses are equal to or exceed the static shear strength.

$$\tau_e = \tau - \tau_d = \tau - \mu_d \sigma_n$$
$$\tau_s = C_s + \mu_s \tau_s \qquad \text{[Eq. 8.18]}$$
$$\tau \geq \tau_s$$

Where τ_e is the ESS, τ is the shear stress prior to slip, τ_s is the static shear strength, τ_d is the dynamic shear strength, C_s the static cohesion, μ_s is the static friction coefficient, μ_d is the dynamic friction coefficient and σ_n is the normal stress on the geological feature. The third line in Equation 8.18 is the condition required for slip to occur.

A sufficiently large stress drop is required to sustain an unstable slip along a structure, similar to the excess energy required to sustain an unstable strain failure as discussed in 8.1.1. If the ESS is in the order of magnitude of 5 to 10 MPa an unstable movement on a pre-existing plane might occur if the shear stress is equal to or larger than the shear strength. (Ryder, 1987)

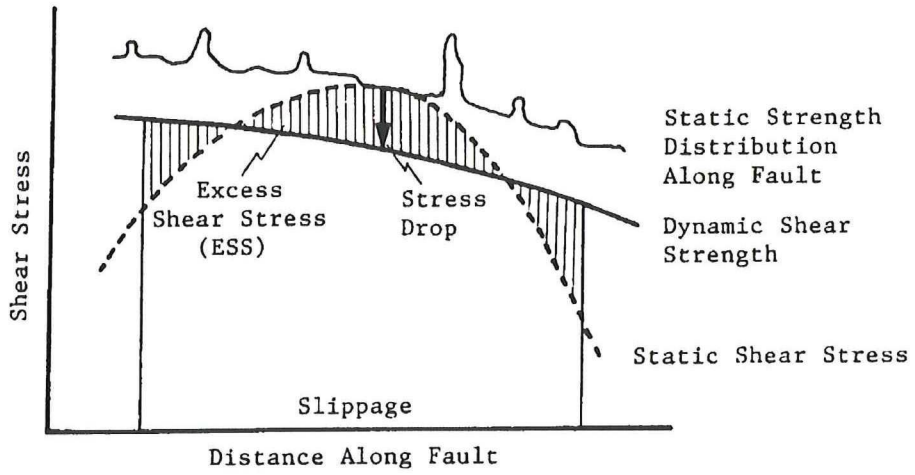

Figure 8.7: The concept of excess shear stress and initiation of slippage on a fault. (Hedley, 1992, after Ryder, 1987)

The concept of ESS is illustrated in Figure 8.7. The static shear strength varies along the fault due to local irregularities (large local differences) and to variations in the normal stress on the fault (smooth variations). The dynamic shear strength is only dependant on the normal stress on the joint, assuming zero cohesion and a constant dynamic friction coefficient. The concept of taking the dynamic friction constant is important as it makes the ESS method practically applicable to underground mining.

By doing so the ESS is also somewhat conservative; local highs in the dynamic friction would decrease the event magnitude prediction significantly. The dashed line represents the static shear stress, which is a combination of virgin and induced stresses. If at some point the shear stress touches the static shear strength the shear strength would reduce to the dynamic shear strength. This stress drop is unbalanced and will force the adjacent rock to displace along the fault as well. The displacements will halt when the ESS has become sufficiently negative. (Ryder, 1997)

The start of the analysis of the shear stress-strength assessment is by looking into the Mohr circle. In case of dynamic shear strength the cohesion reduces to zero and failure initiates if the angle 2β-φ is 90 degrees or less as can be seen in Figure 8.8.

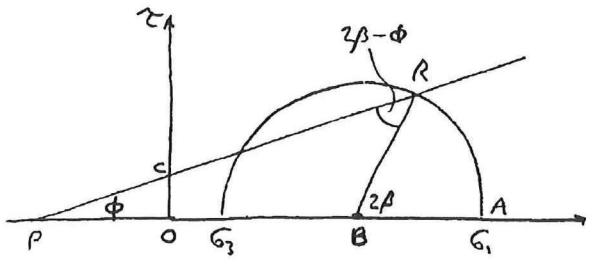

Figure 8.8: The Mohr circle (McKinnon, 2006)

By law of sines:

$$\frac{BR}{\sin\phi} = \frac{PB}{\sin(2\beta-\phi)}$$

$$\frac{\tau_m}{\sin\phi} = \frac{\sigma_m}{\sin(2\beta-\phi)} \qquad \text{[Eq. 8.19]}$$

With

$$BR = \frac{1}{2}(\sigma_1 - \sigma_3) = \tau_m$$

$$PB = \frac{1}{2}(\sigma_1 + \sigma_3) + c\cot\phi = \frac{1}{2}(\sigma_1 + \sigma_3) = \sigma_m \qquad \text{[Eq. 8.20]}$$

$$2\beta - \phi \le \frac{1}{2}\pi$$

A way of looking at the problem is to calculate the maximum friction angle. If the friction angle is lower than the dynamic friction angle of the existing plane there might be slippage and the shear and normal forces need to be calculated for the

orientation of the plane of the structure. The lines of text inserted into Examine3D are shown in Figure 8.9.

$$\frac{\sigma_m \sin\phi}{\tau_m} \leq 1$$

$$\sin\phi \leq \frac{\tau_m}{\sigma_m} = \frac{\sigma_1 - \sigma_3}{\sigma_1 + \sigma_3} \qquad \text{[Eq. 8.21]}$$

$$\phi \leq \sin^{-1}\left(\frac{\sigma_1 - \sigma_3}{\sigma_1 + \sigma_3}\right)$$

```
* minimum friction angle for excess shear stress
option_3_title = "req max phi"
option_3 = asin((s1-s3)/(s1+s3))*360/(2*3.14159)
```

Figure 8.9: Lines of text inserted into Examine3D to evaluate potential for fault slip.

By creating iso-surfaces with the values for the maximum dynamic friction angles for potential slippage a quick assessment can be made if geological structures with corresponding or lower dynamic friction angles are present in the volume encompassed by the iso-surface. This provides a quick and easy way to select the structures that can display large ESS and that need more attention. Once structures are selected the actual shear and normal stresses need to be calculated for the actual orientation of the structure as the criteria presented here are the maximum shear stresses and minimal normal stresses possible for a structure with an optimal orientation. After the dynamic shear strength and cohesion are included in the calculation the ESS can be calculated to provide an upper bound estimate of the magnitude of a potential event.

8.4 The effect of backfill in transverse open stoping

Backfill is used in Lappberget to provide a work floor for subsequent cuts and is placed after completion of the stope. The backfill also provides a passive support system in that it only starts to provide support after the host rock reacts upon it. The amount of support pressure backfill can provide depends of the amount and rate of volumetric closure of the host rock, the time of backfill placement and the stiffness characteristics of the backfill. When compared to an unfilled stope, backfill will reduce the total volumetric closure, decrease the increase in stress in rock abutments, increase the strength of the wall rocks by providing confining pressure and absorb the

energy that would otherwise have been released seismically. Some of these effects are small depending on the fill properties and state of stress. (Hedley, 1992)

One of the conclusions of a study done by Hedley in 1992 on seismic energies in cut and fill mining in elastic rock masses is that early placement of backfill with a high stiffness reduces the liberated seismic energy. It should be noted that as backfill is placed in the last stage of mining, most deformation has already taken place. (Hedley, 1992).

Since backfill in transverse open stoping is only placed after the stope has been mucked out the effect of reducing the volumetric closure is very limited. The main attributes that backfill needs to have is to produce an adequate work floor for the subsequent cut within a limited time frame and to remain its integrity (minimize dilution) when the adjacent stopes are blasted. (Brady and Brown, 2004) As a result it is justified to not take backfill into account when modeling.

8.5 Correlation to seismicity

The correlation of the aforementioned tools to actual seismicity is ideally obtained from the rock mass that is being studied. This is a problem as there is no seismic data available from Lappberget. If data would be available more sophisticated methods could be used by correlating numerical modeling with the history of seismic events in the area to come up with a probabilistic relationship (Beck and Brady, 2002). This, however, is not the case.

8.5.1 ERR

The relationship between ERR and rockbursts appears to be site specific. Figure 8.10 is based on rockbursts in longwall mining in South African gold mines. While this figure could be a great asset in evaluating mine layouts in those longwall operations, it has little use outside of these specific conditions. Severe pillar bursts occurred in the Elliot lake and Kirkland lake mines in Northern Ontario with stress levels approaching 150 MPa, yet the ERR was in the order of magnitude of 0.5 MJ/m2. This is approximately 1% of the values found critical in South Africa (Hedley, 1992)

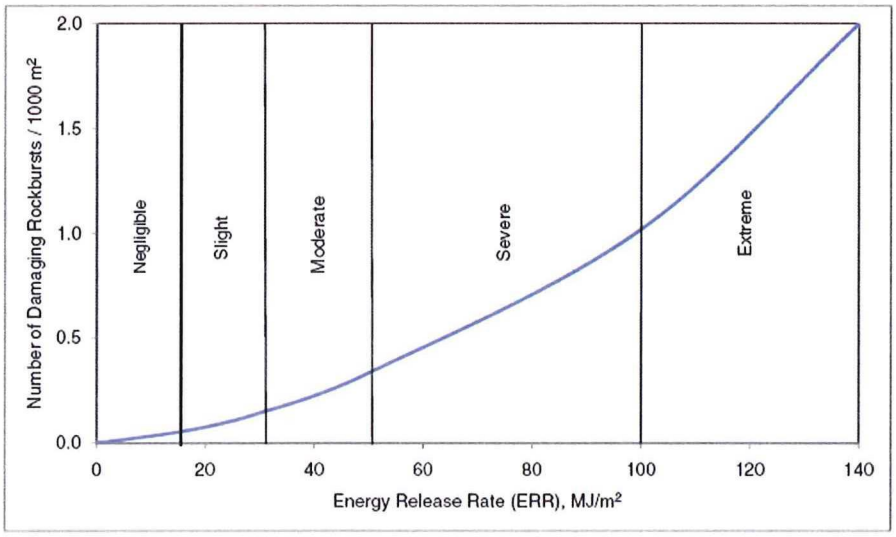

Figure 8.10: Correlation between rate of rockbursting and calculated ERR observed in deep South African gold mines. COMRO 1988

While the exact values of ERR are not to be compared directly with mines in other conditions, it does provide a quick and easy indication of specific areas with higher seismic potential. The limitations or ERR should always be considered, as it is based on elastic volumetric closure and gives hardly any information on behavior of failed rock masses. (Larsson, 2004 and Hedley, 1992)

In this thesis the total strain energy in the rock will be evaluated in relation to that failure criteria and loading history, as outlined in 8.3.1.

8.5.2 ESS

A robust way of indicating the upper level of fault-slip movements was proposed (Ryder, 1987) using the seismic moment (M_0), defined by Equations 8.23.

$$M_0 = GV$$
$$V = \int Ride.dA \qquad \text{[Eq. 8.23]}$$
$$G = \frac{E}{2(1+\upsilon)}$$

Where G is the shear modulus, which can be expressed in terms of Young's and the Poisson ratios. The ride is the displacement along the fault and A is the area of the fault where displacement occurred. The seismic moment in turn relates to seismic magnitude (Richter scale) by Equation 8.24.

$$1.5M = \log_{10} M_0 - 9.1 \qquad \text{[Eq. 8.24]}$$

The displacements and areas on a fault can be estimated by numerical analysis if the cohesion can be reduced to zero and if the friction angle can be used. Alternatively an analytical approximation can be used (Ryder, 1987). In the Western Deep mine the ESS has been used in predicting the upper boundary of rock bursts associated with dykes (James et al., 2007).

While this method has shown good correlations in the past it should be noted that stress analysis in fault-slip related rockbursts should take progressive movement along faults into account. Ryder used a boundary element method similar to the one used in this thesis that assumes the rockmass to continuously deform in an elastic way under the advance of mining fronts (Brady and Brown, 2004). More success has been gained in using the ESS as a back analysis method for major rockbursts (Hedley, 1992).

Urbancic and Trifu analyzed two large events in the Lockerby mine in Sudbury that were associated with a schist shear zone in a sill pillar. The two events were caused by sill pillar extraction and were recorded with a microseismic system. After the events took place various stress components were calculated, such as shear stress, normal stress, and stress drop components. Based on those results it was concluded that high stress release estimates are not necessarily indicators for fault-slip potential, and that the probable cause of the two large fault slip events was due to local variations in the shear stress relative to normal stress. (Urbancic and Trifu, 1998).

The fault-slip type of failure seems to be more complicated to assess as the area that seems to be most likely to give is in the weak rock types (talc) at or near the hanging wall contact. The geometry of these rock types appears irregular and this makes the calculation of excess shear stresses on the geometry of these weaknesses very

complicated. In fault-slip failure a boundary element method alone is likely not sufficient to draw conclusions. Other factors, such as differences in rock mass properties become more relevant. In addition of the Examine3D models a Phase2 model was built to put the boundary element models into perspective.

The occurrence of softer rock types in the hanging wall might be positive for Lappberget from a seismicity point of view. If there would be a major failure mechanism along this zone it would mean that the stresses are less likely to accumulate much energy that would later be released though seismic events. The energy would then be dissipated though gradual failure (and associated displacement).

8.6 Blasting and seismicity

As noted in 8.1.3 predicting the exact timing of a rockburst is impossible. This should not come as a great surprise as the many underlying factors that lead to a rockburst are poorly understood. (Hedley, 1992)

It is, however, possible to look at the distribution of rockbursts and/or seismic events in terms of days and weeks. In some cases, such as in the Coeur d'Alene district in the USA and typical South African mines, the majority of events occur during or just after blasting (Hedley, 1992). For the Coeur d'Alene mines between 70 and 80% of the seismic events occurred with or within one hour of blasting (Whyatt et al, 2002). In other cases, such as the Quirke mine (Elliot lake, Canada), there was no such relationship. (Hedley, 1992)

Blasting can trigger a large share of the seismic events, but it is probably not only the blast vibrations that trigger the seismicity. It is the instantaneous removal of rock and the subsequent rock mass response to the change that is thought to trigger a large part of the seismicity. The more rock is removed the greater the stress redistribution and hence the more seismicity that takes place. Centralized blasting has its advantages as all of the stress distribution in the mine occurs simultaneously and thus the interaction of stress redistributions could trigger more seismicity. (Hedley, 1992)

8.7 References

Beck, D.A., and B.H.G. Brady, 2002, *Evaluation and application of controlling parameters for seismic events in hard-rock mines.* Int. J. of Rock Mechanics and Mining Sciences 39 (2002) 633-642.

Brady, B.H.G. and E.T. Brown, 2004, *Rock mechanics for underground mining*, Kluwer academic publishers, Dordrecht, the Netherlands.

Brummer, R. K., and P. P. Andrieux, 2002. *A Design Methodology for Destress Blasting*, in NARMS-TAC 2002: Mining and Tunnelling Innovation and Opportunity, Vol. 1, pp. 165-172. R. Hammah et al., Eds. Toronto: University of Toronto Press.

Hedley, D.F.G., 1992, *Rockburst handbook for Ontario hardrock mines*, CANMET special report SP92-1E, Canada communication group, Ottawa, Canada

James, J.V., T. Rangasamy and S.P. Petho, 2007, *Excess Shear Stress analysis of seismicity associated with dykes.* Proc. 4th international seminar on deep and high stress mining, Perth, Australia, p21-30.

Larsson, K., 2004, *Seismicity in mines, a review*, technical report, 2004:22, Luleå University of Technology, Luleå, Sweden.

Larsson, K., 2004, *Mining induced Seismicity in Sweden*, Licentiate thesis, 2004:80, Luleå University of Technology, Luleå, Sweden

McKinnon, S.D., 2007, *Stress distributions and failure around excavations*, notes for the course "Stability analysis in mine design" at Queens University department of mining engineering, Kingston, Canada.

Myrvang, A., 2001, *Bergmekanikk*, notes for the course "Rock and soil mechanics" at the NTNU – institutt for geologi og begteknikk, Trondheim, Norway. (in Norwegian)

Ryder, J.A., 1987, *Excess shear stress (ESS): An engineering criterion for assessing unstable slip and associated rockburst hazards*. Proc. 6th international Rock Mech. Congr., Montreal, p1211-1215.

Urbancic, T.I., and C.I. Trifu, 1998, *Shear zone stress release heterogeneity associated with two mining induced events of M 1.7 and 2.2*, Tectonophysics 289 (1998) 75-89.

Whyatt, J., W. Blake, T. Williams and B. White, 2002, *Sixty years of rock bursting in the Coeur d'Alene district of Northern Idaho: Lessons learned and remaining issues*, Transactions –SME 2002, VOL 312, p. 171-178, USA

Pyroxene boulder presentation by Falconbridge...

9. Predicting seismicity

In this chapter all of the previous chapters will be combined to investigate the potential for seismicity. The chapter is split up in two parts: the first part is directed towards strain related seismicity where the geometry and sequence of the stopes will play an important role. The second part is related to geological features and examines the potential for slip along structures and other non-elastic behaviour of the kind.

9.1 Strain related seismicity

As pointed out in Chapter 8, evaluation of strain related seismicity assumes elastic conditions as a starting point. This part will evaluate the calculated energies based on elasticity models versus the expected plasticity.

9.1.1 Pillars – vertical alignment

For the pillars on the footwall drifts planes of measuring points were inserted into the Examine3D models. These horizontal planes are located on three levels halfway the pillar height and in four vertical lines as shown in Figure 9.1. The horizontal lines of planes are located at the 1080 and 926 levels and the vertical lines are between stopes 6 – 7, 12 – 13, 14 – 15 and 20 – 21. The pillars on 1080 and 926 levels will be discussed in 9.1.2.

The anticipated results are, as noted in Chapter 5, that the pillars will disappear in the stress shadow once nearby mining progressed to the next stage. The issue might be in the pillars that are in the active areas.

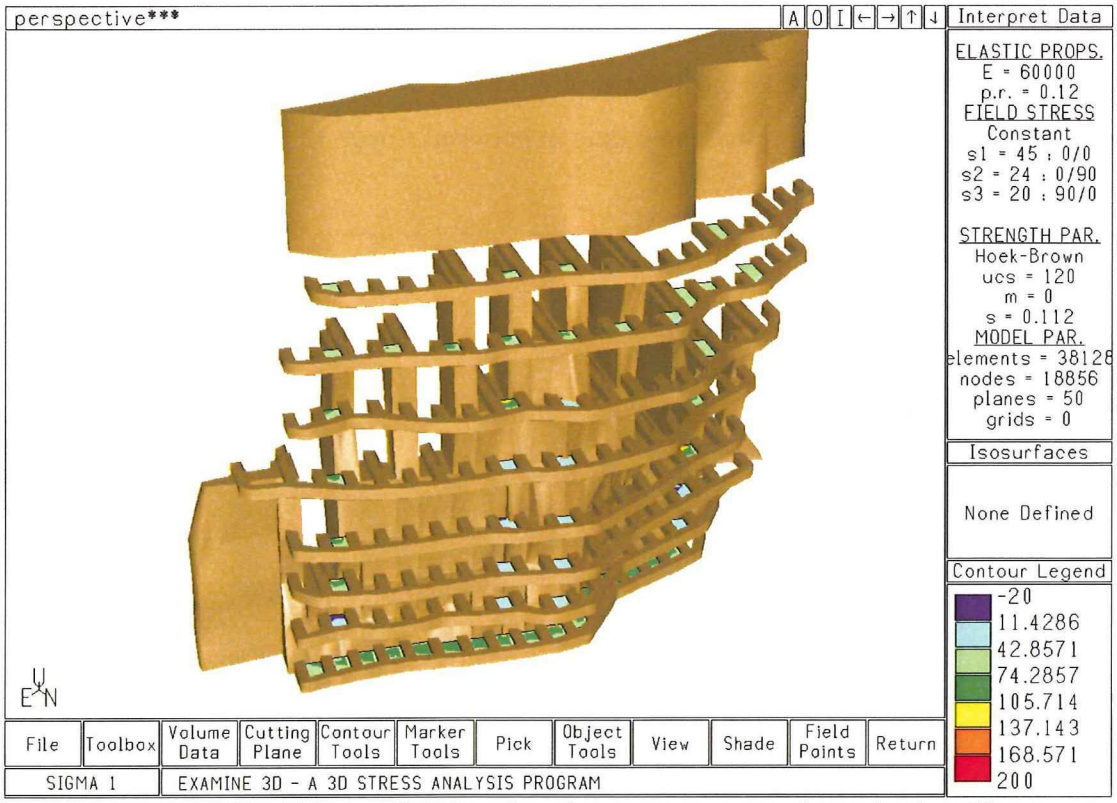

Figure 9.1: The 2013 model showing the measurement planes in the pillars.

The values for the planes were averaged out to represent the total pillar condition. In addition the maximum strain energy in the plane was calculated. For the remainder of the analysis the average strain energies, stresses etc. were used. The relationship between the average and maximum strain energy is shown in Figure 9.2.

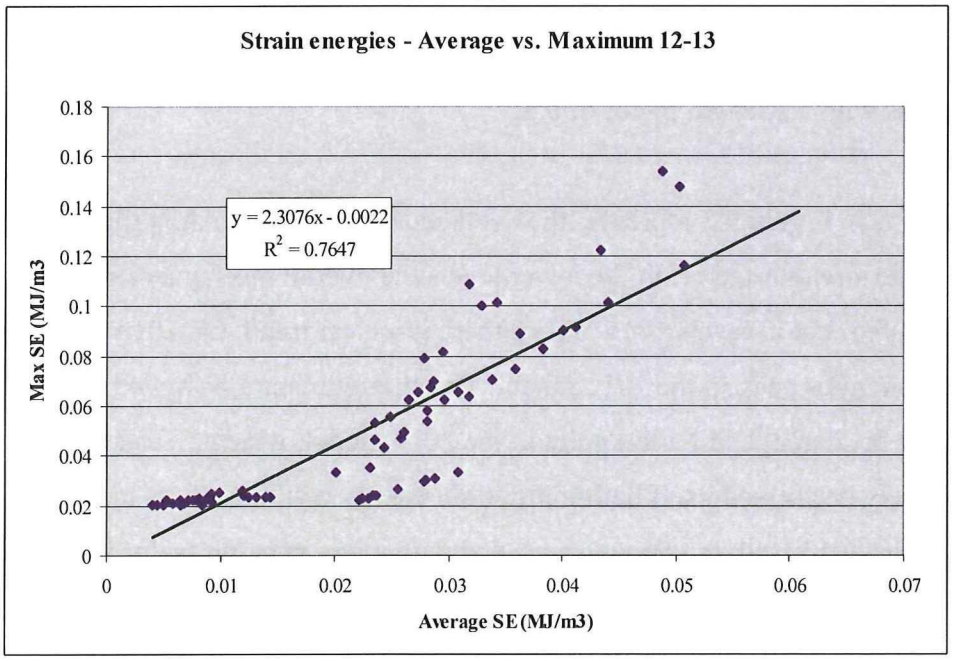

Figure 9.2: Average and maximum strain energies

From Figure 9.2 it can be concluded that the maximum strain energy is approximately two to three times larger than the average strain energy. The values for the plot are for all of the measurement points of the pillars in between stopes 12 and 13.

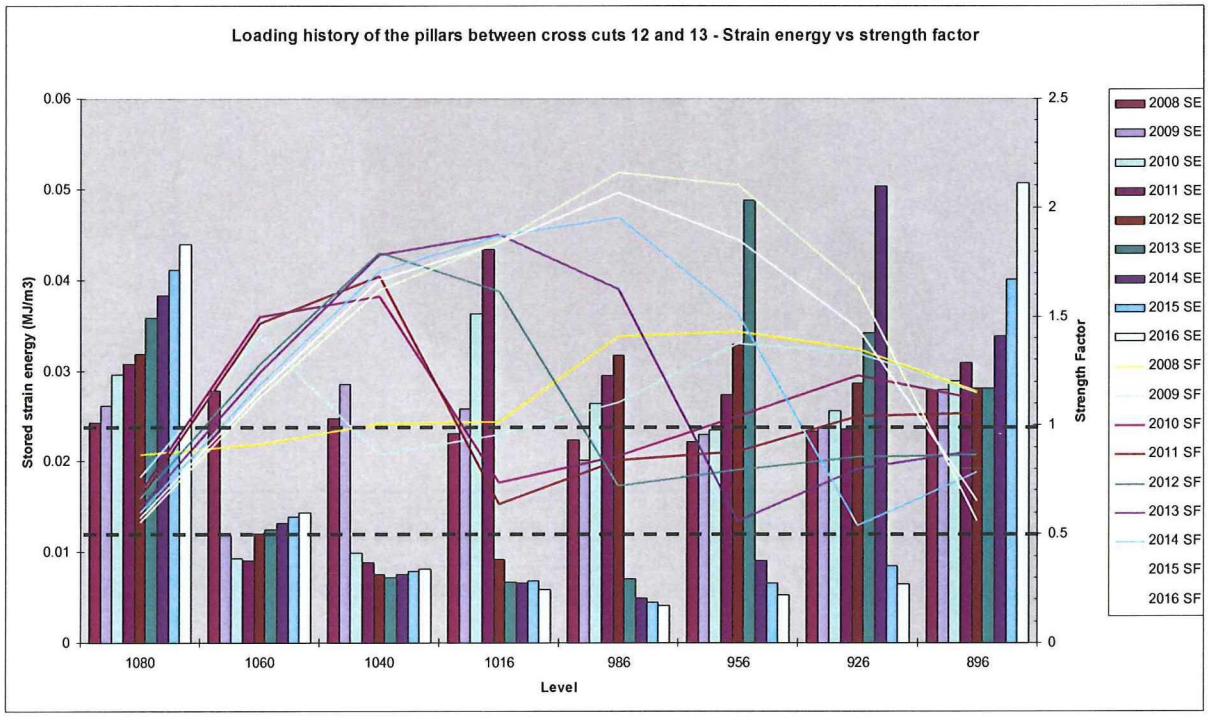

Figure 9.3: Loading history of the pillars between stopes 12 and 13.

Figure 9.3 might be somewhat confusing at first due to the large amount of data. The two horizontal dashed lines are based on the failure criterion. Damage initiates at a strength factor of 1, as calibrated by Anders Nyström (Nyström, 2005). Unstable cracking might start from approximately $^2/_3$ of the UCS (Martin, 1997), which corresponds with a strength factor of 0.5.

The columns in Figure 9.3 represent the average strain energy in the pillar. The lines represent the strength factor. In the lower levels the overall mechanism somewhat more obscured, but in levels 1016 and up there is a clear trend. On 1016 for example, the strain energies peak in the 2011 model. The strength factor however was already well below the damage initiation point in the 2010 model, which means that the pillar already likely destressed itself before the strain energy could reach its maximum. Similarly the 2013 peak in 956 was preceded with a low strength factor in 2012 and the 2014 peak in 926 was preceded with a low strength factor in 2013.

This seems to be coherent with the Phase2 model. The amount of yielded elements per node in the model is shown in Figure 9.4 ranging from zero failed elements (blue) to 100% yielded (red). The plastic zone on the footwall concentrates around the pillar zone of the succeeding level. As noted in Chapter 7, this effect is likely smaller for primary stopes and likely larger for secondary stopes.

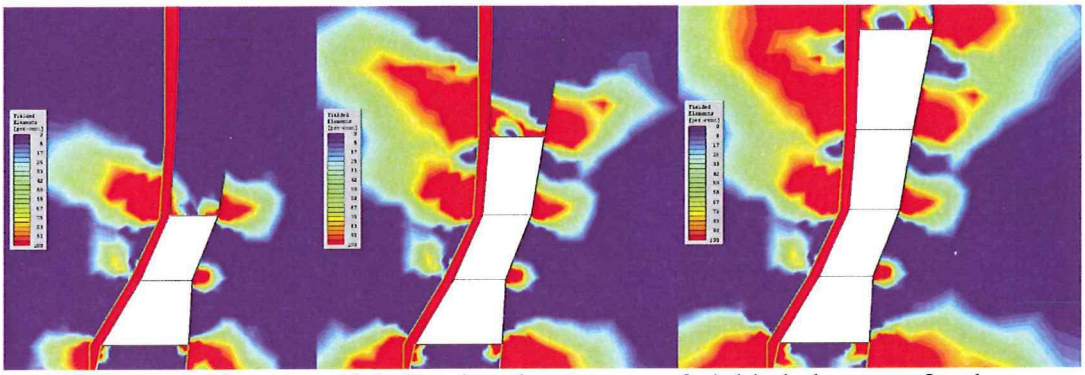

Figure 9.4: Phase2 model showing the amount of yielded elements for three succeeding stages.

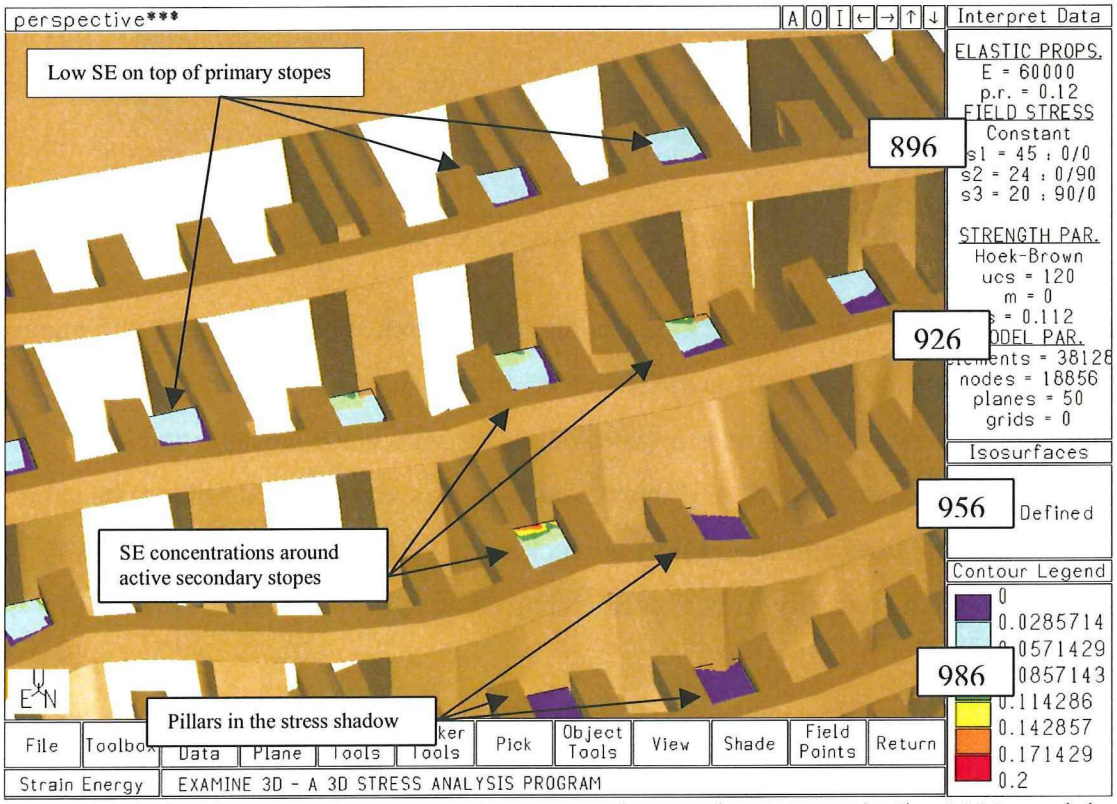

Figure 9.5: Strain energy concentrations around secondary stopes in the 2013 model.

Figure 9.5 shows a part of the 2013 model. The vertical line of pillars on the left is also shown in Figure 9.3. In Figure 9.3 the peak in strain energy of 2013 is clearly seen in the picture as the strain energy concentrations are highest on 956 level. The

pillar on 986 in 2013 lies in the stress shadow, and this is coherent with the strain energy for 986 in 2013 in Figure 9.3. The pillars on top of the primary stopes as pointed out in Figure 9.5 have low strain energies.

Figure 9.6: The 2013 model with $\sigma_1 - \sigma_3$ shown in the pillars.

Figure 9.6 is similar to Figure 9.5, except that the difference between major and minor principal stresses is shown. This difference is effectively the failure criterion. Initiation of some failure starts at approximately 40 MPa while unstable cracking starts at approximately 80 MPa. However, as the rock starts failing it will not be able to sustain the stresses and as an effect the rock starts destressing. The stress paths will at least have to be partially redistributed and lower stresses in the failed area are the result.

In conclusion, the pillars are deemed unlikely to display any violent failure. The modelled strain energy concentrations are most likely dissipated through gradual failure that is initiated in the pillars in the stages prior to the peak concentrations. In this paragraph only the pillars between 12 and 13 were discussed. The other vertical lines showed similar trends. The loading history plots of those lines can be found in Appendix D.

9.1.2 Pillars – 1080 and 926 levels

The two horizontal lines of planes in the pillars are located on 1080 and 926 levels. 1080 was chosen because it is a location where the stresses bend around Lappberget and where they will likely accumulate. The loading history of 1080 level is shown in Figure 9.7.

At the moment of writing, mining has not caught up to the 2008 model yet. The observations of pillar deterioration are therefore not yet up to par with the strength factors shown in Figure 9.7. The early signs of pillar deterioration are there though.

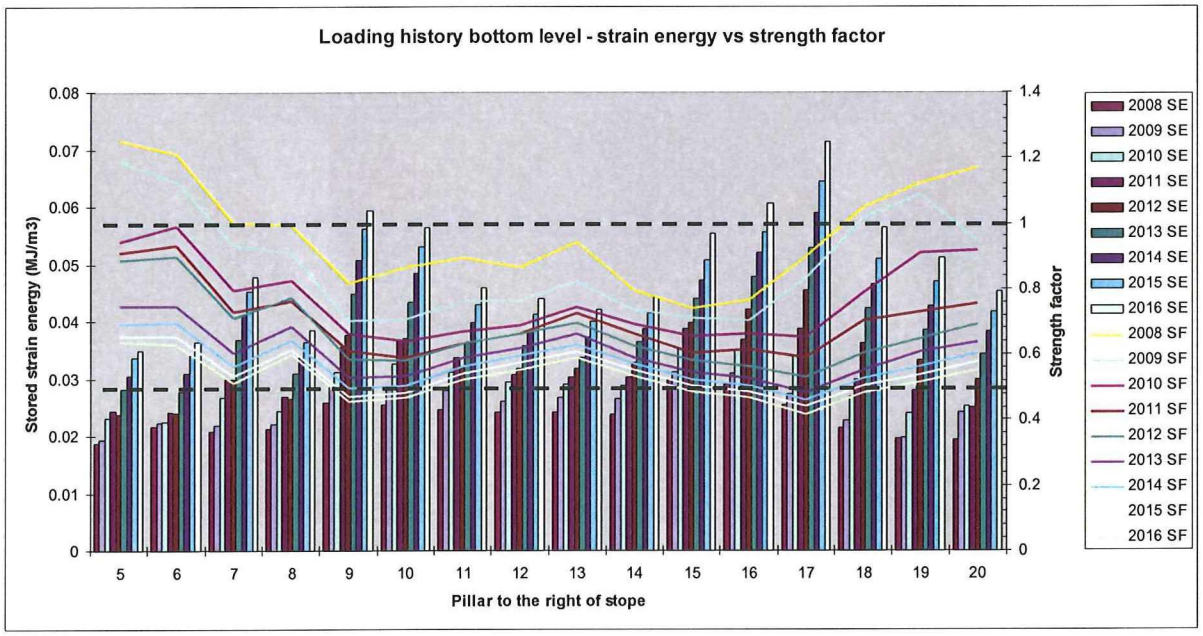

Figure 9.7: Loading history of the pillars on 1080 level.

The strength factor varies over the strike of the ore. This has two probable causes: at the flanks there is intact rock in the proximity and in the centre there are mining activities in the levels above. The strength factor only decreases as mining progresses. Failure in the rock mass decreases the stress sustaining capacity and thus the stored strain energies and very low strength factors shown in Figure 9.7 will likely not be reached.

All mining activities on 1080 level are scheduled to have terminated in 2011. After this time the level will be of no further use from a mining point of view. There might be some additional core drilling to further define the part of Lappberget below 1080

level. Although it is not likely that there will be any type of violent failures as failure initiates, other types of failure could occur because the 1080 level remains a level with dynamic stresses; it does not fully disappear behind the stress shadow.

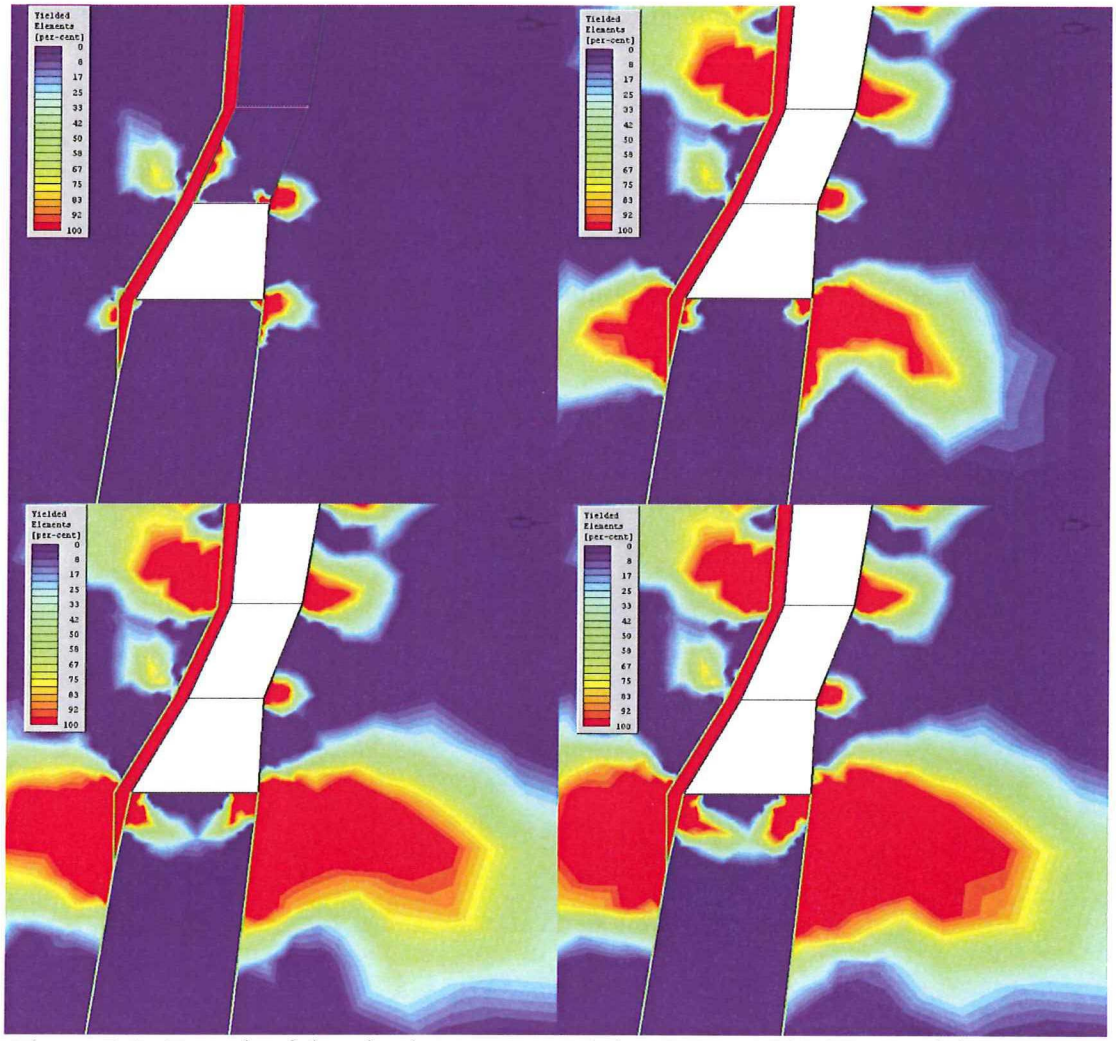

Figure 9.8: Growth of the plastic zone around the FW on 1080. The model stages are 1080 for the top left, 1040 for the top right, 986 for the bottom left and 926 for the bottom right picture.

The growth of the plastic zone at 1080 level is illustrated by the yielded elements in the simple Phase2 model shown in figure 9.8. In the first few stages of the model the growth is the fastest and as the mining progresses in the upper levels the growth slows down.

The effect of the stress shadow is shown in Figure 9.9. This is the plot of the loading history of the pillars in 926 level. In the first three models there is hardly any change in the strength factor as no mining activities take place in the vicinity. The first real

change in the strength factor occurs in the 2011 model when the upper accesses of first primary stopes reach 926 level around stopes 12 to 16. Some failure should then be taking place around that area in the 2012 model before the first secondary stope reaches the 926 level in the 2013 model. There is a peak in the strength factor in the pillar between stopes 14 and 15 for the 2014 model; it is here that the first secondary stope is taken at 926 level which causes the pillar to disappear behing the stress shadow. This shadow expands in the 2015 model where the two adjacent secondary stopes are mined. In the last model all stopes are mined and as a result all pillars on the 926 level disappear in the stress shadow. Analogous to the vertical line of pillars that was discussed in 9.1.1 the strain energies reach their maximum after the strength factor indicated some degree of failure. This means that the strain energy has likely dissipated through the process of failure before it could reach its maximum.

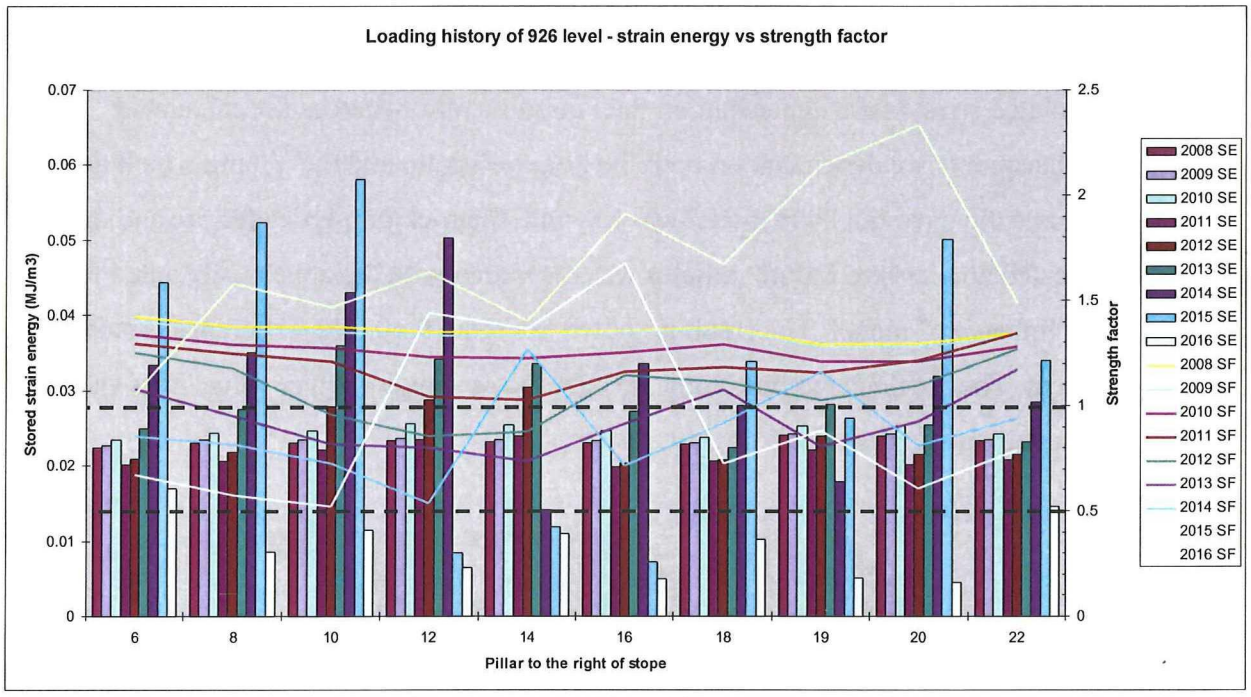

Figure 9.9: Loading history of the pillars on 926 level.

In conclusion it can be noted that the levels that disappear in the stress shadow will probably not cause any violent failure. The bottom level will likely dissipate the strain energy through gradual failure rather than violent failure. The bottom level can potentially be sealed off or be regarded as a non-entry area in the 2011 stage provided that all potential core drilling has been carried out. Until that time the overall stability of the level, as in all levels but especially on 1080, should be closely monitored.

9.1.3 Secondary stopes

The secondary stopes are not in the limestone, for which the depth of failure was calibrated. The UCS value for the ore was picked at 200 MPa and the Young's modulus at 90 GPa (Table 7.3). For all of the Examine3D models the parameters for limestone were entered, but adding in a few constant factors can approximate the properties for the ore. The difference in the Poisson ratio is neglected (0.12 for limestone vs. 0.15 for the ore). The strain energies need to be multiplied with a factor of 1.5. The strength factor needs to be multiplied by a factor of 120/200 = 0.6 to get a more accurate estimation for the depth of failure. This has not been calibrated, but is based on the measured UCS values for ore and the experience of the limestone calibration. It is strongly recommended to develop (calibrate) some sort of failure criteria in the ore.

There is an error in using simple factors to account for different rock properties. The calculated stresses are dependant on the Poisson's ratio whereas the calculated displacements are dependant on both the Poisson's ratio and the Young's modulus. To evaluate the error the 2008 model was run with the rock properties for ore and the indicated zone where failure initiates was compared with the zone recalculated from the "limestone" model. The result is shown in Figure 9.10. The difference is small but present. The recalculated limestone strength factor shows a lower value. This should be kept in mind when analysing the results.

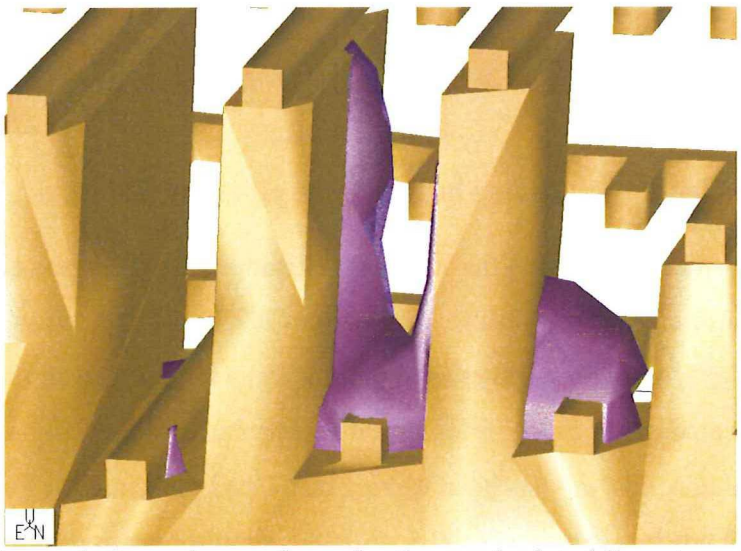

Figure 9.10: Strength factor iso-surfaces for the recalculated limestone (blue) and ore (orange) properties.

In each of the models the strength factor of the previous model was plotted. In addition the iso-surface for the failure criterion of the model itself was added as a transparent iso-surface. Such an outcome is shown in Figure 9.11.

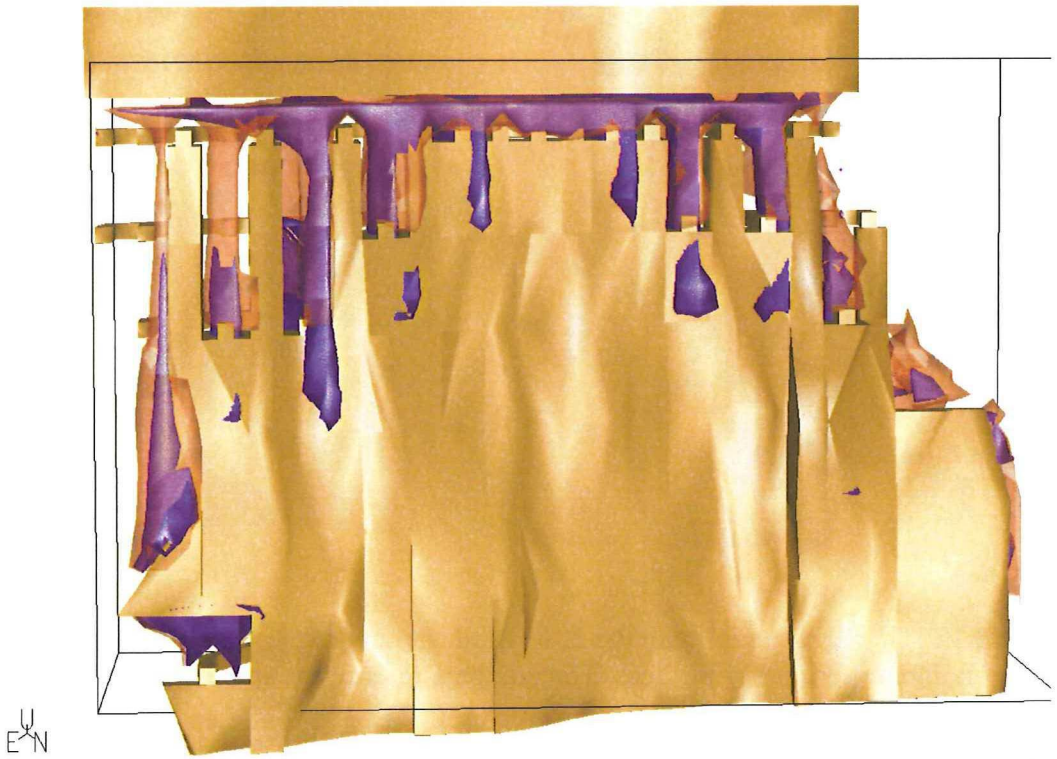

Figure 9.11: The 2015 model with the 2015 (transparent orange) and 2014 (solid blue) failure criterion iso-surfaces.

The situation as in Figure 9.11 is exactly as expected. The model indicates failure in all secondary stopes in the 2014 model. This failure progresses in the 2015 model so that all secondary stopes are likely effectively destressed for the 2016 model. The verdict for this model is therefore rather simple; the stopes will likely have shown some degree of failure before energy can accumulate.

In models showing an earlier stage in the life of Lappberget the situation might be a little more complicated. Figure 9.12 shows the 2010 model with the 2010 and 2009 failure criterion iso-surfaces. From the picture it can be seen that there is no indication of previous failure in stope 14 and 8, so the top accesses for these stopes might be excavated in highly stressed ground. It is in these drifts/stopes that the potential for some degree of strain related seismicity is the highest for this model. The model outcomes similar to Figures 9.11 and 9.12 can be found in Appendix E.

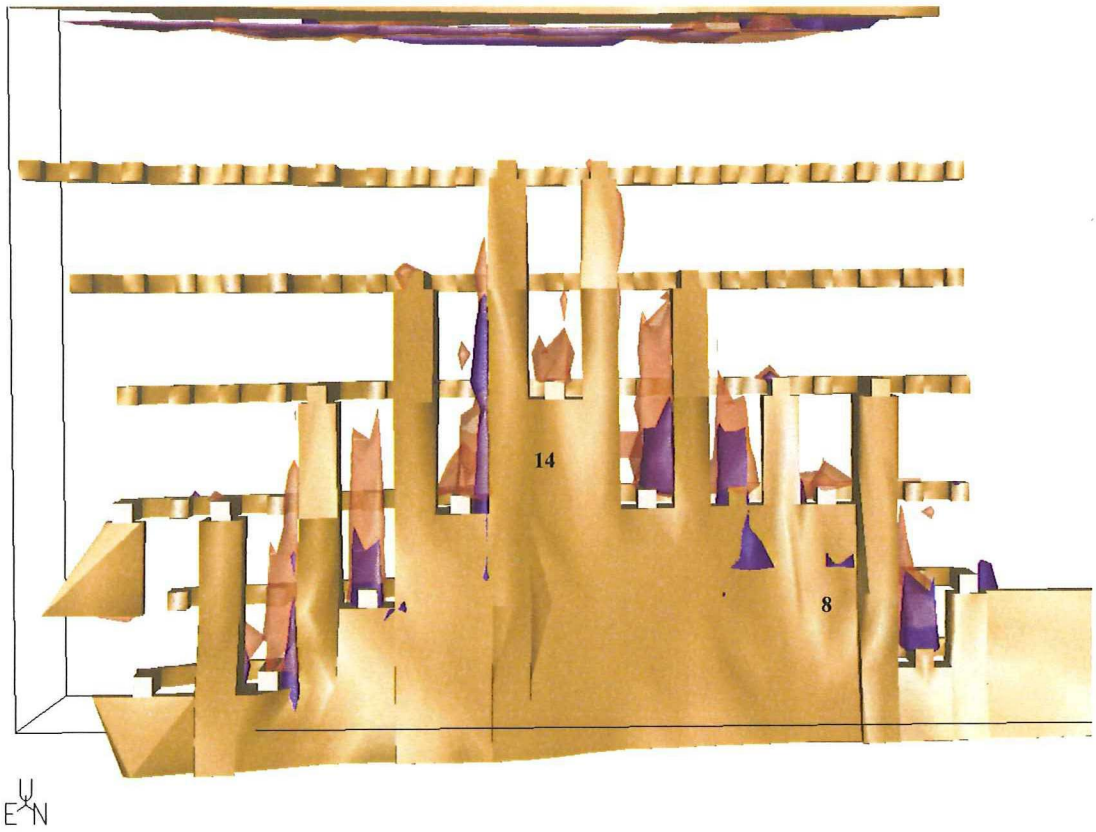

Figure 9.12: The 2011 model with the 2011 (transparent orange) and 2010 (solid blue) failure criterion iso-surfaces. The numbers refer to the stope numbers.

From all models the potentially problematic stopes have been summarized in Table 9.1. The stresses and strain energies (SE) in this table are taken at the location where the top access will be excavated in the previous model. Those drifts are anticipated to have the most risk for rockbursting when they are constructed. Not only because of the chance of seismicity but also because people could be working there.

The values for these locations are based on the BEM and should be placed in the proper context. If one assumes that the skarn-talc rock mass at the hanging wall contact has roughly the same properties as the limestone in the footwall, the depth of failure in the hanging wall can be estimated by creating iso-surfaces of the strength factor of 1. It turns out that all iso-surfaces run into the hanging wall. An example is shown in Figure 9.13, where the yellow iso-surface is extended even from the problematic stopes from the 2014 model (stope 18 and 8) into the hanging wall. The expectation is that the stresses modelled in the BEM will turn out lower in reality.

Table 9.1: Potential problematic secondary stopes. The stresses and strain energies are taken on the location of the top access for those stopes in the previous model. HW gives an indication of the ore/hanging wall contact.

Model	Stope	Level	σ1	σ3	SE	HW
			MPa	MPa	kJ/m^3	
2016	None					
2015	None					
2014	18	986-956	70-85	0-20	30-90	Failed
	8	986-956	60-85	0-20	30-100	Failed
2013	22	1040-1060	45-95	5-25	30-120	Failed
	8	1016-986	40-60	0-20	30-60	Failed
2012	14	986-956	50-70	0-20	30-90	Failed
	16	1016-986	50-90	0-20	30-90	Failed
2011	20	1080-1060	55-105	5-15	30-150	Failed
	16	1040-1016	55-85	0-20	30-60	Failed
	14	1016-986	55-75	0-15	30-60	Failed
	8	1040-1016	45-75	0-20	30-60	Failed
2010	All	1080-1016	35-65	0-20	30-90	Failed
2009	All	1060-1040	40-70	0-20	30-90	Failed
2008	N/A					

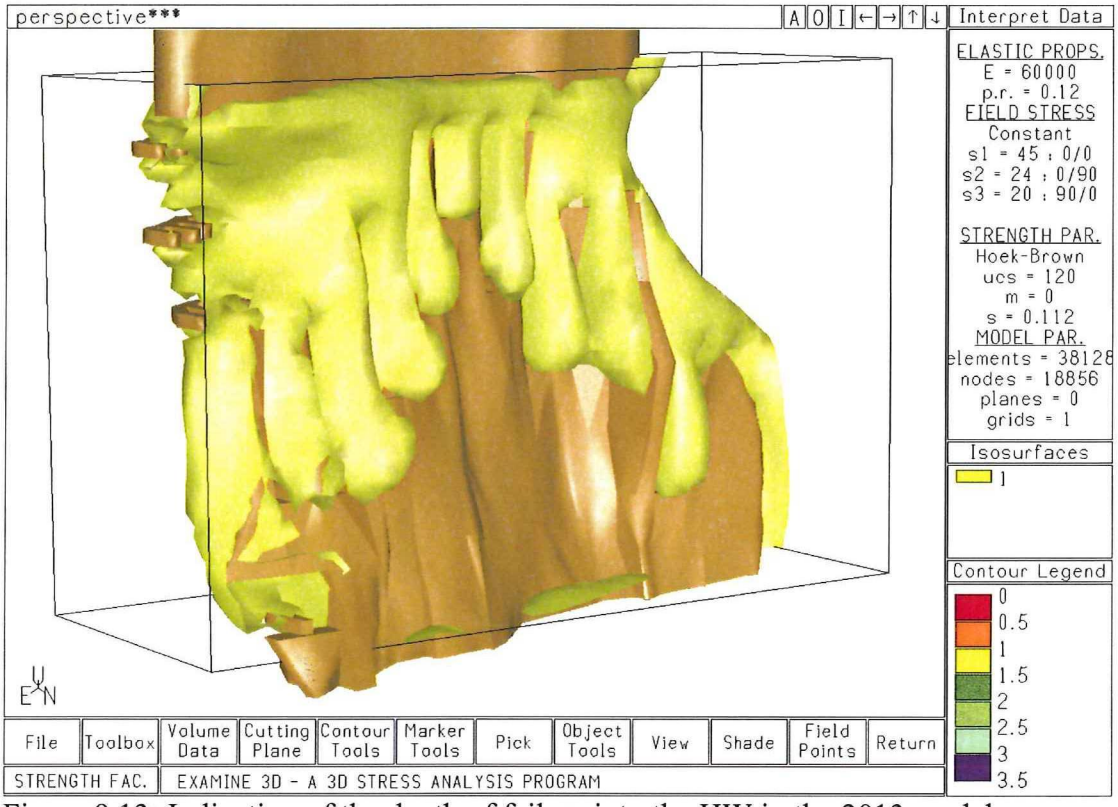

Figure 9.13: Indication of the depth of failure into the HW in the 2013 model.

Failure in both the hanging wall and footwall causes the stresses in the stopes to reduce. As a result of the reduction of stresses, the failure in the ore might not be as extensive as modelled in Examine3D. Figure 9.14 shows the amount of yielded elements in the elasto-plastic model and has the iso-lines of the strength factor from the elastic model that indicates the depth of failure. The strength factor in Phase2 is very similar to the strength factor in Examine3D. It appears that the yielded zone can be reasonably approximated with the strength factor for most stages. When the sill pillar yields in the ore, it seems that the yielded zone is not as extensive in the HW and FW as indicated in the elastic model.

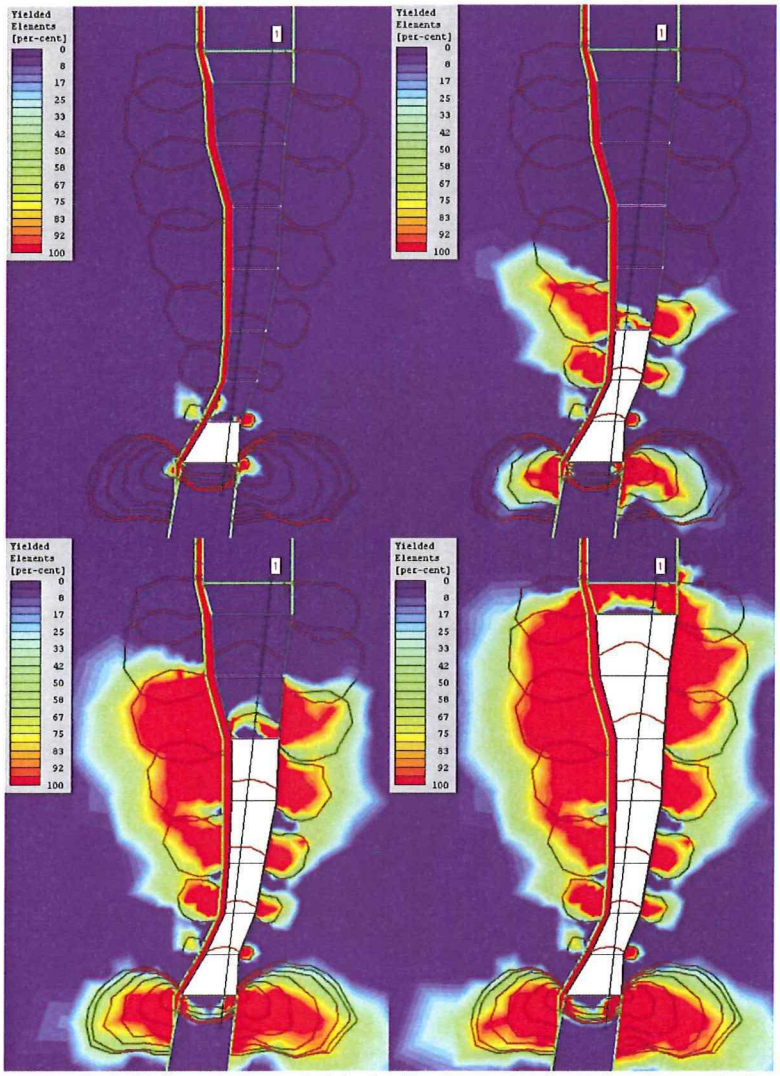

Figure 9.14: Strength factor vs. yielded elements in the elastic and elasto-plastic models. Note the line running through all the stopes; along this line the data points for Figure 9.15 were gathered. For some obscure reason number 1 on this line is the end point. The 1080 stage is in the top left, the 1040 stage in the top right, the 986 stage bottom right and 926 stage bottom right.

The resulting reduction of stresses can be indicated with Figure 9.15. For both models a query line was inserted into the models at exactly the same position with the exact same query point intervals along the line. A third model in Phase2 was made where all materials are elasto-plastic except for the ore (named the semi-plastic model). This should give an indication of the stress reduction in the ore due to the yielded zones in the FW and HW. Again this is not completely correct either, as the plastic zones of the ore and the other zones will likely interact. The yielded zones on either side of the ore are nearly identical in the plastic and semi-plastic models.

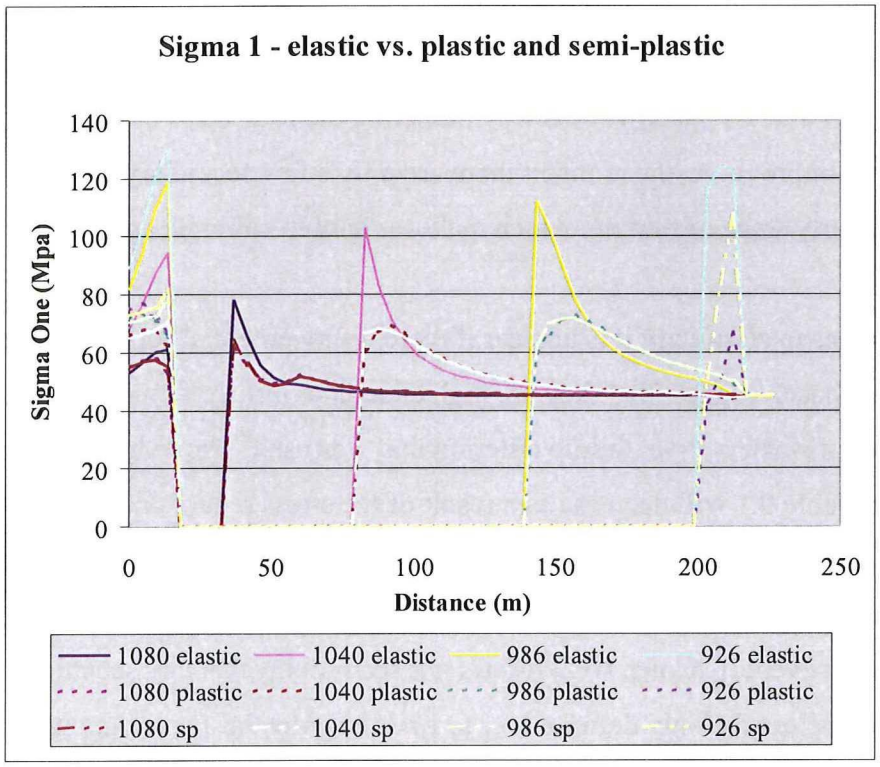

Figure 9.15: Sigma 1 in the elastic vs. elasto-plastic models.

The main result is that the stress reduction in the ore in the plastic model is mainly due to the plasticity of the HW and FW, as the values for the plastic and semi-plastic model are not very different. The exception is the sill pillar where stresses seem to increase towards the top. In this part the stress will likely exceed the strength and plasticity will occur.

In conclusion, it can be said that the stresses are probably reduced significantly due to failure of the hanging wall and the footwall as indicated by the Phase2 models. The

exact amount of stress reduction due to the created stress shadow in comparison to the Examine3D models is hard to determine with the available modeling software. To get a more accurate picture of how this should work fundamentally a three-dimensional failure modeling method can be used. It is the question if this would approximate the real conditions with the limited information available of the distribution of the different rock masses.

When it comes to secondary stopes it is important to keep track of all observations in the top access drifts and possibly compliment it with convergence measurements to get a sense of plasticity around the drift perimeter. Based on observations the virgin stresses could be calibrated to account for the plastic zone in the FW and HW, which puts the ore in a stress shadow. This way modeling the rock mass in the secondary stopes could improve. At the moment there are only a few secondary stopes and it is only in the early stage of mining, which makes it hard to calibrate anything.

When it comes to seismicity it is unclear if there is any potential for it. The indicated stresses by Phase2 suggest that they are high enough to initiate failure according to the, somewhat conservative, failure criterion that was used. The indicated strain energies in Table 9.1 will decrease as a result of the stress reduction. Whether or not the rock will fail and if there will be any seismicity is unclear. When comparing the strain energies in the secondary stopes with the strain energy found for the Kanalmalmen event (Chapter 10.2) it does not seem likely that any seismicity will occur. Nonetheless the only definite way to find the potential for seismicity is once a seismic event occurs.

9.1.4 Sill pillar considerations

As can be seen in Figures 9.11 and 9.12 failure in the ore starts in the sill pillar from an early stage. Similar images of the other models can be found in Appendix E. These indicated plasticity zones are likely to be smaller than modelled due to failure in the hanging wall and footwall. The exact same arguments are valid: failure can probably not be accurately predicted when failure in the HW and FW obscures the stress situation in the sill pillar. Figure 9.15 shows that stresses around the sill pillar can get high despite the failure zone. In the plastic Phase2 model from Figure 9.14 it shows

extensive failure in the sill pillar occurs, even though the backfill properties in the above cut and fill area are probably too optimistic.

The strain energies in the sill pillar are high in the Examine3D model. They reach up to about 200 kJ/m3, which is in the same order of magnitude as the Kanalmalmen case. This value is not realistic though, as gradual failure in that region will prevent the rock from reaching that amount of energy. Furthermore failure in the FW and HW will significantly reduce the stresses in the sill pillar. Similarly to the secondary stopes, it is unlikely that the rock mass can accumulate enough energy to display any strain related seismicity because of the probable gradual failure of the rock and the reduction of stresses in the sill pillar due to FW and HW failure. Developing a failure criterion based on observations in the ore should provide clarification.

9.2 Seismicity related to geological features

The Zinkgruvan case in Chapter 10.1 shows that the majority of the seismic events there might be due to a large-scale fault, which is running in the footwall. At present no such large structure is known in the vicinity of Lappberget.

If such a structure would be present close to Lappberget an upper-bound value can be estimated with the ESS method (Chapter 8.3.2). Looking into the maximum dynamic friction angle required to sustain slippage can provide a quick assessment. An example of the maximum required friction angle is shown in Figures 9.16 and 9.17 for the 2013 and 2015 models, respectively. It can be seen that the area for the potential for slip along a structure increases as mining progresses.

The influence of a plastic zone on a possible nearby structure is not straightforward. It could reduce or increase the stresses depending on the distance from the plastic zone, but the resulting change in the normal and shear stress will likely depend on the orientation of the hypothetical structure too. If there would be any structures close to the hanging wall (in or very near the indicated zone of plasticity) there is a good chance that the rock will fail gradually and will not be able to accumulate stresses/energy for a sudden (violent) failure.

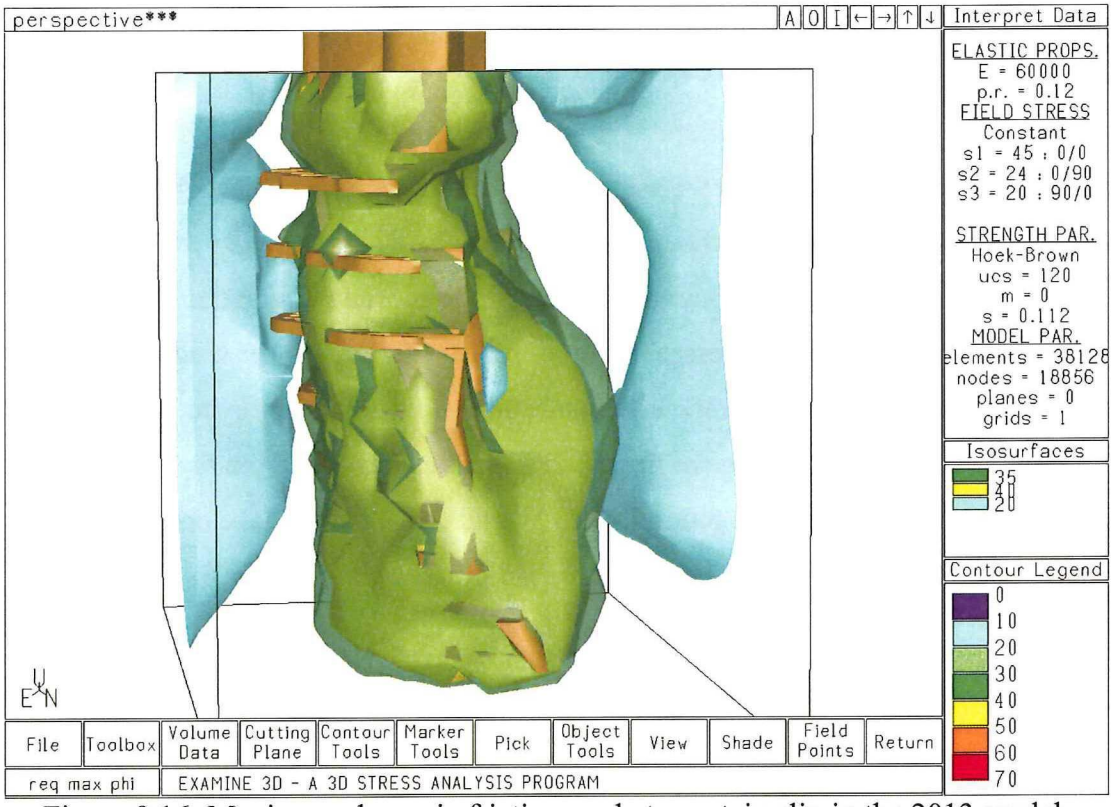

Figure 9.16: Maximum dynamic friction angle to sustain slip in the 2013 model.

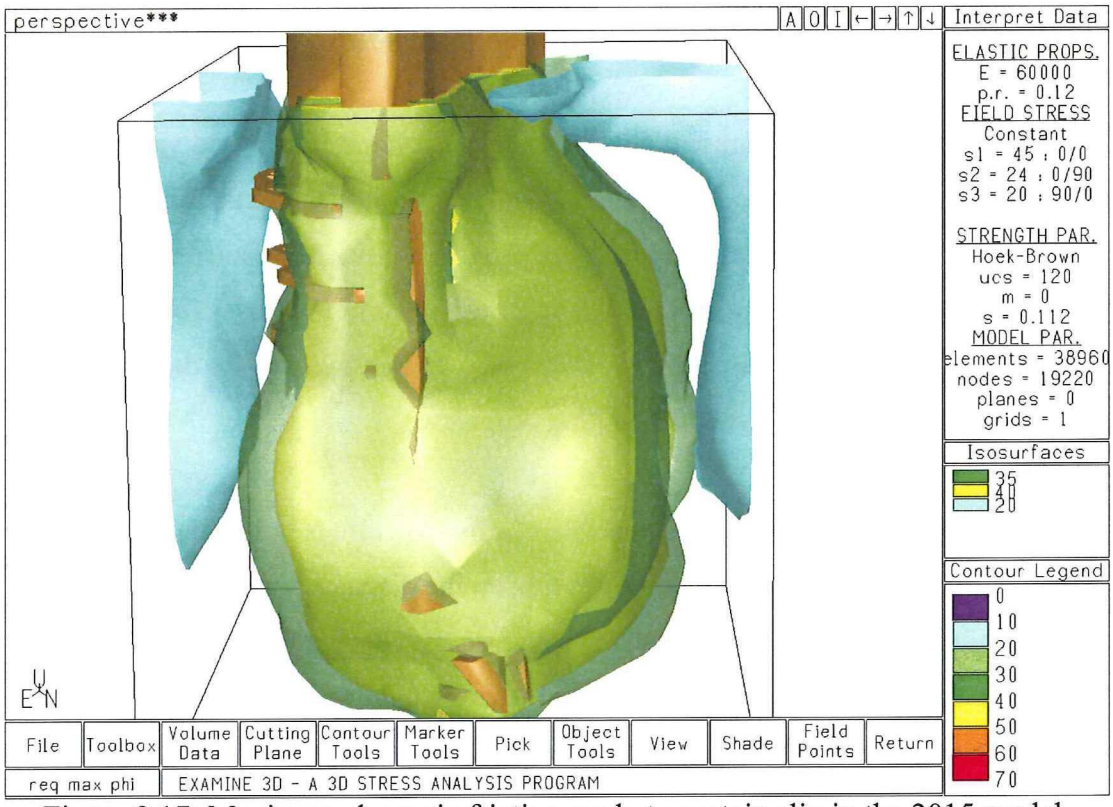

Figure 9.17: Maximum dynamic friction angle to sustain slip in the 2015 model.

9.3 Discussion on the results

The main issue in this chapter is the trade-off between results from a method that assumes a homogeneous elastic rock mass and the expected and modelled plasticity. Modelling the plasticity was done by a two-dimensional finite element method, which has some inevitable errors in itself. Not only representing the geometry of the stopes is a problem, the geometry of the different rock masses and their properties are hard to capture in the model because of both geological uncertainty and the lack of a representative plane strain situation.

The pillars on the footwall drift are likely the easiest to assess. The prognosis is that they will destress themselves prior to reaching maximum strain energies. This was determined by analysing the calibrated strength factors versus the progressive loading. The mechanism seems to be confirmed by the Phase2 model outcomes.

There will most likely be plastic zones in the HW and FW. These plastic zones will likely reduce the stress in the ore (stopes, sill pillar) significantly as indicated by Figure 9.15, which would in turn lower the strain energies in the ore. A stress reduction also means that the rock in secondary stopes might not fail prior to mining activities. Calibration of the models should be carried out through observations and convergence measurements.

At present there are no significant structures such as dykes and faults known to be in the vicinity of Lappberget. If such a structure would exist, an upper-bound estimation of fault-slip event magnitudes can be obtained by using the ESS method. Although this method is somewhat conservative and has some fundamental errors it is a good starting point. With the Examine3D software the normal and shear stresses can be calculated after some manipulation of the modelled data. The influence of any plastic zone is not straightforward and likely depends on the distance and orientation of the structure. By evaluating the maximum dynamic shear strength (in the most optimal orientation of the fault) a quick estimation can be made if the structure has any potential to sustain a fault-slip movement. If this is the case, the static shear strength and the shear stresses can be examined. This will require some serious guessing as the

cohesion of faults are known to vary significantly and the dynamic and static shear strength coefficients are hard to measure.

The ESS method assumes a planar structure, which, especially on a large scale, is usually the case. There are some more drawbacks to this method as outlined in Chapter 8.5.2 and 8.3.2.

This chapter can be concluded with the note that strain related seismicity is likely not going to occur in the pillars. For the secondary stopes it is not likely that any strain related seismicity will occur, as the modelled stresses will either be reduced by the failed zones in the FW and HW or will cause the rock in the stopes to fail gradually before sufficient energy can accumulate. This is based on the case study of Kanalmalmen in Chapter 10.2. The fault-slip potential depends on the occurrence, location and orientation of any significant structures. Any structures that are very close to the hanging wall of Lappberget will likely be destressed due to gradual failure of the weak ore/HW contact.

There should be a disclaimer here. The only definite way of finding the potential for seismicity is by experiencing seismicity. Prediction will improve with calibration of the models and experience that comes along with mining Lappberget. This thesis is focussed on finding the potential violent failure, but there are other forms of instability that could cause trouble, such as fall-out of wedges in the destressed footwall infrastructure.

9.4 References

Martin, C.D., 1997, *The effect of cohesion loss and stress path on brittle rock strength*. Can. Geotech. J. 34: 698-725 (1997).

Nyström, A., 2005, *Numerical analysis of stope dimensions for large scale mining of the Lappberget ore body and prognosis of mining conditions*, New Boliden AB internal report TG_REP2005/004, Boliden, Sweden. (in Swedish)

Rocscience, 2003, *Examine3D*, version 4.0992, Toronto, Canada

Rocscience, 2008, *Phase2*, version 6.028, Toronto, Canada

10. Case studies

In this Chapter two case studies will be discussed and modelled similar to the modelling done on Lappberget. This should provide an idea of conditions necessary for seismic events. The first case study is on an orebody in the Zinkgruvan mine that showed some seismicity. This mine is equipped with a microseismic monitoring system that provides estimations for location and magnitude of the event. The second case is on an orebody in Garpenberg where an event took place of which the tremors were felt on surface. While the magnitude was not recorded the location was known and it might prove a useful case as rock and stress conditions are similar to Lappberget.

10.1 Zinkgruvan

Zinkgruvan is an old mine in the Bergslagen district in Sweden near the tourist town Askersund. The mine has been continuously in operation since 1857 (Figure 10.1) and is currently owned by the Canadian mining firm Lundin Mining. Zinkgruvan produced approximately 800 ktons of ore annually over the years 2004 to 2006 with approximately 10% Zn, 5% Pb and 95 g/ton Ag grades. (Lundin website, 2008)

Figure 10.1: Zinkgruvan mine (Wikipedia, 2008)

The mine consists of several orebodies, of which Nygruvan and Burkland are the major ones. They are separated by the Knalla fault. Figure 10.2 shows the crude regional geology around Zinkgruvan. Nygruvan runs approximately NW-SE while Burkland is oriented roughly perpendicular in the NE-SW direction. Both ore bodies are lead-zinc deposits. In addition there is a copper deposit located in the hanging wall in Burkland, but that has not been touched yet except for one exploration drift. Nygruvan is steeply dipping towards the NE, while Burkland is dipping steeply towards the North. (Sjöberg, 2005)

The rock conditions, mining geometries and stresses in Burkland resemble conditions in Lappberget and as a result this case study will be limited to Burkland and its seismic events only.

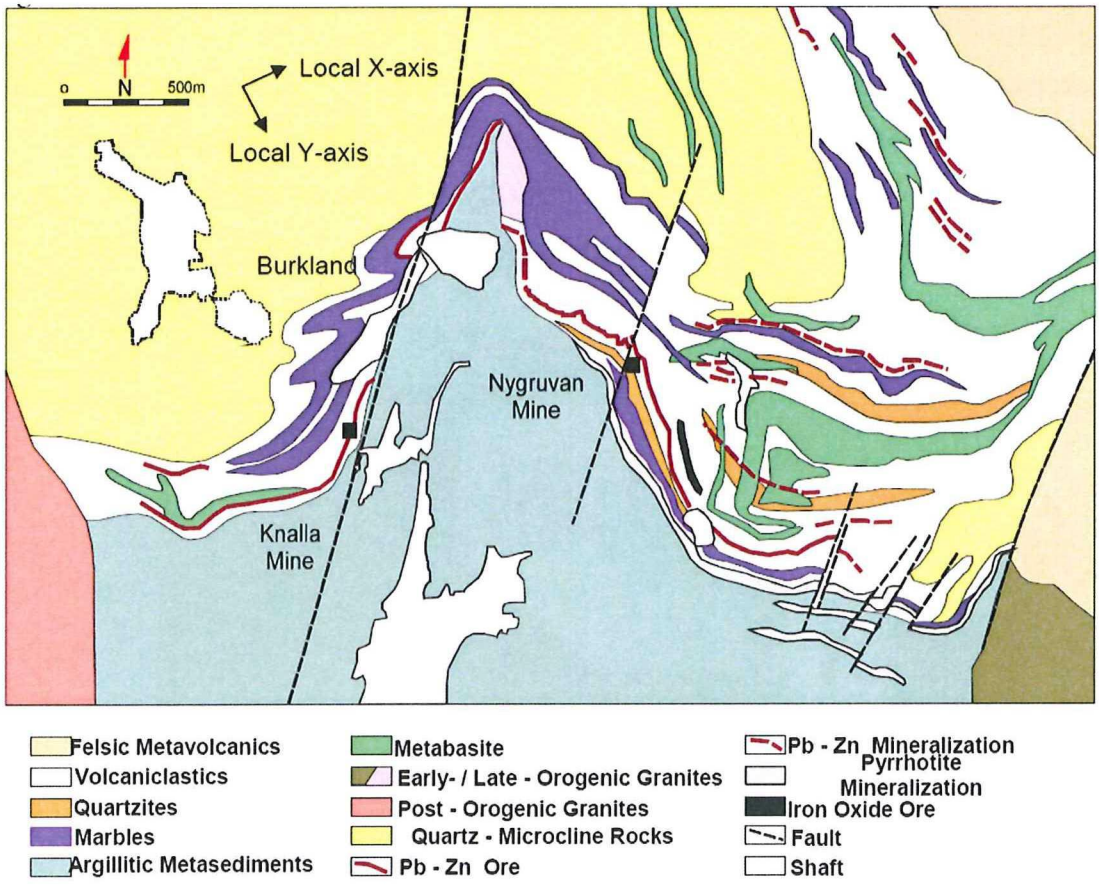

Figure 10.2: Regional geology around Zinkgruvan (Sjöberg, 2005)

10.1.1 Mining Burkland

Zinkgruvan is using its own coordinate system where the X-axis is roughly parallel to Nygruvan and thereby roughly perpendicular to Burkland. The X-axis is oriented 54.995° off of the geographic North, as shown in Figure 10.3.

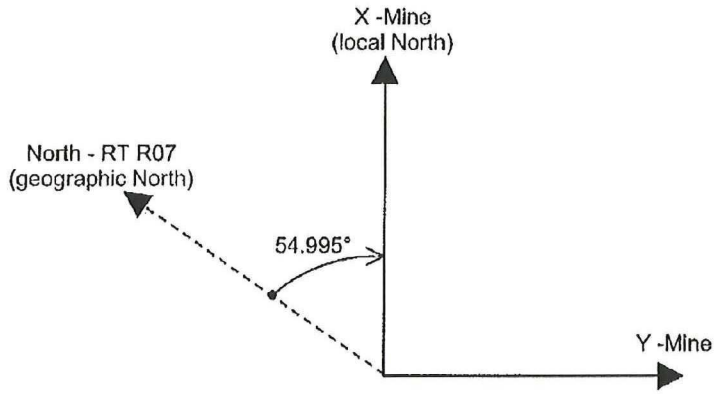

Figure 10.3: Local mine coordinate system and true North. (Sjöberg, 2005)

In Burkland a longhole open stoping method is used. The primary stopes are 30m in height (+5m for the drift) and 20m wide along the strike of the ore. These stopes are backfilled with 4-6% cement filled backfill. The secondary stopes are 25m wide and have 2-3% cement in the backfill. A small cross section is included in Figure 10.5 to give an idea of the mining geometry. The copper ore body is included in this figure as well; it is located on the left in the picture in the hanging wall. Previously larger stopes were used but this led to additional dilution and in some cases cave-ins from the hanging wall. As a result the stope sizes were reduced to avoid these problems. (Sjöberg, 2005)

The mining geometries for the case study were provided as triangulations that could easily be imported into Examine3D. Three major seismic events happened in Burkland and the mine geometry at those times as well as the indicated event magnitudes and locations were provided (Nyström, 2008 and Askemur, 2008). The input parameters used in the modelling will be discussed in the next section.

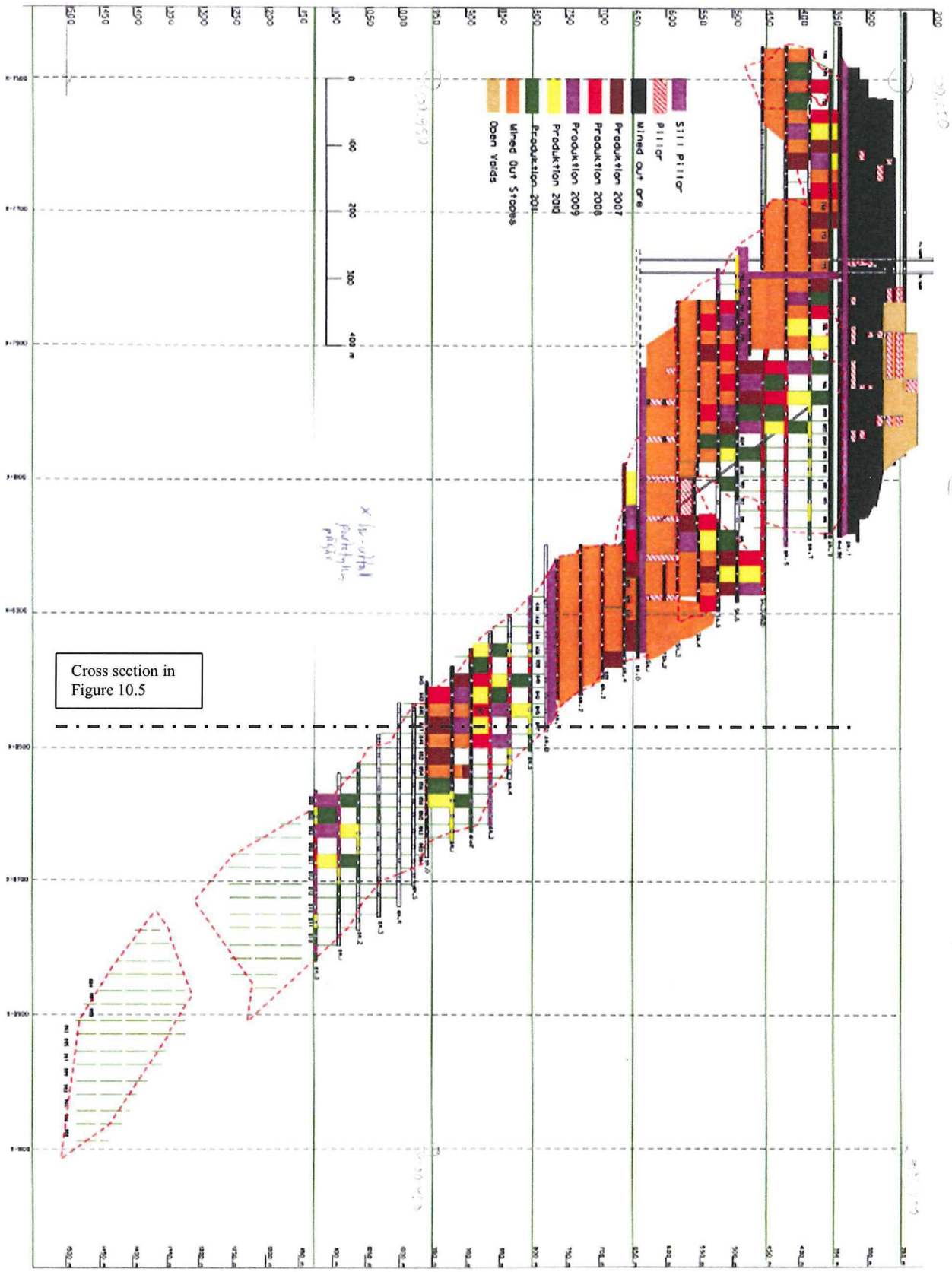

Figure 10.4: Mining layout of the Burkland Zn-Pb orebody (Askemur, 2008)

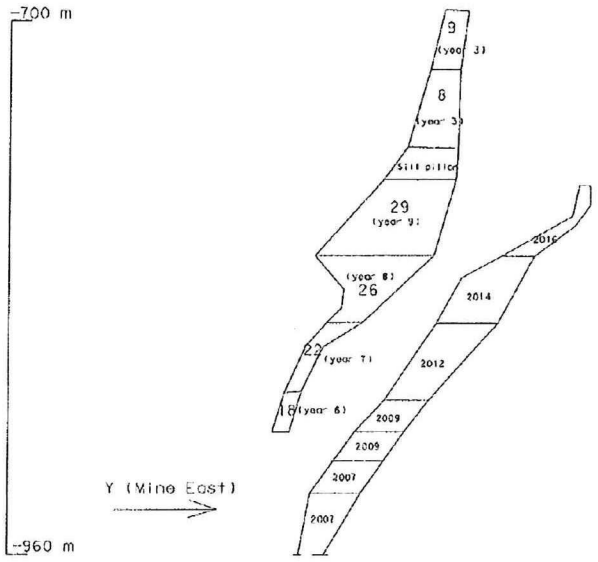

Figure 10.5: Cross section at X ≈ 8475, with the copper ore body in the hanging wall. (Sjöberg, 2005) This cross section is indicated on Figure 10.4.

10.1.2 Geology and Geomechanical properties

Stresses

Stress measurements in Burkland at depth proved to be difficult. Stress induced fractures and natural structures caused measurements to fail. The successful measurements at depth were carried out in the zinc ore at 965m and those indicated high stresses ($\sigma_H \sim 65$MPa, $\sigma_h \sim 45$MPa) of which the major principal stress is oriented roughly perpendicular to the strike of the orebody. Some core disking was observed in quartz rich parts of the core, which indicates that the stress varies locally. An upper bound value for the maximum horizontal stress was estimated at 70 MPa. The orientation of the major horizontal stress seems to comply with slabbing that occurred in the exploration drift in the hanging wall. The experiences with failure in bored raises are less straightforward, here the influence of the Knalla fault and previous mining activities complicated the state of stress. (Sjöberg, 2005)

The picked stress profile is identical to the one used in the report by Sjöberg. It is a rough estimation, where the maximum horizontal stress is oriented E-W (090/00) and the minor horizontal stress N-S (000/00) in the local mine coordinate system. Furthermore a zero intercept was picked, although locked in stresses are widely

experienced in Scandinavia. Equations 10.1 to 10.3 were used in Examine3D. Due to time constraints the study by Sjöberg could not back-calculate these stresses, but these equations should provide a good starting point. (Sjöberg, 2005)

$$\sigma_H = 0.068z \quad \text{[Eq. 10.1]}$$

$$\sigma_h = 0.047z \quad \text{[Eq. 10.2]}$$

$$\sigma_v = 0.028z \quad \text{[Eq. 10.3]}$$

Geology

The general stratigraphy from the footwall of the zinc ore to the hanging wall at the copper ore (Figure 10.5) is (Sjöberg, 2005):

1. **Biotite Leptite**; relatively competent rock, with varying contents of biotite. GSI rating between 50 and 60 based on estimations and previous experience by Sjöberg.
2. **Leptite and/or Skarn-leptite**; varies from very competent and of high strength to weak and highly fractured, but generally more competent than the hanging wall counterpart. GSI in the range of 50 to 65, although some parts with lower GSI occur intermittently.
3. **Zinc-lead ore**; competent and of high strength throughout the mining horizon. Consistent GSI ratings between 60 and 70, sometimes up to 80.
4. **Leptite and/or Skarn-leptite**; Varies from very competent and of high strength to weak and highly fractured, most often at the immediate hanging wall contact. Areas with low GSI of around 35 occur (sometimes lower), but the major parts are between 50 and 65.
5. **Limestone/marble**; fairly high degree of metamorphosis rendering this rock type relatively high strength, although significantly weaker and softer than the surrounding leptites. GSI between 60 and 65, sometimes up to 80.
6. **Copper ore**; relatively competent but judged slightly weaker and softer than the lead-zinc ore. GSI between 55 and 65, locally up to 80.
7. **Quartz-feldspar leptite**; very competent with high strength and stiffness, and with typically brittle behaviour. GSI in the range between 70 and 85.

There are a few structures present in the area. A brecciated fault zone between the zinc-lead and copper ore bodies has been indicated, as well as a crushed zone in the footwall side of the zinc-lead ore. (Sjöberg, 2005)

Rock mass properties and failure criteria

In the report by Sjöberg two-dimensional plastic modelling was done to investigate mining of the copper ore in the footwall. In his model he used the values for the Young's modulus and Poisson ratio as listed in Table 10.1. In his analysis he used the Mohr-Coulomb failure criterion, which is different from the Hoek-Brown criterion that was used for Lappberget. The UCS values for the different rock masses are listed in Table 10.1 as well.

Table 10.1: Rock properties for Burkland (Sjöberg, 2005)

Rock type	UCS (MPa)	Young's modulus (GPa)	Poisson ratio
Biotite leptite (Zn-Pb FW)	175 +/- 75	60	0.25
Zinc-lead ore	225	75	0.25
Leptite and/or Skarn leptite (Zn-Pb HW)	175 +/- 75	70	0.25
Limestone/Marble (Cu FW)	100	55	0.25
Copper ore	165	65	0.25
Quartz-feldspar leptite (Cu HW)	300	71	0.33

For Examine3D only one value for the elasticity can be entered. From a quick assessment it looks as though most of the seismicity took place in the ore or in the footwall of the zinc-lead deposit, so the Young's modulus will be taken as 70 GPa, the Poisson ratio as 0.25 and the UCS as 200 MPa. The input parameters for Examine3D are shown in Figure 10.6.

Some calibration for elastic models is available. Observed failure mechanisms were modelled which provides the stress level criteria as listed in Table 10.2. Note that the picked failure criterion in Figure 10.6 is still conservative, as $\sigma_1 - \sigma_3 = {}^1/_3\ \sigma_c = 67$ MPa. Since this failure criterion is supposed to indicate the initiation of failure it is deemed adequate for this exercise. In the discussion of model results the range of values in Table 10.2 will be discussed as well.

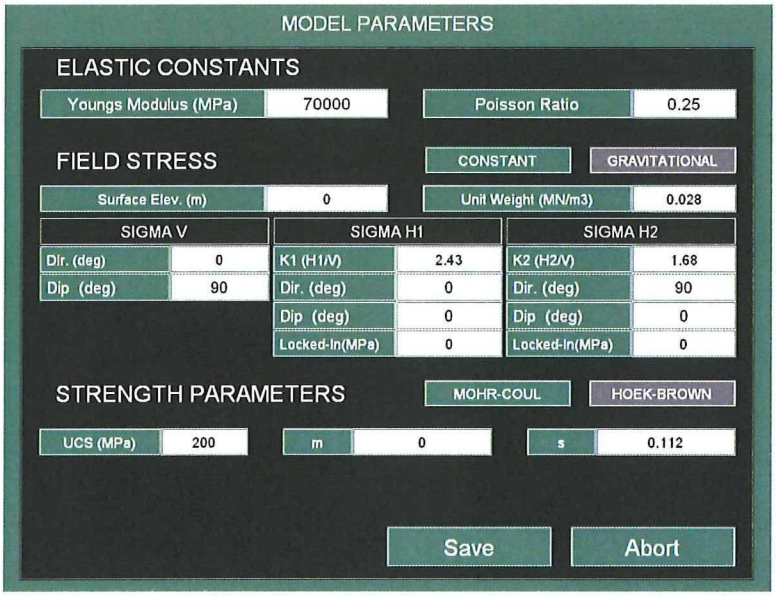

Figure 10.6: Parameters used in all models for Burkland. Note that Sigma H1 and H2 have been rotated, this is because the mine geometry is rotated.

Table 10.2: Stress level criteria for Burkland. The values are calculated elastic stresses normal to the ore body. (After Sjöberg, 2005)

Failure mode	Stress (MPa)
Severe sill pillar damage	125
Floor heave/cracking in benches	100
Foundation failure in the hanging wall	100
Foundation failure in weak hanging wall	75

10.1.3 Seismic events and model results

The seismic events that were picked up in Burkland with a positive magnitude are listed in Table 10.3. The magnitude in this table is a local mine seismic magnitude, which gives values slightly less than the Richter scale. The location of the events is given fairly accurate with a precision of 10 meters or less. (Askemur, 2008)

Table 10.3: Seismic events with positive magnitude in Burkland. The geometries at the time of the events in yellow have been modelled. (Askemur and Nyström, 2008)

Date	Magnitude	X	Y	Z
2003-03-14	0.2	8024	1820	451
2003-03-14	0.1	7959	2091	682
2005-06-02	0.0	8263	1964	798
2005-12-31	0.2	7895	1970	630
2006-05-25	0.6	7897	1952	629
2007-02-14	0.1	8434	2053	765
2007-03-23	0.7	8375	1940	844
2007-04-13	0.0	8366	2024	812
2007-05-11	**1.0**	**8498**	**1954**	**965**
2007-05-28	0.7	7982	2036	480
2007-06-26	0.0	7817	1979	246
2007-08-18	0.7	7945	1960	690
2007-08-18	**1.6**	**7981**	**2012**	**674**
2007-10-01	0.5	8665	1867	963
2007-11-09	0.1	8477	1914	976
2007-11-17	0.4	8117	2002	723
2007-12-18	0.3	8223	2098	568
2007-12-25	0.7	8233	2087	580
2008-02-19	**1.0**	**8334**	**2015**	**685**
2008-02-22	0.1	8053	1991	304

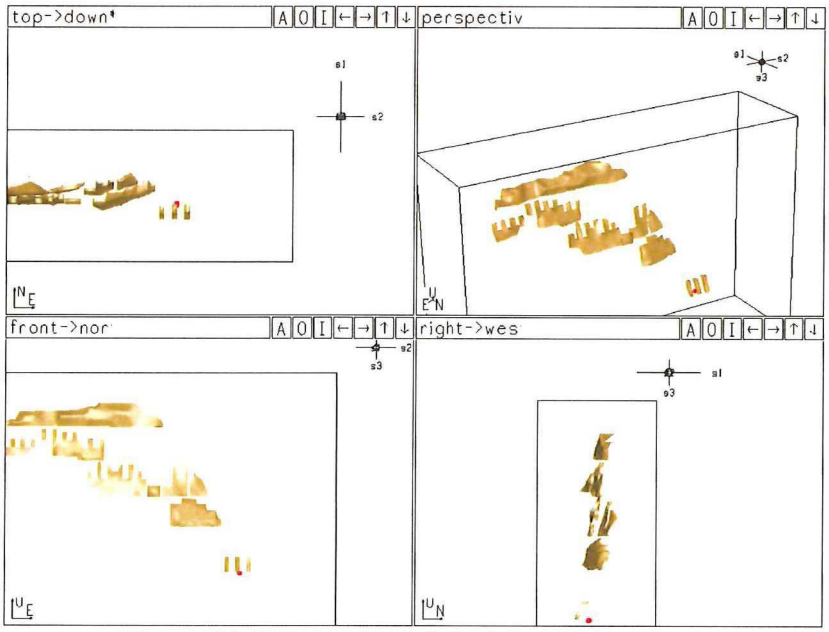

Figure 10.7: Location of the May 2007 event.

The first model is for the May 2007 event with a magnitude of 1.0. No other events with positive magnitude were recorded in the timeframe around the event. The location of the event is shown in Figure 10.7. It was located by the monitoring system

under the deepest stopes in production at the time and it appears to be in the biotite leptite footwall.

The first event did not display any anomalies. The strength factor at that point is 1.67 with a major principal stress component of 66 MPa. The strain energy as calculated is 30 kJ/m3. Even if there would be a large error in the location this event cannot be explained with this model, as there are no anomalies in the area. The major principal stress in the area surrounding the event is shown in Figure 10.8.

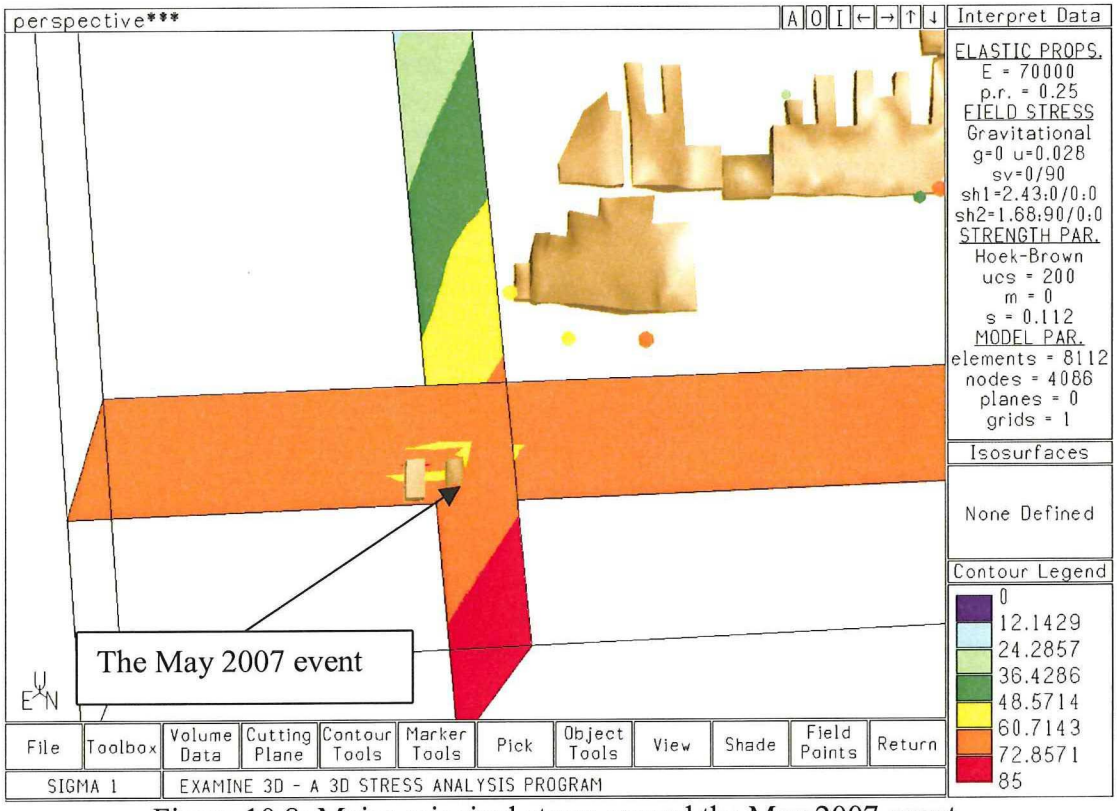

Figure 10.8: Major principal stress around the May 2007 event.

The next event has a magnitude of 1.6 on the local mine seismic magnitude. This event was localised in the footwall. Another event happened on that day close to the larger event with a magnitude of 0.7. This event is located very close to the footwall-ore contact. Figure 10.9 shows the two events. There might not be a relation between the two events, but since the two are located so close to each other and happened on the same day they very well might be. The times of the events were not provided so it is not possible to say which one might have triggered the other.

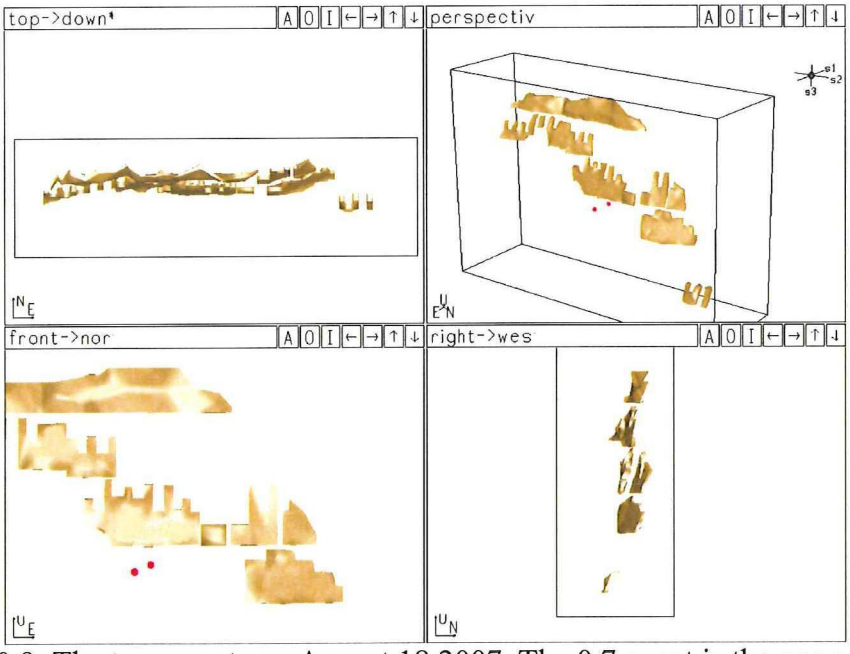

Figure 10.9: The two events on August 18 2007. The 0.7 event is the one on the left which appears to be at the ore/footwall contact and the 1.6 event is the one on the right which is in the footwall.

Similarly to the first event there are no clear indicators for the events. The strength factors are 2.5 and 1.9 for the small and large event, respectively. The strain energies for both locations according to the model are 17 kJ/m3. The large event happened at 674 meters below surface, whereas the closest excavations are at approximately 630 meters below surface.

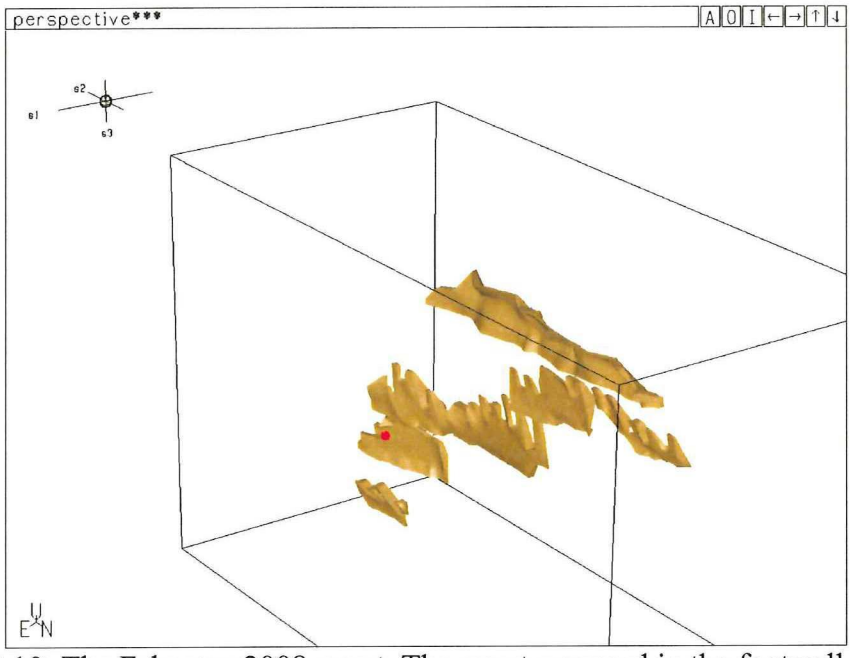

Figure 10.10: The February 2008 event. The event occurred in the footwall at the ore contact and hard to see in a plan or section view.

Figure 10.10 shows the third and last event that was modelled. It was located near the edge of the stress shadow. The stresses are very low at this point, with σ_1 = 14 MPa, σ_2 = 10 MPa and σ_3 = 20 kPa, so failure should not occur according to the criterion. The strain energy at the location of the event is very small.

Since the stresses are so low the tensile strength of the rock might be important. The minor principal stress is still positive, albeit small, in the model, but the stress varies locally and as a result the minor principal stress might become negative. While movement on the plane normal to a potential tensile stress might be possible, the stresses in the stress shadow are small and as such it is not likely that this would cause a high-energy event. In addition, most rock masses have a non-existent tensile strength, which would imply that the rock would destress itself from the time small tensile stresses are present.

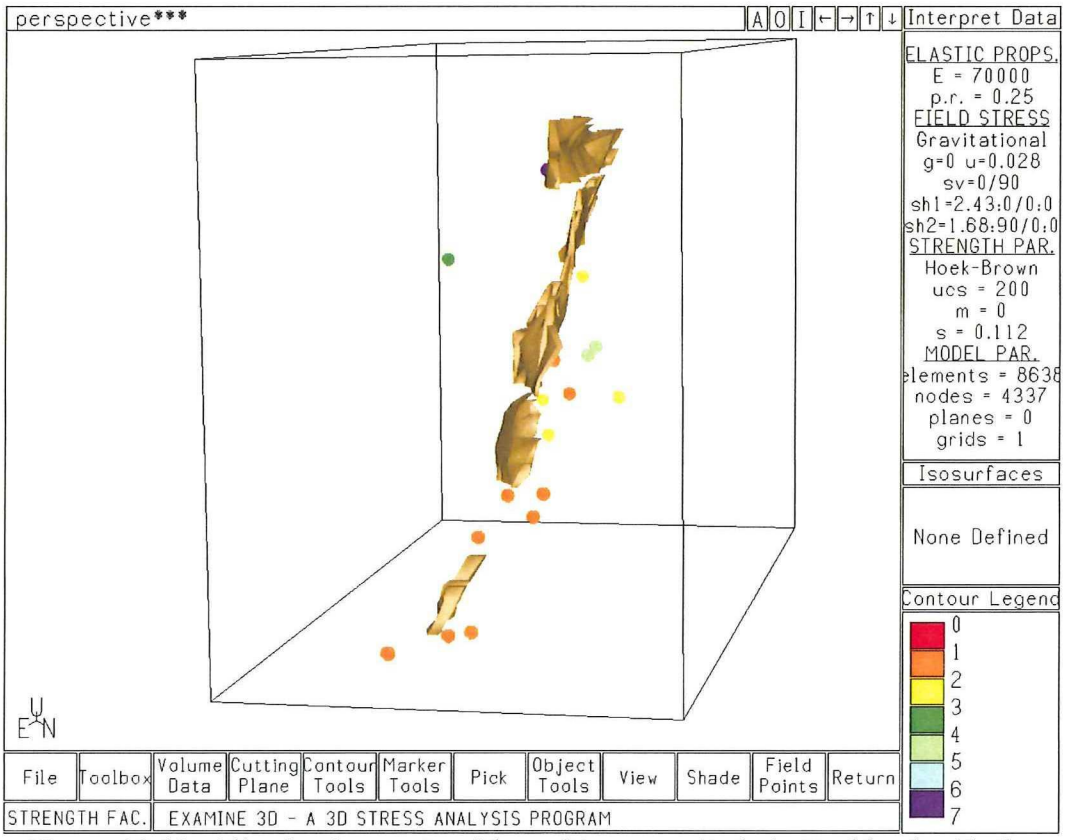

Figure 10.11: All seismic events with positive magnitude in Burkland with the geometry of the February 2008 event.

When looking at the location of the events it is clear that the majority occurred in the footwall. Figure 10.11 shows the location of all the events. The strength factor in this figure has little meaning to the values, as the model is calculated for the February 2008 geometry. Of the twenty events, four appear to be in the hanging wall, four in the ore or very near to the ore-footwall contact and the remaining twelve in the footwall.

Since there are no extremes in any parameter around the events, they have to be caused by something that was not captured by the model. The infrastructure for example is not included in the models, although it is hard to envision that drifts alone could create the conditions for such large events. Another factor that might have played a role in the cause(s) for the events is the large spread in rock properties for the biotite leptite in the footwall (Table 10.1). Furthermore the stresses vary locally as noted earlier.

There is a fault, the Knalla fault, running in the footwall. From stress observations and measurements there was no evident stress rotation present, which implies that the fault is well healed and interlocked and capable of transferring shear stresses. (Sjöberg, 2005) Maybe on a smaller scale there is a large local difference in the fault's properties leading to local stress concentrations while keeping a regional stress transferring capability, similar by the case of the Lockerby mine in Sudbury described in 8.5.2. The author does not know the exact location and orientation of the Knalla fault at the moment of writing.

The above speculations could all have contributed in creating the conditions for the events. There are probably more factors that played a part. Whatever the cause is, the only thing that is clear is that the boundary element method used in these models could not explain the occurrences of the seismic events. Further analysis is needed before the mechanism(s) behind these events is(are) understood.

10.2 Sill pillar failure in Kanalmalmen ore body in Garpenberg

Kanalmalmen is a small orebody in the southern part of the Garpenberg mine as is shown in Figure 10.12. By the end of 2003 mining activities in this ore body were reduced to sill pillar mining by cut and fill operations. The failure that took place in week 47 of that year could be felt in the town of Garpenberg and it is estimated to have a magnitude between 1 and 2 (Nyström, 2008).

This case could be interesting as it might provide some insight in sill pillar failures in particular. Furthermore, the rock and stress conditions are likely very similar to Lappberget which makes it all the more suitable for analysis.

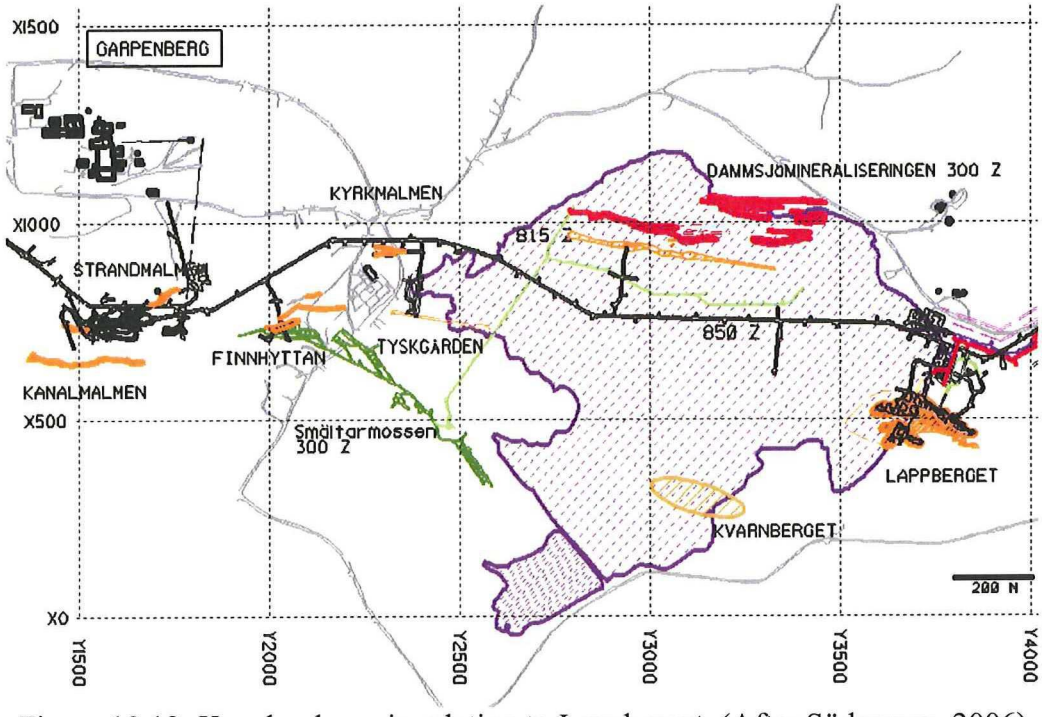

Figure 10.12: Kanalmalmen in relation to Lappberget. (After Söderman, 2006)

The mine geometry just prior to failure is shown in Figure 10.13. The approximate estimated location is shown in this figure as well (Nyström, 2008). The geometry was triangulated and could, after some minor alterations, be used in Examine3D for further analysis (Rocscience, 2003).

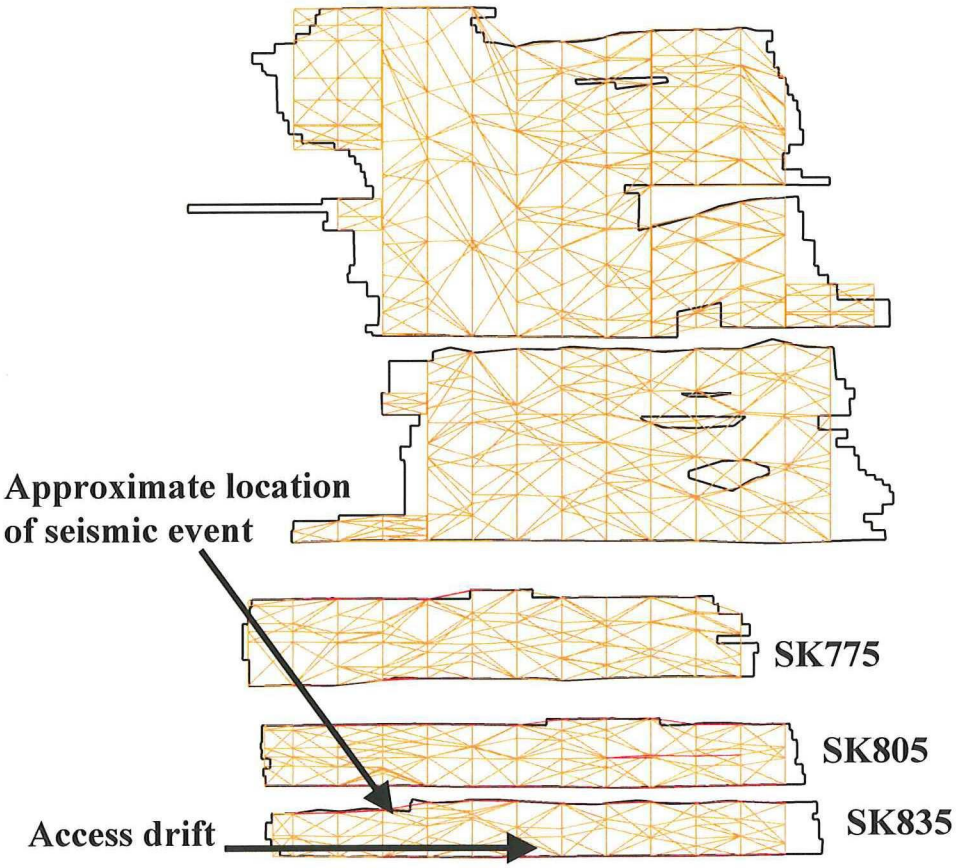

Figure 10.13: longitudinal view from the hanging wall on Kanalmalmen. The triangulation is shown in orange. (After Nystrom, 2008)

In Kanalmalmen two distinct zones can be distinguished. The contact is approximately at the point where the access drift connects to the ore. On the left of that drift (on the right of Figure 10.13) the rock mass is of poor quality with soft schistose contact zones between the ore and the host rock. On this side the encountered problems are related to convergence and large deformations, but there have not been any cases of violent failure. On the right side (left in Figure 10.13) the rock mass is much stronger and stiffer and it is in this zone that the seismic event occurred. After the seismic events sill pillar mining in this part of Kanalmalmen was stopped (Nyström, 2008).

The rock mass properties and stresses have not been measured in this part of the mine. The assumption is made that they are similar to Lappberget. Since Examine3D is a fully elastic modelling program the only real issue with this assumption is the orientation of the far field stress tensor. The major stress component is approximately oriented perpendicular to the ore, which makes the assumption more valid.

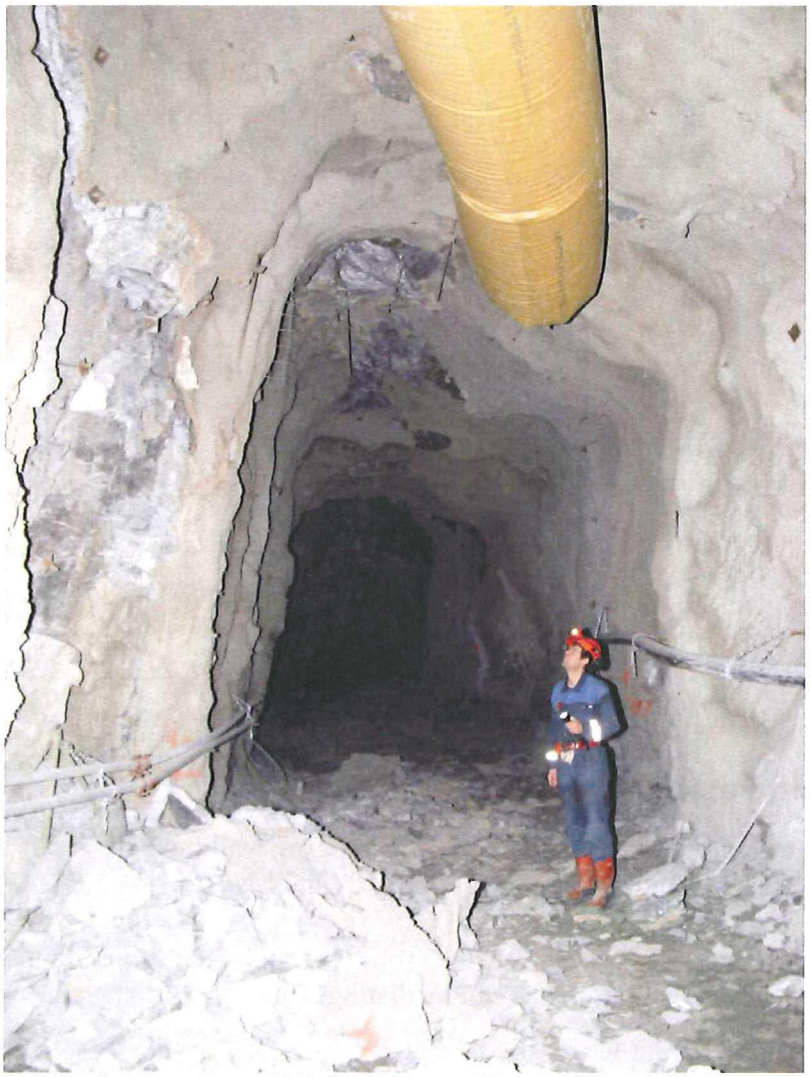

Figure 10.14: Displaced material from the wall and along the centre of the back further down the drift. Anders can, in this case, be used as a scale. (Nyström, 2008)

During the event some material was displaced from the wall as can be seen in Figure 10.14. A bit further down the drift more loose from the back can be seen lying on the floor. The displaced material from the back roughly follows the centreline of the drift shown in Figure 10.14. The backs and shoulders of drifts in Kanalmalmen were supported with rebar (mix of resin and cement grouted) at approximately 1 m spacing and 3 cm fibercrete (steel fibres). In addition shotcrete arches were constructed every ~10m by bolting the profile at a bolt spacing of 1m and applying local fibrecrete with a thickness of ~10cm. These arches functioned to stop the propagation of failure along the hanging wall. The footwall side did not sustain any (visible) damage. Some opened joints along the foliation at the access drift could be seen as well as some small failures. The left side was not influenced by these events on the right side. Some

cracks that existed prior to the event could be seen in the fibercrete on the hanging wall side. (Nyström, 2008).

The experience with sill pillar mining in Kanalmalmen on other levels was that the final cuts usually gave no problems as fracturing had already taken place and had effectively destressed itself. It was in the cuts prior to that when the ground was still in the process of destressing that usually gave the problems. In retrospect, it appears that this did not happen in the sill pillar above SK835. If the sill pillar had fractured the energy would have dissipated over the mining progress similar to the other previously mined sill pillars. It might be due to a local anomaly in the strength of the rock that caused two things: accumulation of strain energy and not failing at higher stress.

The geometry just prior to the event was imported into Examine3D and the strain energy was calculated in the area of the rockburst. The highest level of strain energies that still show occurrences in the area was used to create iso-surfaces. This is shown in Figure 10.15.

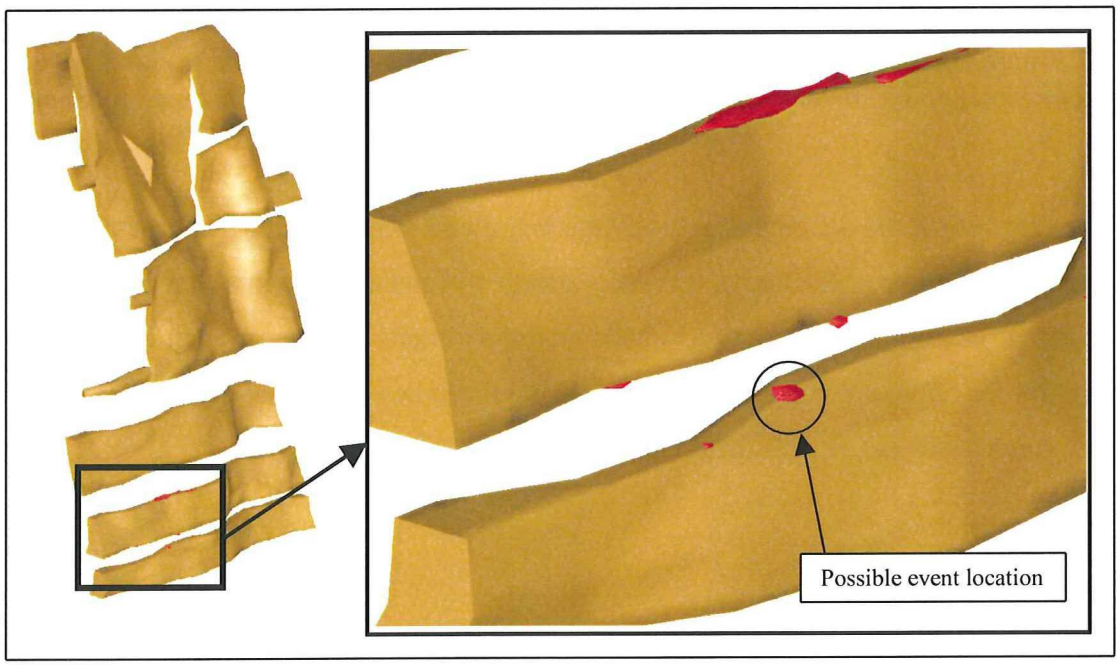

Figure 10.15: Geometry with 250 kJ/m3 strain energies around the area of the event.

Figure 10.15 also shows that the strain energies in SK805 are equally high or even higher than in SK835, so strain energy alone is not a satisfactory criterion for the event. Figure 10.16 shows the major principal stress around the failed pillar. The

stresses just around the stopes SK805 and SK835 are equal in magnitude, the average stress in the pillar however is a lot higher because the pillar is smaller.

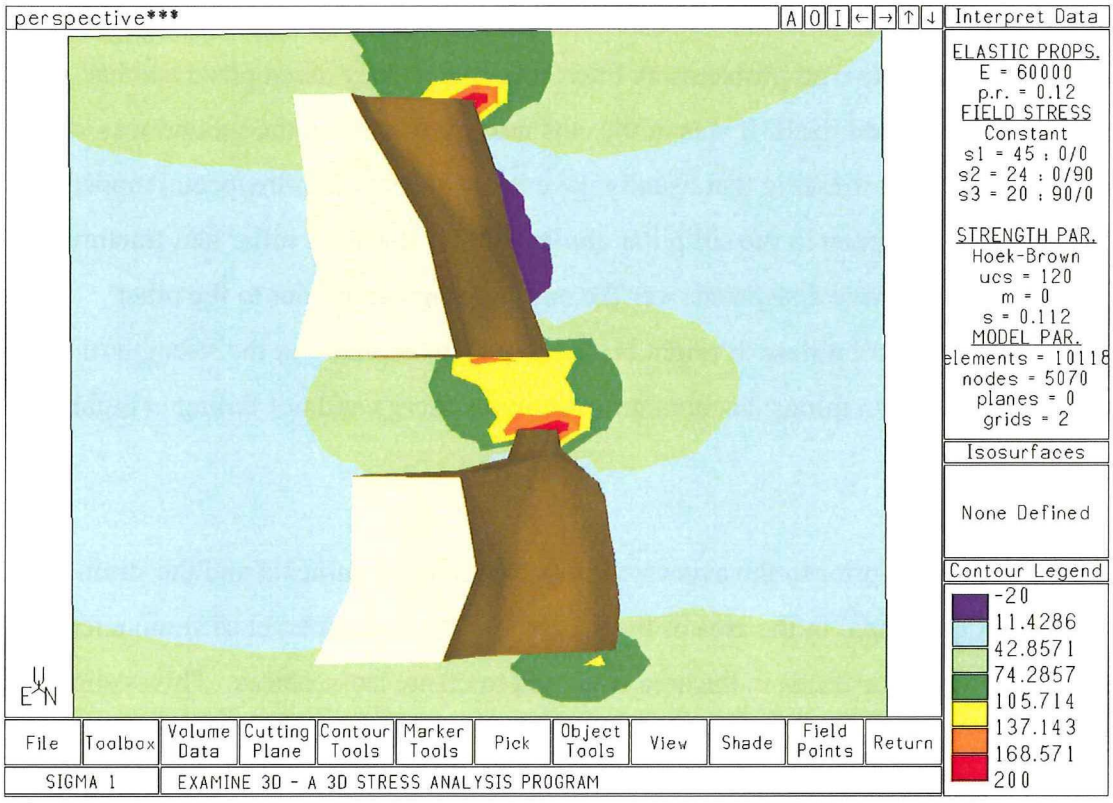

Figure 10.16: Major principal stress around the event area. The plane cuts the excavation approximately perpendicular at the location of the possible event location as indicated in Figure 10.X4.

When looking at the difference between the major and minor principal stresses in Figure 10.17 it becomes clear that there is a large difference throughout the pillar ranging from 85 in the centre to 130 MPa on the perimeter. If the same failure criterion for Lappberget is used ($\sigma_1 = \sigma_3 + {}^1/_3\,\sigma_c$) it can be shown that even very strong rock masses will fail at such differences.

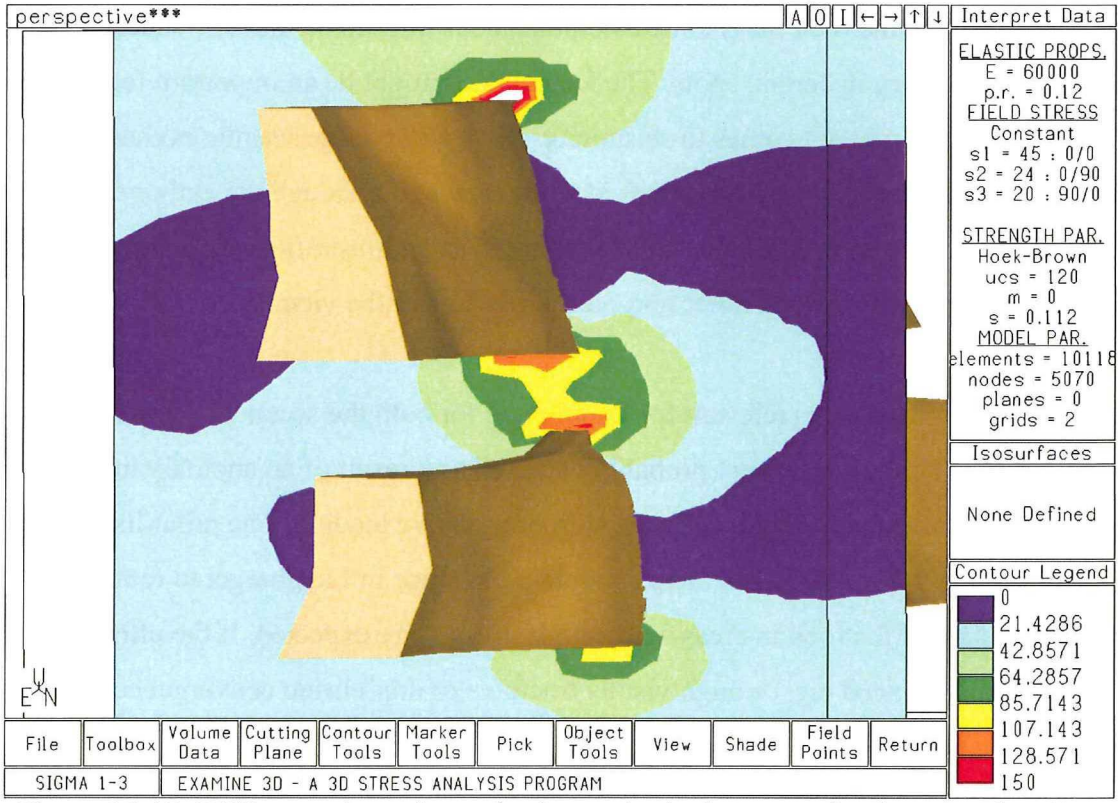

Figure 10.17: Difference in major and minor principal stresses for the event location in Kanalmalmen. The difference is essentially the basis for the utilized failure criterion.

The most plausible explanation for the event is that the rock mass was locally unusually strong which caused energy to accumulate in the pillar. As the stresses overcame the strength of the pillar all of that energy was released instantly causing a seismic event of which the radiated energy could be felt on surface. The one spot shown on Figure 10.15 could be the point where the event initiated, as it showed high strain energy and is in the right location. Only a small amount of material was displaced as support ensured to maintain an interlocking pattern of fragments. Since material was displaced over the length of the drift it is likely that the entire pillar was destressed, but this is hard to say as management decided to terminate mining in this area. This single event is the only occurrence of seismicity in Kanalmalmen.

10.3 Comparisons and recommendations

The Zinkgruvan case showed that the three-dimensional boundary element method did not suffice in finding an explanation for the experienced seismic events. It did not

suffice to assume the rock mass to be a homogeneous infinite medium in which energy accumulates in certain spots. The Knalla fault might be an important feature in the local geology when it comes to seismicity. Most of the large seismic events occurred in the footwall where the fault is running trough although the author does not know the exact location. This case can be regarded as an illustration of the importance of the structural geology and other non-elastic features in the vicinity.

The Kanalmalmen case is relevant for Lappberget for both the secondary drifts and the sill pillar. The seismic event probably occurred as a result of an anomaly in the rock strength of the sill pillar combined with progressive loading. The pillar likely destressed due to the event. A strategy should be in place in Lappberget to routinely check the state of the rock in areas where high stresses are expected. If the effects of failure are not noticed e.g. through visible fractures or non-elastic convergence care should be taken.

The convergence of the sill pillar in Kanalmalmen was unfortunately not measured at the time. The hypothesis is that the sill pillar did not fail gradually, but instantly. If the rock had failed gradually the perimeter probably would have shown some non-elastic convergence due to the expansion of rock after peak strength. If there is any truth in this hypothesis a measurement program on 1080 and 1060 in stope 10 should be expanded to other stopes. These measurements combined with the models in Examine3D and observations could prove to be a useful tool in assessing the state of the rock mass surrounding the excavations. If the convergence is lacking in stopes that are modelled to be highly stressed care should be taken in the mining activities in those areas.

If more case studies are deemed necessary to evaluate the risk of seismicity in Lappberget it is important to select the cases that resemble rock, mining and stress conditions in Garpenberg. Other than Zinkgruvan there are no suitable cases in Sweden and it could be worthwhile to look abroad for mines experiencing rock bursts. Stress conditions in Northern Ontario are similar to Scandinavia and there is a long history in rockburst research. Examples of mines with similar mining methods and experience with seismicity are the Hemlo operations (Williams mine especially) in Marathon, Laronde in Quebec, Garson in Sudbury and Macassa in Kirkland Lake

(McKinnon, 2008). Another mine that might be worth looking at is the Thayer Lindsley mine in Sudbury where seismicity is experienced despite (or because of?) some weak rock masses. (Carlisle, 2008)

10.4 References

Askemur, T., 2008, *Personal communication.*

Carlisle, 2008, *Personal communication*

Brady, B.H.G. and E.T. Brown, 2004, *Rock Mechanics for underground mining*, Kluwer Academic Publishers, Dordrecht, the Netherlands

McKinnon, S.D., 2008, *Personal communication*

Nyström, A., 2008, *Personal communication.*

Lundin Mining Cooperation, 2008, http://www.lundinmining.com/s/Zinkgruvan.asp

Rocsience, 2003, *Examine3D*, version 4.0997, Toronto, Canada.

Sjöberg, J., 2005, *Rock Mechanics Analysis of the Copper Orebody*, SwedPower report for Zinkgruvan mining AB, Luleå, Sweden

Söderman, T., 2006, *Garpenberg area*, presentation on the New Boliden AB operations in Garpenberg

Wikipedia, 2008, http://sv.wikipedia.org/wiki/Zinkgruvan_%28gruva%29

11. Conclusions and recommendations

The aim of the thesis is to indicate areas in Lappberget with a risk for induced seismicity. The conclusions of this thesis are in no way definite, as there is always room for improvement in prediction. The conclusions are listed in 11.1, whereas some suggestions for future work are given in 11.2.

11.1 Conclusions

The considerable length of this report is mainly due to the attempt to summarize all relevant available information. Not all information, the chapters on geology and stresses for example, is used as material to come to these conclusions. What one might see as excess information, e.g. extensive geology descriptions and information on convergence measurements, can also be seen as illustrations of the complexity of the overall geomechanics in Lappberget.

The pillars will not likely display strain related seismicity, as progressive loading will push the stresses past the calibrated strength before the maximum strain energy is attained. The energy will be dissipated through existing or new micro fractures. The bottom level will not disappear in the stress shadow and remains subject to a dynamic state of stress. While violent failure is unlikely, other types of instability might occur.

Plastic zones will likely grow on the footwall and hanging wall as mining progresses. These plastic zones can reduce the stresses in the **secondary stopes** significantly, which in turn might not show any signs of gradual failure. The stress reduction will also cause the strain energy to drop. The chance for seismicity in secondary stopes is small, as the strain energy in the stopes does not reach the strain energy in the order of magnitude from the Kanalmalmen case, even when looking at fully elastic models.

Fault slip movements along geological structures are hard to assess. At present, no large significant structures are known in the vicinity of Lappberget. The weak hanging wall – ore contact will likely not give any problems as failure will happen gradually without the ability to accumulate enough energy. If there would be any significant structure the ESS method can be used to get a conservative prediction of

the magnitude of a possible event. Whether or not any slip will occur depends on the orientation, location and properties of the fault.

The **only definite way of finding the potential for seismicity** is by experiencing seismicity. Prediction will improve with calibration of the models and experience that comes along with mining Lappberget. This thesis is focussed on finding the potential violent failure, but there are other forms of instability that could cause trouble, such as fall-out of wedges in the destressed footwall infrastructure. The occurrence of seismic events does not automatically lead to structural instability, but also depends on a number of things such as the applied support and distance from excavations.

11.2 Recommendations

The prediction of gradual failure in the (secondary) stopes can be improved by **calibration**. Observations and convergence measurements should be used to get a better failure criterion and an improved understanding of the state of stress. This calibration should ideally be based on a large number of stopes. For this reason it could be a good idea to archive pictures and observations of each stope from the earliest stage possible, possibly augmented with calibration measurements. This failure criterion can then be used for the sill pillar too.

A similar calibration could be used to assess the structural integrity of stopes by comparing stope designs with the Cavity Monitoring System (CMS) scans. This could lead to an improved estimate for **dilution**.

The **overall geomechanics** can be improved by getting a better sense of the distribution of rock masses and by looking into possible significant structural geology. The extend and location of the apparent strong and intact rock mass at the new potential shaft location should be included. Three-dimensional failure modelling software might shed more light on the stress situation in the secondary stopes and sill pillar.

Recommendations for **additional cases** were included in 10.3. Northern Ontario has a number of mines with similar mining methods and with experience in seismicity.

Appendix A – Geological maps of excavations

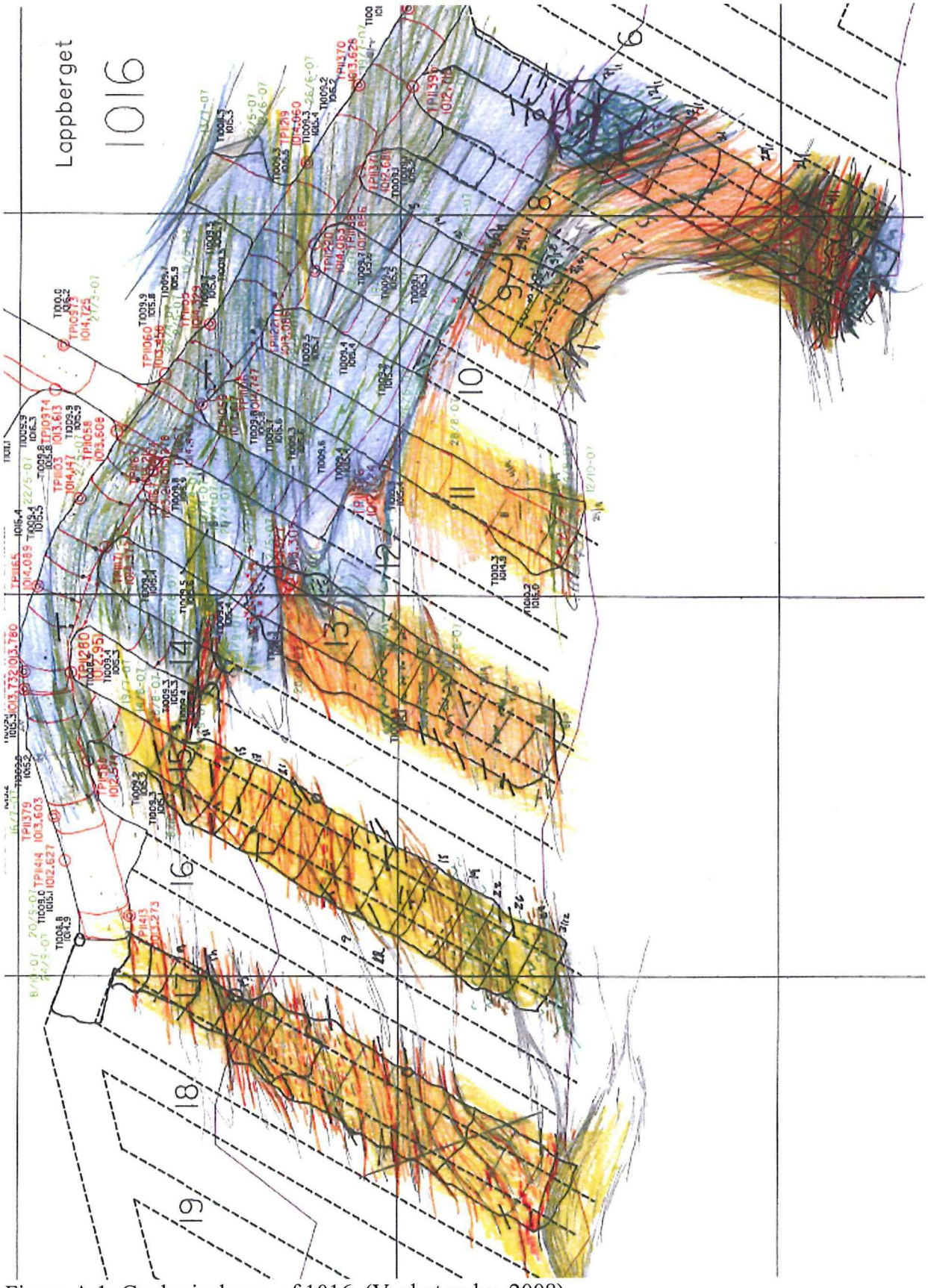

Figure A.1: Geological map of 1016. (Vyskytensky, 2008)

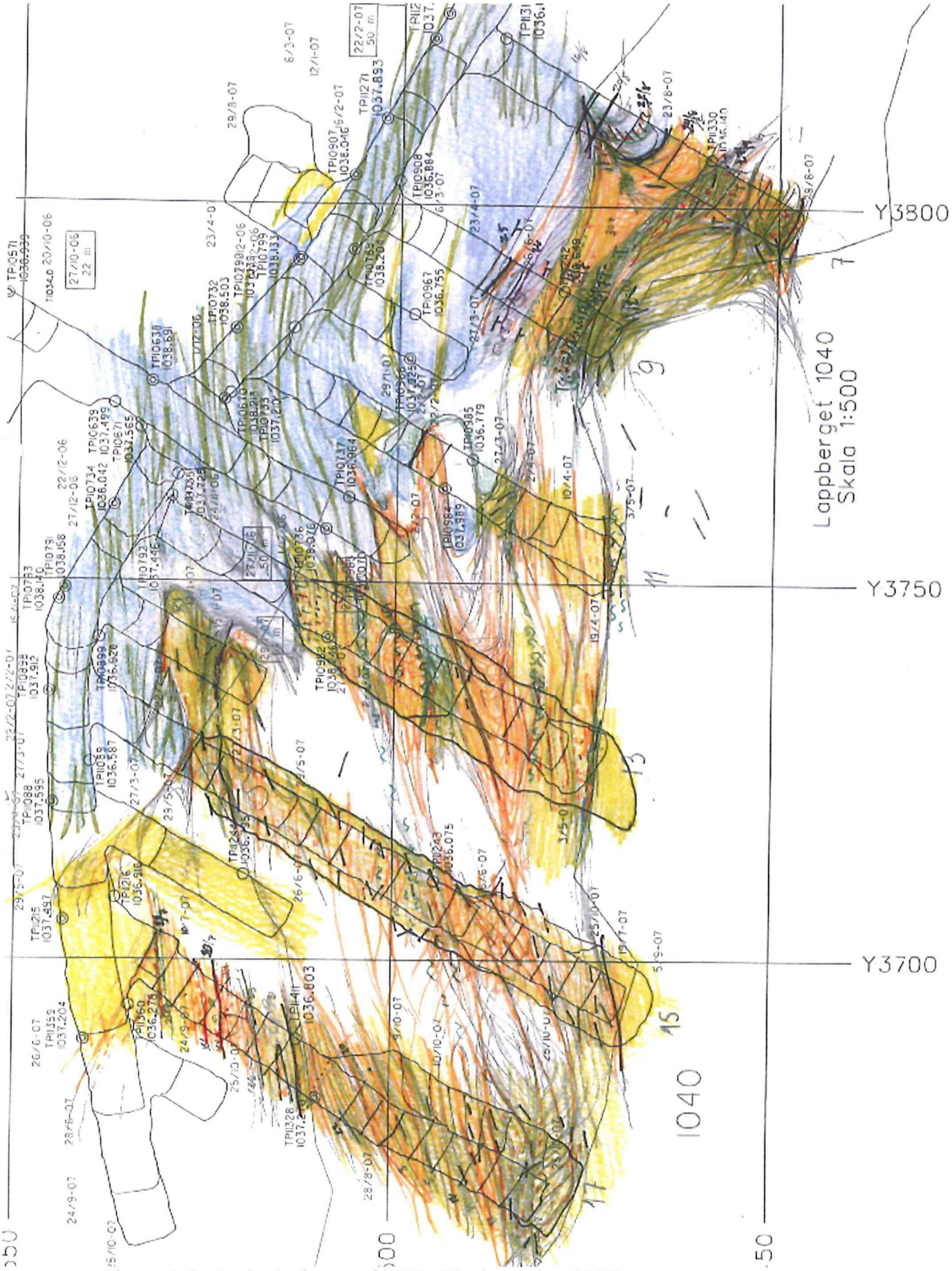

Figure A.2: Geological map of 1040. (Vyskytensky, 2008)

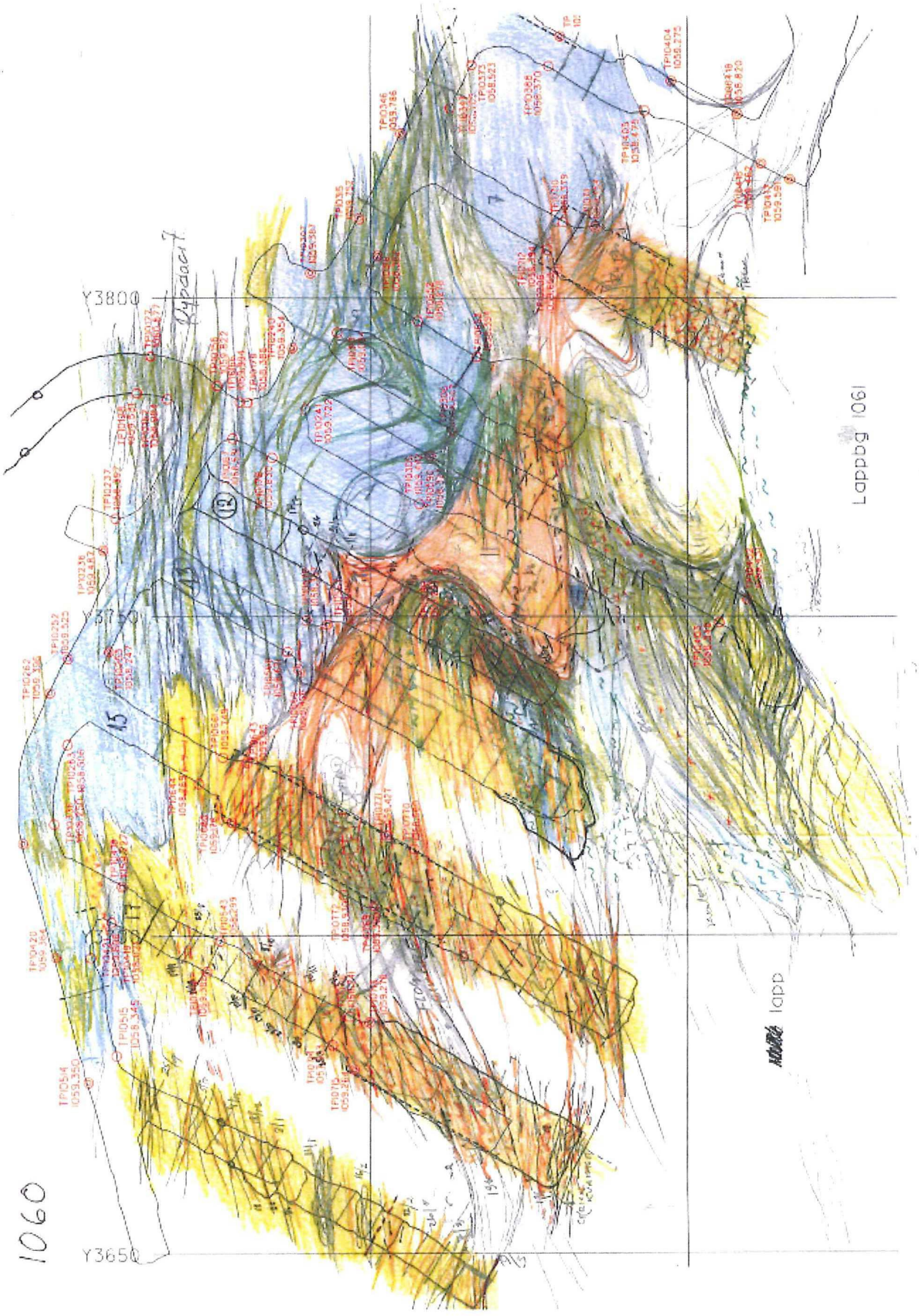

Figure A.3: Geological map of 1060. (Vyskytensky, 2008)

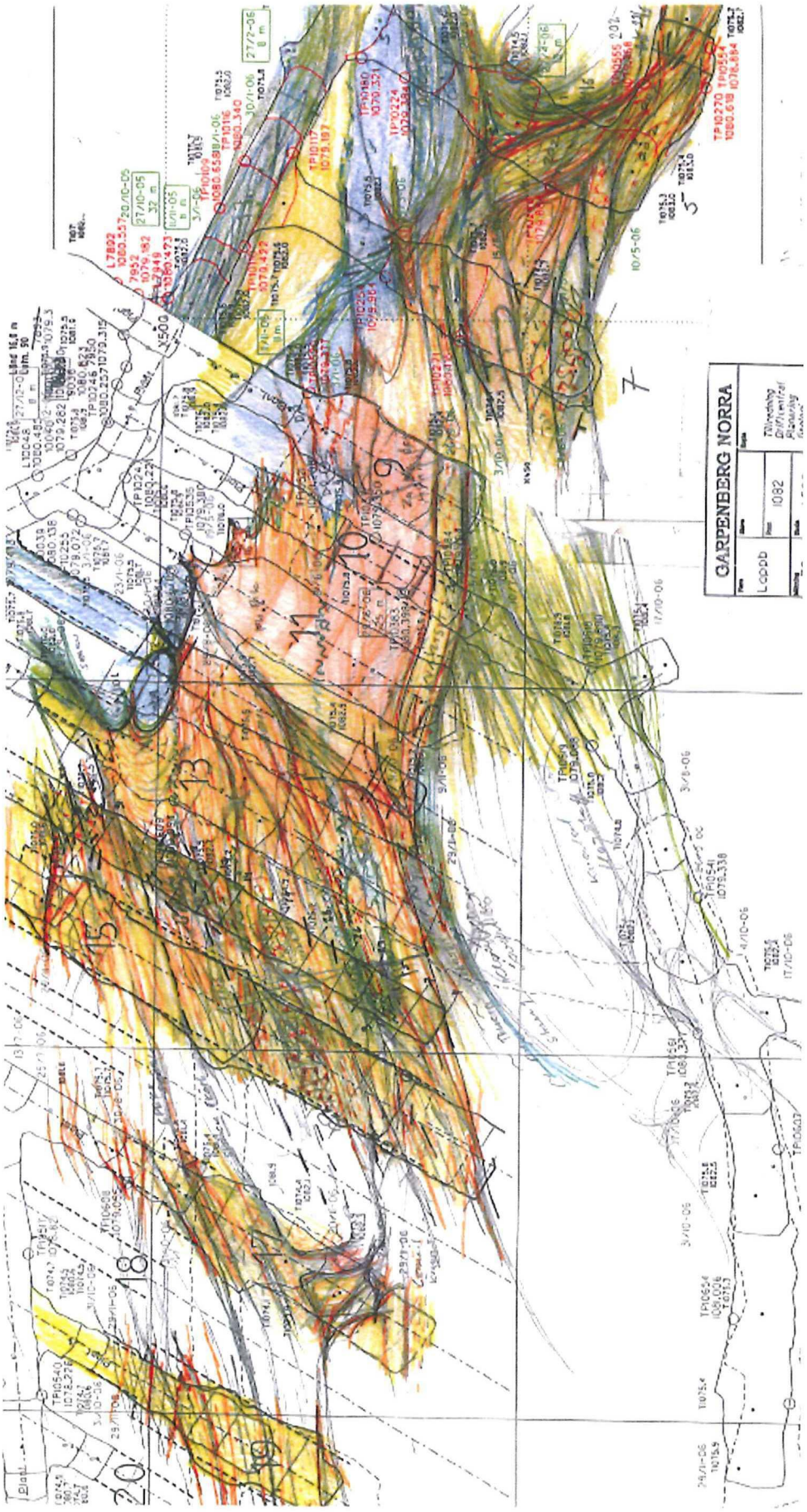

Figure A.4: Geological map of 1080 (1/2). (Vyskytensky, 2008)

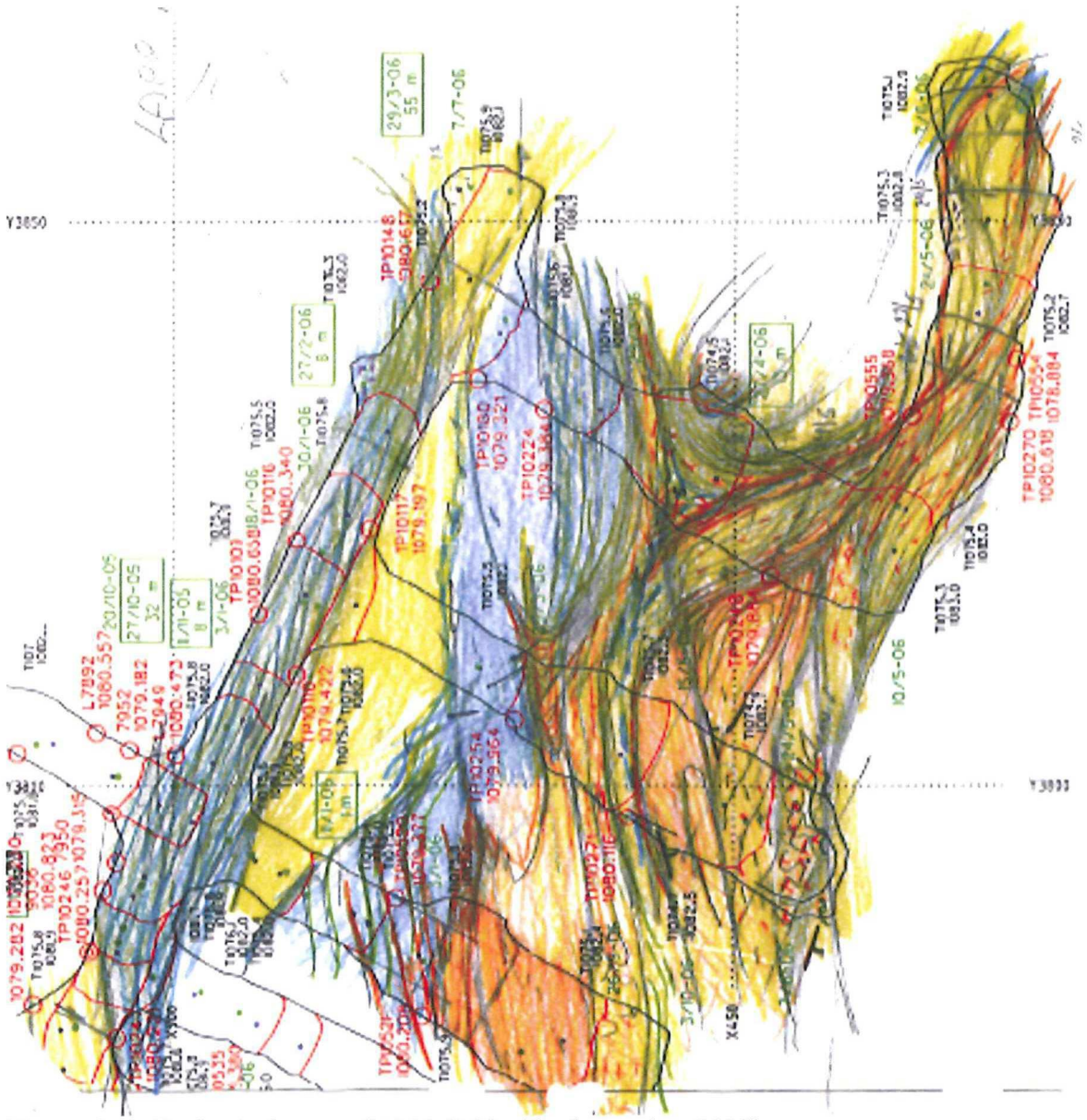

Figure A.5: Geological map of 1080 (2/2). (Vyskytensky, 2008)

Appendix B – Model geometries in Examine3D

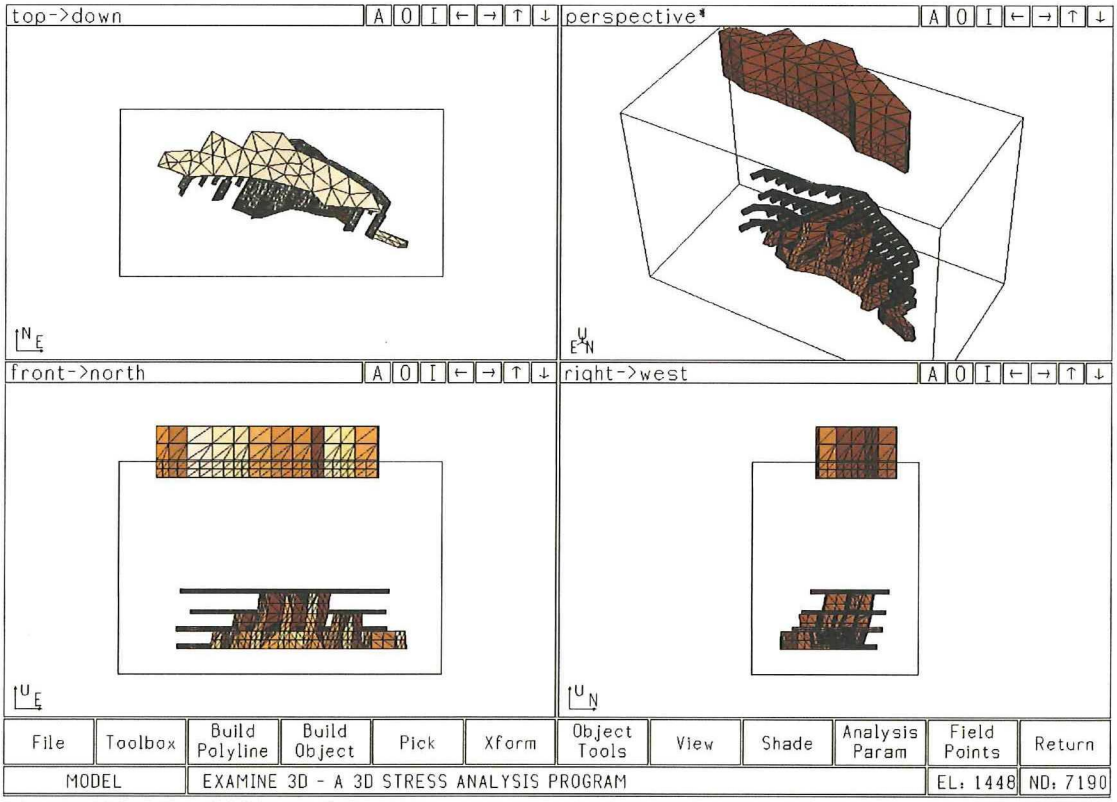

Figure B1: The 2008 model

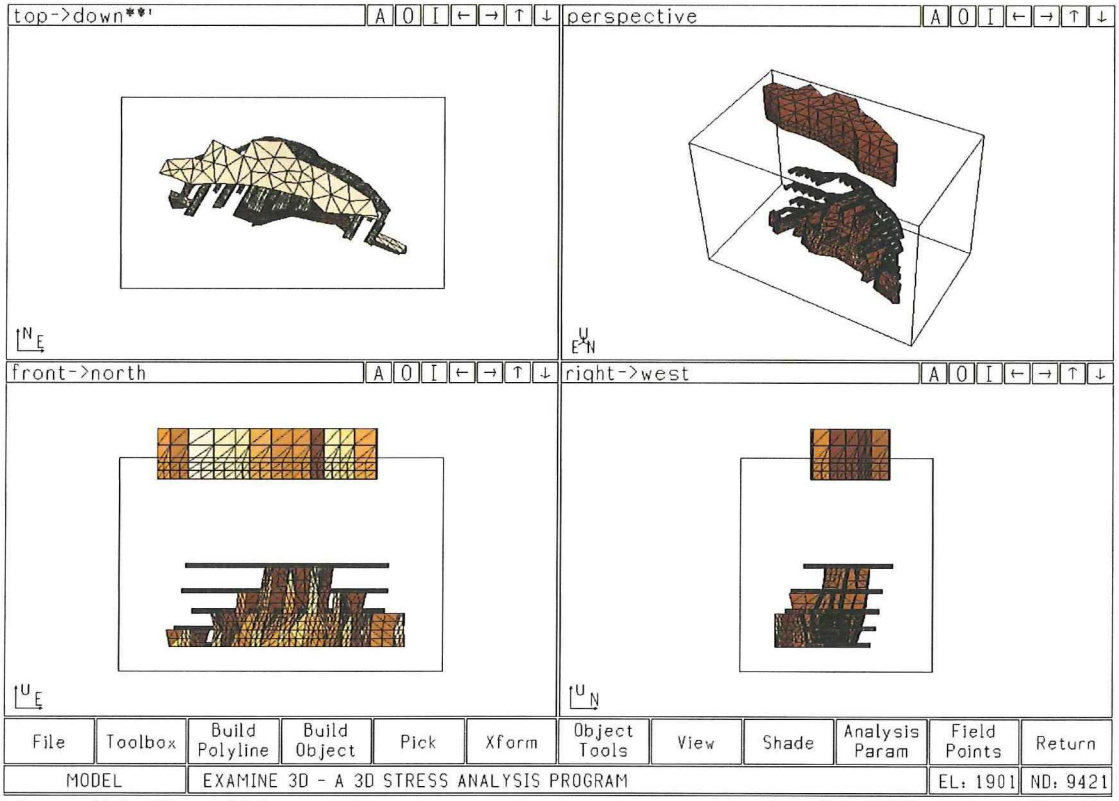

Figure B2: The 2009 model

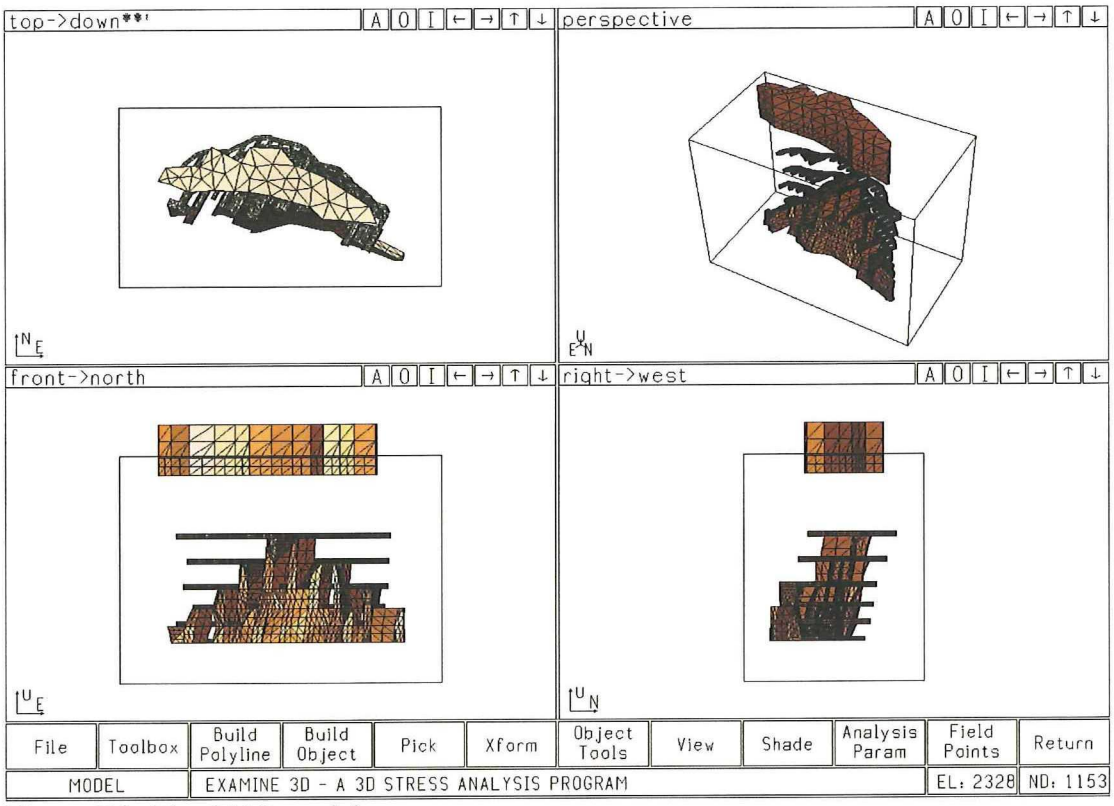

Figure B3: The 2010 model

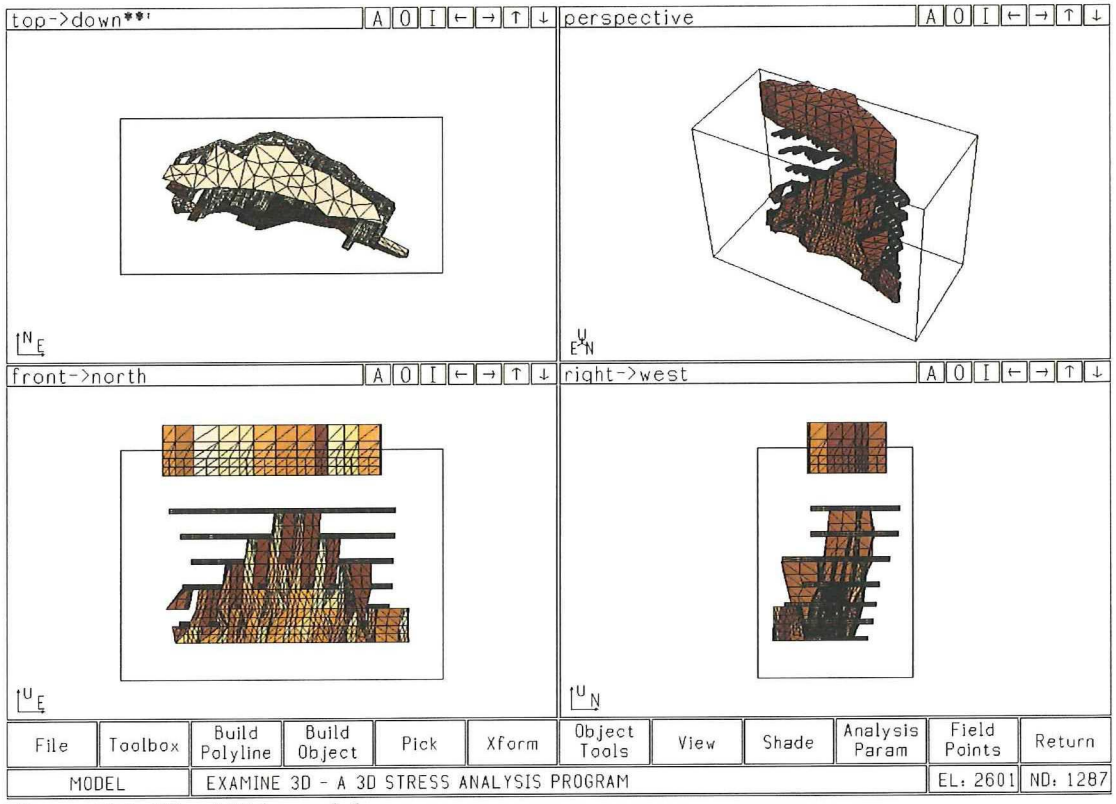

Figure B4: The 2011 model

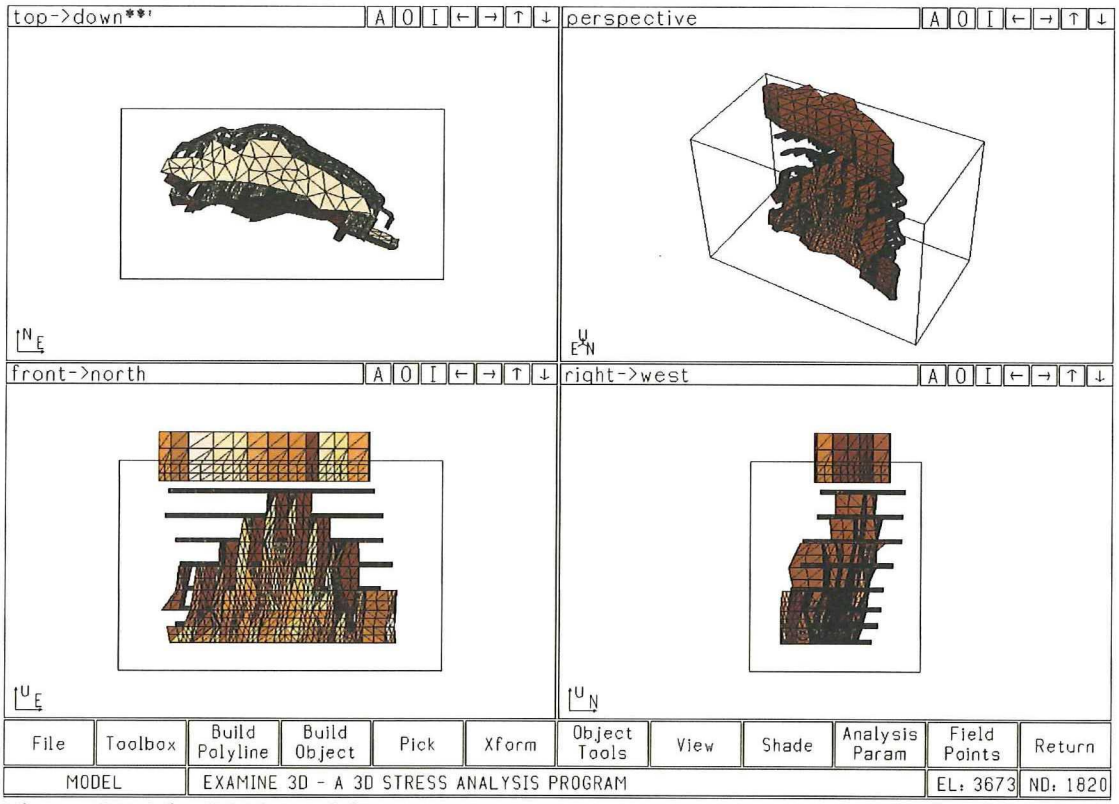

Figure B5: The 2012 model

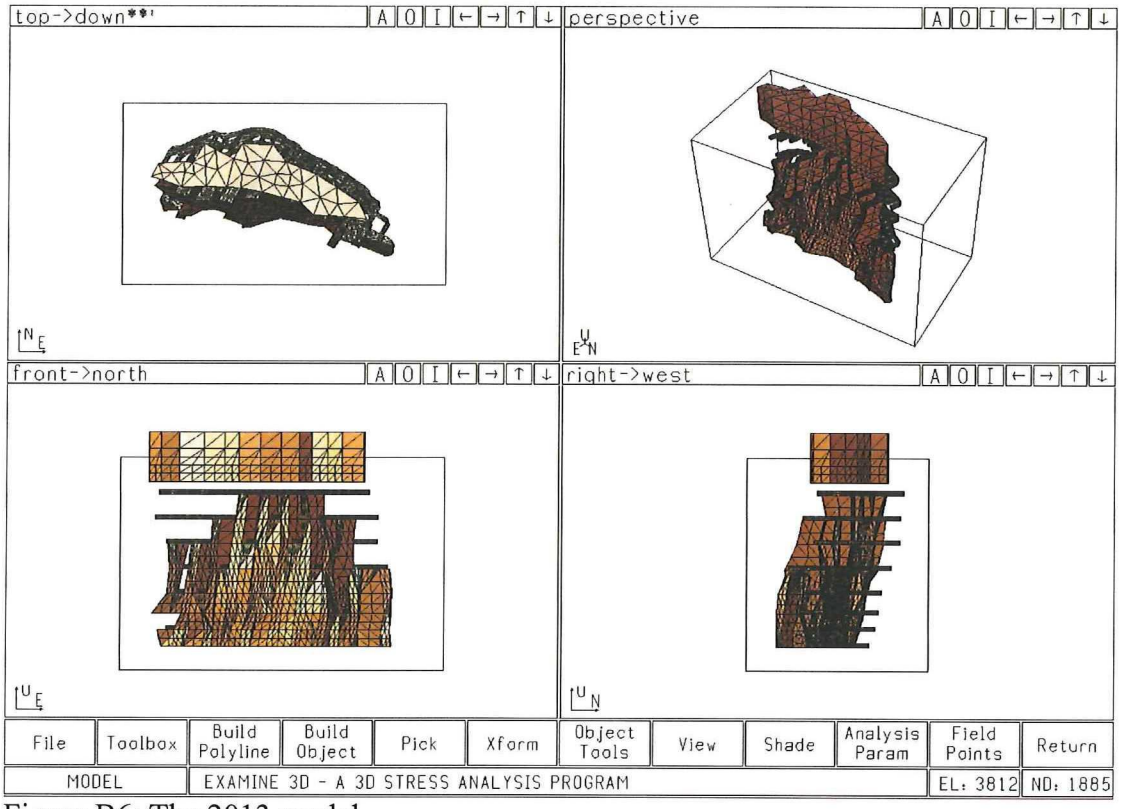

Figure B6: The 2013 model

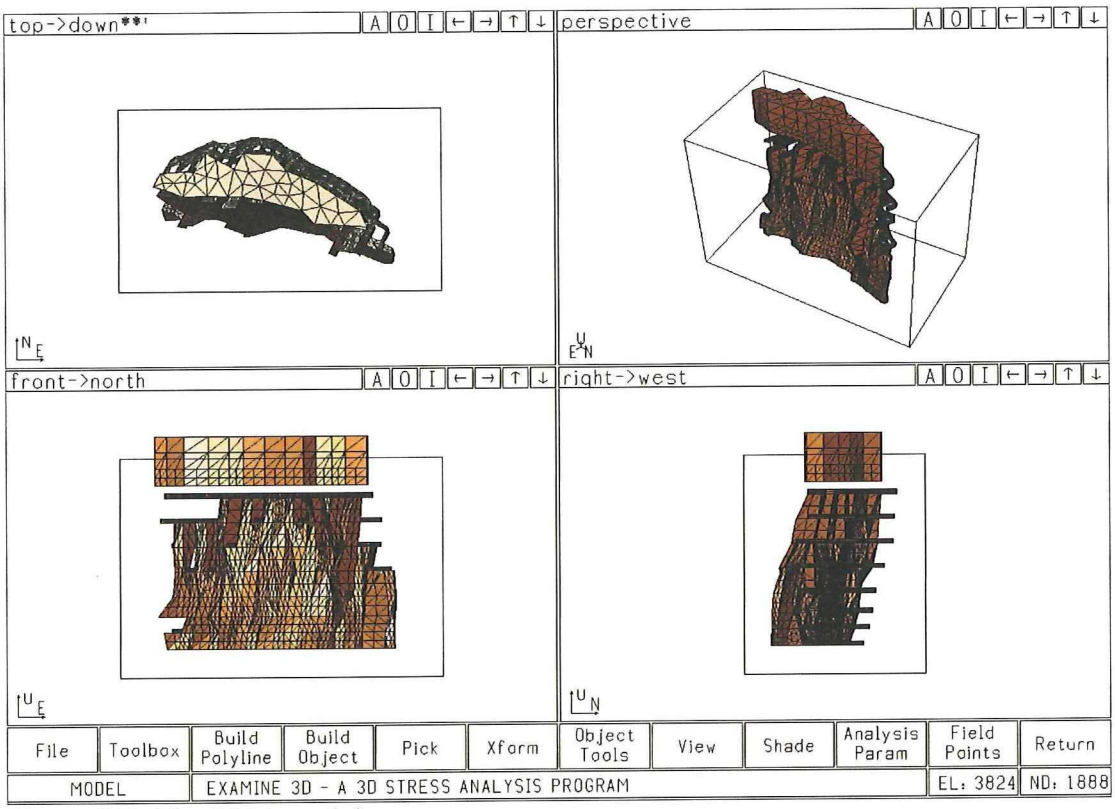

Figure B7: The 2014 model

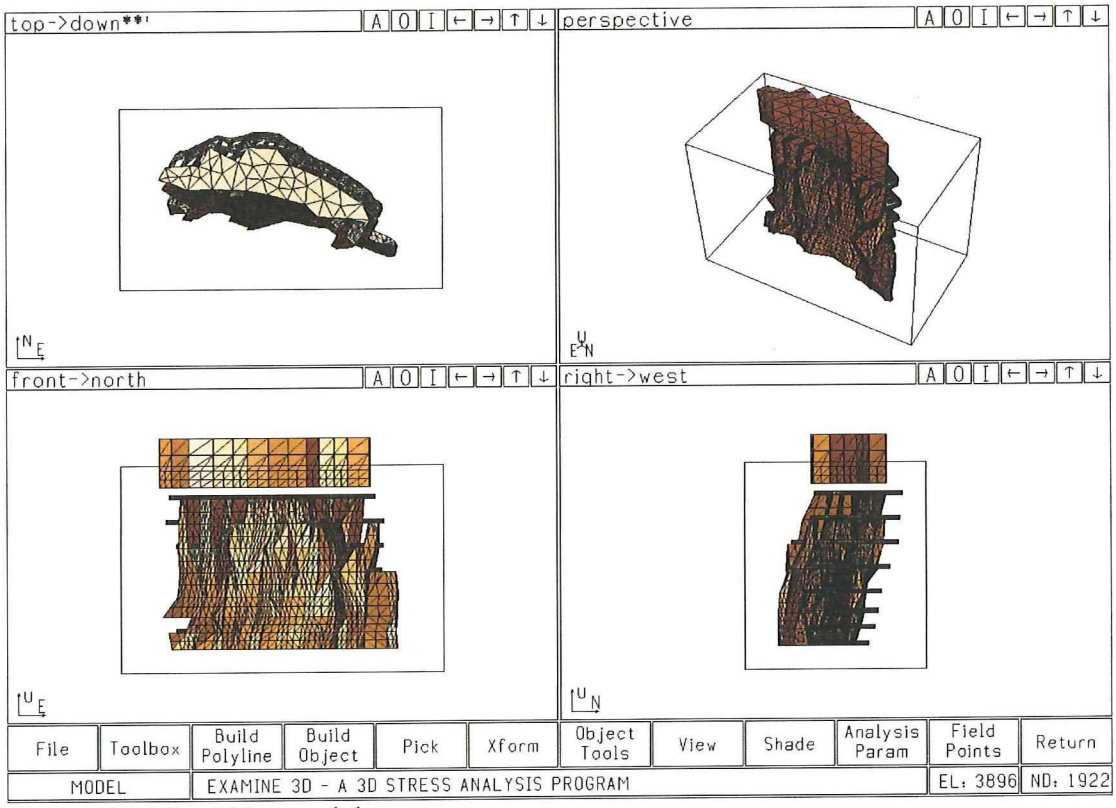

Figure B8: The 2015 model

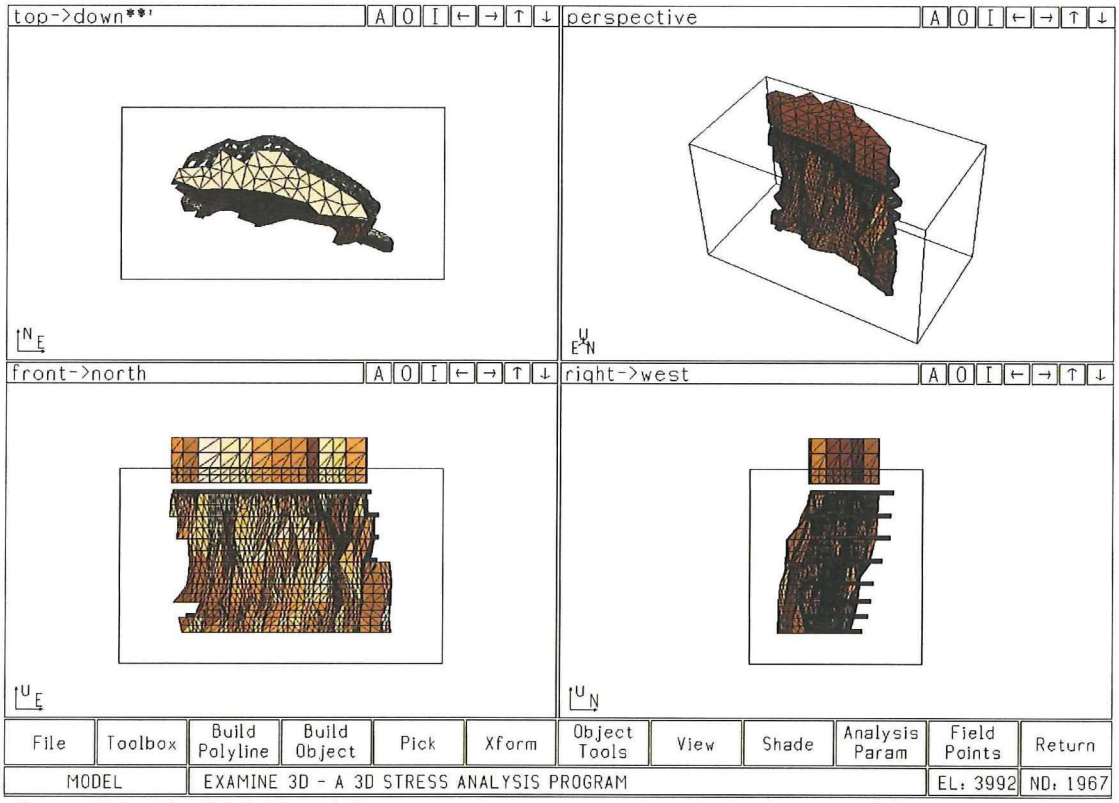

Figure B9: The 2016 Model

Appendix C – Stages and model geometry in Phase2

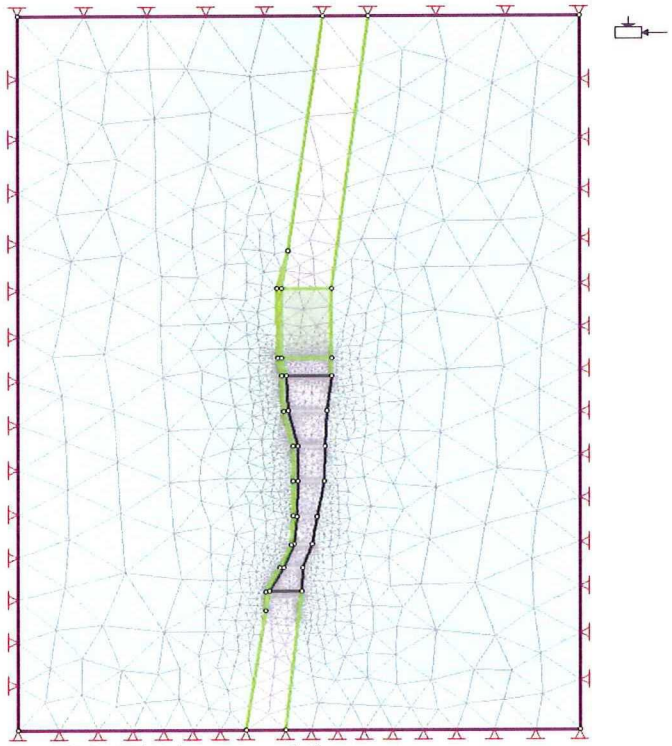

Figure C.1: The base model

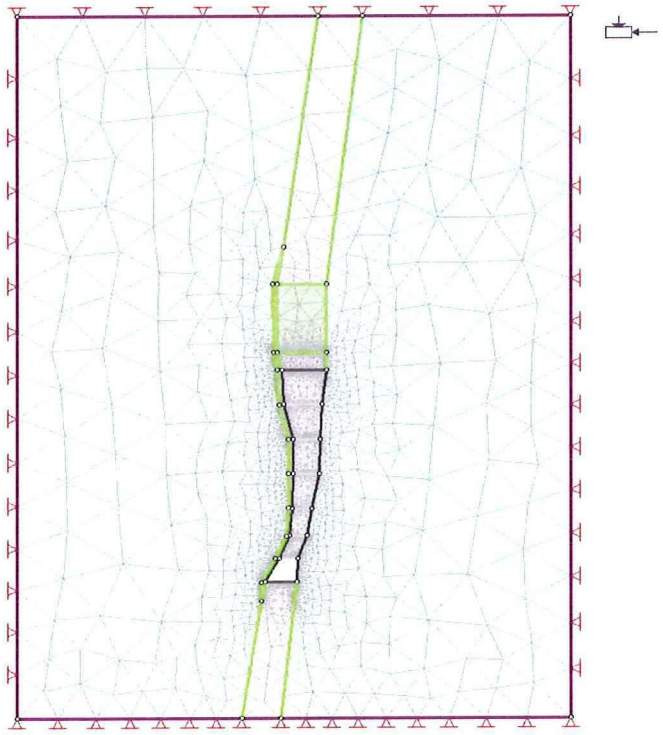

Figure C.2: The 1080 model

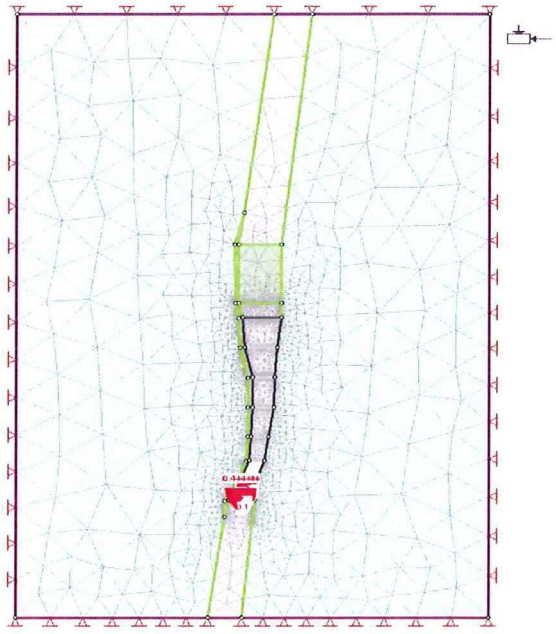

Figure C.3: The 1060 model

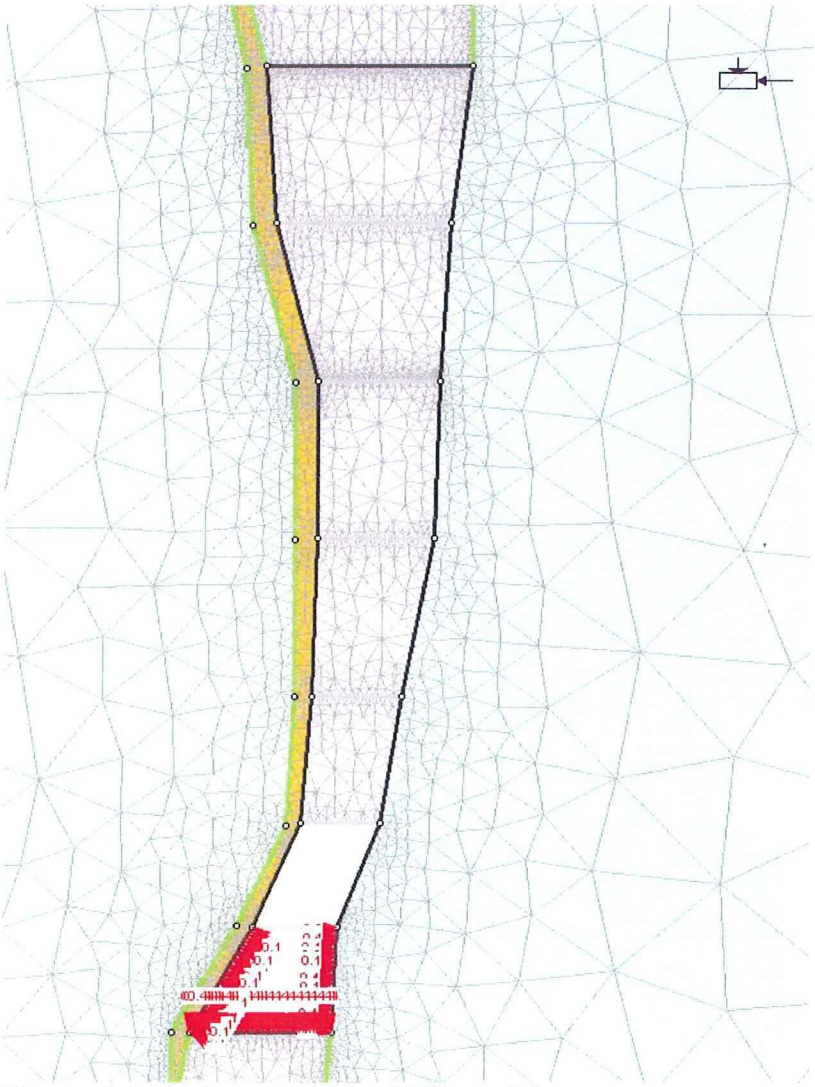

Figure C.4: A close-up of the 1060 model

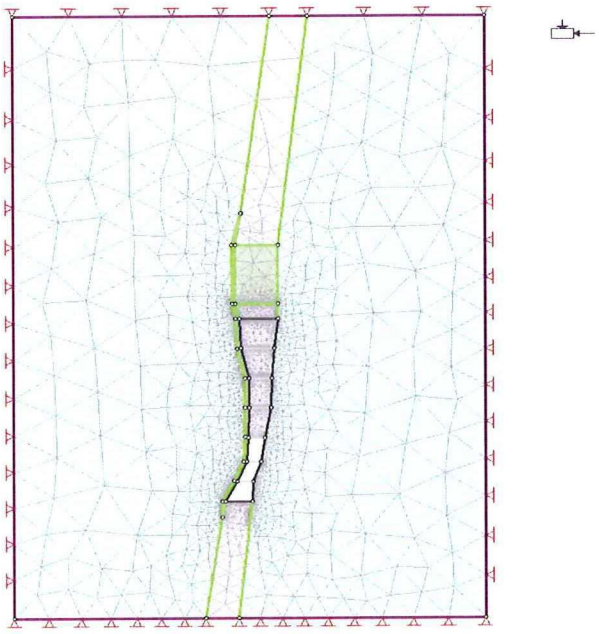

Figure C.5: The 1040 model

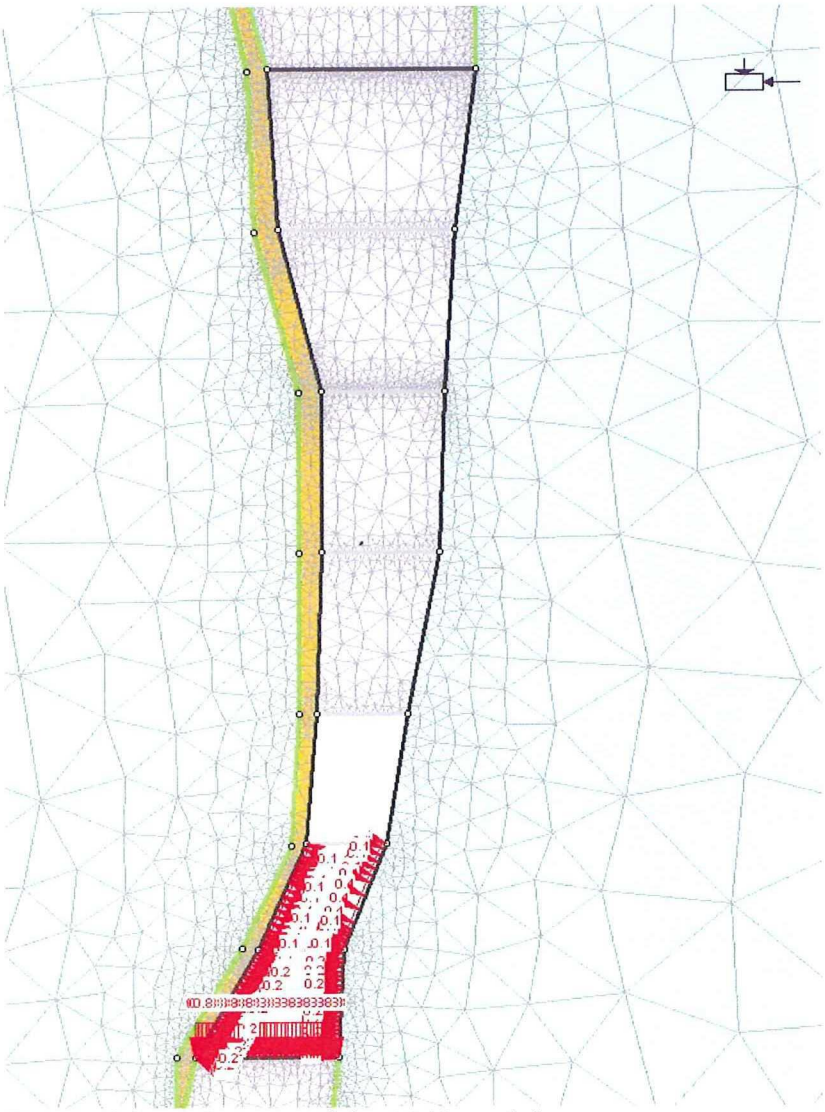

Figure C.6: A close-up of the 1040 model

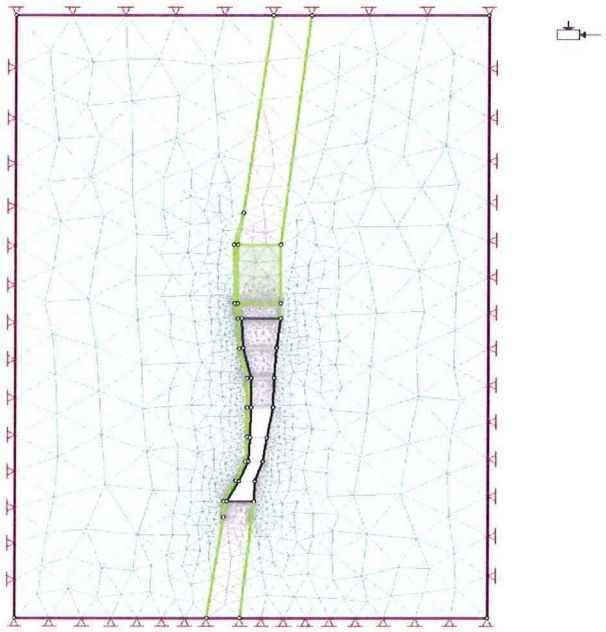

Figure C.7: The 1016 model

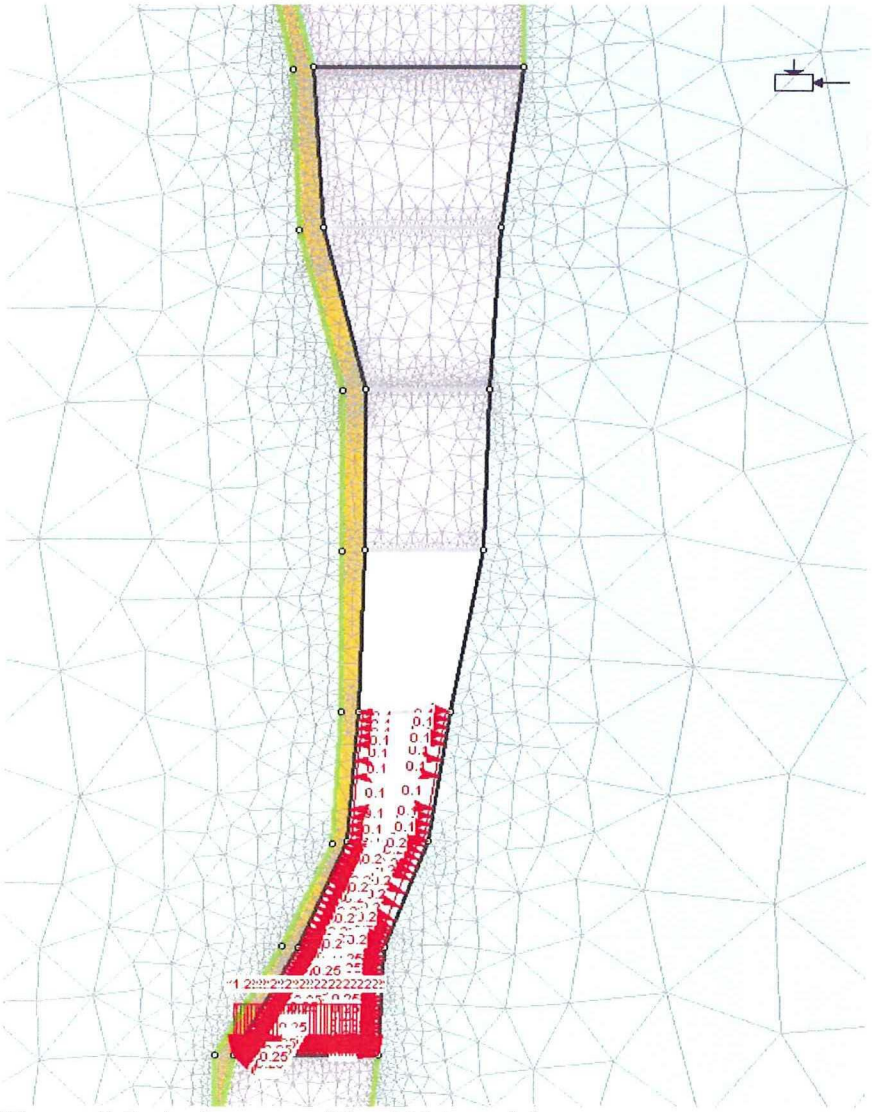

Figure C.8: A close-up of the 1016 model

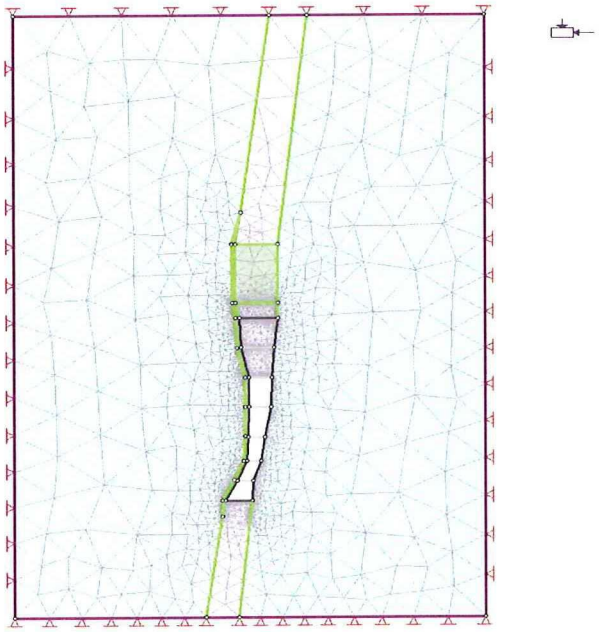

Figure C.9: The 986 model

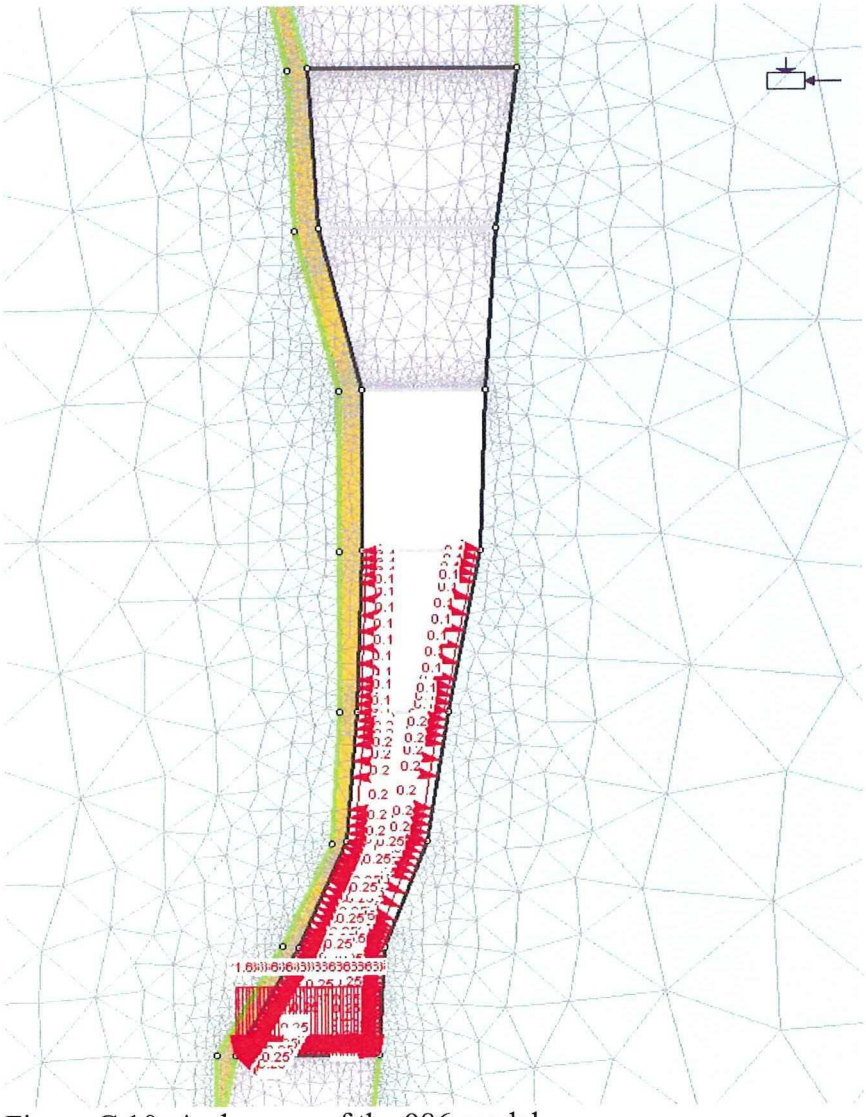

Figure C.10: A close-up of the 986 model

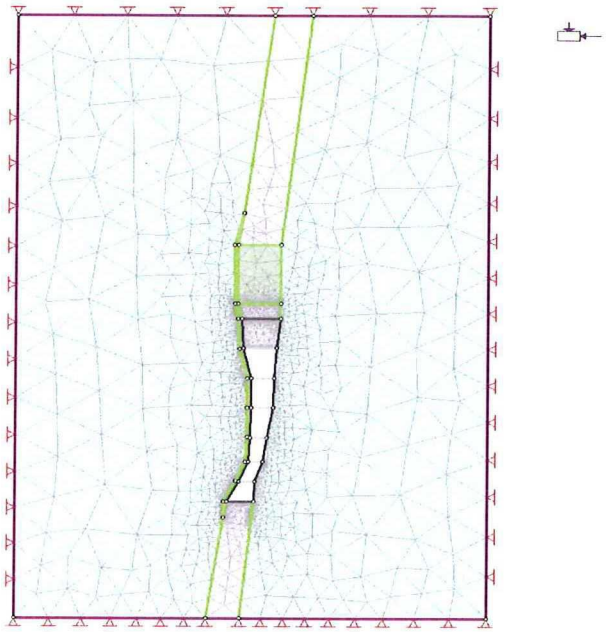

Figure C.11: The 956 model

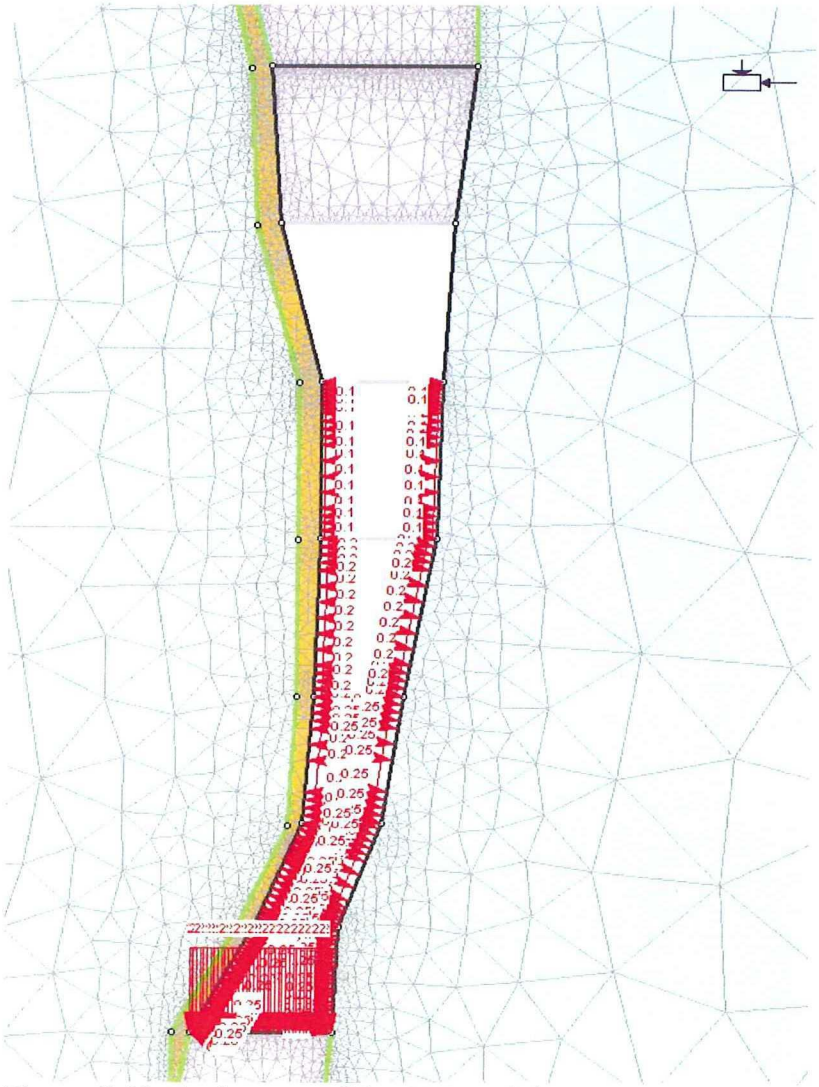

Figure C.12: A close-up of the 956 model

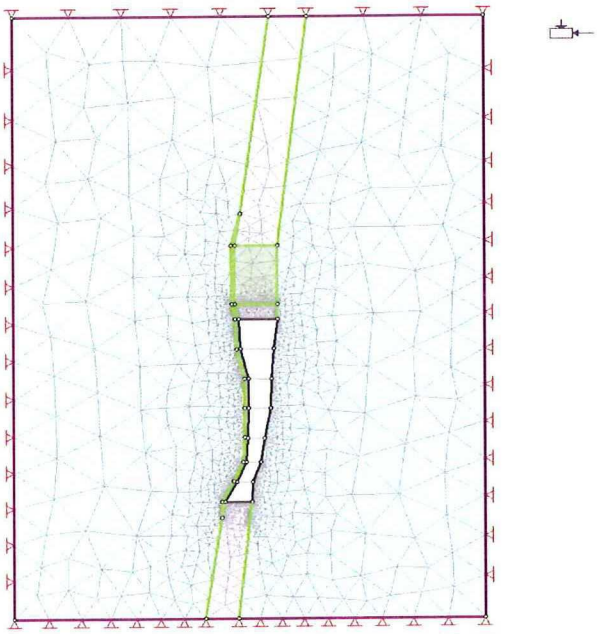

Figure C.13: The 926 model

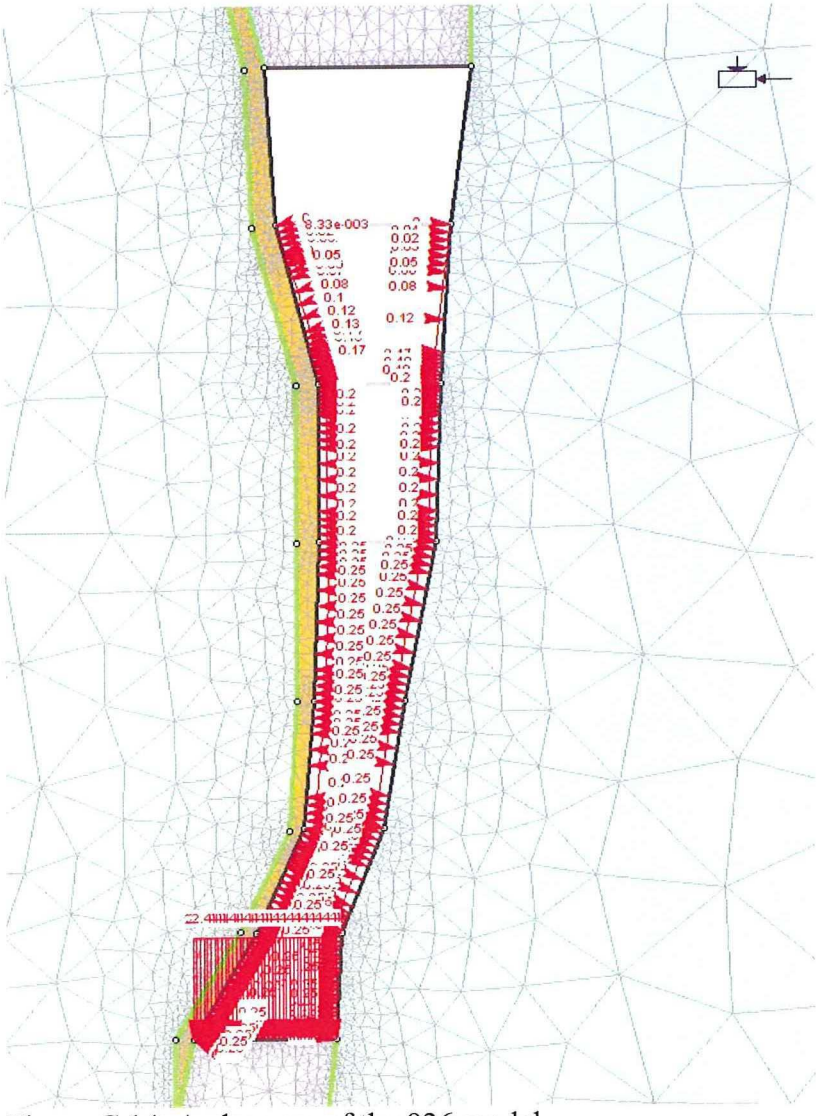

Figure C.14: A close-up of the 926 model

Appendix D – Loading histories in the pillars

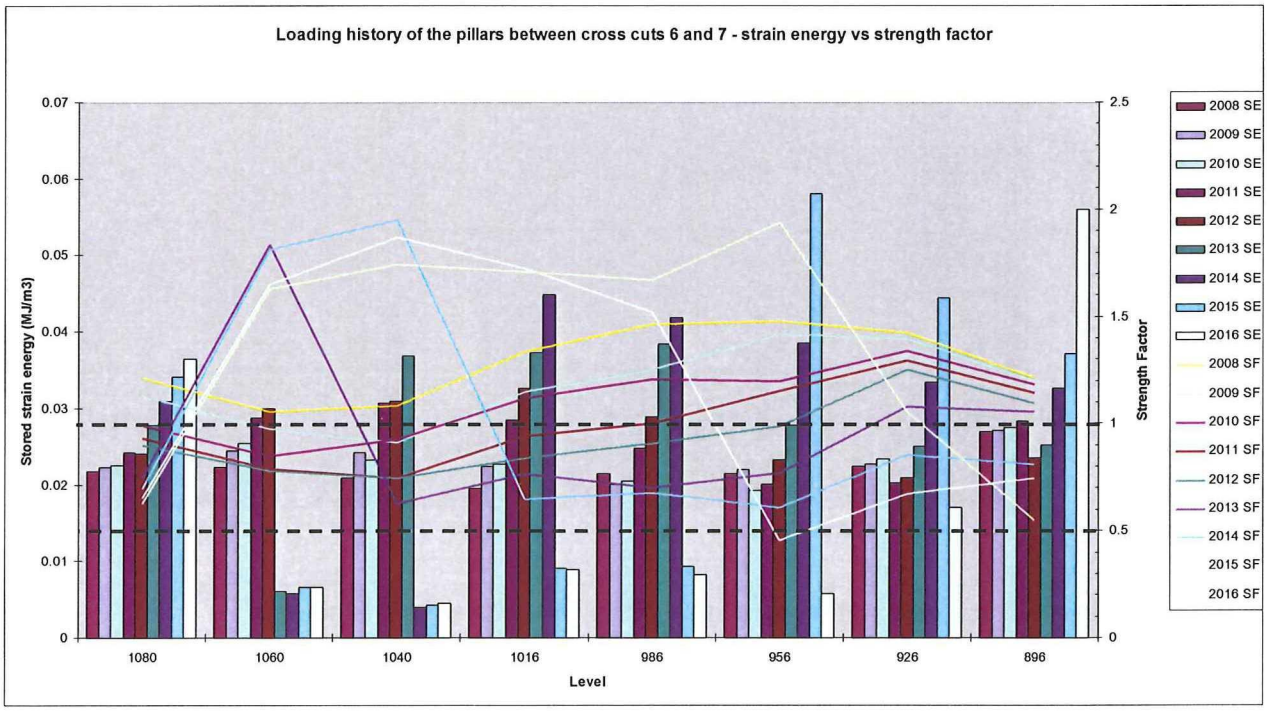

Figure D.1: Loading history of the pillars between stopes 6 and 7.

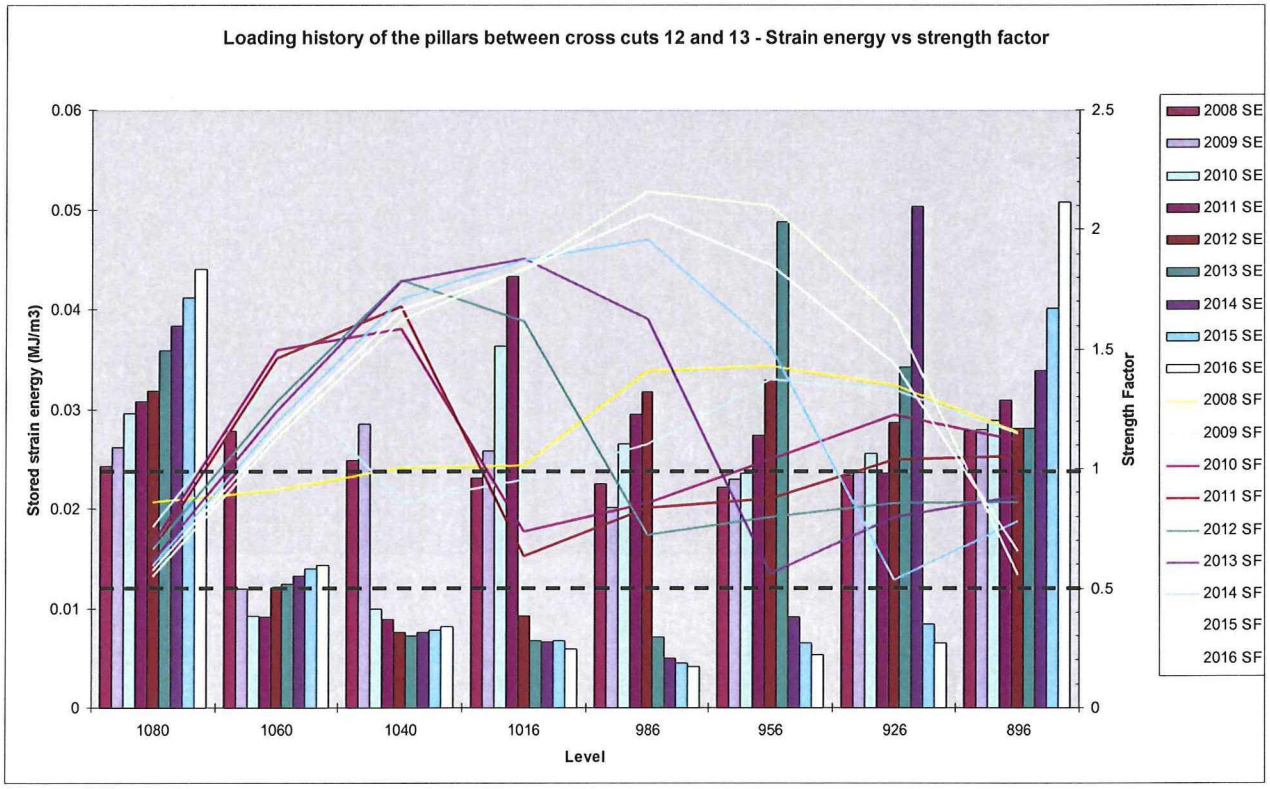

Figure D.2: Loading history of the pillars between stopes 12 and 13

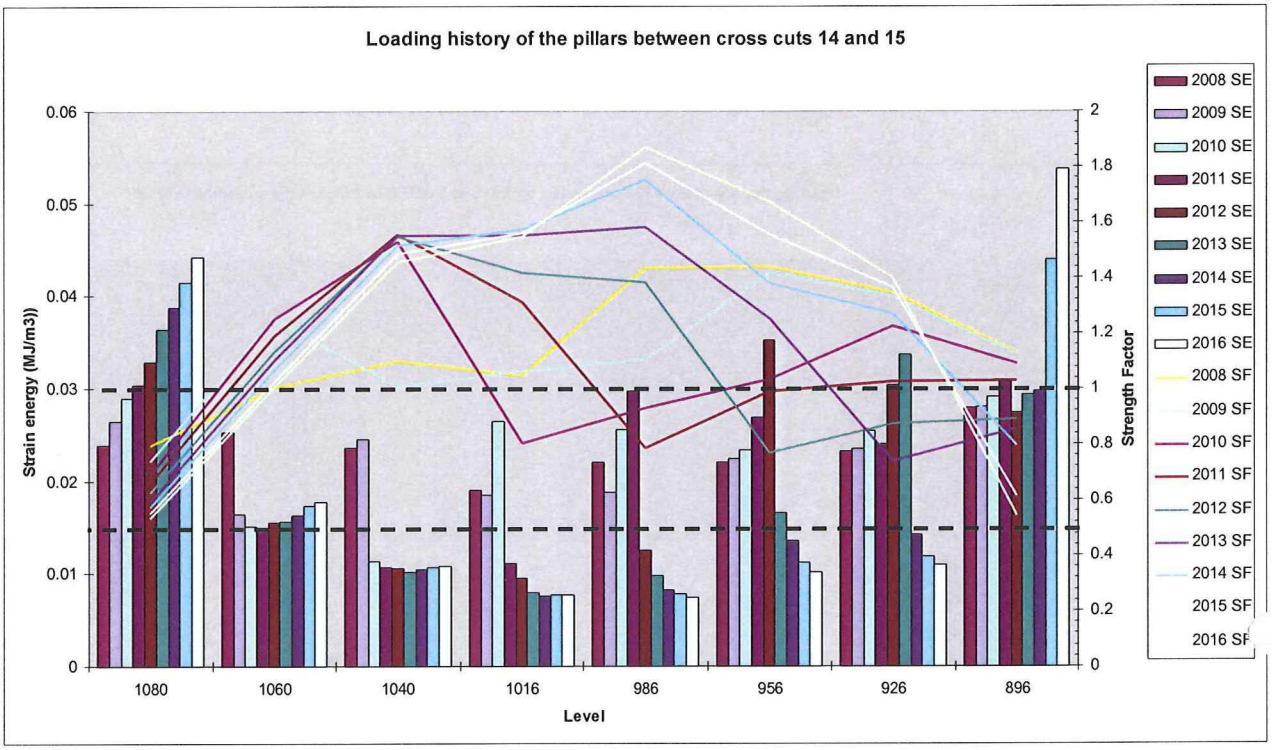

Figure D.3: Loading history of the pillars between stopes 14 and 15

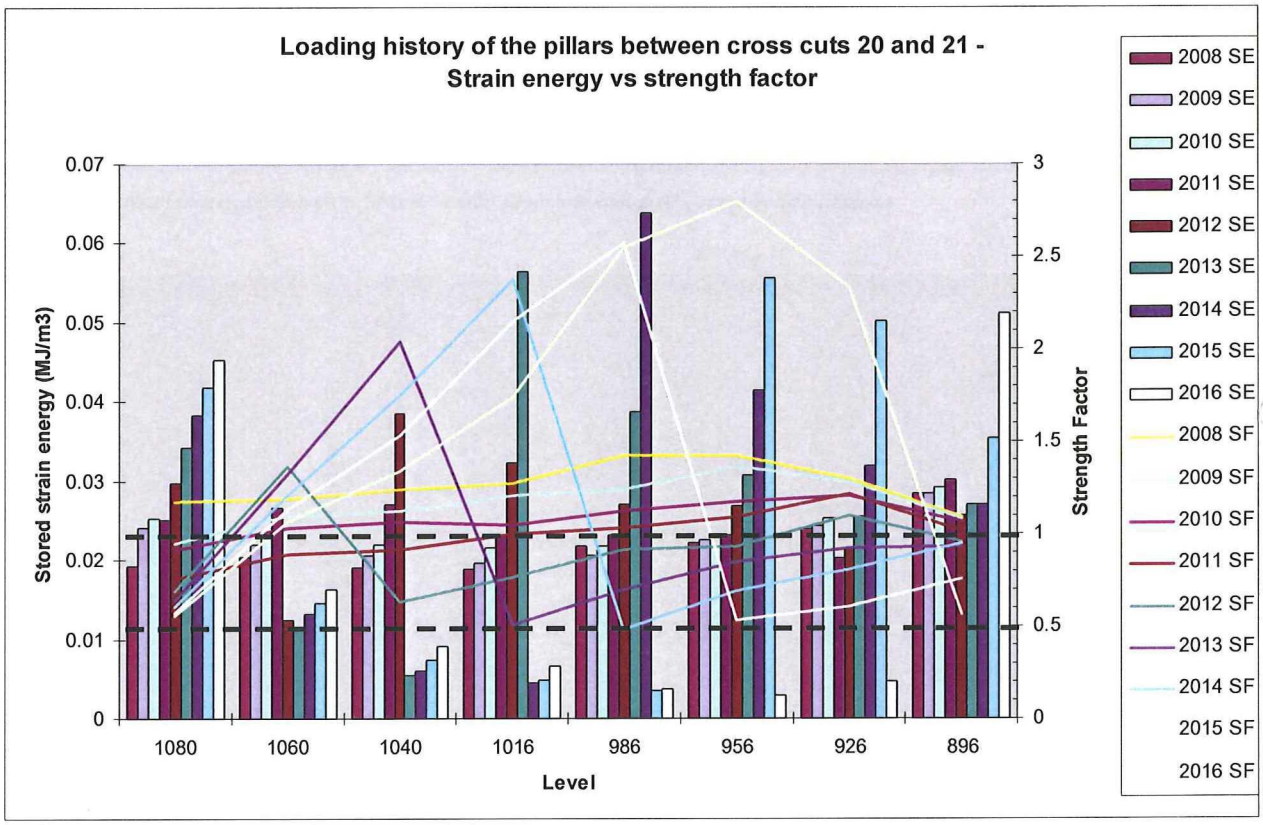

Figure D.4: Loading history of the pillars between stopes 20 and 21

Appendix E – Failure in secondary stopes

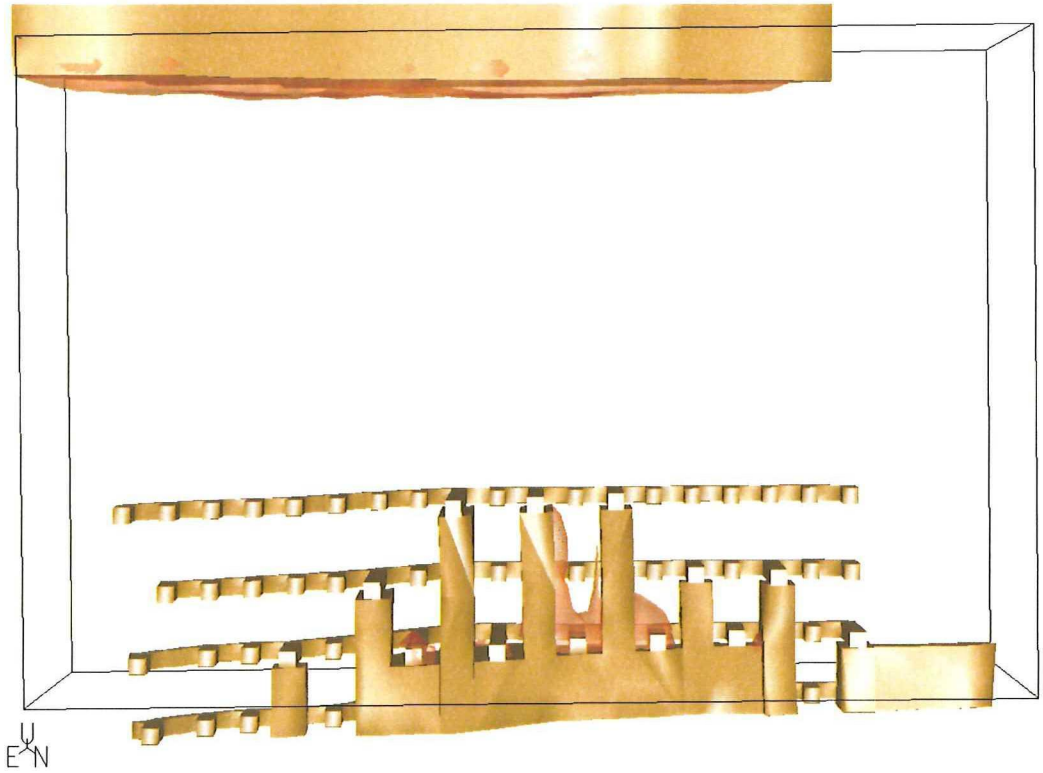

Figure E.1: The 2008 model with the 2008 (transparent orange) failure criterion iso-surface.

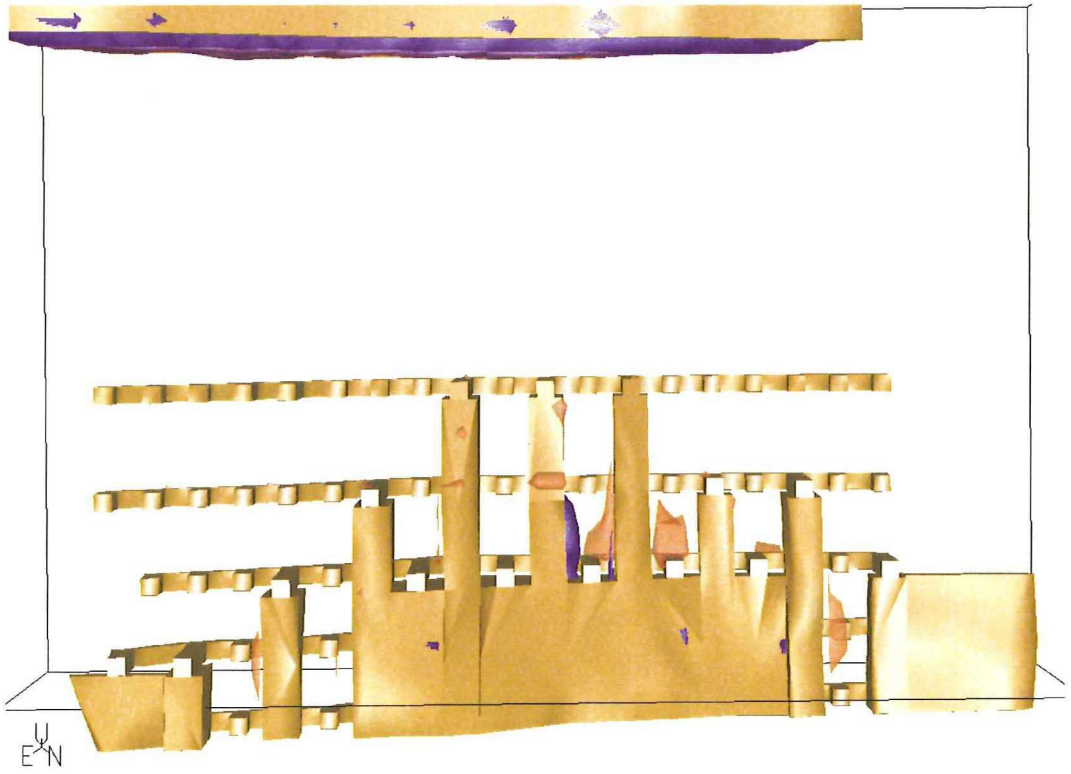

Figure E.2: The 2009 model with the 2009 (transparent orange) and 2008 (solid blue) failure criterion iso-surfaces.

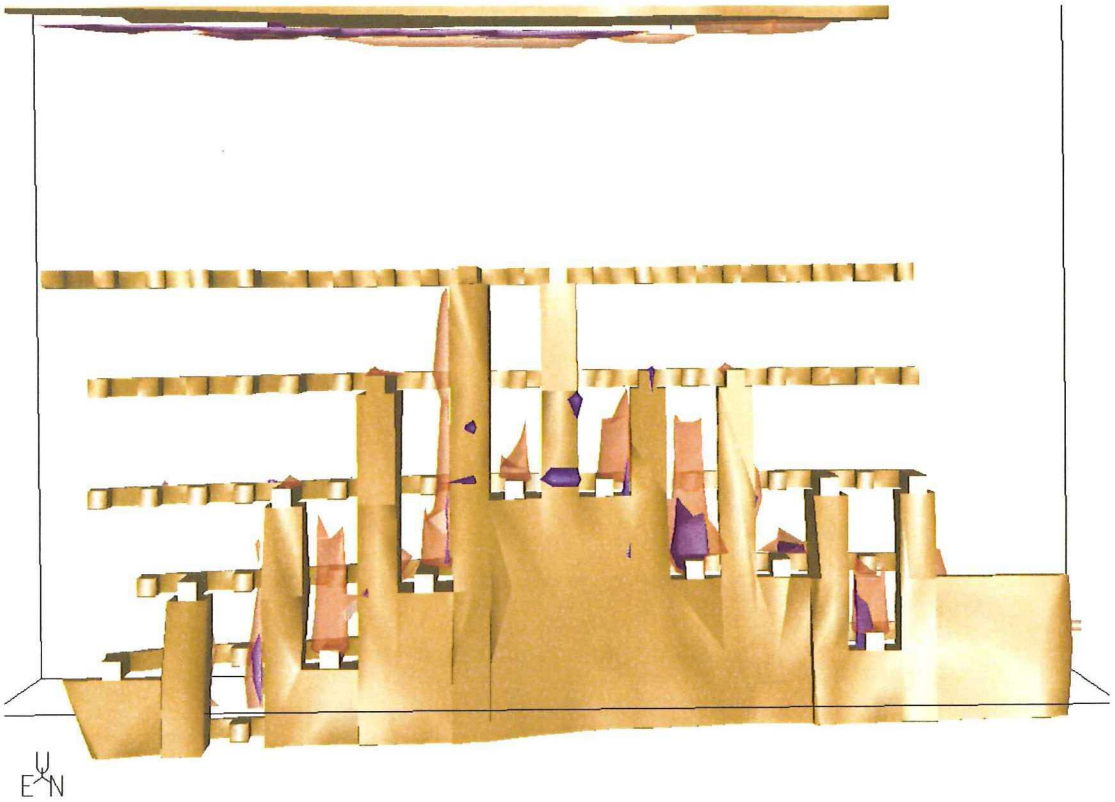

Figure E.3: The 2010 model with the 2010 (transparent orange) and 2009 (solid blue) failure criterion iso-surfaces.

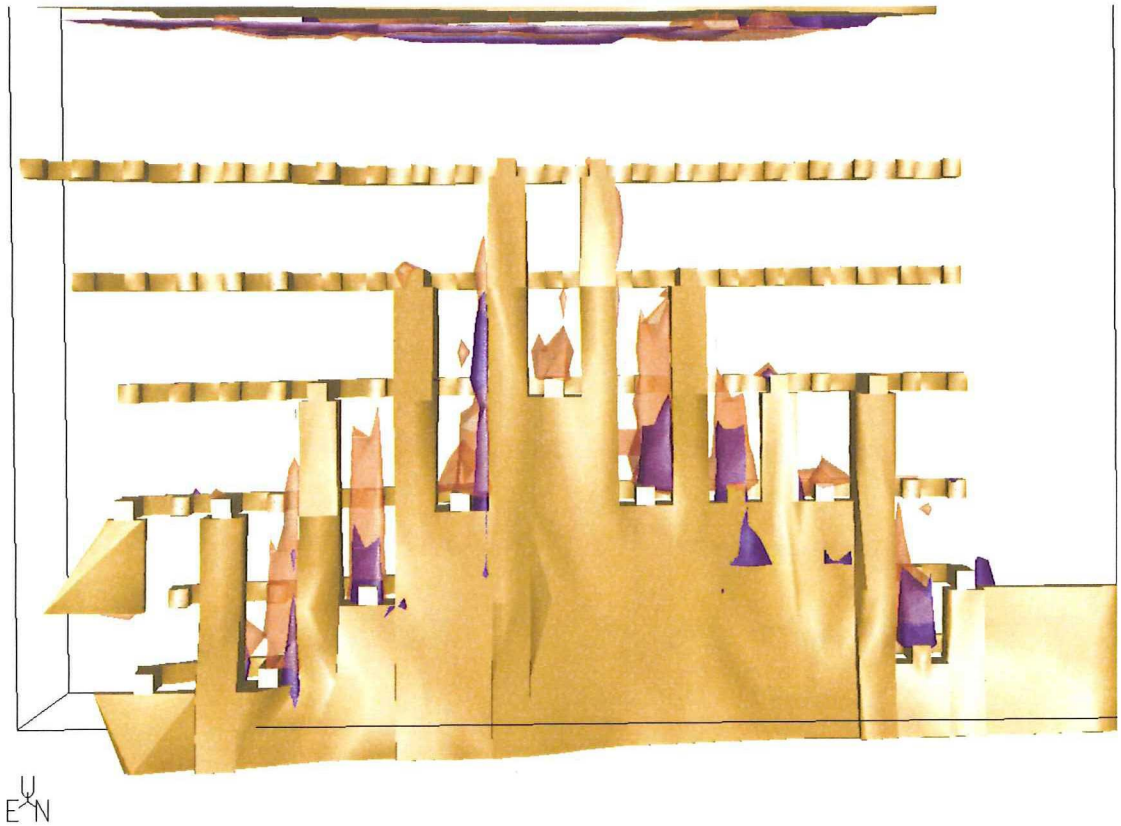

Figure E.4: The 2011 model with the 2011 (transparent orange) and 2010 (solid blue) failure criterion iso-surfaces.

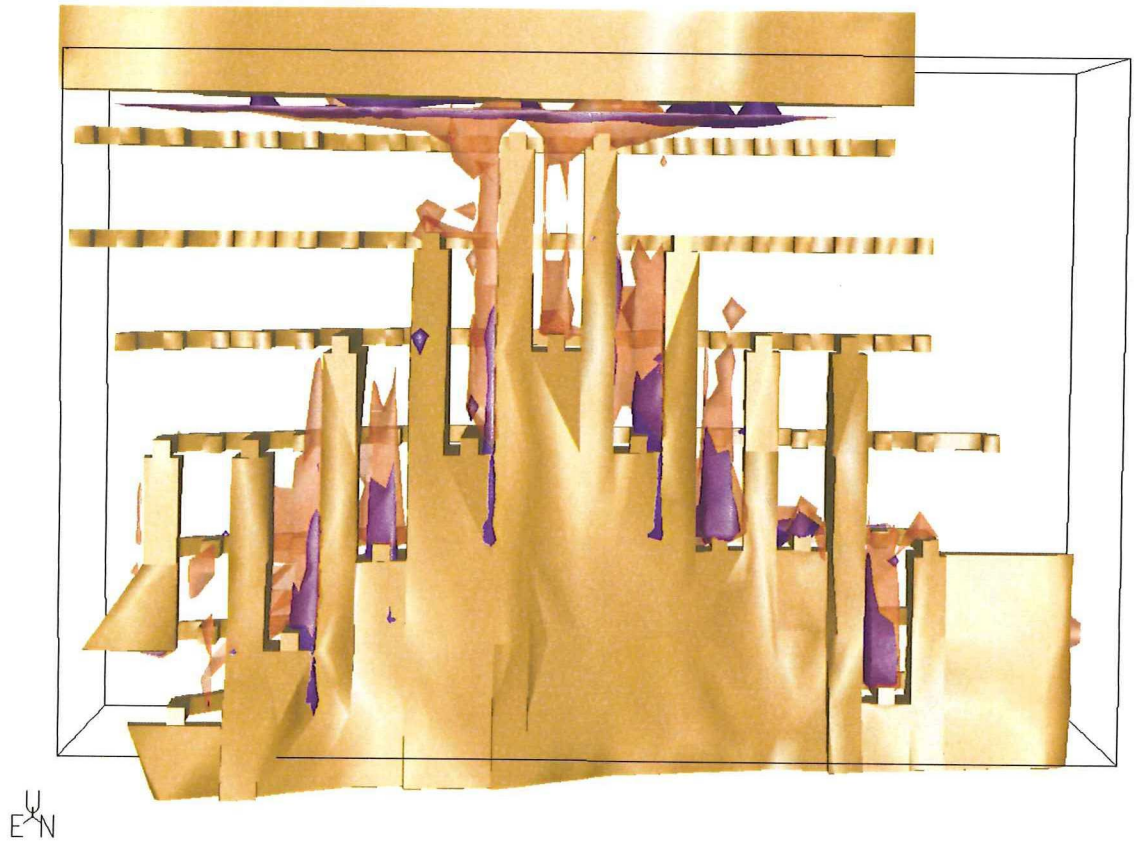

Figure E.5: The 2012 model with the 2012 (transparent orange) and 2011 (solid blue) failure criterion iso-surfaces.

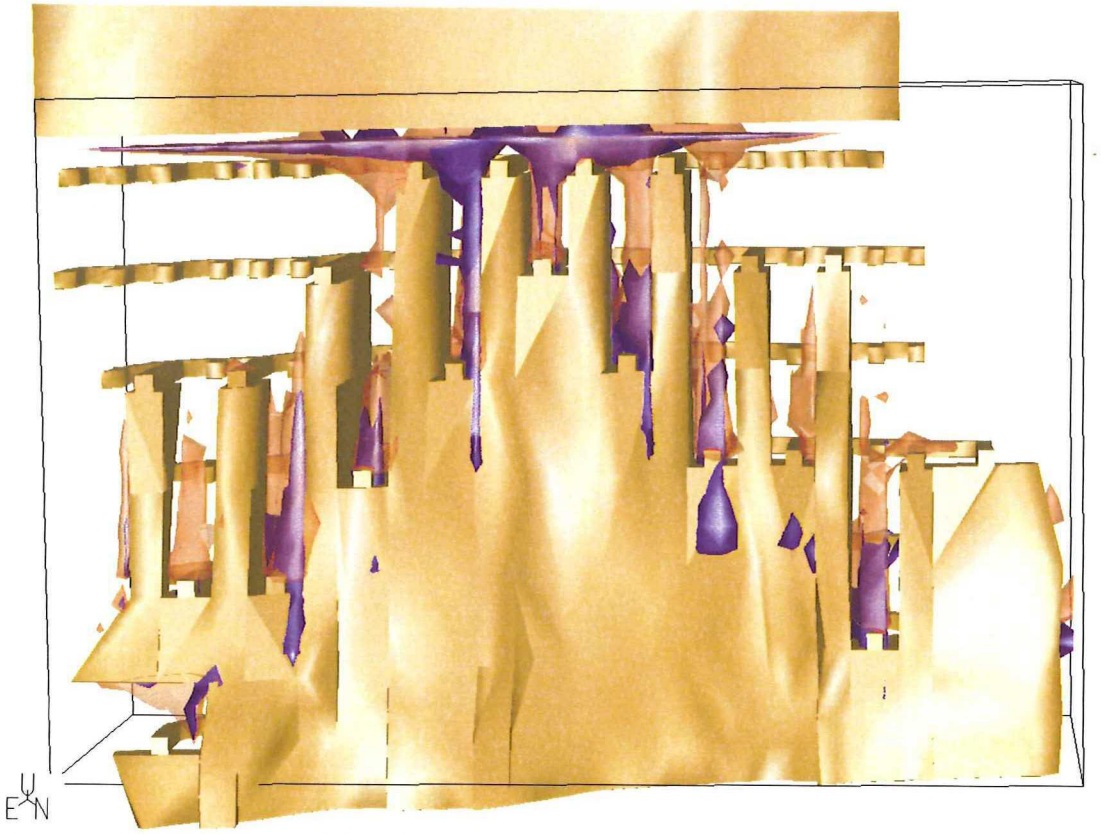

Figure E.6: The 2013 model with the 2013 (transparent orange) and 2012 (solid blue) failure criterion iso-surfaces.

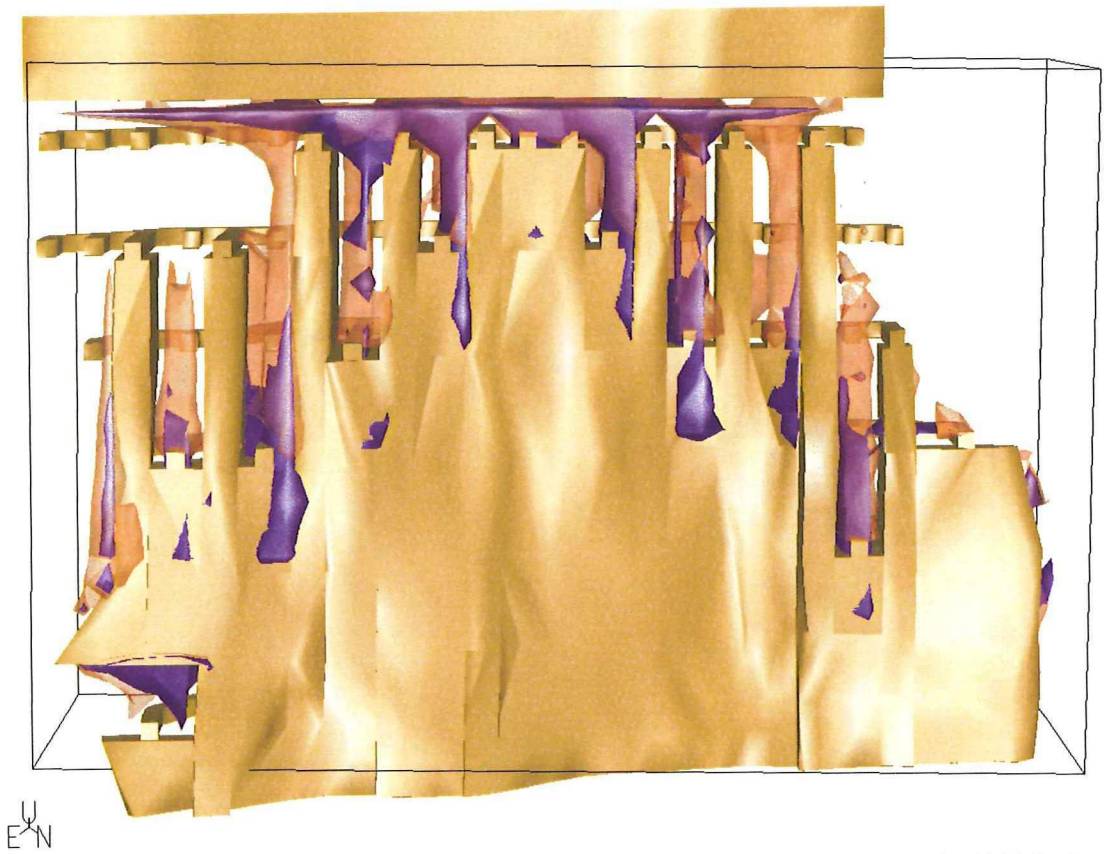

Figure E.7: The 2014 model with the 2014 (transparent orange) and 2013 (solid blue) failure criterion iso-surfaces.

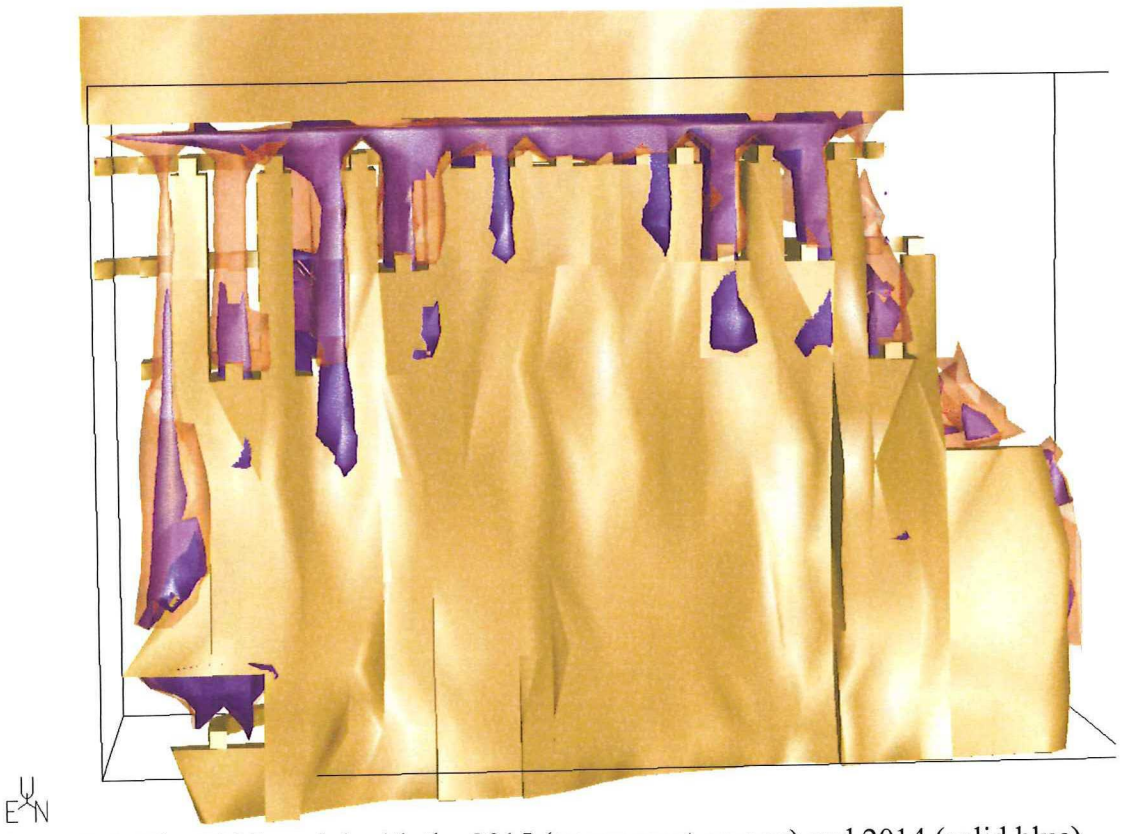

Figure E.8: The 2015 model with the 2015 (transparent orange) and 2014 (solid blue) failure criterion iso-surfaces.

Figure E.9: The 2016 model with the 2016 (transparent orange) and 2015 (solid blue) failure criterion iso-surfaces.